Advances in Methods and New Insights into the Mechanisms of Microplastic Transport and Retention in Rivers, Streams and Lakes

DISSERTATION

zur Erlangung des akademischen Grades eines

Doktors der Naturwissenschaften (Dr. rer. nat.)

in der

Bayreuther Graduiertenschule für
Mathematik und Naturwissenschaften (BayNAT)

der Universität Bayreuth

vorgelegt von

Jan-Pascal Boos

geboren in *Bottrop*

Bayreuth, 2023

Die vorliegende Arbeit wurde in der Zeit von August 2019 bis Juli 2023 an der Universität Bayreuth am Lehrstuhl für Hydrologie unter Betreuung von Herrn PD Dr. Sven Frei angefertigt.

Vollständiger Abdruck der von der Bayreuther Graduiertenschule für Mathematik und Naturwissenschaften (BayNAT) der Universität Bayreuth genehmigten Dissertation zur Erlangung des akademischen Grades eines Doktors der Naturwissenschaften (Dr. rer. nat.).

Form der Dissertation: Kumulative Dissertation

Dissertation eingereicht am: 06.07.2023

Zulassung durch das Leitungsgremium: 26.07.2023

Wissenschaftliches Kolloquium: 15.03.2024

Amtierender Direktor: Prof. Dr. Jürgen Köhler

Prüfungsausschuss:

PD Dr. Sven Frei (Gutachter)
Prof. Dr. Martin Obst (Gutachter)
Prof. Dr. Stefan Peiffer (Vorsitz)
Prof. Dr. Stephan Gekle

(Drittgutachter: Prof. Dr. Tobias Schütz)

Acknowledgements

Table of Contents

Summary

The ubiquity of microplastics (MPs) in the environment has raised global concerns due to their potential adverse effects on organisms. MPs can be transported over long distances and have been detected in remote environments. However, the processes governing the transport of MPs through the environment remain largely unknown, mainly due to their unique combination of size, shape, density and surface properties. This dissertation aims to investigate the mechanisms involved in the transport and retention of MPs in rivers, streams and lakes, focusing on physical processes and biotic interactions.

Study 1 introduced innovative quantitative methods for the spatio-temporal investigation of the transport and retention dynamics of small MPs (1-10 µm) in a laboratory flume, where a rippled streambed induced small-scale hyporheic exchange. MPs were monitored in the surface water with two fluorometers, allowing a continuous mass balance. Migration through the streambed was monitored with a laser-induced Fluorescence-Imaging-System. Detection limits below 3 µg/L for 1 µm polystyrene beads allowed for accurate tracking of MPs. Results showed advective transfer of MPs between the surface water and the streambed. MPs infiltrated up to 10 cm below the ripple crest. These direct experimental observations indicate that hyporheic exchange plays a crucial role in controlling the fate of MPs in fluvial environments.

In study 2, the quantification technique introduced in study 1 was used to systematically analyze the effects of MPs size, sediment type and flow conditions on the dynamics of particle transport and retention in a rippled streambed. As particle size increased (1, 3 and 10 µm), the maximum infiltration depth into the coarse streambed decreased (11, 10 and 7 cm), with 10 µm particles being partially retained. In the fine sand experiment, MPs experienced significant retardation in the streambed and exhibited slow release to the surface water, with 22 % not being recovered at the outflow location. Conversely, the high-flow experiment demonstrated efficient flushing of MPs from the streambed, resulting in the shortest residence times.

Study 3 presented a hybrid approach to modeling the transport of MPs. A computational fluid dynamics model was developed with openFOAM and calibrated with experiments such as in study 2. The integrated model solved the flow in the surface water and the hyporheic zone and reproduced the transport of MPs following advection and dispersion. The model accurately represented the transport of 1 µm particles but did not capture the delayed transport of 10 µm MPs through the streambed. The larger MPs were affected by retardation processes that increased with flow path length, suggesting interactions in the streambed.

Summary

Study 4 investigated the vertical transport of microplastics in lakes by combining field measurements, laboratory experiments and a 1D random walk model. Four experiments were conducted to investigate the effect of MPs size (1-5, 28-48 and 53-63 µm) and hydrodynamic conditions (thermal stratification and lake turnover). The model accurately predicted residence times for larger particles but overestimated them by a factor of 10 for the smallest MPs. Residence times of small MPs were 12 times shorter during lake turnover than during thermal stratification, but no resuspension was observed. These results suggest that additional mechanisms, such as aggregation or biotic interactions, are crucial factors controlling the transport of small MPs in lakes.

In study 5, the effect of biotic interactions on MPs transport in lakes was investigated using laboratory experiments and numerical models. A physical model, influenced by particle settling and mixing, was compared to a biological model that additionally included the interaction with a filter feeder (*Daphnia*). Following uptake, particles were egested and embedded in faecal pellets, significantly increasing particle settling velocity by 3 to 5 orders of magnitude. As a result, the residence time of small MPs (< 5 µm) in the lake decreased from 15 years in the abiotic model to 1 year in the biotic model. This allowed for particle sedimentation considering a lake flushing time of 4 years. The transport of larger MPs (15 µm) was similarly influenced by both biological and physical processes.

Study 6 investigated the effects of MPs exposure on an aquatic filter feeder (*Dreissena bugensis*). Fragments of different polymers within a comparable size range ($20 - 120$ µm) were characterized in-depth to analyze the polymer-specific impact on the organism. The exposure conditions were comparable as confirmed by flow velocity measurements. Interestingly, mussels did not cease filtration when exposed to MPs. Ingested MPs caused polymer-dependent adverse effects, as indicated by changes in biochemical markers. The strongest negative effects were observed for recycled PET, which was attributed to its chemical composition, including additives and residual monomers.

The integration of laboratory experiments, field measurements and numerical modeling has highlighted the complex processes involved in the dynamics of MPs transport and retention. The results indicate the influence of physical, physicochemical and biological mechanisms on the fate of MPs, which exhibit high mobility in rivers, streams and lakes.

Zusammenfassung

Die Verbreitung von Mikroplastik (MP) in der Umwelt hat weltweit Besorgnis über seine potenziell schädlichen Einflüsse auf Organismen ausgelöst. MP kann über große Entfernungen transportiert werden und wurde selbst in entlegenen Gebieten detektiert. Wie der Transport von Mikroplastik durch die Umwelt gesteuert wird, ist aufgrund der einzigartigen Kombination von Größe, Form, Dichte und Oberflächeneigenschaften weitgehend unbekannt. Diese Dissertation untersucht die Mechanismen, die den Transport und Rückhalt von MP in Flüssen, Bächen und Seen kontrollieren, mit Fokus auf physikalischen Prozessen und biotischen Interaktionen.

In Studie 1 werden innovative quantitative Methoden zur Untersuchung der räumlich-zeitlichen Transport- und Retentionsdynamik von kleinem MP (1-10 µm) in einer Laborrinne vorgestellt, in der ein geriffeltes Flussbett einen kleinräumigen hyporheischen Austausch erzeugt. MP wurde im Oberflächenwasser mithilfe zweier Fluorometer überwacht, die eine kontinuierliche Massenbilanz ermöglichten. Die Migration durch das Flussbett wurde mit einem laserinduziertem Fluoreszenz-Imaging-System untersucht. Nachweisgrenzen unter 3 µg/L für 1 µm große Polystyrolkugeln erlaubten eine genaue Verfolgung von MP. Es zeigte sich ein advektiver Transfer von MP zwischen dem Oberflächenwasser und dem Flussbett, mit einer maximalen Infiltrationstiefe von 10 cm unter dem Riffelkamm. Diese direkte Beobachtung unterstützt die Hypothese, dass der hyporheische Austausch den Verbleib von MP in Fließgewässern steuert.

In Studie 2 wurde die in Studie 1 eingeführte Quantifizierungsmethode zur systematischen Untersuchung des Einflusses von Partikelgröße, Sedimenttyp und Strömungsbedingungen auf den Transport und die Retentionsdynamik von MP in einem geriffelten Flussbett verwendet. Die Ergebnisse zeigten, dass mit zunehmender MP-Größe (1, 3 und 10 µm) die maximale Eindringtiefe im groben Flussbett abnahm (11, 10 und 7 cm), wobei 10 µm MP teilweise zurückgehalten wurde. Im Feinsandexperiment wurde MP im Flussbett stark verzögert und nur langsam an das Oberflächenwasser abgegeben. Hierbei wurden 22 % des MP am unteren Auslass des Gerinnes nicht wiedergefunden. Im Gegensatz dazu zeigte das Experiment mit höherem Abfluss eine effiziente Ausspülung von MP aus dem Flussbett, was zu den kürzesten Verweilzeiten führte.

In Studie 3 wurde ein hybrider Ansatz zur Modellierung des Mikroplastiktransports vorgestellt. Das neu entwickelte numerische Strömungsmodell in openFOAM wurde mit Experimenten wie in Studie 2 kalibriert. Das integrierte Modell erfasste die Strömung sowohl im Oberflächenwasser als auch in der hyporheischen Zone und stellt den Transport von MP durch Advektion und Dispersion dar. Das Modell bildete den Transport von 1 µm großem MP genau ab, konnte aber

Zusammenfassung

den verzögerten Transport von 10 μm großem MP nicht erfassen. Darüber hinaus nahm die Verzögerung im Flussbett mit zunehmender Fließweglänge zu, was auf die Bedeutung von Partikelwechselwirkungen hinwies.

Studie 4 untersuchte das vertikale Transportverhalten von Mikroplastik in Seen durch Feldmessungen, Laborexperimente und einem 1D Random-Walk-Modell. Vier Experimente wurden durchgeführt, um den Einfluss der MP-Größe (1-5, 28-48 und 53-63 μm) und der hydrodynamischen Bedingungen (thermische Schichtung und Durchmischung) zu untersuchen. Die Verweilzeiten von größerem MP wurden vom Modell gut vorausgesagt, aber für das kleinste MP um das Zehnfache überschätzt. Im Vergleich zur thermischen Schichtung war die Verweilzeit von kleinem MP während der Durchmischung des Sees 12-mal kürzer, wobei keine Resuspension beobachtet wurde. Diese Ergebnisse deuten darauf hin, dass zusätzliche Mechanismen wie Aggregationen oder biologische Interaktionen den Transport von kleinem MP in Seen steuern.

Studie 5 untersuchte den Einfluss biotischer Interaktionen auf den MP-Transport in Seen durch Laborexperimente und numerische Modelle. Zwei Systeme wurden verglichen: Ein physikalisches Modell, das das Absinken von MP und Durchmischung erfasst, und ein biologisches Modell, das zusätzlich die Interaktion mit einem Filtrierer (*Daphnia*) berücksichtigt. Das nach der Aufnahme wiederausgeschiedene MP war in Fäkalpellets eingebettet, was die Sinkgeschwindigkeit um 3 bis 5 Größenordnungen erhöhte. Die Verweilzeit von kleinem MP (< 5 μm) im See sank von 15 Jahren im abiotischen Modell auf 1 Jahr im biotischen Modell, was bei einer Wasseraustauschzeit von 4 Jahren zur Sedimentation führte. Der Transport von größerem MP (15 μm) wurde in ähnlichem Ausmaß durch biologische und physikalische Prozesse beeinflusst.

Studie 6 untersuchte die Effekte einer MP-Exposition auf einen aquatischen Filtrierer (*Dreissena bugensis*). Fragmente verschiedener Polymere ähnlicher Größe (20 – 120 μm) wurden eingehend charakterisiert, um spezifische Effekte auf den Organismus zu untersuchen. Die Exposition war vergleichbar, was durch Messungen der Fließgeschwindigkeit bestätigt wurde. Interessanterweise änderten die Muscheln ihr Filtrationsverhalten trotz Exposition nicht. MP-Aufnahme verursachte polymerabhängige negative Effekte, wie Veränderungen biochemischer Marker belegten. Stärkste negative Effekte traten bei rezykliertem PET auf, was auf die chemische Zusammensetzung, insbesondere Additive und Restmonomere, zurückgeführt wurde.

Laborexperimente, Feldmessungen und numerische Modelle haben die komplexen Prozesse untersucht, die am Transport und der Retention von MP beteiligt sind. Die Ergebnisse verdeutlichen den Einfluss physikalischer, physikalisch-chemischer und biologischer Mechanismen auf den Verbleib von MP, das eine hohe Mobilität in Flüssen, Bächen und Seen aufweist.

1 Introduction

1.1 Microplastics – a novel environmental contaminant

Plastic products have become essential in modern society and their consumption is closely tied to socioeconomic developments (Koelmans et al., 2019). Global plastic production has been steadily increasing, reaching 391 Mt/a in 2021, equivalent to 50 kg/a per person (PlasticsEurope, 2022). Unfortunately, inadequate management of plastic waste after use results in an uncontrolled release into the environment, with projections indicating a potential tripling from 60-90 Mt/a in 2015, to 155-265 Mt/a in 2060 (Lebreton and Andrady, 2019). Plastic contamination has surpassed planetary boundaries and has become a global concern (Persson et al., 2022). While various remediation strategies have been developed (Padervand et al., 2020), it is imperative to shift from a linear 'throwaway lifestyle' to a circular economy (Koelmans et al., 2019). Addressing plastic waste generation and its release into the environment also aligns with targets 12.4 and 12.5 of the Sustainable Development Goals (United Nations, 2015).

Microplastics (MPs) are microscopic plastic particles ranging in size from 1 µm to 5 mm (Frias and Nash, 2019). They can be categorized as primary MPs, intentionally produced for applications like cosmetics, or secondary MPs, which result from the degradation or fragmentation of larger items like tires or litter. Therefore, MPs vary widely in size, density, shape and surface characteristics. While some insights can be derived from studies on natural sediments (Waldschläger et al., 2022) or engineered nanoparticles (Hüffer et al., 2017), the unique combination of particle properties requires specific research to understand their behavior in the environment.

MPs are highly mobile in the environment, being transported over long distances and penetrating various environmental compartments in a 'microplastic cycle' (Bank and Hansson, 2022). The deep sea is a major sink for MPs (Woodall et al., 2014). Most marine plastics originate from terrestrial sources and were transported by rivers and streams. (Schmidt et al., 2017). MPs can enter fluvial systems through both point sources like wastewater treatment plants (Mintenig et al., 2017) and diffuse sources such as agricultural runoff (Bigalke et al., 2022) or atmospheric fallout (Allen et al., 2019). The high spatio-temporal variability of particle numbers in rivers (Mintenig et al., 2020) and the detection of MPs in streambed sediments (Frei et al., 2019) highlight the significance of retention processes within fluvial systems (Schwarz et al., 2019).

1.2 Microplastic transport mechanisms in rivers, streams and lakes

Fluvial systems play multiple roles in the dynamics of MPs, acting as conduits, potential sinks and secondary sources (Mani et al., 2015). Particles can become trapped in surface water eddies,

deposited at the streambed interface, or retained in the streambed. On a larger scale, the transport of MPs is influenced by catchment characteristics and hydrology (Baldwin et al., 2016). Certain areas with low flow velocities, such as lakes (Tibbetts et al., 2018) or dammed river sections (Watkins et al., 2019), promote particle sedimentation to the streambed, leading to reduced concentrations in the surface water. Conversely, high-flow events can remobilize MPs, significantly increasing their concentrations in the surface water by an order of magnitude (Gündoğdu et al., 2018). Small, (sub-)pore-scale MPs are particularly relevant due to their high mobility in fluvial systems and their presence in streambed sediments (Frei et al., 2019). Notably, these particles are not completely removed during drinking water treatment processes, which can result in human exposure to MPs (Pivokonsky et al., 2018).

The transport of MPs is influenced by a combination of particle properties, hydrodynamic flow characteristics and biogeochemical interactions. Gravitational settling of MPs is influenced by its physical characteristics, including particle size, density and shape (Ahmadi et al., 2022). Smaller MPs with densities similar to water exhibit low sinking velocities and can have prolonged residence times in the water column (Elagami et al., 2022). However, the transport behavior of MPs differs from that of mineral particles with high density and spherical shape, for which transport formulae are well established. In the case of MPs, both the settling velocity and the critical shear stress required for particle erosion have been found to be lower than expected based on theoretical predictions (Elagami et al., 2022; Waldschläger and Schüttrumpf, 2019b).

1.2.1 Hydrodynamic influences in fluvial systems

In rivers and streams, the settling behavior of MPs is superimposed by larger hydrodynamic forces, resulting in a hydraulic sorting of the deposited particles (Woodward et al., 2021). The ubiquitous detection of MPs in the surface flow, at the streambed interface and in streambed sediments (Shahul Hamid et al., 2018) highlights the influence of interactions between surface and subsurface flow. For small, (sub-)pore-scale MPs, advective transfer from the surface water across the interface into the streambed sediments has been considered as a potential mechanism to transport particles into the hyporheic zone (Frei et al., 2019).

The hyporheic zone serves as an important ecosystem, where surface water and groundwater are hydraulically connected (Boano et al., 2014). This region exhibits increased nutrient turnover and supports a high level of biological diversity in close proximity to the streambed interface (Lewandowski et al., 2019). The exchange of water in the laminar regime follows Darcy's law and is influenced by factors such as (i) the hydraulic conductivity of the streambed sediments, (ii) the hydraulic gradient between the streambed interface and the sediments and (iii)

the flux of groundwater into and out of the surface water (Saenger, 2000; Storey et al., 2003). Hyporheic exchange occurs at various scales, ranging from the local alluvium to the larger river catchment scale. This thesis focuses on small-scale, vertical exchange driven by the streambed topography which plays a crucial role in biogeochemical turnover (Gomez-Velez et al., 2015). Common bedforms found in natural rivers are ripples or dunes, which form under subcritical flow conditions with low Froude numbers (Engelund and Fredsoe, 1982).

Bedform-induced hyporheic flow is primarily driven by advective pumping and diffusion plays a negligible role (Elliott, 1991). The stream water infiltrates at the upstream stoss side of the bedform, migrates through the porous medium and re-enters the surface water at the downstream lee side of the bedform (Elliott and Brooks, 1997). This mechanism is discussed to facilitate the transfer of small, (sub-)pore-scale MPs from the surface water into the hyporheic zone (Frei et al., 2019). However, the behavior of conservative tracers is not directly transferable to MPs, which were detected in shallower depths of the streambed, where they were additionally retained (Harvey et al., 2012). The extent of MPs retention depended on the hydrodynamic characteristics, and during high-flow events, previously stored MPs could be remobilized back into the surface water (Harvey et al., 2012; Hurley et al., 2018). Simulations from headwater streams have demonstrated significant temporal variation in the residence times of MPs in streambed sediments, ranging from a few hours to several years (Drummond et al., 2022).

Column experiments have provided insight into the mobility of MPs in porous media flow, highlighting the influence of sediment properties and physicochemical interactions (Lu et al., 2021a; 2021b). The infiltration depth of larger MPs (>100 µm) was found to be related to the particle-to-sediment grain size ratio (Waldschläger and Schüttrumpf, 2020). However, it is challenging to extrapolate the results of simplified column experiments to the complex dynamics of MPs transport in rivers and streams, where three-dimensional hydrodynamic forces play a significant role. The specific contributions of advective transfer and sedimentation-erosion-cycles in controlling the transfer of MPs between the surface water and the streambed, as well as the mechanisms affecting particle transport within porous media are still not well understood.

1.2.2 Hydrodynamic influences in lake systems

Unlike rivers and streams, lake systems exhibit low flow velocities, particularly in the longitudinal direction (Bek et al., 2019). This allows for the isolation of vertical transport processes and the analysis of key factors controlling particle settling behavior. In lakes, particle transport is primarily influenced by the stability of the water column, changing between thermal stratification and lake turnover, as well as wind forcing and seiches (Bek et al., 2019). These

hydrodynamic conditions exhibit spatial and seasonal variations, mostly due to water temperatures, which can induce both turbulent mixing and laminar flows in the water column. While turbulent mixing accelerates sedimentation and burial of natural material, it can also result in the resuspension of previously deposited material (Weyhenmeyer et al., 1997).

Studies indicate that MPs can undergo temporary or permanent retention in lakes (D'Avignon et al., 2022; Dusaucy et al., 2021). However, the understanding of MPs transport processes in lakes is still limited: Many studies investigating MPs settling behavior have been conducted in controlled laboratory settings (Elagami et al., 2022; Waldschläger and Schüttrumpf, 2019a) and it remains unclear, how these findings can be applied to the more complex conditions found in real lakes. For instance, studies suggest that small MPs may have prolonged residence times in the water column (Elagami et al., 2022), which increases the likelihood of interactions with other water constituents or biota, thereby potentially influencing the transport behavior of MPs.

1.2.3 The influence of interactions between particles and biota

In the aquatic environment, MPs can be degraded due to a variety of mechanical, chemical and biological processes (Klein et al., 2017), that may significantly alter their transport behavior in rivers, streams and lakes. In addition, aggregation with other particles or solutes can increase the settling velocity of MPs, facilitating their efficient removal from the water column (Schmidtmann et al., 2022). The formation of biofilms on MPs can affect settling velocities (Elagami et al., 2022; Rummel et al., 2017) and is discussed to have a more pronounced effect on smaller particles with a high surface-to-volume ratio (Fazey and Ryan, 2016).

MPs in aquatic systems can interact with freshwater biota (Scherer et al., 2018) and enter the food chain through filter feeders such as mussels (Hoellein et al., 2021) or *Daphnia* (Imhof et al., 2017). Apart from the direct physical impact, sorbed chemicals can leach out and trigger immune responses on the organism (Redondo-Hasselerharm et al., 2023). Given their ability to bioaccumulate in higher trophic levels (Bhatt and Chauhan, 2023), MPs pose a threat to aquatic communities (Anbumani and Kakkar, 2018). However, it remains unclear which specific physicochemical properties of MPs are particularly harmful for aquatic organisms.

Finally, biotic interactions, such as particle storage in organisms or deposition in biological matrices, can also influence particle transport behavior in the water column and lead to particle immobilization (Cole et al., 2023). Additionally, bioturbation in freshwater sediments can increase the vertical propagation of MPs (Frank et al., 2023). Further research is needed to evaluate whether such biotic interactions significantly alter MPs transport in relation to the hydrodynamic and physical forces which naturally occur in rivers, streams and lakes.

2 Objectives and structure

This research was conducted as part of the Collaborative Research Centre 1357 'Microplastics' at the University of Bayreuth and focused on investigating the transport patterns of microplastics (MPs) in fluvial systems. Despite the ubiquitous detection of MPs in rivers, streams and lakes, the mechanisms that control the dynamics of particle transport and retention within these environments are still not fully understood. To address this knowledge gap, the studies in this thesis aimed to evaluate and explore four main hypotheses:

1. Small, (sub-)pore-scale MPs are mobile in fluvial systems and can be advectively transferred between the surface water and the streambed sediments (studies 1 and 2)

2. The ratio of particle-to-streambed grain size can be used as an indicator of particle infiltration and retention in the streambed (studies 2 and 3)

3. The hydrodynamic characteristics of the surface flow affect MPs infiltration and retention in the streambed sediments (studies 2 and 3) as well as its residence time in the water column (study 4)

4. MPs interact with organisms in the water column and near the streambed, significantly affecting MPs transport (study 5) and inducing stress on biota (study 6).

Various research techniques were used to address these hypotheses. Laboratory experiments in a water flume (studies 1-3) investigated MPs migration between surface water and the streambed. These results served to validate a numerical model which is introduced in study 3. In addition to this focus on MPs transfer in an idealized laboratory setting, field experiments (study 4) analyzed MPs transport in real lakes. The influence of biotic interactions on MPs transport in lakes was studied by combining laboratory experiments with numerical models (study 5). Lastly, the effect of MPs exposure on biota was studied under laboratory settings in glass aquaria (study 6).

The objective of study 1 was to develop a novel monitoring technique to spatio-temporally quantify MPs transport in an experimental flume, which was influenced by both surface flow and bedform-induced subsurface flow. The methods involved a continuous monitoring of MPs concentrations using fluorometers in the surface water, as well as a laser-induced Fluorescence-Imaging-System to track MPs transfer between (i) the surface water, (ii) the streambed interface and (iii) in the streambed sediments. The reliability of these quantification methods was assessed, and the setup was used for an initial experiment investigating the transport of 1 µm MPs in the flume.

In study 2, the newly developed monitoring technique was employed to systematically investigate the effects of particle size (1, 3 and 10 µm), streambed sediments (fine and coarse sand) and hydrodynamic conditions (low and high flow) on the dynamics of MPs transport and retention in both surface water and streambed sediments. The study additionally included hydrodynamical measurements to gain insights into the physical mechanisms controlling the infiltration of MPs into the streambed.

In Study 3, a hybrid modeling approach using openFOAM was developed and validated using the novel MPs transport monitoring techniques. The digital twin approach provided additional information and addressed the limitations of the experimental methods by providing a more comprehensive understanding of particle transport and retention throughout the study domain and characterizing hyporheic flow velocities. By comparing the transport processes of 1 µm and 10 µm beads, valuable insights into the mechanisms influencing the fate of MPs in streambed sediments were obtained.

Study 4 focused on MPs transport behavior in natural settings and presented field experiments which were conducted at lake 'Großer Brombachsee'. By studying the vertical transport pattern in the lake, which is characterized by less pronounced longitudinal flow compared to rivers and streams, the influence of particle properties on MPs residence times in the water column was analyzed under realistic hydrodynamic conditions. Fluorometric techniques, which were developed in study 1, were used to monitor MPs transport in the lake.

In study 5, the influences of hydrodynamic conditions and biotic interactions on particle transport in lake systems were examined. Laboratory measurements were conducted to gather data on particle settling velocity after egestion by filter feeders (*Daphnia*). This information was used to compare particle transport in two different lake models. The first model focused on the physical aspects of MPs transport, considering gravitational settling and turbulence. The second model, a physico-biological model, considered additional factors such as particle uptake and egestion by *Daphnia*.

Study 6 investigated the influence of polymer type and chemical composition of MPs on benthic filter feeders (*Dreissena bugensis*). The mussels were exposed to particles in a glass aquarium, where a submerged pump induced a circular flow. The study analyzed the behavioral response of these organisms by comparing their filtration rate when exposed to natural particles and MPs. The uptake of MPs into the organisms was visually inspected, and biochemical markers were examined to assess the induced stress level of the organism.

3 Materials and methods

3.1 Laboratory flume experiments (studies 1 – 3)

3.1.1 Experimental setup and hydrodynamic characterizations

MPs transport experiments were conducted in a water flume (dimensions: 5 x 0.086 x 0.30 m, G.U.N.T. GmbH), which was inclined between 0 and 3 mm/m (Figure 1). To monitor discharge continuously, an electromagnetic flowmeter (Jumo GmbH) was employed, and mean surface flow velocities ranged from 0.06 to 0.17 m/s in the flume. Particle aggregation was prevented by using deionized water in the flume, operated in (i) a closed-circuit setup for study 1 and (ii) an open circuit setup for studies 2-3 to avoid particle recirculation. Weirs were strategically positioned to define a study domain that was homogeneously filled with unimodal sands of two distinct size classes (coarse and fine sand) for the experiments. The mean diameter of the sands was 1.0 and 0.4 mm. The streambed was manually formed into a series of stable ripple structures to replicate natural stream conditions (Fox et al., 2014). Additionally, in studies 2-3, the morphology of the entire streambed was measured using a 2D laser profiler (wenglor GmbH).

In studies 2 and 3, ultrasonic sensors (WayCon GmbH) were used to monitor the water surface elevation at six locations. Particle-Image-Velocimetry (PIV, ILA_5150 GmbH) was employed to measure flow velocities in longitudinal and vertical directions (x-z-plane) in the surface water. The flow field was illuminated along the flume centerline using an LED sheet ($\lambda \approx 520$ nm), allowing for image acquisition using a CMOS camera (iDS Imaging GmbH). The longitudinal position of the PIV system was adjustable to analyze the flow field over a selected bedform as well as its two adjacent ripples. Average flow velocities were obtained by merging 9 individual PIV measurements, each consisting of 1000 frames captured at a frequency of 40 Hz.

3.1.2 Innovative spatio-temporal analysis techniques

The experiments were conducted using polystyrene beads of 1, 3 and 10 µm in diameter (Poly-Sciences Inc.). The particles had a density of 1050 kg/m^3 and were internally fluorescently dyed. In addition, the surface of the MPs was coated to prevent aggregation. Prior to disposal, water containing MPs from previous studies passed through a cascade of membrane filters (Fuhr GmbH) with mesh sizes 0.45 µm and 0.04 µm multiple times which removed most MPs.

The volumetric concentration of MPs in the surface water was measured by two portable fluorometers (FL24, Albillia Co.). They were installed at the inflow and outflow of the study domain and recorded at a frequency of 0.5 Hz. Peristaltic pumps were used to extract water from the flume, pass it through the flow cell of the fluorometers and then return it back to the flume.
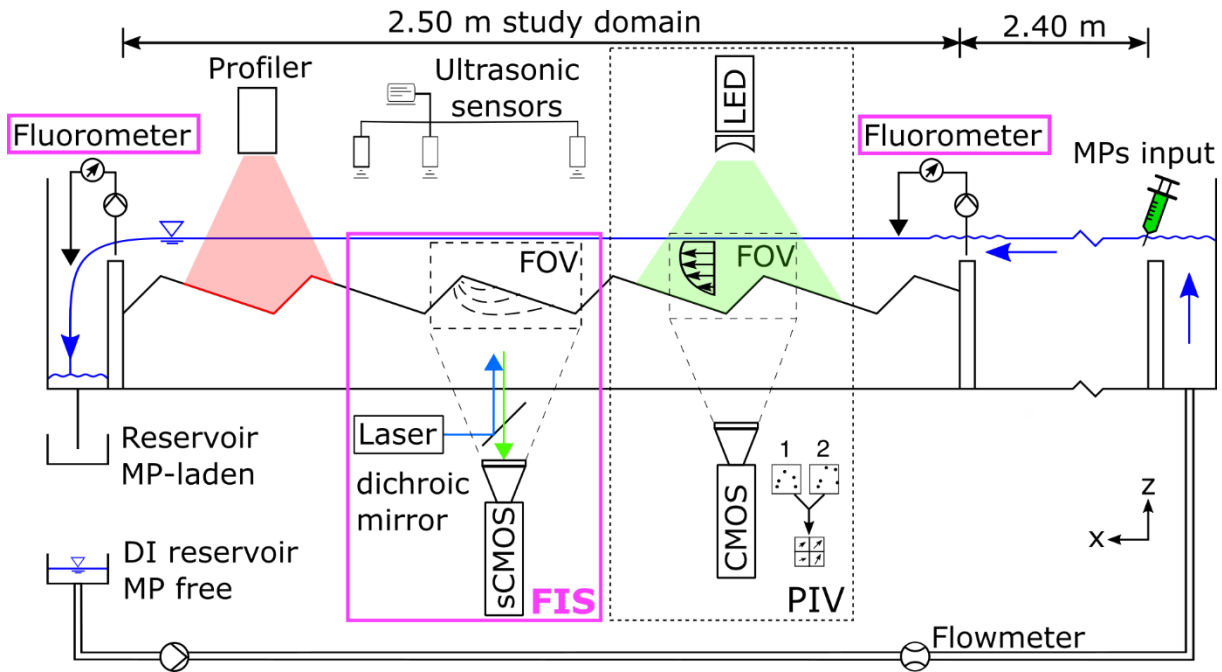
Figure 1: Setup of the flume experiments: Microplastics (MPs) were tracked in the surface water, using fluorometers, and at a monitored bedform with a Fluorescence-Imaging-System (FIS). Surface flow velocities were acquired with Particle-Image-Velocimetry (PIV), water levels with ultrasonic sensors and bedform morphology with a laser profiler. Flow velocities and MPs infiltration pattern were analyzed sequentially for the same bedform. This figure is included as Figure 1 in Study 2.

A Fluorescence-Imaging-System (FIS) was developed to capture the fluorescent signal of MPs at one selected bedform structure. The FIS allowed for the continuous detection of MPs (i) in the surface flow, (ii) at the streambed interface and (iii) in the pore space of the streambed at the glass interface of the flume. The measurements were conducted at a frequency of $0.5 – 8$ Hz. For excitation of the fluorescent dye in the MPs, two diode-pumped solid state-lasers with a wavelength of 457 nm (CNI Ltd) were used. The optical path of the laser light was deflected orthogonally to the monitored bedform with a 45° dichroic mirror (Chroma Technology Corp). This arrangement effectively minimized the amount of laser excitation light that entered the sensor of a scientific CMOS camera (Andor Zyla 5.5, Oxford Instruments), which was used for capturing the images.

The calibration of both detection systems, the fluorometers and the FIS, spanned over four orders of magnitude and used a set of 16 standards, resulting in approximately 30 measurements for the fluorometers and 80 measurements for the FIS. To calibrate the FIS, a 10 cm long flume section was isolated and filled with MPs suspensions in (i) the surface water and (ii) the pore space of the streambed sediments. Additionally, a purpose-built glass tank measuring 60 cm x 30 cm x 5 cm was positioned in the flume to calibrate larger areas. Due to the heterogeneous

intensity distribution in the laser beam, the fluorescence intensity varied throughout the field of view of the camera. To account for this, linear regressions were performed locally, averaging squares of 10 x 10 pixels. Quantification limits were determined from the calibration curves (Funk et al., 1985).

3.1.3 Quantification of the dynamics of microplastic transport

To compare MPs transport across different experimental scenarios, concentrations c [ML^{-3}] obtained from fluorometer and FIS measurements in the surface water and the pore water of the streambed sediments were normalized to mass transfer rates $\dot{m}$ [T^{-1}], by considering the flume discharge Q [L^3T^{-1}] and MPs input mass m_0 [M]:

$$\dot{m}(t) = \frac{c(t) \cdot Q(t)}{m_0}$$

The fluorometers continuously measured the temporal evolution of MPs concentration in the surface water at both the inflow and outflow of the study domain. By integrating the mass transfer rate over time, the number of MPs that has been entering and leaving the study domain could be determined. The value at the end of each experiment represented the total amount of MPs recovered at the measurement locations, allowing for comparisons of MPs retention among different experimental scenarios. For studies 2 and 3, the difference between the mass flux at the inflow and outflow was interpreted as MPs present in the study domain. This approach assumed that the location of the fluorometer measurements adequately represented the entire cross-sectional area.

The FIS dataset served to analyze the dynamics of MPs infiltration into the bedform structure. Breakthrough curves were generated by extracting particle concentrations at multiple depths (1-11 cm) below the ripple crest, and all layers were averaged over 1 cm depth. Experimental artefacts were reduced by rejecting the first and last 5 % of MPs detection in each layer. The onset of detectable infiltration at each depth indicated the time of arrival of the plume front, and its slope ($\partial z/\partial t$) was used to calculate vertical propagation velocities. In addition to systematically analyzing spatially averaged light intensities for all particles, the FIS provided sufficient resolution to monitor individual particle positions in the streambed for the larger, 10 µm MPs. For these particles, a quantification of the infiltration dynamics was additionally performed using two approaches: (i) the mean position of the infiltrated MPs (center of mass) was determined by averaging individual particle positions over space, and (ii) the plume front was calculated by connecting the outermost particles.

3.2 Numerical flume model (study 3)

In study 3, an integrated three-dimensional hydrodynamic model was developed using the open-FOAM toolbox for computational fluid dynamics. The model considered both air and water flow and employed the interFoam solver to accurately simulate free-surface flow dynamics. The volume-of-fluid method was used to track the interface between air and water. To capture larger turbulences, such as those occurring in the wake of the bedform structures, a large eddy simulation model was employed. The streambed sediments were represented as a porous continuum, incorporating friction-induced pressure losses based on Darcy's law. This approach allowed for the integrated simulation of the hydrodynamic conditions in both surface flow and subsurface flow in the flume. For the transport of MPs, a scalar transport model was used. It considered advective and dispersive processes and was modified with an additional advective retardation factor to account for the potential retardation of particles in the streambed. This approach modeled MPs as a conservative tracer.

The experimental setup from study 2 was used to calibrate the numerical model. MPs transport experiments were conducted with 1 µm and 10 µm PS microbeads, with a sediment grainsize of 1.0 mm and a mean surface velocity of 0.06 m/s. The entire experimental dataset was used for the calibration, including (i) hydrodynamic characteristics (discharge, water levels, and velocity fields above the monitored bedform), (ii) sediment topography, (iii) MPs concentrations in the surface water (fluorometer dataset) and (iv) MPs concentrations in the surface water and in the pore water of the streambed sediments at the monitored bedform (FIS dataset). In addition to replicating the laboratory results, the numerical model provided additional insights into MPs transport. It enabled the investigation of the three-dimensional distribution of MPs throughout the entire study domain and captured the temporal changes in particle distribution in both surface water and the streambed sediments. Furthermore, the model facilitated the analysis of hyporheic flow patterns, providing valuable information on MPs transport mechanisms.

3.3 Lake field experiments (study 4)

In study 4, field experiments were performed at lake 'Großer Brombachsee' to analyze the transport behavior of MPs in a natural environment. A circular plastic enclosure ('mesocosm'), measuring 12 m in depth and 3 m in diameter, was anchored to the lake bottom. Distinct size ranges of MPs (1-5 µm, 28-48 µm and 53-63 µm) were added individually in separate experiments to examine the influence of particle size on transport under low hydrodynamic forces during thermal stratification. Another experiment using 1-5 µm MPs was conducted during lake turnover to assess the impact of turbulent convective mixing on particle transport. Portable

fluorometers (studies 1-3), were used to monitor MPs at two locations: 1 m below the lake surface and 0.5 m above the mesocosm bottom.

The temperature profile in the lake mesocosm was measured at 1 m intervals, and water velocities were monitored 1 m below the surface with a 3D acoustic Doppler velocimeter. Particle settling velocities were obtained from (i) calculations for the 1-5 µm MPs using Stokes' law, (ii) laboratory results for the 28-48 µm and 53-63 µm MPs using PIV (studies 2-3), and (iii) field data based on the times when 50 % of the particles were detected by the fluorometers. Furthermore, the residence times of MPs in the lake were calculated by determining the duration from the initial detection of surface-near MPs until 95 % of the particles reached the bottom-near location. This analysis emphasized the tailing behavior of the breakthrough curve. Finally, the observed particle transport in the lake was compared to a 1D random walk model that incorporated the settling velocities of MPs. The model simulated the transport of MPs based on vertical settling of the particles and random displacements caused by turbulence.

3.4 Modeling of microplastic transport in lakes under biotic interactions (study 5)

Study 5 investigated the importance of biotic influences on the transport dynamics of MPs (0.5, 5 and 15 µm) in lake systems. Generic virtual experiments were conducted and parametrized for both a large lake (Lake Constance, Germany) and a small lake (Esthwaite Water, UK). Lake temperature profiles represented summer thermal stratification. Two models were developed to simulate particle transport: The abiotic system focused on purely physical transport processes and considered turbulent mixing and particle settling, which was estimated from Stokes' law. In contrast, the biotic system incorporated the physical processes of the abiotic system and additionally considered biotic interactions, as caused by the uptake by organisms, such as unselective filter feeders (*Daphnia*). The model represented the ability of the organisms to ingest MPs, temporarily store them in their intestinal tract and excrete them embedded in faecal pellets. Both models simulated particle transport as a series of transfer functions, rather than spatio-temporally resolving lake hydrodynamics.

The model incorporated experimental data obtained from laboratory conditions where *Daphnia* were exposed to distinct types of MPs (PS fragments of 17.7 µm and PS spheres of 3 µm). The faeces produced by the organism were collected from the bottom of the glass beakers. The sinking velocities of these faecal pellets were subsequently determined by performing experimental measurements using the PIV system from studies 2-4. To visually confirm the presence

of particles embedded in faecal pellets, *Daphnia* were exposed to fluorescent PS measuring 10 µm. The faecal pellets were subsequently examined by fluorescence microscopy.

3.5 Laboratory experiments on the influence of microplastics on biota (study 6)

Study 6 examined the effect of MPs on aquatic filter feeders (*Dreissena bugensis*), which reside at the streambed interface. MPs feeding experiments were conducted for four different polymers: PET, PS, PE and PLA, as well as mussel fragments as natural control particles in the size range of 20 – 120 µm. To visually confirm the uptake of MPs into the organism, the mussels were additionally exposed to fluorescently coated PS, and soft tissues of the mussels were analyzed by fluorescence microscopy. The behavior of the mussels was analyzed by monitoring their filtration activity in the presence of MPs. In addition, biochemical markers such as enzymes and the proteome were analyzed to evaluate the induced stress on the organisms.

Particle exposure to the organisms was realized by transporting the particles as a suspended load in the water column. A submersible pump was used to create a circular flow. Flow velocities were measured based on the positioning of the mussels during the exposure experiments to investigate the transport of MPs, ensuring that hydrodynamic forces were sufficient to suspend particles with the highest density (mussel fragments, 2590 kg/m³) and the lowest density (PS, 1050 kg/m³). A 2D laser Doppler velocimeter (TSI Inc.) provided high-resolution measurements of the vertical profile of longitudinal and vertical velocity components. Friction velocities were calculated by (i) fitting the profile of the mean horizontal velocity components to the logarithmic law of the wall and (ii) the mean of height-dependent Reynolds stresses, calculated from velocity fluctuations. Thresholds for particle erosion and suspension were obtained from calculations based on particle characteristics.

4 Summary of individual results and discussions

4.1 Study 1: Tracking Microplastics Across the Streambed Interface: Using Laser-Induced-Fluorescence to Quantitatively Analyze Microplastic Transport in an Experimental Flume

This study introduced novel detection techniques to accurately quantify the spatio-temporal transport of MPs through an experimental water flume featuring a rippled streambed. To assess MPs concentrations in the surface water and calculate mass balances, two fluorometers were positioned at the inflow and outflow of a study domain. In the study domain, particle transport through a specific monitored bedform was measured using a Fluorescence-Imaging-System.

The measurement techniques exhibited a linear relationship within the concentration range of 0.4 to 4,000 µg/L with an R^2 value of 0.97 for the fluorometers and R^2 exceeding 0.99 for the FIS. The detection limits for the fluorometers and the FIS were determined as 0.6 µg/L and 3.1 µg/L, respectively. Hence, these measurement techniques yielded reliable data for the quantitative assessment of MPs concentrations. To assess the reproducibility of the novel measurement techniques, experiments were conducted without sediments, indicating a variation in MPs recovery rate between 80 and 90 %. This discrepancy in the mass balance was likely caused by a heterogeneous concentration of MPs in the surface water. The fluorometers extracted water from a single point in the center of the flume, assuming it was representative of the entire cross section. The FIS focused near the inner water-glass-interface, where the no-slip condition results in lower flow velocities and reduced MPs transport in proximity to the boundary.

An experiment was conducted to analyze the transport of 1 µm MPs through the flume with a rippled streambed (sediment grain size of 1.0 mm) under the influence of bedform-induced hyporheic exchange. Surface water measurements indicated a wider breakthrough and a lower peak at the outflow location compared to the inflow location. As a result, the upper measurement site was primarily controlled by advective processes, and the lower site, in contrast, was affected by a combination of advection, dispersion and likely retardation in the streambed sediments. After approximately 100 s at the inflow position and 140 s at the outflow position, the concentration of MPs increased again due to water recirculation. Consequently, the tailing behavior of the breakthrough curve could not be analyzed. The FIS monitoring provided first experimental evidence of MPs infiltration at the upstream stoss side and particle release at the downstream lee side of the bedforms. At shallow depths of the streambed, peak concentrations were higher and arrived more quickly. MPs infiltration depth was observed to extend to a

maximum of two times the bedform height. Following the initial breakthrough, surface water concentrations at the inflow, outflow and above the bedform became comparable and gradually decreased over the course of the 5-hour experiment. Besides the possibility of particle deposition within the flume system, this trend indicated MPs retention in the streambed sediments.

This study introduced innovative techniques for the quantification of spatio-temporal dynamics of MPs transport in the surface water and in the streambed of a water flume. Methodically, the experiments contributed to optimizing the positioning of the fluorometers at the inflow and outflow of the study domain, as well as refining the settings of the FIS to achieve a high dynamical range while avoiding camera sensor oversaturation. Scientifically, the study provided first experimental evidence of the advective transfer of (sub-)pore-scale MPs into the streambed along with particle release from the streambed. The observed pattern of infiltration at the stoss side and release at the lee side resembled a pattern commonly observed for dissolved tracers.

4.2 Study 2: Assessing the Behavior of Microplastics in Fluvial Systems: Infiltration and Retention Dynamics in Streambed Sediments

In this study, five pulse-injection experiments were conducted to analyze the factors controlling the dynamics of MPs infiltration and retention in a rippled streambed. MPs transport was monitored using the novel techniques described in study 1, which involved tracking surface flow concentrations at the inflow and outflow of the study domain using fluorometers as well as monitoring infiltration at a specific bedform using the FIS. The experiments systematically varied three key parameters: (i) MPs size, with particles of 1, 3 and 10 µm diameter; (ii) streambed grain size, employing coarse and fine sediments with mean grain sizes of 1.0 mm and 0.4 mm, respectively; and (iii) hydrodynamic conditions, alternating between low-flow and high-flow regimes with mean surface flow velocities in the study domain between 0.06 m/s and 0.11 m/s.

The experiment conducted under high-flow conditions exhibited the highest and fastest peak in MPs surface water concentration at the outflow location. Across all experiments with coarse sediments, the breakthrough curves displayed a delayed decrease in MPs concentration at longer times, with the experiment with 3 µm MPs showing an additional secondary increase in concentration. Notably, the experiment conducted with fine sediment displayed multiple secondary peaks. These observations suggest that the transport of MPs was not controlled by advection and dispersion alone, but also involved particle infiltration into, retardation in, and release from the streambed. In the fine sediment experiment, approximately 22 % of MPs remained in the study domain until the end of the experiment (after 1800 s), indicating significant retardation effects at the streambed interface or in the streambed sediments.
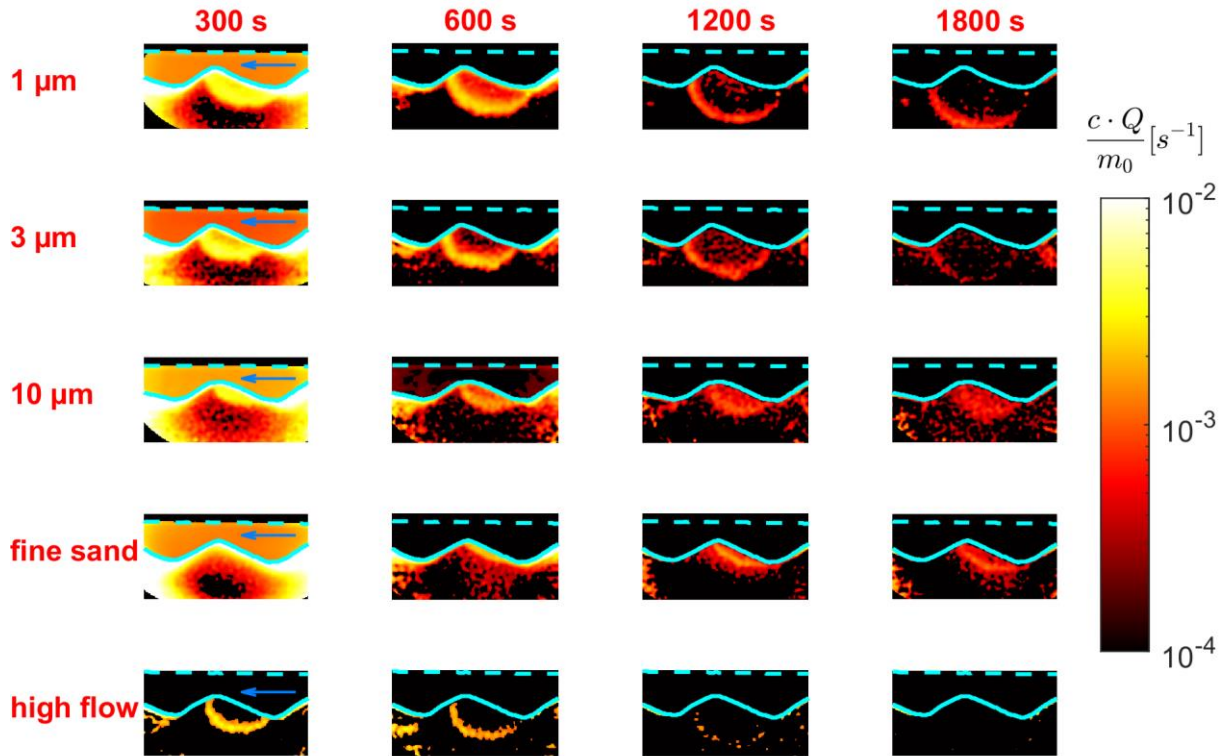
Figure 2: Microplastic infiltration into the streambed, monitored with the Fluorescence-Imaging-System. Four snapshots of planar microplastic concentration fields (as mass transfer rates) are shown for five different experiments, varying particle diameter, sediment grain size and flow conditions. The reference for all experiments was the experiment with 1 µm beads, coarse sediment and low flow conditions (first row). For the other experiments, one characteristic was systematically changed. The air-water interface is shown as a dashed line in cyan, the streambed-water interface as a solid line in cyan. The main surface flow is from right to left (blue arrow). This figure is included as Figure 4 in Study 2.

MPs transport at the selected bedform showed a consistent pattern of particle infiltration at the upstream stoss side of the bedform structure and release at the downstream lee side (Figure 2). This pattern aligned with both the measured surface flow conditions and simulated subsurface flow conditions. In the experiments with coarse sediment, the penetration depth of particles varied depending on their size. Specifically, the 1 µm particles exhibited the deepest infiltration with 11 cm, followed by the 3 µm particles with 10 cm and the 10 µm particles with 7 cm. In contrast, the fine sediment experiment with 1 µm MPs displayed the shallowest infiltration of 5 cm, suggesting that MPs retardation caused by interactions with the streambed sediment played a significant role. Interestingly, the particle-to-sediment grain size ratio could not solely account for the substantial difference in infiltration depth observed between the coarse sediment experiment with 3 µm MPs (ratio of 0.0029) and the fine sediment experiment with 1 µm MPs (ratio of 0.0028). Despite having similar ratios, infiltration depth decreased from 10 cm to 5 cm in the fine sediment experiment. The vertical propagation velocity in the streambed decreased

exponentially with depth and this decrease was more pronounced for larger particles. In the high-flow experiment, no particles were detected at the end of the experiment (Figure 2), indicating that streambeds can be effectively flushed from MPs even if the bedform remains stable. However, in all other experiments, particles remained in the streambed until the end of the experiment indicating retardation in the porous medium. Furthermore, the FIS monitoring allowed for the individual detection of 10 µm MPs. After approximately 1500 s, the center of mass of all infiltrated particles and the plume front changed only slightly, indicating MPs retention in the streambed. Towards the end of the experiment (1800 s), a constant number of approximately 300 particles was detected in the bedform. This finding suggested that particle transport in the streambed was not solely controlled by advective and dispersive processes, but that retention or retardation mechanisms, such as physical straining and interactions between particles and the streambed sediments played a significant role.

In summary, this study investigated the effects of particle size, streambed characteristics and hydrodynamic flow conditions on the complex transport and retention dynamics of MPs in a fluvial model environment. Building upon the findings of study 1, this work suggests that MPs are highly mobile in rivers and streams, and advective pumping plays a significant role in the transfer of MPs between surface water and the streambed. Particles exhibited prolonged residence times in fine sediments and the largest, 10 µm particles were partially retained in the streambed.

4.3 Study 3: Integrated Numerical Modelling to Quantify Transport and Fate of Microplastics in the Hyporheic Zone

In this study, a hybrid modeling approach was employed to investigate the transfer of MPs between surface water and the streambed in riverine systems. An integrated, three-dimensional hydro-numerical model was developed in openFOAM, which was calibrated using experimental data obtained from laboratory experiments like those conducted in study 2. The experiments analyzed the transport of 1 µm and 10 µm MPs through a flume environment with a rippled streambed composed of sediments with a grainsize 1.0 mm, under a mean surface flow velocity of 0.06 m/s.

The comparison between the physical and numerical experiments indicated a close match in water elevations and flow velocities. In the laboratory experiments, a recirculation area was observed in the lee of the ripple crest, and this characteristic was accurately represented in the numerical model with a permeable streambed. However, when an impermeable streambed was simulated, the surface flow did not exhibit backward-facing eddies, highlighting the importance

of an integrated model to accurately represent the hydrodynamics of the flow field. The simulations indicated the development of hyporheic flow, which directed water from the upstream stoss side of the bedform into deeper layers of the streambed sediments and back into the surface flow at the downstream lee side. Hyporheic flow cells were primarily confined to single ripples, and an additional underflow was observed which was attributed to the inclination of the flume.

The simulated infiltration pattern of MPs in the streambed sediments and the arrival times of peak concentrations within the first 7 cm below the ripple crest closely matched the laboratory results. The numerical model indicated that after 500 s, more MPs were present in the streambed sediments than in the water surface compartment. Subsequently, MPs were released from the streambed, leading to a gradual decrease of MPs in the system over the duration of the experiment. Both models suggested that most MPs were transported in the surface water, as indicated by higher MPs concentrations and flow velocities. Furthermore, the numerical model demonstrated that MPs infiltration patterns varied longitudinally from bedform to bedform, and laterally between the glass-interface (where the laboratory data were acquired) and the flume centerline. These findings indicated the significance of small-scale velocity distribution on particle transport dynamics.

The numerical model closely represented the transport of 1 µm MPs, where an advection-dispersion-model for particle transport was used. However, for the 10 µm particles, propagation in the streambed sediments was reduced, indicating particle retardation. Using a single advective retardation factor was not sufficient to closely match the experimentally observed peak arrival times at various depths below the surface. The retardation of particles was not constant, but rather increased with flow length and in deeper regions of the streambed, suggesting particle retention in the streambed sediments.

The integrated modelling approach indicated that the transfer of MPs into the streambed was driven by advective pumping and particle release from the streambed was the main source of MPs in the later stages of the experiment. Retention of 1 µm MPs in the streambed was negligible. However, the larger 10 µm MPs exhibited retardation in the streambed, which increased with flow path length, indicating particle retention. This suggested the involvement of additional physicochemical processes that contribute to the (temporary) immobilization of particles, which were not represented in the numerical modeling approach.

4.4 Study 4: Quantifying microplastic residence times in lakes using mesocosm experiments and transport modelling.

Study 4 aimed to investigate the vertical transport behavior of MPs in a low-flow environment within a lake mesocosm, combining laboratory experiments, field measurements and numerical models. The sinking velocities were determined using Stokes' law for the smallest, 1-5 µm MPs and measured with Particle-Image-Velocimetry in the laboratory for the bigger, 28-48 µm and 53-63 µm MPs. Sinking velocities were additionally derived from particle breakthrough curves in the lake mesocosm. Furthermore, the study assessed particle residence time in the lake by comparing the measured data with the results of a 1D random walk model.

Consistent with theoretical predictions, the settling behavior of MPs was strongly influenced by particle size, with smaller particles exhibiting lower settling velocities and consequently longer residence times in the water column. The measured particle residence time closely matched the model results for the 28-48 µm and 53-63 µm MPs. However, the model overestimated the actual residence time in the lake for the smaller, 1-5 µm MPs by a factor of 10. This suggested the contribution of additional factors, such as physicochemical or biotic interactions, which accelerated the deposition of small MPs in the in-lake mesocosm. Given longer residence times in the lake, these particles were more likely to interact with other water constituents. In addition, the relative impact of surface aggregation increases for small particles which exhibit a high surface-to-volume ratio.

The influence of hydrodynamics on particle transport was studied by comparing the transport of 1-5 µm MPs between summer (thermal stratification) and autumn conditions (lake turnover). During lake turnover, particle residence time in the lake decreased by a factor of 12, indicating rapid transport to the sediments. This effect was associated with increased vertical transport velocities due to the influence of turbulent convective mixing, which increased the probability of aggregation phenomena by resuspending material from the sediments. However, the absence of MPs resuspension in the experiment indicated an efficient immobilization of MPs in the lake.

In this study, MPs transport was examined in a near-to-nature system. The settling velocity in the lake aligned with theoretical expectations and laboratory experiments, increasing with particle size. However, small MPs (1-5 µm) exhibited shorter residence times in the lake than anticipated. Lake turnover, characterized by turbulent convective mixing, accelerated particle transport. These findings highlight the importance of lake hydrodynamics and additional mechanisms, such as physicochemical aggregation and biological interactions, for small MPs with high surface-to-volume ratios.

4.5 Study 5: Filter feeders are key to small microplastic residence times in stratified lakes: A virtual experiment

In study 5, the influence of biological interactions on particle transport in lake systems was investigated. Laboratory measurements and numerical simulations were employed to compare particle residence times in two lake models: a purely physical model driven by turbulent mixing and particle settling, and a physico-biological model that additionally considered the ingestion, storage and egestion of MPs in the form of faecal pellets by filter feeders, specifically *Daphnia*.

In the abiotic system, small MPs with sizes below 5 µm exhibited low settling velocities. When MPs were embedded in faecal pellets, their settling velocities increased significantly by 3 to 5 orders of magnitude. The pellets exhibited a settling velocity of approximately 1 mm/s, regardless of the size of the incorporated particle. This accelerated transport resulted in a decrease in particle residence time from over 15 years for small MPs (< 5 µm) in the purely physical model to approximately 1 year in the biotic model. Considering a water residence time of 4 years in lake Constance, particle immobilization by deposition to the bed was controlled by biotic interactions. The model also indicated that most small MPs passed through the organisms. The biological pathway played a dominant role in controlling particle transport for MPs smaller than 5 µm. For larger particles (15 µm), both biological and physical pathways had comparable importance. Furthermore, the significance of biological interactions on particle transport varied with the population size of *Daphnia*, indicating a seasonal variation of the transport pattern that can be expected in natural lake systems.

Through virtual experiments, this study demonstrated the significant influence of biotic interactions on the transport of MPs in lakes. Filter-feeding organisms, such as *Daphnia*, played a crucial role by incorporating, storing and subsequently releasing MPs through faecal pellets. This biological process significantly increased particle settling velocity and allowed particles to settle to the sediment instead of being carried away during lake flushing. Biotic interactions were particularly notable for smaller particles and increased with *Daphnia* population.

4.6 Study 6: In-depth characterization revealed polymer type and chemical content specific effects of microplastic on *Dreissena bugensis*

In study 6, the influence of MPs polymer type and chemical composition on a benthic filter feeder (*Dreissena bugensis*) was investigated. The mussels were exposed to MPs in a glass aquarium where a circular water flow was generated by a submersible pump. The impact of MPs on the organism was addressed by monitoring filtration activity and biochemical markers, such as enzyme activity and proteomic alterations.

Measurements of the flow velocities at the locations, where the mussels were positioned, indicated friction velocities between 9 – 16 mm/s The critical threshold for particle erosion was calculated as 9 mm/s for the heaviest (mussel fragments) and 3 mm/s for the lightest particles (polystyrene). This suggested that all particles were transported as suspended load during the experiment, ensuring a comparable exposure of the mussels to the different particle types.

The filtration behavior of the mussels was not affected by exposure to MPs or natural particulate matter, in contrast to exposure to dissolved contaminants, which cause mussels to cease filtration. Accordingly, fluorescence microscopy analysis confirmed the presence of MPs in the digestive tract of the mussels. However, exposure to MPs resulted in increased stress levels in the mussels, as indicated by biochemical markers. The magnitude of the effect depended on the type of polymer, and highest adverse effects were found for recycled PET fragments. The increase in stress was attributed to the presence of additional chemicals, such as additives or residual monomers, which could leach into the mussel's digestive tract after ingestion.

In summary, this study demonstrated that aquatic organisms inhabiting the streambed of rivers and lakes can incorporate MPs, resulting in adverse effects that vary based on the chemical composition of MPs. Mussels were able to filter MPs from the predominantly horizontal flow pattern in the water column. However, it is important to consider that in natural riverine systems, hyporheic exchange can lead to an additional vertical flow component, potentially increasing the exposure of organisms to MPs at the streambed.

5 Conclusion

Despite the ubiquitous presence of MPs in aquatic environments, there is still a lack of comprehensive knowledge regarding the specific mechanisms that control MPs transport. This thesis aimed to enhance the mechanistical understanding of the fundamental processes that govern the dynamics of MPs transport and retention in rivers, streams and lakes.

5.1 Main findings on microplastic transport mechanisms

MPs transport in riverine systems was studied using an experimental flume with a rippled streambed, where MPs were introduced to the surface water in a pulse injection. Although most MPs was quickly transported downstream in the surface water, studies 1-3 indicated that small, (sub-)pore-scale MPs (1-10 µm) were advectively transferred between surface water and the streambed. Transport patterns in the hyporheic zone resembled the infiltration of a dissolved solute, with particles being transferred across the streambed interface at the upstream stoss side of the bedform, transported through the streambed and released at the downstream lee side. Since turbulent hydrodynamic forces inhibit the deposition of small MPs on the streambed (Drummond et al., 2020), the results clearly indicated that hyporheic exchange is a crucial transport mechanism responsible for transferring small MPs into streambed sediments. The streambed acts as a retardation zone for MPs and displays spatial variability in terms of infiltration and release areas. In addition, temporal variations in the role of the streambed were observed, transitioning from a temporary sink for MPs to a secondary source. Following the passage of the initial contamination plume in the surface flow, MPs release from the streambed became the primary source of MPs in the surface water (study 3). These findings highlight that rivers and streams play a significant role not only as conduits for MPs transport from terrestrial sources to the sea, but also as influential factors on MPs retention and transport dynamics.

Particle size played a significant role in MPs transport dynamics. Smaller particles exhibited lower settling velocities in the surface flow (study 4). Furthermore, particle mobility and infiltration depth in the streambed increased for smaller particles (1 µm MPs), while larger, 10 µm MPs infiltrated into shallower regions of the streambed (studies 2-3). Individual particle tracking (study 2) and numerical modeling (study 3) indicated that 10 µm particles experienced prolonged retardation in the streambed, which increased with flow path length (study 3). However, the duration of the flume experiments was insufficient to confirm permanent particle retention in the streambed. The grain size of the streambed also influenced MPs infiltration, with fine sediments limiting infiltration to shallower regions and retarding a high fraction of MPs until the end of the experiment (study 2). This behavior could not be solely explained by the ratio

between particle and sediment grain size, which deviated from previous findings in column experiments (Waldschläger and Schüttrumpf, 2020). These results highlight the complexity of MPs transport in three-dimensional flows within fluvial systems, connecting surface water and the hyporheic zone.

The hydrodynamic characteristics of the flow exerted an important influence on particle transport and infiltration. The numerical model showed that particle infiltration patterns varied longitudinally from bedform to bedform and laterally within bedforms (study 3). This indicated the influence of small-scale velocity distributions in the surface water, since transfer was governed by advective pumping, transferring particles between the surface water and the streambed. Higher surface flow velocities led to faster particle breakthrough in both surface water and the streambed (study 2). Although bedforms remained stable in all experiments, increased flow conditions resulted in efficient particle flushing from the bedform: Unlike in the low-flow experiments, no particles were detected within the streambed sediments at the end of the experiment. Particle settling behavior in the lake field experiment also depended on flow hydrodynamics, with convective mixing in the water column reducing the residence time of MPs in lakes (study 4).

In natural environments, MPs transport patterns may differ significantly from results of laboratory studies. Despite the typical resuspension of particles during lake turnover (Evans, 1994), this effect was not observed for MPs in study 4, suggesting particle immobilization in the lake. Furthermore, the residence time of small MPs in lakes was much shorter than expected, indicating rapid sedimentation. Based on physical settling processes alone, MPs deposition was not anticipated as the residence time exceeded the flushing time of the lake (study 5). These findings emphasize the complex transport behavior of MPs in rivers, streams and lakes and suggest the involvement of additional mechanisms that modify transport behavior. Interactions with other suspended particles, solutes or biota, can enhance particle settling velocity and contribute to particle deposition to lake sediments.

Interactions between biota and MPs were investigated in studies 5 and 6. When MPs were ingested and egested by organisms, they became embedded in a biological matrix, significantly increasing particle settling velocity (study 5). In lakes, this biological pathway can play a crucial role in transporting small MPs from the surface to the sediments. This effect is particularly relevant for small MPs due to their longer residence times in the water column, which increases the likelihood of particle interaction. Additionally, the higher surface-to-volume ratio enhances the relative impact of surface aggregation processes. The importance of biological interactions

depended on organism population, suggesting a seasonal variation in MPs transport (study 5). Similar effects can be expected for riverine environments, where benthic filter feeders such as mussels can ingest suspended MPs from the water column (study 6). Following egestion, particles may become immobilized due to increased settling velocity in the biological matrix and deposit near the organism (Cole et al., 2023), creating a sink of biologically altered MPs on the streambed. In addition, particle uptake by the organism can induce stress on the organism, with the severity depending on the polymer type (study 6). PET fragments exhibited the highest adverse effects, likely attributed to their specific chemical composition. Such sublethal effects may gradually increase at higher trophic levels and thereby affect ecosystem functions, indicating the risk associated with MPs exposure to aquatic organisms (Schwarzer et al., 2022).

5.2   Implications for natural fluvial environments

In natural rivers and streams, streambed sediments have been found to contain high abundances of pore-scale MPs smaller than 100 µm (Frei et al., 2019). Studies 1-3 demonstrated that MPs ranging from 1 to 10 µm can be advectively transferred from the surface water across the streambed interface, exhibiting high mobility in the streambed sediments. While the laboratory flume experiments primarily observed small-scale hyporheic exchange within individual bedforms, exchange in natural fluvial systems occurs at various spatial and temporal scales (Boano et al., 2014). Larger variations of the hydraulic head gradient, as caused by pool-riffle sequences (Frei et al., 2018), lead to the formation of deeper hyporheic flow cells, which have the potential to transfer highly mobile, small MPs into deeper regions of the streambed. This phenomenon is particularly pronounced during losing conditions, when stream water infiltrates into the aquifer, potentially allowing (sub-)pore-scale MPs to reach shallow groundwater as discussed by Frei et al. (2019). Conversely, seasonal variations in groundwater levels can result in gaining conditions, causing previously stored MPs to be released back into the stream water following the subsurface flow. These findings highlight that streambeds can serve as temporal sinks, conduits and sources for MPs.

Furthermore, the retardation of MPs in the streambed is influenced by flow conditions in the surface water (study 2). During baseflow conditions, MPs can be advectively transferred into the streambed. However, during increased discharges, even when the bedform remains stable, MPs can be effectively flushed from the top layers of the streambed sediments. These flushed MPs are subsequently released into the surface water and transported downstream as suspended load. The resuspension of MPs can become the main source of MPs in the surface flow, creating a time lag between the contamination event and the abundance of particles in the stream. This

suggests a legacy effect in natural systems, as particles can have prolonged residence times in the catchment (Drummond et al., 2022). Therefore, retention and release of MPs from the streambed depends on the temporal evolution of river discharge and may follow a seasonal pattern. During higher flow events followed by strong rainfalls or snowmelt, it is expected that MPs will be mobilized not only from the top layers, but also from deeper layers of the streambed. This can result in an increased concentration of MPs in the surface water (Ockelford et al., 2020). In addition to particle release caused by bedform erosion, the enhanced advective transfer of MPs out of the streambed is expected to contribute to the significant reduction (up to 70 %) of MPs loads detected in sediments after flooding events (Hurley et al., 2018).

MPs exhibited a prolonged retardation in the experiment with fine sand (study 2). Therefore, fine sediments can function as hotspots for MPs contamination, significantly retarding their transport through the sediment and limiting infiltration to shallower depths of the streambed. Since fine sediment loads have been continuously increasing due to catchment management and climate change (Burt et al., 2016; Owens et al., 2005), MPs immobilization in streambed sediments is projected to increase. This can lead to enhanced MPs residence times on the streambed interface and in shallow regions of the streambed and is particularly problematic for benthic organisms, which may become increasingly exposed to MPs. Benthic filter feeders play a critical role as primary entry points for MPs into the food webs of rivers and streams (Huang et al., 2021). Particle exposure to the organism causes adverse effects on the organism (study 6, compare Redondo-Hasselerharm et al. (2023)). This problem is further exacerbated by the fact that small MPs are particularly mobile in fluvial systems (studies 1-3) and can be easily incorporated by aquatic organisms (Cole et al., 2013).

In addition, studies 4 and 5 indicated that the transport of small MPs in low-flow environments, such as lakes, is strongly influenced by interactions with other water constituents. The storage of MPs in faecal pellets resulted in higher sedimentation rates to the streambed, increasing particle immobilization (study 5). Similar effects are anticipated to impact particle transport in rivers, both in surface flow and streambed sediments, where mussels can ingest and egest MPs (study 6). In natural rivers and streams, the interaction between particles and biota is additionally facilitated by hyporheic exchange, which transfers MPs from the surface water to the streambed interface, where benthic filter feeders reside. Compared to pristine MPs, the advective transfer of particles embedded in biological matrices may be hindered or limited due to the size of the aggregation matrix. Additionally, particle stickiness enhances the potential for further interactions on the streambed. These processes suggest a (temporal) sink for biologically altered MPs on the streambed.

5.3 Research outlook

This thesis integrated laboratory, field and numerical experiments to investigate the fundamental mechanisms governing the transport and retention of MPs in rivers, streams and lakes. While new insights into the complex behavior of MPs were gained, certain aspects remained unresolved due to experimental limitations and time constraints. Therefore, further research is needed to improve our understanding of the dynamics of MPs in aquatic environments.

Firstly, the laboratory experiments analyzing transport of MPs between the surface and the streambed focused on a specific subset of MPs with variable size (1-10 µm), but otherwise consistent properties such as low density (polystyrene, 1050 kg/m³), spherical shape and pristine surface characteristics. However, it is important to consider that small particles with different shape, such as fragments or fibers, may exhibit different transport and retention processes due to their higher interaction potential in porous media. Altered surface characteristics, such as surface charge, can cause physicochemical interactions between MPs and suspended particles in the surface water or the streambed sediments. The specific influence of these factors on MPs transport in fluvial systems with pronounced three-dimensional flow components remains unclear and requires further investigation. In addition, the transport behavior of larger and denser particles was not analyzed in the transport experiments. Due to higher settling velocities, these particles may exhibit different behavior in the surface water, such as a greater tendency to deposit on the streambed near the upstream regions of the flow rather than following water flow in the surface water. The increased size of the particles may additionally inhibit infiltration into the streambed sediments, resulting in preferential accumulation areas on the streambed.

Secondly, bedform structures in natural rivers and streams are highly mobile, since hydrodynamical conditions exhibit a large spatio-temporal variability. Fluctuations in stream flow may exceed the critical motion threshold, leading to the erosion of sediment at the upstream face of the bedform and deposition at the downstream face, causing the migration of bedform structures in the direction of streamflow. It is crucial for future research to investigate whether these highly dynamic, transient sedimentation and erosion cycles enhance the transfer of MPs into streambed sediments, and whether particles are preferentially stored in deeper regions of the streambed or remobilized back into the stream. High-flow events have been shown to cause preferential deposition of clay particles (< 2 µm) in the streambed sediments (Teitelbaum et al., 2021). It is possible that MPs exhibit similar behavior, and once transported into deeper layers, they may be less influenced by advective exchange and become immobilized in the streambed for extended periods, increasing the potential to interact with benthic organisms.

5 Conclusion

Thirdly, the influence of hyporheic exchange conditions requires further research. If the stream exhibits losing conditions, it is necessary to investigate how deep MPs can infiltrate into the hyporheic zone, and whether significant quantities of MPs can reach shallow groundwaters. Long-term experiments are needed to investigate particle mobility, in particular whether particles can infiltrate deeper into the sediment and potentially connect with other hyporheic flow cells or hyporheic underflow. In addition, the flume experiments could only indicate an increased retardation of small MPs in the streambed, suggesting particle retention for the bigger MPs in the streambed sediments. This conceptual shortcoming can be overcome with a pore-scale model of MPs transport in streambeds that specifically tracks the transport pathways of individual particles and analyzes the interactions between MPs and sediment grain surfaces.

Finally, future research is needed to investigate the existence and significance of preferential deposition areas for particles or particle aggregations in riverine systems, particularly in proximity to benthic filter feeders. The larger size of aggregated particles and the increased likelihood of interactions due to the stickiness of the biological matrix suggest that these particles may exhibit less infiltration into the streambed and have an extended residence time, increasingly affecting benthic communities. In addition, physicochemical interactions in the streambed, which are influenced by water chemistry and the properties of the porous medium, can play a crucial role in particle transport, as demonstrated in column experiments. However, it remains unclear whether larger-scale hyporheic exchange or small-scale physicochemical interactions in the streambed will dominate the transport behavior of small MPs in natural rivers and streambeds with complex three-dimensional flow characteristics.

In conclusion, the research findings have demonstrated that small MPs exhibit high mobility in aquatic systems. Both physical processes, such as advective transfer across the streambed interface, and biological mechanisms, including ingestion and egestion by filter feeders, play significant roles in determining the residence time of MPs in aquatic systems. These insights contribute to our mechanistic understanding of the fundamental transport and retention processes controlling the complex behavior of MPs in rivers, streams and lakes.

6 References

Ahmadi, P., Elagami, H., Dichgans, F., Schmidt, C., Gilfedder, B.S., Frei, S., Peiffer, S., Fleckenstein, J.H., 2022. Systematic Evaluation of Physical Parameters Affecting the Terminal Settling Velocity of Microplastic Particles in Lakes Using CFD. Front. Environ. Sci. 10. doi:10.3389/fenvs.2022.875220.

Allen, S., Allen, D., Phoenix, V.R., Le Roux, G., Durántez Jiménez, P., Simonneau, A., Binet, S., Galop, D., 2019. Atmospheric transport and deposition of microplastics in a remote mountain catchment. Nature Geosci. doi:10.1038/s41561-019-0335-5.

Anbumani, S., Kakkar, P., 2018. Ecotoxicological effects of microplastics on biota: a review. Environmental science and pollution research international 25 (15), 14373–14396. doi:10.1007/s11356-018-1999-x.

Baldwin, A.K., Corsi, S.R., Mason, S.A., 2016. Plastic Debris in 29 Great Lakes Tributaries: Relations to Watershed Attributes and Hydrology. Environmental science & technology 50 (19), 10377–10385. doi:10.1021/acs.est.6b02917.

Bank, M.S., Hansson, S.V., 2022. The Microplastic Cycle: An Introduction to a Complex Issue, in: Bank, M.S. (Ed.), Microplastic in the environment. Pattern and process. Environmental contamination remediation and management. Springer; University of Massachusetts, Institute of Marine Research, Cham, Switzerland, Amherst, pp. 1–16.

Bek, M.A., Lowndes, I.S., Hargreaves, D.M., Negm, A.M., 2019. Lakes and Their Hydrodynamics, in: Negm, A.M., Bek, M.A., Abdel-Fattah, S. (Eds.), Egyptian Coastal Lakes and Wetlands: Part I, vol. 71. The Handbook of Environmental Chemistry. Springer International Publishing, Cham, pp. 197–214.

Bhatt, V., Chauhan, J.S., 2023. Microplastic in freshwater ecosystem: bioaccumulation, trophic transfer, and biomagnification. Environmental science and pollution research international 30 (4), 9389–9400. doi:10.1007/s11356-022-24529-w.

Bigalke, M., Fieber, M., Foetisch, A., Reynes, J., Tollan, P., 2022. Microplastics in agricultural drainage water: A link between terrestrial and aquatic microplastic pollution. The Science of the total environment 806 (Pt 4), 150709. doi:10.1016/j.scitotenv.2021.150709.

Boano, F., Harvey, J.W., Marion, A., Packman, A.I., Revelli, R., Ridolfi, L., Wörman, A., 2014. Hyporheic flow and transport processes: Mechanisms, models, and biogeochemical implications. Rev. Geophys. 52 (4), 603–679. doi:10.1002/2012RG000417.

Burt, T., Boardman, J., Foster, I., Howden, N., 2016. More rain, less soil: long-term changes in rainfall intensity with climate change. Earth Surf. Process. Landforms 41 (4), 563–566. doi:10.1002/esp.3868.

6 References

Cole, M., Artioli, Y., Coppock, R., Galli, G., Saad, R., Torres, R., Vance, T., Yunnie, A., Lindeque, P.K., 2023. Mussel power: Scoping a nature-based solution to microplastic debris. Journal of Hazardous Materials 453, 131392. doi:10.1016/j.jhazmat.2023.131392.

Cole, M., Lindeque, P., Fileman, E., Halsband, C., Goodhead, R., Moger, J., Galloway, T.S., 2013. Microplastic ingestion by zooplankton. Environmental science & technology 47 (12), 6646–6655. doi:10.1021/es400663f.

D'Avignon, G., Gregory-Eaves, I., Ricciardi, A., 2022. Microplastics in lakes and rivers: an issue of emerging significance to limnology. Environ. Rev. 30 (2), 228–244. doi:10.1139/er-2021-0048.

Drummond, J.D., Nel, H.A., Packman, A.I., Krause, S., 2020. Significance of Hyporheic Exchange for Predicting Microplastic Fate in Rivers. Environ. Sci. Technol. Lett. 7 (10), 727–732. doi:10.1021/acs.estlett.0c00595.

Drummond, J.D., Schneidewind, U., Li, A., Hoellein, T.J., Krause, S., Packman, A.I., 2022. Microplastic accumulation in riverbed sediment via hyporheic exchange from headwaters to mainstems. Science advances 8 (2), eabi9305. doi:10.1126/sciadv.abi9305.

Dusaucy, J., Gateuille, D., Perrette, Y., Naffrechoux, E., 2021. Microplastic pollution of worldwide lakes. Environmental pollution (Barking, Essex : 1987) 284, 117075. doi:10.1016/j.envpol.2021.117075.

Elagami, H., Ahmadi, P., Fleckenstein, J.H., Frei, S., Obst, M., Agarwal, S., Gilfedder, B.S., 2022. Measurement of microplastic settling velocities and implications for residence times in thermally stratified lakes. Limnology & Oceanography 67 (4), 934–945. doi:10.1002/lno.12046.

Elliott, A.H., 1991. Transfer of solutes into and out of streambeds.

Elliott, A.H., Brooks, N.H., 1997. Transfer of nonsorbing solutes to a streambed with bed forms: Laboratory experiments 33 (1), 137–151. doi:10.1029/96WR02783.

Engelund, F., Fredsoe, J., 1982. Sediment Ripples and Dunes. Annu. Rev. Fluid Mech. 14 (1), 13–37. doi:10.1146/annurev.fl.14.010182.000305.

Evans, R.D., 1994. Empirical evidence of the importance of sediment resuspension in lakes. Hydrobiologia 284 (1), 5–12. doi:10.1007/BF00005727.

Fazey, F.M.C., Ryan, P.G., 2016. Biofouling on buoyant marine plastics: An experimental study into the effect of size on surface longevity. Environmental pollution (Barking, Essex : 1987) 210, 354–360. doi:10.1016/j.envpol.2016.01.026.

Fox, A., Boano, F., Arnon, S., 2014. Impact of losing and gaining streamflow conditions on hyporheic exchange fluxes induced by dune-shaped bed forms. Water Resour. Res. 50 (3), 1895–1907. doi:10.1002/2013WR014668.

Frank, Y.A., Vorobiev, D.S., Vorobiev, E.D., Samarinova, A.A., Antsiferov, D.V., Strezov, V., 2023. Ability of benthic oligochaetes to bury microplastics in aquatic bottom sediments. The Science of the total environment 857 (Pt 3), 159687. doi:10.1016/j.scitotenv.2022.159687.

Frei, S., Azizian, M., Grant, S.B., Zlotnik, V.A., Toundykov, D., 2018. Analytical modeling of hyporheic flow for in-stream bedforms_ Perturbation method and implementation. Environmental Modelling & Software (111), 375–385. doi:10.1016/j.envsoft.2018.09.015.

Frei, S., Piehl, S., Gilfedder, B.S., Löder, M.G.J., Krutzke, J., Wilhelm, L., Laforsch, C., 2019. Occurence of microplastics in the hyporheic zone of rivers. Scientific reports 9 (1), 15256. doi:10.1038/s41598-019-51741-5.

Frias, J.P.G.L., Nash, R., 2019. Microplastics: Finding a consensus on the definition. Marine pollution bulletin 138, 145–147. doi:10.1016/j.marpolbul.2018.11.022.

Funk, W., Dammann, V., Vonderheid, C., Oehlmann, G. (Eds.), 1985. Statistische Methoden in der Wasseranalytik: Begriffe, Strategien, Anwendungen. VCH, Weinheim.

Gomez-Velez, J.D., Harvey, J.W., Cardenas, M.B., Kiel, B., 2015. Denitrification in the Mississippi River network controlled by flow through river bedforms. Nature Geosci 8 (12), 941–945. doi:10.1038/ngeo2567.

Gündoğdu, S., Çevik, C., Ayat, B., Aydoğan, B., Karaca, S., 2018. How microplastics quantities increase with flood events? An example from Mersin Bay NE Levantine coast of Turkey. Environmental pollution (Barking, Essex : 1987) 239, 342–350. doi:10.1016/j.envpol.2018.04.042.

Harvey, J.W., Drummond, J.D., Martin, R.L., McPhillips, L.E., Packman, A.I., Jerolmack, D.J., Stonedahl, S.H., Aubeneau, A.F., Sawyer, A., Larsen, L.G., Tobias, C.R., 2012. Hydrogeomorphology of the hyporheic zone: Stream solute and fine particle interactions with a dynamic streambed. J. Geophys. Res. 117 (G4). doi:10.1029/2012JG002043.

Hoellein, T.J., Rovegno, C., Uhrin, A.V., Johnson, E., Herring, C., 2021. Microplastics in Invasive Freshwater Mussels (Dreissena sp.): Spatiotemporal Variation and Occurrence With Chemical Contaminants. Front. Mar. Sci. 8. doi:10.3389/fmars.2021.690401.

Huang, W., Song, B., Liang, J., Niu, Q., Zeng, G., Shen, M., Deng, J., Luo, Y., Wen, X., Zhang, Y., 2021. Microplastics and associated contaminants in the aquatic environment: A review

6 References

on their ecotoxicological effects, trophic transfer, and potential impacts to human health. Journal of Hazardous Materials 405, 124187. doi:10.1016/j.jhazmat.2020.124187.

Hüffer, T., Praetorius, A., Wagner, S., Kammer, F. von der, Hofmann, T., 2017. Microplastic Exposure Assessment in Aquatic Environments: Learning from Similarities and Differences to Engineered Nanoparticles. Environmental science & technology 51 (5), 2499–2507. doi:10.1021/acs.est.6b04054.

Hurley, R., Woodward, J., Rothwell, J.J., 2018. Microplastic contamination of river beds significantly reduced by catchment-wide flooding. Nature Geosci 11 (4), 251–257. doi:10.1038/s41561-018-0080-1.

Imhof, H.K., Rusek, J., Thiel, M., Wolinska, J., Laforsch, C., 2017. Do microplastic particles affect Daphnia magna at the morphological, life history and molecular level? PloS one 12 (11), e0187590. doi:10.1371/journal.pone.0187590.

Klein, S., Dimzon, I.K., Eubeler, J., Knepper, T.P., 2017. Analysis, Occurrence, and Degradation of Microplastics in the Aqueous Environment. Springer International Publishing 58, 51–67. doi:10.1007/978-3-319-61615-5_3, 51-67.

Koelmans, B., Pahl, S., Backhaus, T., Bessa, F., van Calster, G., Contzen, N., Cronin, R., Galloway, T., Hart, A., Henderson, L., Kalčíková, G., Kelly, F., Kolodziejczyk, Marku, E., Poortinga, W., Rillig, M., van Sebille, E., Steg, L., Steidl, J., Steinhorst, J., Syberg, K., Thompson, R., Wagner, M., van Wezel, A., Wyles, K., Wright, S.L., 2019. A scientific perspective on microplastics in nature and society. Evidence review report no. 4. SAPEA, Berlin.

Lebreton, L., Andrady, A., 2019. Future scenarios of global plastic waste generation and disposal. Palgrave Commun 5 (1). doi:10.1057/s41599-018-0212-7.

Lewandowski, J., Arnon, S., Banks, E., Batelaan, O., Betterle, A., Broecker, T., Coll, C., Drummond, J.D., Gaona Garcia, J., Galloway, J., Gomez-Velez, J., Grabowski, R., Herzog, S., Hinkelmann, R., Höhne, A., Hollender, J., Horn, M., Jaeger, A., Krause, S., Löchner Prats, A., Magliozzi, C., Meinikmann, K., Mojarrad, B., Mueller, B., Peralta-Maraver, I., Popp, A., Posselt, M., Putschew, A., Radke, M., Raza, M., Riml, J., Robertson, A., Rutere, C., Schaper, J., Schirmer, M., Schulz, H., Shanafield, M., Singh, T., Ward, A., Wolke, P., Wörman, A., Wu, L., 2019. Is the Hyporheic Zone Relevant beyond the Scientific Community? Water 11 (11), 2230. doi:10.3390/w11112230.

Lu, T., Gilfedder, B.S., Peng, H., Niu, G., Frei, S., 2021a. Effects of clay minerals on the transport of nanoplastics through water-saturated porous media. The Science of the total environment 796, 148982. doi:10.1016/j.scitotenv.2021.148982.

Lu, T., Gilfedder, B.S., Peng, H., Peiffer, S., Papastavrou, G., Ottermann, K., Frei, S., 2021b. Relevance of Iron Oxyhydroxide and Pore Water Chemistry on the Mobility of Nanoplastic Particles in Water-Saturated Porous Media Environments. Water Air Soil Pollut 232 (5). doi:10.1007/s11270-021-05125-z.

Mani, T., Hauk, A., Walter, U., Burkhardt-Holm, P., 2015. Microplastics profile along the Rhine River. Scientific reports 5, 17988. doi:10.1038/srep17988.

Mintenig, S.M., Int-Veen, I., Löder, M.G.J., Primpke, S., Gerdts, G., 2017. Identification of microplastic in effluents of waste water treatment plants using focal plane array-based micro-Fourier-transform infrared imaging. Water research 108, 365–372. doi:10.1016/j.watres.2016.11.015.

Mintenig, S.M., Kooi, M., Erich, M.W., Primpke, S., Redondo-Hasselerharm, P.E., Dekker, S.C., Koelmans, A.A., van Wezel, A.P., 2020. A systems approach to understand microplastic occurrence and variability in Dutch riverine surface waters. Water research 176, 115723. doi:10.1016/j.watres.2020.115723.

Ockelford, A., Cundy, A., Ebdon, J.E., 2020. Storm Response of Fluvial Sedimentary Microplastics. Scientific reports 10 (1), 1865. doi:10.1038/s41598-020-58765-2.

Owens, P.N., Batalla, R.J., Collins, A.J., Gomez, B., Hicks, D.M., Horowitz, A.J., Kondolf, G.M., Marden, M., Page, M.J., Peacock, D.H., Petticrew, E.L., Salomons, W., Trustrum, N.A., 2005. Fine-grained sediment in river systems: environmental significance and management issues. River Res. Applic. 21 (7), 693–717. doi:10.1002/rra.878.

Padervand, M., Lichtfouse, E., Robert, D., Wang, C., 2020. Removal of microplastics from the environment. A review. Environ Chem Lett 18 (3), 807–828. doi:10.1007/s10311-020-00983-1.

Persson, L., Carney Almroth, B.M., Collins, C.D., Cornell, S., Wit, C.A. de, Diamond, M.L., Fantke, P., Hassellöv, M., MacLeod, M., Ryberg, M.W., Søgaard Jørgensen, P., Villarrubia-Gómez, P., Wang, Z., Hauschild, M.Z., 2022. Outside the Safe Operating Space of the Planetary Boundary for Novel Entities. Environmental science & technology 56 (3), 1510–1521. doi:10.1021/acs.est.1c04158.

Pivokonsky, M., Cermakova, L., Novotna, K., Peer, P., Cajthaml, T., Janda, V., 2018. Occurrence of microplastics in raw and treated drinking water. The Science of the total environment 643, 1644–1651. doi:10.1016/j.scitotenv.2018.08.102.

PlasticsEurope, 2022. Plastics - the Facts 2022.

6 References

Redondo-Hasselerharm, P.E., Rico, A., Koelmans, A.A., 2023. Risk assessment of microplastics in freshwater sediments guided by strict quality criteria and data alignment methods. Journal of Hazardous Materials 441, 129814. doi:10.1016/j.jhazmat.2022.129814.

Rummel, C.D., Jahnke, A., Gorokhova, E., Kühnel, D., Schmitt-Jansen, M., 2017. Impacts of Biofilm Formation on the Fate and Potential Effects of Microplastic in the Aquatic Environment. Environ. Sci. Technol. Lett. 4 (7), 258–267. doi:10.1021/acs.estlett.7b00164.

Saenger, N., 2000. Identifikation von Austauschprozessen zwischen Fließgewässer und hyporheischer Zone 115.

Scherer, C., Weber, A., Lambert, S., Wagner, M., 2018. Interactions of Microplastics with Freshwater Biota, in: Wagner, M., Lambert, S. (Eds.), Freshwater Microplastics, vol. 58. The Handbook of Environmental Chemistry. Springer International Publishing, Cham, pp. 153–180.

Schmidt, C., Krauth, T., Wagner, S., 2017. Export of Plastic Debris by Rivers into the Sea. Environmental science & technology 51 (21), 12246–12253. doi:10.1021/acs.est.7b02368.

Schmidtmann, J., Elagami, H., Gilfedder, B.S., Fleckenstein, J.H., Papastavrou, G., Mansfeld, U., Peiffer, S., 2022. Heteroaggregation of PS microplastic with ferrihydrite leads to rapid removal of microplastic particles from the water column. Environmental science. Processes & impacts 24 (10), 1782–1789. doi:10.1039/d2em00207h.

Schwarz, A.E., Ligthart, T.N., Boukris, E., van Harmelen, T., 2019. Sources, transport, and accumulation of different types of plastic litter in aquatic environments: A review study. Marine pollution bulletin 143, 92–100. doi:10.1016/j.marpolbul.2019.04.029.

Schwarzer, M., Brehm, J., Vollmer, M., Jasinski, J., Xu, C., Zainuddin, S., Fröhlich, T., Schott, M., Greiner, A., Scheibel, T., Laforsch, C., 2022. Shape, size, and polymer dependent effects of microplastics on Daphnia magna. Journal of Hazardous Materials 426, 128136. doi:10.1016/j.jhazmat.2021.128136.

Shahul Hamid, F., Bhatti, M.S., Anuar, N., Anuar, N., Mohan, P., Periathamby, A., 2018. Worldwide distribution and abundance of microplastic: How dire is the situation? Waste management & research 36 (10), 873–897. doi:10.1177/0734242X18785730.

Storey, R.G., Howard, K.W.F., Williams, D.D., 2003. Factors controlling riffle-scale hyporheic exchange flows and their seasonal changes in a gaining stream: A three-dimensional groundwater flow model. Water Resour. Res. 39 (2). doi:10.1029/2002WR001367.

Teitelbaum, Y., Dallmann, J., Phillips, C.B., Packman, A.I., Schumer, R., Sund, N.L., Hansen, S.K., Arnon, S., 2021. Dynamics of Hyporheic Exchange Flux and Fine Particle Deposition Under Moving Bedforms. Water Resources Research 57 (4). doi:10.1029/2020WR028541.

Tibbetts, J., Krause, S., Lynch, I., Sambrook Smith, G., 2018. Abundance, Distribution, and Drivers of Microplastic Contamination in Urban River Environments. Water 10 (11), 1597. doi:10.3390/w10111597.

United Nations, 2015. Transforming our World: The 2030 Agenda for Sustainable Development: A/RES/70/1.

Waldschläger, K., Brückner, M.Z., Carney Almroth, B., Hackney, C.R., Adyel, T.M., Alimi, O.S., Belontz, S.L., Cowger, W., Doyle, D., Gray, A., Kane, I., Kooi, M., Kramer, M., Lechthaler, S., Michie, L., Nordam, T., Pohl, F., Russell, C., Thit, A., Umar, W., Valero, D., Varrani, A., Warrier, A.K., Woodall, L.C., Wu, N., 2022. Learning from natural sediments to tackle microplastics challenges: A multidisciplinary perspective. Earth-Science Reviews 228, 104021. doi:10.1016/j.earscirev.2022.104021.

Waldschläger, K., Schüttrumpf, H., 2019a. Effects of Particle Properties on the Settling and Rise Velocities of Microplastics in Freshwater under Laboratory Conditions. Environmental science & technology 53 (4), 1958–1966. doi:10.1021/acs.est.8b06794.

Waldschläger, K., Schüttrumpf, H., 2019b. Erosion Behavior of Different Microplastic Particles in Comparison to Natural Sediments. Environmental science & technology 53 (22), 13219–13227. doi:10.1021/acs.est.9b05394.

Waldschläger, K., Schüttrumpf, H., 2020. Infiltration Behavior of Microplastic Particles with Different Densities, Sizes, and Shapes-From Glass Spheres to Natural Sediments. Environmental science & technology 54 (15), 9366–9373. doi:10.1021/acs.est.0c01722.

Watkins, L., McGrattan, S., Sullivan, P.J., Walter, M.T., 2019. The effect of dams on river transport of microplastic pollution. The Science of the total environment 664, 834–840. doi:10.1016/j.scitotenv.2019.02.028.

Weyhenmeyer, G.A., Håkanson, L., Meili, M., 1997. A validated model for daily variations in the flux, origin, and distribution of settling particles within lakes. Limnology & Oceanography 42 (7), 1517–1529. doi:10.4319/lo.1997.42.7.1517.

Woodall, L.C., Sanchez-Vidal, A., Canals, M., Paterson, G.L.J., Coppock, R., Sleight, V., Calafat, A., Rogers, A.D., Narayanaswamy, B.E., Thompson, R.C., 2014. The deep sea is a major sink for microplastic debris. Royal Society open science 1 (4), 140317. doi:10.1098/rsos.140317.

Woodward, J., Li, J., Rothwell, J., Hurley, R., 2021. Acute riverine microplastic contamination due to avoidable releases of untreated wastewater. Nat Sustain 4 (9), 793–802. doi:10.1038/s41893-021-00718-2.

6 References

7 Publications and manuscripts

Contribution statement

Study 1: Tracking Microplastics Across the Streambed Interface: Using Laser-Induced-Fluorescence to Quantitatively Analyze Microplastic Transport in an Experimental Flume

Status: Published in *Water Resources Research*, Volume 57, Issue 12, first published online: 03 December 2021, https://doi.org/10.1029/2021WR031064

Authors: **Jan-Pascal Boos**, Benjamin-Silas Gilfedder, Sven Frei

Own contribution: Study design 80 %, data collection 100 %, data processing and analysis 100 %, interpretation of the results 80 %, preparation of the manuscript 80 %

Author contribution: **JPB developed the laboratory setup and designed the study, performed all experiments, wrote the software to analyze the data, interpreted the results and prepared the manuscript.** BSG conceived the project, assisted in study design, interpretation of the results and revised the manuscript. SF conceived and supervised the project, designed the study, interpreted the results and helped by reviewing and editing of the manuscript. **JPB is the corresponding author.**

Study 2: Assessing the Behavior of Microplastics in Fluvial Systems: Infiltration and Retention Dynamics in Streambed Sediments

Status: Published in *Water Resources Research*, Volume 60, Issue 2, first published online: 23 February 2024, https://doi.org/10.1029/2023WR035532

Authors: **Jan-Pascal Boos**, Franz Dichgans, Jan H. Fleckenstein, Benjamin-Silas Gilfedder, Sven Frei

Own contribution: Study design 90 %, data collection 90 %, data processing and analysis 90 %, interpretation of the results 80%, preparation of the manuscript 80 %

Author contribution: **JPB developed the laboratory setup and designed the study, collected data, wrote the software for data processing, interpreted the results, and prepared the manuscript.** FD built the numerical model, analyzed its data and helped during the review of the manuscript. JHF conceived the project, assisted with the numerical model, and reviewed the manuscript. BSG conceived the project and reviewed the manuscript. SF conceived and supervised the project, assisted in the study design, interpreted the results, and reviewed and edited the manuscript. **JPB is the corresponding author.**

Study 3: Integrated Numerical Modelling to Quantify Transport and Fate of Microplastics in the Hyporheic Zone

Status: Published in Water Research, Volume 243, 1 September 2023, 120349, https://doi.org/10.1016/j.watres.2023.120349

Authors: Franz Dichgans, **Jan-Pascal Boos**, Pouyan Ahmadi, Sven Frei, Jan H. Fleckenstein

Own contribution: Study design 30 %, data collection 50 %, data processing and analysis 40 %, interpretation of the results 20 %, preparation of the manuscript 10 %

Author contribution: FD co-developed the research idea, developed the numerical modeling setup, assisted with the flume experiment setup, carried out the numerical modeling and validation, processed, analyzed and interpreted the numerical and laboratory datasets, and wrote the initial draft of the manuscript. **JPB developed the laboratory setup and carried out the flume experiment, processed the experimental dataset and assisted in the data interpretation**. PA assisted in data interpretation. SF supported the laboratory experiments. JHF conceived the project, co-developed the research idea, and assisted in the data interpretation. **All authors contributed to reviewing and editing the manuscript**.

Study 4: Quantifying microplastic residence times in lakes using mesocosm experiments and transport modelling

Status: Published in *Water Research,* Volume 229, 1 February 2023, 119463, https://doi.org/10.1016/j.watres.2022.119463

Authors: Hassan Elagami, Sven Frei, **Jan-Pascal Boos**, Gabriele Trommer, Benjamin-Silas Gilfedder

Own contribution: Study design 0 %, data collection 20 %, data processing and analysis 10 %, interpretation of the results 10 %, preparation of the manuscript 10 %. Fluorometer part (method development to quantify microplastics transport, also used in studies 1-3) 90 %.

Author contribution: HE built the mesocosm setup, performed all experiments, worked on data analysis and interpretation, and wrote the manuscript. SF built the mesocosm, helped with conducting the experiments, assisted in data interpretation, built the random walk model, did all simulations, and worked on writing and editing the manuscript. **JPB assisted in data interpretation and worked on writing and editing the manuscript**. GT assisted with planning the experiments and provided lake monitoring data and logistics. BSG conceived the project, built the mesocosm, helped with conducting the experiments, assisted in data interpretation, and worked on writing and editing the manuscript.

Study 6: In-depth characterization revealed polymer type and chemical content specific …

Study 5: Filter feeders are key to small microplastic residence times in stratified lakes: A virtual experiment

Status: Published in *Science of the Total Environment,* Volume 890, 10 September 2023, 164293, https://doi.org/10.1016/j.scitotenv.2023.164293

Authors: Benjamin-Silas Gilfedder, Hassan Elagami, **Jan-Pascal Boos**, Julian Brehm, Matthias Schott, Lorenz Witt, Christian Laforsch, Sven Frei

Own contribution: Study design 10 %, data collection 10 %, data processing and analysis 10 %, interpretation of the results 0 %, preparation of the manuscript 10 %. PIV part (method development and experiments to analyse settling behavior of faecal pellets, also used in studies 2-3) 80 %

Author contribution: B.S. Gilfedder was responsible for the paper concept, writing the paper, and data analysis. H. Elagami was responsible for data assimilation from existing literature and paper revision and discussion of results. **J.P. Boos conducted the PIV measurements to quantify the settling velocities of Daphnia faeces and editing of the paper.** J. Brehm, M. Schott, L. Witt designed, conducted and analysed the data from the Daphnia faeces settling experiments, while C. Laforsch supervised these experiments and assisted with the data analysis. S. Frei designed and conducted the modelling, helped with the interpretation of the data and assisted in writing the paper.

Study 6: In-depth characterization revealed polymer type and chemical content specific effects of microplastic on Dreissena bugensis

Status: Published in *Journal of Hazardous Materials,* Volume 437, 5 September 2022, 129351, https://doi.org/10.1016/j.jhazmat.2022.129351

Authors: Julian Brehm, Magdalena V. Wilde, Lukas Reiche, Lisa-Cathrin Leitner, Benedict Petran, Marcel Meinhart, Simon Wieland, Sven Ritschar, Matthias Schott, **Jan-Pascal Boos**, Sven Frei, Holger Kress, Jürgen Senker, Andreas Greiner, Thomas Fröhlich, Christian Laforsch

Own contribution: Study design 5 %, data collection 5 %, data processing and analysis 5 %, interpretation of the results 5 %, preparation of the manuscript 5 %. LDV part (method, experiments, analysis, and figures, required to ensure comparable microplastics transport during the feeding experiments) 100 %.

Author contribution: J.B. and C.L. designed the research study. J.B., L.R., S.R. performed behavior, ROS enzyme experiments, and sampling for proteome analysis. J.B. analyzed the data.

J.B and S.R. performed the uptake experiment. L.W. and T.F. performed the proteome analysis. B.P., L.L, M.M., S., and S.W. performed physico-chemical particle characterizations and data analysis. **JP.B performed the LDV experiment and data analysis**. S.F, H.K., T.F., A.G., J.S. and C.L. provided instruments and expert advice. All authors read and commented on the manuscript.

J.B and S.R. performed the uptake experiment. L.W. and T.F. performed the proteome analysis.

Study 1: Tracking Microplastics Across the Streambed Interface: Using Laser-Induced-Fluorescence to Quantitatively Analyze Microplastic Transport in an Experimental Flume

Authors: **Jan-Pascal Boos**, Benjamin-Silas Gilfedder, Sven Frei

Water Resources Research®

Key Points:

- Novel methodology for the analysis of microplastic (MP) transport in a water flume
- Quantitative, spatiotemporal information of MPs through fluorometric techniques
- First direct observation of advective transport of MPs through the hyporheic zone using natural sediments

Correspondence to:

J.-P. Boos,
Jan-Pascal.Boos@uni-bayreuth.de

Tracking Microplastics Across the Streambed Interface: Using Laser-Induced-Fluorescence to Quantitatively Analyze Microplastic Transport in an Experimental Flume

Jan-Pascal Boos[1] [ID], **Benjamin Silas Gilfedder[1,2]** [ID], **and Sven Frei[1]** [ID]

[1]Department of Hydrology, Bayreuth Center of Ecology and Environmental Research (BAYCEER), University of Bayreuth, Bayreuth, Germany, [2]Limnological Research Station, Bayreuth Center of Ecology and Environmental Research (BAYCEER), University of Bayreuth, Bayreuth, Germany

Abstract Rivers and streams are a primary transport vector for microplastics (MPs), connecting terrestrial sources to marine environments. While previous studies indicated that pore-scale MPs can accumulate in streambed sediments, the specific MPs transport and retention mechanisms in fluvial systems remain poorly understood. As part of this technical note, we present a novel method for a quantitative analysis of the spatiotemporal transport and retention of pore-scale MPs in an experimental flume. A continuous mass balance for MPs in surface water was achieved using two online fluorometers, while a laser-induced Fluorescence-Imaging-System was developed to track and quantify the spatial migration of MPs through the streambed sediments. The detection limit was <1 μg/L for 1 μm polystyrene microbeads with the fluorometers and 3 μg/L for the Fluorescence-Imaging-System. The system was able to quantitatively track the advective transfer of MPs into the streambed sediments: a process that has yet not been observed experimentally. Results showed that MPs infiltrated into the streambed sediments up to a depth twice the bedform amplitude. This work provides a novel experimental method to quantitatively monitor MP transport through porous media and advective exchange of MP across the streambed interface.

1. Introduction

Microplastics (MPs), synthetic polymer particles smaller than 5 mm (Frias & Nash, 2019), are omnipresent in the hydrosphere (Andrady, 2011; Li et al., 2020) as well as in marine, riverine and limnic biota (Carbery et al., 2018; Jemec et al., 2016; Windsor et al., 2019). Detection of MPs in remote areas such as the deep-sea (Woodall et al., 2014), polar regions (Peeken et al., 2018) and remote lakes (Free et al., 2014) as well as their accumulation in ocean gyres (Law et al., 2010) highlight the importance of understanding transport mechanisms responsible for distributing MPs from source areas to these various environmental compartments. The majority of marine MPs is transported to the ocean by rivers and streams (Meijer et al., 2021). MPs enter stream and river systems through both point and diffuse sources including wastewater treatment plants, the atmosphere and surface runoff (Skalska et al., 2020).

The mobility and retention of MPs in fluvial systems depends on catchment properties (Baldwin et al., 2016), hydrodynamic characteristics (Haberstroh et al., 2020), physicochemical interactions (Lu, Gilfedder, Peng, Niu, & Frei, 2021; Lu, Gilfedder, Peng, Peiffer, et al., 2021) and particle properties (Waldschläger & Schüttrumpf, 2019a). MP accumulation has been observed in low flow regimes such as lakes and reservoirs (Tibbetts et al., 2018) as well as behind flow obstacles (Los Santos et al., 2021; Watkins et al., 2019) and morphological streamed features such as ripples and dunes (Mani et al., 2019), constituting either temporary or permanent retention areas (Horton & Dixon, 2018).

High numbers of MPs have been detected in surface flow, at the streamed interface and in streamed sediments (Shahul Hamid et al., 2018). Along with sedimentation, advective transfer of MPs across the streamed interface into the sediments has been discussed as a potential transport pathway for pore-scale MPs into the hyporheic zone (HZ) and shallow groundwater (Frei et al., 2019). Similar to aqueous phase contaminants (Elliott & Brooks, 1997), pore-scale MPs have also been shown to be mobile in porous media such as streamed sediments (Drummond et al., 2020) or alluvial aquifers (Goeppert & Goldscheider, 2021). Contrarily, MPs can be retained in streamed sediments due to physical clogging of pores (Nizzetto et al., 2016) or sorption effects (Lu, Gilfedder,

Writing – review & editing: Jan-Pascal Boos, Benjamin Silas Gilfedder, Sven Frei

Peng, Peiffer, et al., 2021). During flooding, previously retained MPs can be re-mobilized from the streambeds by erosion (Ockelford et al., 2020).

MP transport in rivers and streams depends on particle characteristics such as shape, size, density and surface characteristics (Kowalski et al., 2016). As the mathematical formulation of transport equations was originally developed for natural sediments, mainly mineral particles of high density and spherical shape, they are only approximately representative for MPs (Hoellein et al., 2019; Waldschläger & Schüttrumpf, 2019b). Thus, additional studies explicitly investigating the transport mechanisms of MPs in streams and rivers are required. MPs have been found to be stored more shallowly in and released more rapidly from the HZ compared to solutes in field studies (Harvey et al., 2012), highlighting the importance of hyporheic exchange for MPs smaller than 100 µm (Drummond et al., 2020). The mobility of bigger MPs (>600 µm) in porous media was previously investigated using column experiments packed with glass beads, showing that retention strongly depended on the relative particle size (Waldschläger & Schüttrumpf, 2020). However, particle migration was not continuously monitored, and results from column experiments are difficult to transfer to stream systems with pronounced three-dimensional hydrodynamical forces that are directly determined by the specific shape of bed form structures.

While MPs migration between surface flow and the HZ has been postulated (Frei et al., 2019), the detailed exchange mechanisms and the specific roles of advective transfer, erosion and sedimentation of MPs in riverine systems have not been experimentally investigated. As part of this technical note, we present an experimental setup for dynamic monitoring and quantification of pore-scale (1–10 µm) MPs abundances in (a) surface flow, (b) at the streambed interface and (c) in hyporheic sediments for an experimental flume environment. The methodology is versatile as it can be used to establish mass balances for MPs in the surface water as well as quantify the spatiotemporal dynamics of MPs in the sediments. This can be linked to the hydrodynamic conditions and bedform morphology for a deeper mechanistic understanding of the transport and retention behavior of MPs in fluvial systems.

2. Materials and Methods

2.1. Set-Up of the Experimental Flume

The experiments were carried out in a tiltable, closed-circuit flume (G.U.N.T. GmbH) with a rectangular cross-section (500 × 8.6 × 30 cm, Figure 1). The inlet water was intermittently stored in a reservoir of 250 L in which water temperature and water level was continuously monitored using a levelogger (Solinst Ltd). Deionized water was used for all experiments, which was conveyed to the flume by a centrifugal pump (Ebara S.p.A.). Discharge in the flume was adjusted between 0.5 and 2.5 Ls^{-1} using an electropneumatic valve (GF Ltd.) and monitored continuously with an electromagnetic flow meter (Jumo GmbH).

2.2. Microplastic Particles

The experiments were performed with polystyrene (PS) microbeads with a diameter of 1 and 10 µm and density of 1.05 g mL^{-1} (PolySciences Inc.). The particles have an internal fluorescent dye, characterized by an excitation maximum at 441 nm and emission maximum at 486 nm. The stock particles have a concentration of 2.6% in aqueous suspension and are coated with a tenside (sodium dodecyl sulfate). An intermediate dilution was prepared by diluting 100 mg of stock solution in 50 mL deionized water. The final calibration suspensions were obtained by further dilution. Particle numbers were calculated using particle density and size and were $\sim 2 \cdot 10^6$ particles/ µg. The stock suspension was kept dark and refrigerated at 4°C to avoid thermal as well as photochemical degradation. After each experiment, flume and sediments were thoroughly rinsed with deionized water to remove MPs from the system. The signal of any remaining MPs (lower than the detection limit) was incorporated into the blank signal measured in subsequent experiments. MP laden water from previous experiments was repeatedly pumped through a filter cascade of two membrane filter cartridges with mesh 0.45 µm (Fuhr GmbH), until no MPs were detected and subsequently, the water was released into the sewage system.

45
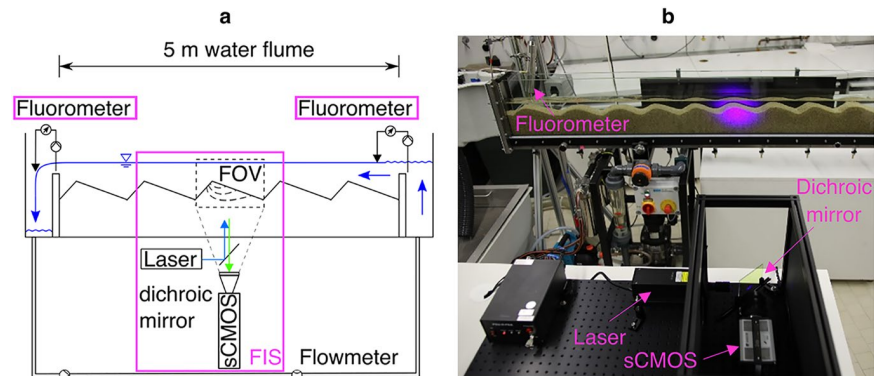
Figure 1. Schematic (a) and photo (b) of the experimental water flume setup showing the applied MPs tracking techniques: Two fluorometers at the inlet and outlet of the flume measure surface water concentrations of MPs. The Fluorescence-Imaging-System (FIS) is used to measure both surface water and pore water MP concentrations by analyzing the fluorescence signal registered by the scientific complementary metal-oxide-semiconductor (sCMOS) sensor. The camera's field of view (FOV) indicates the measurement area.

2.3. Quantification of Microplastic Transport and Retention

2.3.1. Monitoring of MPs in the Surface Water

Continuous in-situ measurement techniques were employed for real-time monitoring of MP abundances in the surface flow. The volumetric particle concentration was measured at the in- and outflow of a control volume with two portable fluorometers (FL24, Albillia Co.) which measure the MP concentration of up to three fluorophores by optical excitation and detection in a flow cell (Schnegg, 2002). Given the fluorescent properties of the MPs, the uranine channel with excitation at 470 nm was selected, using a maximum measurement frequency of 0.5 Hz. Water was extracted from the flume with a peristaltic pump, transferred through the flow cell of the measurement device and returned into the flume. Particle adhesion in the tubing was assumed negligible by choosing a material with smooth inner surface (Tygon E-3609) and minimizing tube length. In contrast to a solute, the fluorescence signal of MP particles passing through the flow cell is discrete in nature and characterized by rapid fluctuations in signal strength and intensity. Calibration of the portable fluorometers was conducted individually for the 1 and 10 µm particles to compare particle detection limits and linearity (Exp. 1 in Table S1 and Figure S1 in Supporting Information S1). Table S1 in Supporting Information S1 provides an overview of the experiments. The measurement signal was corrected by subtracting the blank signal caused by light reflection in deionized water, which was assumed to be stable throughout the experiment. Outliers were removed from the data and a mean value of approximately 30 measurements was used for each calibration standard. The concentrations were grouped in decadal intervals for regression analysis. Quantification and detection limits were calculated using the static model from the calibration curves (Tables S2–S4 in Supporting Information S1).

2.3.2. Manual Sampling of MP in Surface Water and Subsurface Water

Water samples from surface water or pore water were manually collected and analyzed using a laboratory fluorescence spectrometer (LS 55, Perkin Elmer Inc.). The samples were analyzed using a fixed wavelength that matched the peak excitation wavelength of the fluorophore of 441 nm. The emission signal was recorded between 450 and 550 nm with a resolution of 0.5 nm. The peak height at 486 nm as well as the peak area, integrated over the entire measured spectrum and a narrower wavelength interval of 460–540 nm, were used in the linear regression analysis. Triplicates of each sample were analyzed to enhance measurement precision. This method was calibrated for the 1 µm PS beads (Exp. 2).

2.3.3. Monitoring MP Transfer Across the Streambed Interface Using Laser-Induced-Fluorescence Imaging

For a single bedform structure, a scientific complementary metal-oxide-semiconductor (sCMOS) camera (Andor Zyla 5.5, Oxford Instruments) was used to measure the fluorescent signal of MPs in the (a) surface flow, (b) at the streambed interface, and (c) in the pore space of the streambed. Two diode-pumped solid state-lasers (CNI Ltd.,

$\lambda = 457$ nm) were used to excite the fluorescence dye in the MP. For full illumination of the camera sensor, the laser beam was expanded using a 2X Beam Expander (Laser 2000 GmbH). The optical path of the solid-state laser light was diverted perpendicularly to the flow, using a 45° dichroic mirror (Chroma Technology Corp) which significantly reduces the amount of excitation light from entering the detector. The fluorescence light was additionally filtered using a longpass filter (Edmund Optics Inc) mounted on the camera objective (f/0.95, 50 mm focal length) before detection by the imaging sensor (2160*2560 pixel, 6.5 µm pixel length). This Fluorescence-Imaging-System (FIS) was mounted on an optical breadboard which was positioned on a height-adjustable table.

The calibration of the FIS for surface water and porewater was conducted on a 10 cm long, isolated section of the flume filled with (a) MP suspensions and (b) MP suspensions in the pore-space of the streambed sediments (Exp. 3 in Table S1 in Supporting Information S1). The calibration area was centered in the camera's field of view (FOV) to increase measurement sensibility. The dimensions of the calibrated region, the region of interest (ROI), were 7×6 cm with a spatial resolution of 160 µm/Pixel. As fluorescence intensity varied over the field of view, local linear regressions were carried out for squares of 10×10 pixels, yielding individual calibration slopes m. To achieve a homogeneous distribution, m was additionally filtered with a 2d Gaussian filter ($\sigma = 2$). The calibration slope represents the local sensitivity of the FIS, which primarily depends on laser illumination. To account for a potential variation in average light intensity between different calibrations, the slope distribution was normalized by its average value. In the pore-water, the fluorescence signal was heterogeneously distributed caused by a non-reproducible local positioning of grain edges and pore water. Noting a linear correlation for the ROI averaged values (Figure S4 in Supporting Information S1), the calibration slope was obtained by scaling the slope distribution in surface water with the ROI-averaged slope of the pore-water calibration.

An analysis of areas larger than 7×6 cm required an additional calibration, which was conducted using a purpose-built glass tank of dimensions $60 \times 30 \times 5$ cm positioned inside the flume (Exp. 4 in Table S1 in Supporting Information S1). The slope distribution in the water-filled tank was scaled by the average slope of the calibration inside the flume to obtain the final calibration relation. To ensure a reliable quantification, only areas were considered that possessed a correlation coefficient of $R^2 > 0.90$, which coincided with the highest illumination (Figure S3 in Supporting Information S1).

Before and after the experiments, reference measurements were carried out to compensate for a possible change in light illumination and to extract the position of sediment, water and air interfaces. Data acquired prior to MP input was used for background-subtraction. After binning squares of 10×10 pixel, the image was gaussian filtered to achieve higher illumination homogeneity in the pore-water phase. We obtained a vertical profile of MPs in the surface and subsurface water by taking vertical slices at a fixed longitudinal position, averaging the pixel-wise calculated concentrations over a given length (1 cm). The calculations were performed using the image processing toolbox in MATLAB (The MathWorks Inc., 2019).

2.3.4. System Sensitivity

To assess the reproducibility of the analytical measurement techniques, four MPs pulse injection experiments were conducted using deionized water at mean velocity of 0.08 m s^{-1} and without sediments (Exp. 5 in Table S1 in Supporting Information S1). A non-recirculating water flow was chosen to avoid masking the tail of the breakthrough curve by the arrival of recirculated water with higher MP concentrations. The instruments were calibrated prior to each experiment. The fluorometers were positioned at the in- and outflow of the flume (at 0 and 5 m respectively) and the FIS was focusing on an area of 7×6 cm at 3 m along the flume. An obstacle of 10 cm height was positioned at the outflow to ensure that the camera FOV was entirely filled with water. 231 µg of MPs ($\sim 4 \cdot 10^8$ particles) were injected instantaneously into the inlet of the flume, with concentrations of the suspension varying between 46 and 150 mg/L. The experiment finished when the concentration of MPs fell below the detection limit of all measurement devices (~ 4 min). The mass recovery was estimated by temporally integrating MPs breakthrough curves $Q \cdot \int c \ dt$, assuming homogeneity in particle distribution over the cross-section of the flume.

2.3.5. Application Example: Quantification of MPs Mobility and Retention

As a proof of concept, we tested the analytical methods to quantitatively track and quantify the transport and retention behavior of MPs in the flume environment (Exp. 6 in Table S1 in Supporting Information S1). The flume was filled with a coarse sand to represent typical streambed deposits (mean diameter $d_{50} = 1.0$ mm, hydraulic conductivity $K = 3.4 \cdot 10^{-4}$ m/s, porosity $n = 0.29$). A sequence of 17 consecutive ripple bedforms with a crest

length of 15 cm, trough length of 5 cm and amplitude of 3 cm were shaped inside the flume. This geometry was based on an analytical description (Haque & Mahmood, 1985) of bed forms commonly found in streams (Fox et al., 2014) with subcritical flow and low Froude numbers (Engelund & Fredsoe, 1982). Impermeable weirs were used to ensure bedform stability and define the control volume (height 15 cm, located at 80 and 500 cm distance from the flume inlet). Water was recirculated at 0.17 m s^{-1}.

The fluorometers were centered at the weir overflows, measuring at 0.5 Hz. The frame of the FIS was centered on the streambed-water interface of the twelfth bedform (between 3.65 and 3.85 m), to avoid disturbances in the flow field caused by the weirs. The camera aperture was set to its maximum (f/0.95) to enhance light throughput. Images were recorded using an exposure time of 1 s at a frame rate of 0.5 Hz. 26 mg MP of 1 μm diameter were injected as a pulse into the surface flow at the inlet of the flume and the temporal evolution of particle flow (breakthrough) (a) in the surface flow, (b) at the streambed interface and (c) in the streambed sediments was quantitatively monitored using the methods described above.

3. Results and Discussion

3.1. Calibration, Detection, and Quantification Limits

For the two portable fluorometers, the calibration was linear in a range between 0.4 and 4,000 μg/L (lowest R^2 of 0.97, Exp.1, Figure S1a in Supporting Information S1). The detection limit was 0.6 μg/L and the quantification limit was 0.9 μg/L (Table S2 in Supporting Information S1). The fluorometers were less sensitive for the 10 μm particles (detection limit ≈ 50 μg/L) which was attributed to a decrease in particle abundance and surface area in the measurement cell (Text S4 in Supporting Information S1). However, the correlation was still linear with the lowest R^2 being 0.76. Results from the offline fluorescence spectroscopy (Perkin Elmer, Exp. 2, Figure S1b in Supporting Information S1) using the wavelength interval between 460 and 540 nm yielded high coefficients of determination (all $R^2 > 0.93$) and the lowest deviations in triplicate analysis. The detection and quantification limits were comparable to the in-situ fluorometers at 0.5 and 0.8 μg/L, respectively (Table S3 in Supporting Information S1).

For the FIS (Exp. 3), the analysis of a 7 × 6 cm isolated flume section yielded a linear correlation with a mean $R^2 > 0.99$, detection limit of 3.1 μg/L and a quantification limit of 4.7 μg/L (Figure S2 and Table S4 in Supporting Information S1). Small differences in regressions slope were observed in the triplicated calibration, although the position of the FIS was not intentionally changed. The distribution of regression slopes and regression coefficients of the calibration of the FIS for a larger FOV as needed for the infiltration experiment is shown in Figure S3 in Supporting Information S1 (Exp. 4 in Table S1 in Supporting Information S1).

All measurement techniques were characterized by linear relations with high R^2 values, thus providing reliable data for the quantitative evaluation of MPs concentrations. The methods are comparably sensitive as their detection limits are low (<3 μg/L for the 1 μm beads), which reduces the quantity of MPs needed for an individual experiment. These findings agree with previously published data on detection limits for a fluorescence spectrometer using the same 1 μm beads (Goeppert & Hoetzl, 2010).

3.2. Recovery Rate of Pulse Injection Experiments

The MP recovery rates of the Fluorometers and the FIS, acquired in three experiments with linear flow, varied between 80% and 90% (Exp. 5, Figure 2). For the Fluorometers, the MP loss is most likely due to non-uniform MP concentrations in the flume, as in pilot tests particle concentration varied somewhat in vertical and lateral sampling locations. The deviance in FIS data might be caused by the focus being on the inner flume interface: Since the velocity distribution is affected by the no-slip boundary condition located at the water-glass interface, less MP is transported near the boundary, meaning that the lateral integration of the FIS underestimates particle abundance. In addition, experiments with higher flow velocity caused by removing the outflow obstacle displayed a higher recovery rate (>95%). Missing MPs can also be attributed to the adhesion of particles to the glass sides and the bottom of the flume.
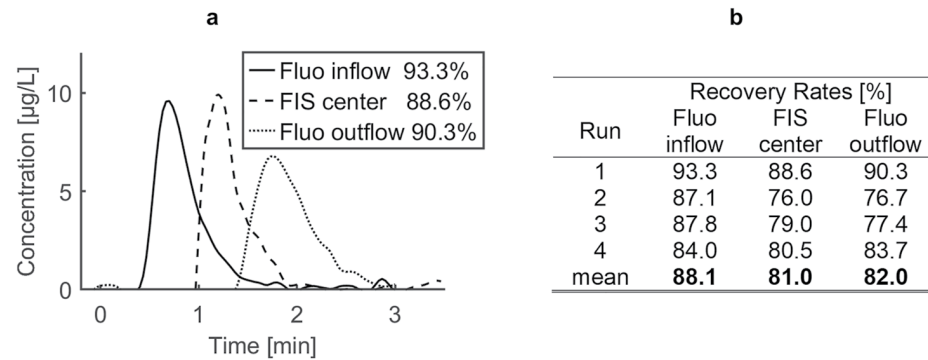
Figure 2. Breakthrough curves of a MP pulse in the flume, with non-recirculating flow and without sediment (Exp. 5). Fluorometer are positioned at in- and outflow (0 and 5 m), the FIS at 3 m. (a) Breakthrough curves for run 1, data is interpolated with splines. (b) Results of the relation of recovered to total MP mass in four experiment runs.

3.3. Quantification of MP Mobility and Retention

In- and outflow MP concentrations of the breakthrough experiment (Exp. 6) are shown in Figure 3a. The time lag between the fluorometers was 22 s, yielding an advective transport velocity of 0.19 m s^{-1}. This agrees with a mean transport velocity of 0.17 m s^{-1}, calculated from the discharge (0.69 L s^{-1}) and the average water depths at bedform crest (26 mm) and trough (40 mm). Comparing the fluorometers, MP peak arrival was delayed by 26 s, indicating minor dispersion effects on peak transport velocity. For the outflow fluorometer the peak concentration was 33% lower (1,740 µg/L vs. 1,170 µg/L), and peak width, measured as full width at half maximum, was 67% higher than at the flume inlet (15 and 25 s). This shows that the breakthrough at the upper fluorometer was mainly influenced by advection, whereas the second measurement site was influenced by advection, dispersion, and probably retention.

The MPs concentration increased again after 99 s at the inflow and 137 s at the outflow due to water recirculation through the flume reservoir. The minimum MPs concentration was 0.1%, respectively 2.3% of peak concentration. An analysis for the recovery during the first pulse of MP yielded 72% for the inflow, and 92% for the outflow fluorometer. The low recovery was most likely caused by a heterogeneous distribution of MPs in the flow closer to the inlet. Details of the tail of the breakthrough curve cannot be evaluated since concentrations were masked by the arrival of MPs-laden recirculated water. After the initial breakthrough, monitoring with Fluorometers yielded similar concentrations of MPs at the in- and outflow of the flume. MPs concentration in the surface water decreased throughout the experiment, beginning at 118 µg/L, and ending at 103 µg/L after five hours (Figure 3a).

For the same experiment, the fluorescence-imaging-system was used to quantify the MPs concentrations in the surface flow above the bedform, at the streambed interface and in the streambed sediments. Depth specific breakthrough curves, averaged over 1 cm depth, are shown in Figure 3b. The datasets show a synchronous peak, independent of sediment depth, at the time of arrival of MP in the surface water (45 s after injection). This effect was physically implausible, given the lower hyporheic flow velocities in the porous medium, which additionally decrease with sediment depth. The effect was attributed to charge spillage (sensor blooming) caused by the oversaturation of individual pixels. The secondary peaks in the subsurface datasets indicated the migration of the MPs plume through the streambed sediments. A non-linear relation between sediment depth and peak arrival time as well as peak concentration could be noticed. Between 1 and 7 cm sediment depth, breakthrough peak time increases from 89 to 251 s, while peak concentration dropped from 630 to 180 µg/L. MPs infiltration was observed to a depth twice the bedform amplitude. After the initial breakthrough, the concentration in the individual sediment depths showed only little variation in time. The FIS data in the surface water showed a declining surface water concentration, starting at 125 µg/L and ending after four hours at 105 µg/L. The values of the FIS data set were similar to the Fluorometer surface water measurements. Figure 3c provides a timeseries of MPs infiltration and a video is available in the supplementary materials.

The application of an injection of MP into the surface water of the flume showed that our experimental setup can be used to investigate transport, exchange and retention of pore-scale MPs in the surface water as well as in the streambed sediments. MP transport in the surface water shows patterns of advection and longitudinal dispersion,
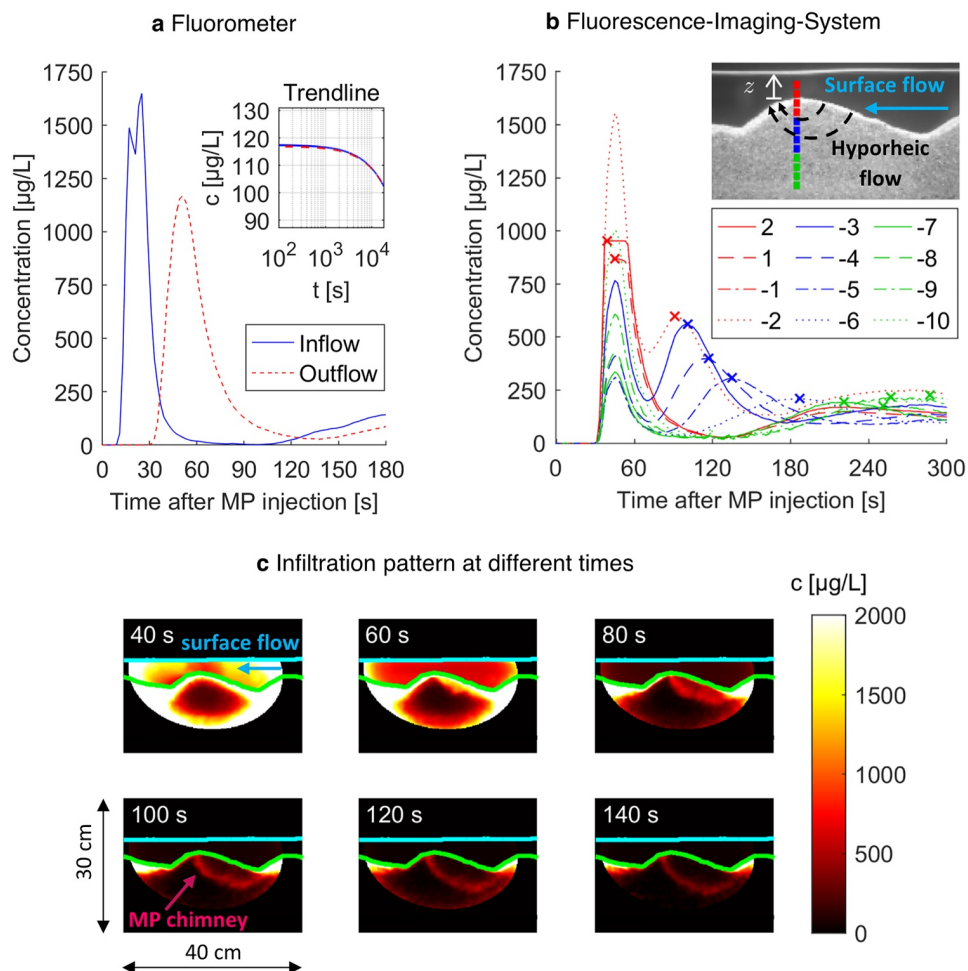
Figure 3. Microplastics (MPs) transport during infiltration experiment (Exp. 6). (a) Concentration in surface water flow at flume inflow and outflow, monitored with Fluorometers. The inset plot shows an exponential trendline. (b) Vertical profile of MPs breakthrough at the ripple crest, slice depth was 1 cm, numeration shows elevation above sediment-water-interface. Peak concentration in the surface is cut off due to over-saturation. Concentration increases after ~2 min due to recirculation. (c) Time series of MPs infiltration, captured with the FIS (air-water-interface in cyan, water-sediment-interface in green, surface flow from right to left). The camera frame is oversaturated at the arrival of MPs in surface water (at 40 s). Particle infiltration depth reaches twice the bedform amplitude. Particles reenter the surface water flow at the downstream face, preferentially in vicinity to the bedform crest.

leading to a less pronounced but lengthier breakthrough in the flume outlet, as has been already noted in previous experiments (Cook et al., 2020). With the FIS system, for the first time, we were able to directly track the advective transfer of MP particles across the streambed interface and flow through the HZ.

Peak concentrations were higher in shallow areas of the sediments. MPs concentrations in the surface water during the peak of the first breakthrough as observed by the FIS, focusing on the center of the control volume, were lower than at the outflow fluorometer. This was probably caused by the oversaturation observed in the FIS. After the first breakthrough, the datasets yielded comparable surface water concentrations (Figure 3a, inset). However, while demonstrating MP infiltration into the streambed sediments, the current data set gives no clear indication on whether particles in the hyporheic zone are immobilized after the first breakthrough or are transported conservatively with the advective flow. Additionally, the surface water concentration continuously decreased during the timescale of the experiment (5 hr). Although this was partially attributed to deposition in the flume apparatus, it is also likely to indicate retention in the streambed sediments. Further, detailed experiments combining

particles, sediment and hydrodynamical characterization are needed to achieve generalizable information on MPs transport and retention.

3.4. Opportunities and Limitations

Using the analytical methods introduced in this work, we can quantitatively study the transport of fluorescent MPs in both surface water and hyporheic sediments in an experimental flume. Mass fluxes for MPs in and out of the control volume were measured using portable fluorometers. For a single bedform, the FIS was successfully used to quantify the migration and re-distribution of MPs (a) in the surface flow, (b) at the streambed interface and (c) in the streambed sediments. By applying the FIS, for the first time the advective transfer of pore-scale MPs from the surface flow into the streambed could be directly observed. This experimental setup can be used to achieve an improved quantitative understanding of the basic mechanisms governing MPs transport and retention in riverine environments. The setup can be used for a large variety of potential application scenarios, such as experiments (a) to investigate how sedimentation and erosion cycles in fluvial systems control MPs abundances in stream flow and streambed sediments, (b) to quantitatively understand retention mechanisms in streambed sediments by using different porous media (e.g., sand, clay, iron-oxides) and non-uniform geochemical conditions (pH, ionic strength), (c) to understand dynamics of re-suspension of MPs during high-flow events which are reported as hot moments of MPs contamination in rivers and streams (Hurley et al., 2018) and (d) to investigate how interactions with biota (uptake and excretion or biofilm formation) is affecting hydrodynamic properties of MPs in rivers and streams.

The methods facilitate an analysis of rapidly changing MPs concentrations, with a maximum sampling frequency of 0.5 Hz using the Fluorometers and 8 Hz using the Fluorescence-Imaging-System. Surface water concentrations of both techniques matched after the initial breakthrough. Due to particle adhesion and mixing in the tubing, the flow to the Fluorometers represents a potential source of error. A significant advantage of the FIS is its non-invasive nature, avoiding disturbances of the hydrodynamic conditions in the flume. However, optical access to a longitudinal flow section is required and therefore, the method is only suitable for a flume with a transparent glass or plexiglass window. In addition, the FIS visualizes subsurface flow only at the sediment-glass interface where the surface flow is influenced by the glass boundary and the subsurface flow by a locally higher porosity (Roozbahani et al., 2014), possibly leading to preferential flow paths. This effect is important for MPs larger than the average pore size of the sediment but was likely to be negligible in our experiment. Indeed, the identified subsurface flow pattern, infiltration at the troughs and exfiltration at the crests, was similar to direct measurements of dissolved tracers in hyporheic sediments (Precht & Huettel, 2004).

The methods can only be applied in combination with fluorescent MPs, which enable a clear separation of MPs from other, non-fluorescent suspended particles. While requiring the additional step of fluorescent staining, cross-contamination with ambient MP and other natural particles is negligible. The measurement also requires stability of the fluorescent signal over time, otherwise decreasing signal strength may be interpreted as lower particle abundances. This can be problematic since fluorescent tracers are known to leach and to degrade after light exposure (Gombert et al., 2017). Therefore, reference measurements with MPs samples stored in the same laboratory should be performed alongside long-term experiments. Quantification with fluorometers worked best for small, pore scale MPs (1 μm), since particle distribution in the flow and in the measurement cell is more homogeneous. With increasing particle size (10 μm), the signal intensity fluctuated which is possibly caused by the irregular passing of particles in the flow cell. Larger and denser particles may restrict the usability of a fluorescence spectrometer if they settle in the cuvette during measurement.

Additionally, we note that by measuring particle concentration in the flume, we track the movement of particle clouds rather than individual particles. For example, 1 μm particles cannot be resolved individually with a pixel size of 6.5 μm. At the detection limit of the fluorometers, a mass concentration of 0.5 μg/L corresponds to abundances of $\approx 10^6$ particles/L. Data on environmentally relevant concentrations of pore-scale MPs are not known due to analytical detection limits, but studies indicate an increasing abundance of smaller particles (Frei et al., 2019; Poulain et al., 2019). Since particle-particle interaction was avoided by tenside coating and an impact of the particles on the hydrodynamics can be neglected due to the small volumetric concentration, the transport mechanisms as observed at the laboratory scale should be transferable to real fluvial systems.

51

4. Conclusion

To our knowledge, the methods presented here are the first published that are able to quantitatively measure MPs transport and retention in a fluvial model environment by simultaneously tracking particle migration in surface flow and in streambed sediments. Using optical techniques, infiltration of MPs into the hyporheic zone was directly visualized and spatiotemporally resolved, which is necessary to gain insights into the mechanisms controlling MP mobility in rivers and streams. The presented method can be used for a combination of pore-scale MPs particles, sediments and bedform structures. This allows for an investigation of various scenarios of MPs transport in fluvial systems, which likely depends on relative particle size, shape, and polymer. Further experiments are necessary to clarify whether infiltrating particles are immobilized permanently in the riverbed sediment, or rather constantly migrate in a dynamic equilibrium. In the future, it will be possible to analyze how small-scale topographical features such as bedforms as well as moving bedforms influence the advective transfer, sedimentation and remobilization of MPs in fluvial systems.

We hope that our experimental setup will help other researchers to implement their own experimental system to investigate the fate of MPs in fluvial ecosystems. Although the presented methods are only partially suitable for application in real stream environments (application of portable fluorometers), we strongly believe that they are very useful to better understand and investigate the fundamental transport and retention mechanisms of MPs in rivers and streams.

Conflict of Interest

The authors declare no conflicts of interest relevant to this study.

Data Availability Statement

The data sets used and analyzed during the current study, as well as the developed MATLAB scripts are published in Zenodo (Boos et al., 2021): https://doi.org/10.5281/zenodo.5706440.

References

Andrady, A. L. (2011). Microplastics in the marine environment. *Marine Pollution Bulletin*, *62*(8), 1596–1605. https://doi.org/10.1016/j.marpolbul.2011.05.030

Baldwin, A. K., Corsi, S. R., & Mason, S. A. (2016). Plastic Debris in 29 Great Lakes Tributaries: Relations to watershed attributes and hydrology. *Environmental Science & Technology*, *50*(19), 10377–10385. https://doi.org/10.1021/acs.est.6b02917

Boos, J.-P., Gilfedder, B. S., & Frei, S. (2021). Data and code for the publication "Tracking microplastics across the streambed interface: Using laser-induced-fluorescence to quantitatively analyze microplastic transport in an experimental flume". https://doi.org/10.5281/zenodo.5706440

Carbery, M., O'Connor, W., & Palanisami, T. (2018). Trophic transfer of microplastics and mixed contaminants in the marine food web and implications for human health. *Environment International*, *115*, 400–409. https://doi.org/10.1016/j.envint.2018.03.007

Cook, S., Chan, H.-L., Abolfathi, S., Bending, G. D., Schäfer, H., & Pearson, J. M. (2020). Longitudinal dispersion of microplastics in aquatic flows using fluorometric techniques. *Water Research*, *170*, 115337. https://doi.org/10.1016/j.watres.2019.115337

Drummond, J. D., Nel, H. A., Packman, A. I., & Krause, S. (2020). Significance of hyporheic exchange for predicting microplastic fate in rivers. *Environmental Science and Technology Letters*, *7*(10), 727–732. https://doi.org/10.1021/acs.estlett.0c00595

Elliott, A. H., & Brooks, N. H. (1997). Transfer of nonsorbing solutes to a streambed with bed forms. *Laboratory experiments*, *33*(1), 137–151. https://doi.org/10.1029/96WR02783

Engelund, F., & Fredsoe, J. (1982). Sediment ripples and dunes. *Annual Review of Fluid Mechanics*, *14*(1), 13–37. https://doi.org/10.1146/annurev.fl.14.010182.000305

Fox, A., Boano, F., & Arnon, S. (2014). Impact of losing and gaining streamflow conditions on hyporheic exchange fluxes induced by dune-shaped bed forms. *Water Resources Research*, *50*(3), 1895–1907. https://doi.org/10.1002/2013WR014668

Free, C. M., Jensen, O. P., Mason, S. A., Eriksen, M., Williamson, N. J., & Boldgiv, B. (2014). High-levels of microplastic pollution in a large, remote, mountain lake. *Marine Pollution Bulletin*, *85*(1), 156–163. https://doi.org/10.1016/j.marpolbul.2014.06.001

Frei, S., Piehl, S., Gilfedder, B. S., Löder, M. G. J., Krutzke, J., Wilhelm, L., & Laforsch, C. (2019). Occurence of microplastics in the hyporheic zone of rivers. *Scientific Reports*, *9*(1), 15256. https://doi.org/10.1038/s41598-019-51741-5

Frias, J. P. G. L., & Nash, R. (2019). Microplastics: Finding a consensus on the definition. *Marine Pollution Bulletin*, *138*, 145–147. https://doi.org/10.1016/j.marpolbul.2018.11.022

Goeppert, N., & Goldscheider, N. (2021). Experimental field evidence for transport of microplastic tracers over large distances in an alluvial aquifer. *Journal of Hazardous Materials*, *408*, 124844. https://doi.org/10.1016/j.jhazmat.2020.124844

Goeppert, N., & Hoetzl, H. (2010). Precise method for continuous measurement of fluorescent microspheres during flow. *Hydrogeology Journal*, *18*(2), 317–324. https://doi.org/10.1007/s10040-009-0517-0

Gombert, P., Biaudet, H., Sèze, R. de, Pandard, P., & Carré, J. (2017). Toxicity of fluorescent tracers and their degradation byproducts. *International Journal of Speleology*, *46*(1), 23–31. https://doi.org/10.5038/1827-806X.46.1.1995

Haberstroh, C. J., Arias, M. E., Yin, Z., & Wang, M. C. (2020). Effects of hydrodynamics on the cross-sectional distribution and transport of plastic in an urban coastal river. *Water Environment Research*, *93*(2), 186–200. https://doi.org/10.1002/wer.1386

Haque, M. I., & Mahmood, K. (1985). Geometry of ripples and dunes. *Journal of Hydraulic Engineering*, *111*(1), 48–63. https://doi.org/10.1061/(ASCE)0733-9429(1985)111:1(48)

Harvey, J. W., Drummond, J. D., Martin, R. L., McPhillips, L. E., Packman, A. I., Jerolmack, D. J., et al. (2012). Hydrogeomorphology of the hyporheic zone: Stream solute and fine particle interactions with a dynamic streambed. *Journal of Geophysical Research*, *117*(G4). https://doi.org/10.1029/2012JG002043

Hoellein, T. J., Shogren, A. J., Tank, J. L., Risteca, P., & Kelly, J. J. (2019). Microplastic deposition velocity in streams follows patterns for naturally occurring allochthonous particles. *Scientific Reports*, *9*(1), 3740. https://doi.org/10.1038/s41598-019-40126-3

Horton, A. A., & Dixon, S. J. (2018). Microplastics: An introduction to environmental transport processes. *Wiley Interdisciplinary Reviews: Water*, *5*(2), e1268. https://doi.org/10.1002/wat2.1268

Hurley, R., Woodward, J., & Rothwell, J. J. (2018). Microplastic contamination of river beds significantly reduced by catchment-wide flooding. *Nature Geoscience*, *11*(4), 251–257. https://doi.org/10.1038/s41561-018-0080-1

Jemec, A., Horvat, P., Kunej, U., Bele, M., & Kržan, A. (2016). Uptake and effects of microplastic textile fibers on freshwater crustacean Daphnia magna. *Environmental Pollution*, *219*, 201–209. https://doi.org/10.1016/j.envpol.2016.10.037

Kowalski, N., Reichardt, A. M., & Waniek, J. J. (2016). Sinking rates of microplastics and potential implications of their alteration by physical, biological, and chemical factors. *Marine Pollution Bulletin*, *109*(1), 310–319. https://doi.org/10.1016/j.marpolbul.2016.05.064

Law, K. L., Morét-Ferguson, S., Maximenko, N. A., & Proskurowski, G. (2010). Plastic Accumulation in the North Atlantic Subtropical Gyre. *Science*, *329*. https://doi.org/10.1126/science.1192321o

Li, C., Busquets, R., & Campos, L. C. (2020). Assessment of microplastics in freshwater systems: A review. *Science of the Total Environment*, *707*, 135578. https://doi.org/10.1016/j.scitotenv.2019.135578

Los Santos, C. B., Krång, A.-S., & Infantes, E. (2021). Microplastic retention by marine vegetated canopies: Simulations with seagrass meadows in a hydraulic flume. *Environmental Pollution*, *269*, 116050. https://doi.org/10.1016/j.envpol.2020.116050

Lu, T., Gilfedder, B. S., Peng, H., Niu, G., & Frei, S. (2021). Effects of clay minerals on the transport of nanoplastics through water-saturated porous media. *Science of the Total Environment*, *796*, 148982. https://doi.org/10.1016/j.scitotenv.2021.148982

Lu, T., Gilfedder, B. S., Peng, H., Peiffer, S., Papastavrou, G., Ottermann, K., & Frei, S. (2021). Relevance of iron oxyhydroxide and pore water chemistry on the mobility of nanoplastic particles in water-saturated porous media environments. *Water, Air, & Soil Pollution*, *232*(5). https://doi.org/10.1007/s11270-021-05125-z

Mani, T., Primpke, S., Lorenz, C., Gerdts, G., & Burkhardt-Holm, P. (2019). Microplastic pollution in benthic midstream sediments of the Rhine River. *Environmental Science & Technology*, *53*(10), 6053–6062. https://doi.org/10.1021/acs.est.9b01363

Meijer, L. J. J., van Emmerik, T., van der Ent, R., Schmidt, C., & Lebreton, L. (2021). More than 1000 rivers account for 80% of global riverine plastic emissions into the ocean. *Science Advances*, *7*(18). https://doi.org/10.1126/sciadv.aaz5803

Nizzetto, L., Bussi, G., Futter, M. N., Butterfield, D., & Whitehead, P. G. (2016). A theoretical assessment of microplastic transport in river catchments and their retention by soils and river sediments. *Environmental Science. Processes & Impacts*, *18*(8), 1050–1059. https://doi.org/10.1039/c6em00206d

Ockelford, A., Cundy, A., & Ebdon, J. E. (2020). Storm response of fluvial sedimentary microplastics. *Scientific Reports*, *10*(1), 1865. https://doi.org/10.1038/s41598-020-58765-2

Peeken, I., Primpke, S., Beyer, B., Gütermann, J., Katlein, C., Krumpen, T., et al. (2018). Arctic sea ice is an important temporal sink and means of transport for microplastic. *Nature Communications*, *9*(1), 1505. https://doi.org/10.1038/s41467-018-03825-5

Poulain, M., Mercier, M. J., Brach, L., Martignac, M., Routaboul, C., Perez, E., et al. (2019). Small microplastics as a main contributor to plastic mass balance in the North Atlantic subtropical gyre. *Environmental Science & Technology*, *53*(3), 1157–1164. https://doi.org/10.1021/acs.est.8b05458

Precht, E., & Huettel, M. (2004). Rapid wave-driven advective pore water exchange in a permeable coastal sediment. *Journal of Sea Research*, *51*(2), 93–107. https://doi.org/10.1016/j.seares.2003.07.003

Roozbahani, M. M., Graham-Brady, L., & Frost, J. D. (2014). Mechanical trapping of fine particles in a medium of mono-sized randomly packed spheres. *International Journal for Numerical and Analytical Methods in Geomechanics*, *38*(17), 1776–1791. https://doi.org/10.1002/nag.2276

Schnegg, P.-A. (2002). *An inexpensive field fluorometer for hydrogeological tracer tests with three tracers and turbidity measurement* (pp. 1484–1488). Groundwater and Human Development.

Shahul Hamid, F., Bhatti, M. S., Anuar, N., Anuar, N., Mohan, P., & Periathamby, A. (2018). Worldwide distribution and abundance of microplastic: How dire is the situation? *Waste Management & Research*, *36*(10), 873–897. https://doi.org/10.1177/0734242X18785730

Skalska, K., Ockelford, A., Ebdon, J. E., & Cundy, A. B. (2020). Riverine microplastics: Behaviour, spatio-temporal variability, and recommendations for standardised sampling and monitoring. *Journal of Water Process Engineering*, *38*, 101600. https://doi.org/10.1016/j.jwpe.2020.101600

The MathWorks Inc. (2019). *MATLAB and image processing toolbox R2019b*. Massachusetts: Natick.

Tibbetts, J., Krause, S., Lynch, I., & Sambrook Smith, G. (2018). Abundance, distribution, and drivers of microplastic contamination in urban river environments. *Water*, *10*(11), 1597. https://doi.org/10.3390/w10111597

Waldschläger, K., & Schüttrumpf, H. (2019a). Effects of particle properties on the settling and rise velocities of microplastics in freshwater under laboratory conditions. *Environmental Science & Technology*, *53*(4), 1958–1966. https://doi.org/10.1021/acs.est.8b06794

Waldschläger, K., & Schüttrumpf, H. (2019b). Erosion behavior of different microplastic particles in comparison to natural sediments. *Environmental Science & Technology*, *53*(22), 13219–13227. https://doi.org/10.1021/acs.est.9b05394

Waldschläger, K., & Schüttrumpf, H. (2020). Infiltration behavior of microplastic particles with different densities, sizes, and shapes-from glass spheres to natural sediments. *Environmental Science & Technology*, *54*(15), 9366–9373. https://doi.org/10.1021/acs.est.0c01722

Watkins, L., McGrattan, S., Sullivan, P. J., & Walter, M. T. (2019). The effect of dams on river transport of microplastic pollution. *Science of the Total Environment*, *664*, 834–840. https://doi.org/10.1016/j.scitotenv.2019.02.028

Windsor, F. M., Tilley, R. M., Tyler, C. R., & Ormerod, S. J. (2019). Microplastic ingestion by riverine macroinvertebrates. *Science of the Total Environment*, *646*, 68–74. https://doi.org/10.1016/j.scitotenv.2018.07.271

Woodall, L. C., Sanchez-Vidal, A., Canals, M., Paterson, G. L. J., Coppock, R., Sleight, V., et al. (2014). The deep sea is a major sink for microplastic debris. *Royal Society Open Science*, *1*(4), 140317. https://doi.org/10.1098/rsos.140317

⊗AGU PUBLICATIONS

Water Resources Research

Supporting Information for

**Tracking microplastics across the streambed interface:
Using laser-induced-fluorescence to quantitatively analyze
Microplastic transport in an experimental flume**

Jan-Pascal Boos *[1], Benjamin-Silas Gilfedder [1,2], Sven Frei [1]

[1]Department of Hydrology, Bayreuth Center of Ecology and Environmental Research (BAYCEER), University of Bayreuth, Universitätsstraße 30, 95440, Bayreuth, Germany

[2] Limnological Research Station, Bayreuth Center of Ecology and Environmental Research (BAYCEER), University of Bayreuth, Universitätsstraße 30, 95440, Bayreuth, Germany

Contents of this file

    Text S1 to S4
    Figures S1 to S5
    Tables S1 to S4

Additional Supporting Information (Files uploaded separately)

    Caption for Movie S1

Introduction

This document provides additional details to describe the following topics

- Overview of the presented experiments (Table S1)
- Dependence of signal quantity on particle size (Text S4)
- Calibration of the fluorometers (Text S3, Figure S1a, Table S2)
- Calibration of the spectrometer (Text S3, Figure S1b, Table S3)
- Calibration of the Fluorescence-Imaging-System (Text S1-S3, Figures S2-S4, Table S4)

1

Text S1.

In Figure S3, we see results of the two-step-calibration of the FIS inside an isolated flume section (7 cm x 6 cm) and a water tank (37 cm x 22 cm). For the center ROI (parts a and b), the averaged slope in the tank was smaller than in the flume (1.039 / 1.749 = 0.59), which is mainly caused by the different water depth along the optical axis (5 mm / 8.6 mm = 0.58). The normalized slope distribution is similar in both calibrations, additionally yielding high correlation coefficients ($R^2 > 0.99$). Therefore, laser illumination in both calibration steps was similar, a necessary requirement for the two-step calibration method, using the average value of the flume ROI and the normalized profile in the tank to describe system sensitivity in the complete FOV area inside the flume. For the whole camera FOV (Figure S3, part c), we see that calibration slope is normally distributed and centered in the image. Although mean slope of the complete FOV is 80 % lower, the binned pixelwise regression shows high correlation coefficients for the complete FOV. The elliptical boundary at $R^2 > 0.9$ corresponds to $m > 0.016$

Text S2.

Figure S4 shows results of the calibration of the Fluorescence-Imaging-System, giving information on the ROI-averaged signal gain (blank-subtracted) in the flume and water tank in the surface water, and in the flume in the pore space. The signal gain in surface water varies, which is mainly caused by the different depths of the calibration volumes (flume 86 mm, tank 50 mm). Although the signal is significantly lower in the pore water than in the surface water, a high R^2 value could be obtained

Text S3.

Tables S2 to S4 show details for the calibrations realized for assessing the system sensibility. Included are the obtained values for the detection limit (DL) and quantification limit (QL), using N calibration standards of fluorescent, 1 µm PS beads. For the Fluorometers and spectrometer, the calibration was repeated with smaller concentrations, until the calculated detection limit was close to the mean of calibrated concentrations. These final metrics (marked in bold) were used to describe the sensitivity of the methods.

2

Text S4.

The detection limit of the online fluorometer was 0.6 µg/L for the 1 um particles and 50 µg/L for the 10 um particles. This could be explained by a loss in signal quality (increase in signal fluctuations caused by the heterogeneous passing of particles) as well as signal quantity (less fluorescence signal) using bigger particles. The fluorescence signal measured by the fluorometer can be described by mass concentration $[ML^{-3}]$ the particle concentration $[\#L^{-3}]$ and the surface area of the particles in suspension $[L^2L^{-3}]$. For given spherical particles with diameter d, density ρ, particle volume $V_{part} = \frac{\pi}{6}d^3$ and surface area $S_{part} = \pi d^2$ in a suspension with mass concentration c:

Particle concentration $N = \frac{c}{\rho V_{part}} = \frac{6c}{\pi \rho d^3}$

Surface area to volume: $SA{:}V = N \cdot S = \frac{6c}{\rho d}$

Under a tenfold higher particle diameter, mass concentration must increase by a factor of 1000 to ensure a constant particle concentration, or a factor of 10 to ensure a constant surface area. From the Fluorometer calibration, mass concentration had to increase by a factor of 83 for the same detection limit, and this lies within both theoretical values. Additionally, changes in the internal staining between the two particles sizes contribute to a difference in signal quantity.

3
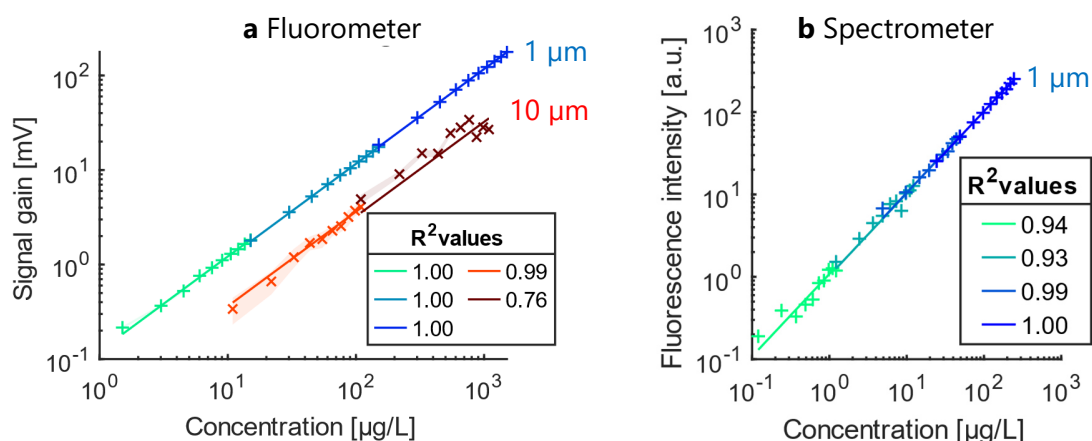
Figure S1. Individual calibration results (Exp. 1 and 2) for the selective measurements, color shades indicate concentration decades. (a) Fluorometer (inflow), with 1 µm (blue) and 10 µm (red) PS beads, data points are averages of approximately 30 measurements. 95% confidence interval boundaries are shown in dashed lines. Signal gain after blank subtraction (1.2 mV). (b) Spectrometer with 1 µm PS beads, data points are averages of triplicates. Fluorescence intensity gain after blank subtraction (3 units)
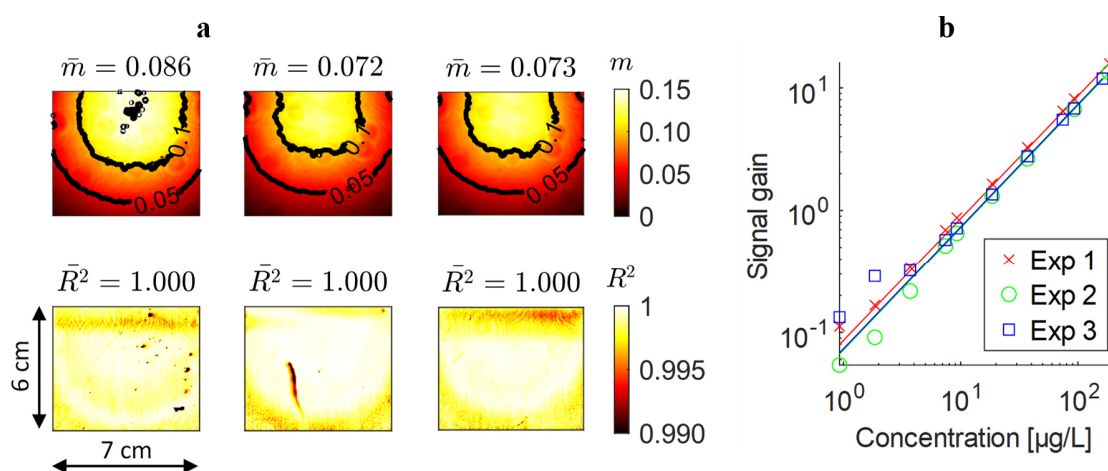
Figure S2. Calibration of Fluorescence-Imaging-System (Exp. 3) for system sensitivity analysis, results of three independent measurements. **(a)** Spatial distribution of slope m and determination coefficient R^2 for the entire camera field of view providing averaged values. Spatial resolution was 36 Pixel/mm. **(b)** Field of view-averaged fluorescence intensities as measured (markers) and calculated from the calibration relation (solid line). Background signal was 102 units)

4

a Flume, center ROI   **b** Tank, center ROI   **c** Tank, complete FOV

$\bar{m} = 1.749$ $\bar{m} = 1.039$ $m/\bar{m}$ $\bar{m} = 0.212$ $m/\bar{m}_{ROI}$

$\bar{R}^2 = 1.000$ $\bar{R}^2 = 0.995$ R^2 $\bar{R}^2 = 0.980$ R^2
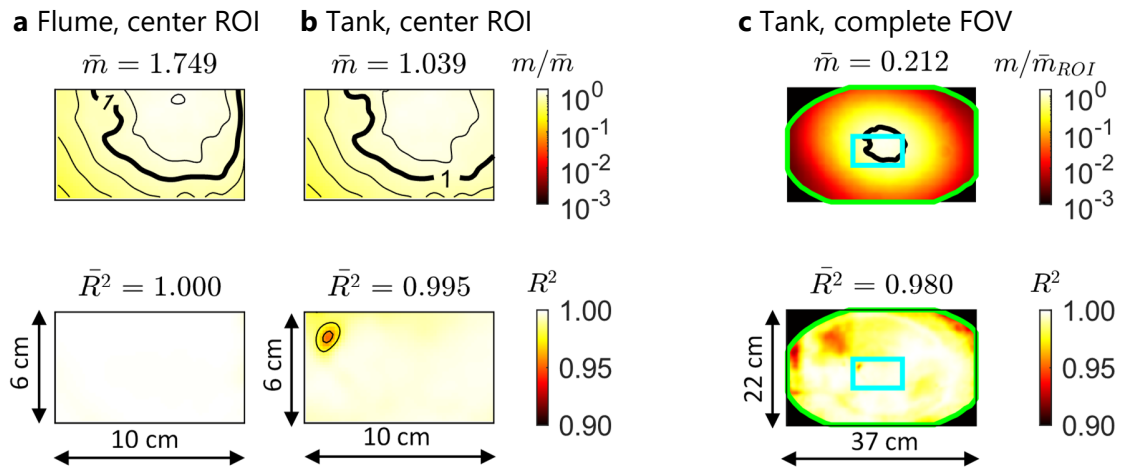
Figure S3: Result of the linear regression analyses of the Fluorescence-Imaging-System (Exp. 4). **(a)**: Calibration in the water flume for the center ROI. **(b)**: calibration in the water tank for the center ROI, which is a detailed view of the whole calibrated area shown in **(c)** (the center ROI is depicted in cyan). While the averaged absolute values ($\bar{m}$) vary, the normalized distribution of calibration slope ($m/\bar{m}$) is similar. Slope isolines are relative to the center ROI average, shown at a 0.2-spacing, and highlighting unity. The green ellipse masks the regions of high correlation ($R^2 > 0.90$), which is used for the outer boundary considered for the calibration. All slope distributions were gaussian filtered ($\sigma = 2$) for homogenization

5
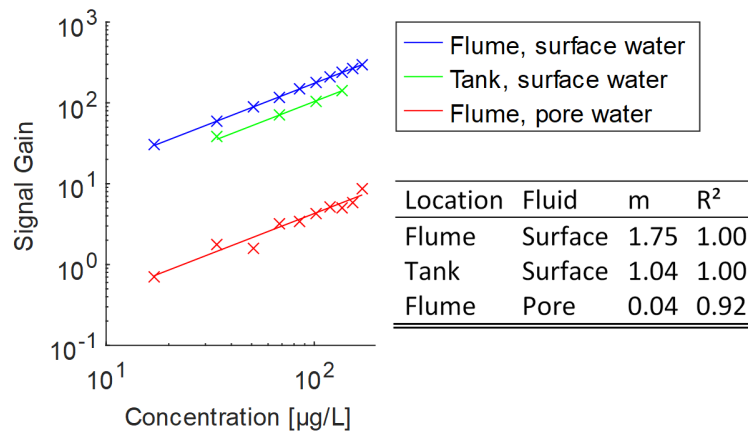
Figure S4: Calibration of the FIS, showing center ROI-averaged data (Exp 4)
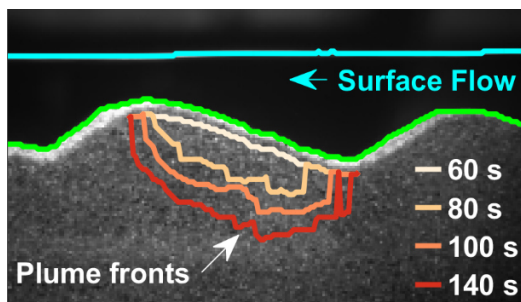
Figure S5: Infiltration fronts after selected timesteps of the infiltration experiment (Exp 6)

6

Exp-Nr	Experiment Type	Measurements	Flume filling	Water flow	MP size [µm]	MP injected
1	Calibration	Fluorometer	-	-	1; 10	-
2	Calibration	Spectrometer	-	-	1	-
3	Calibration	FIS (small FOV)	None	-	1	-
4	Calibration	FIS (large FOV)	None; sediment	-	1	-
5	Recovery Rate	Fluorometer, FIS	None	linear	1	231 µg/ $4 \cdot 10^8$#
6	Infiltration	Fluorometer, FIS	Sediment	recirculating	1	26 mg/ $5 \cdot 10^{10}$#

Table S1. Overview of the presented datasets. FIS = Fluorescence-Imaging-System, FOV = (camera) field of view, MP = microplastics. The experiments were carried out with fluorescent polystyrene microbeads

c_{min} [µg/L]	c_{max} [µg/L]	N [1]	Fluorometer Inflow			Fluorometer Outflow		
			R^2 [-]	DL [µg/L]	QL [µg/L]	R^2 [-]	DL [µg/L]	QL [µg/L]
0.4	4124.0	14	1.000	33.4	50.0	1.000	33.8	50.7
8.2	82.5	10	0.993	11.9	17.6	0.994	10.7	16.0
0.8	8.2	10	0.992	1.3	1.9	0.995	1.0	1.6
0.2	2.1	10	0.987	**0.6**	**0.9**	0.994	**0.6**	**0.9**

Table S2. Calibration details for fluorometers and detection limit (Exp 1)

7

c_{min} [µg/L]	c_{max} [µg/L]	N [1]	R^2 [-]	DL [µg/L]	QL [µg/L]
24.4	243.9	10	0.998	20.5	30.6
4.9	48.8	10	0.995	6.2	9.3
1.2	12.2	10	0.930	5.5	8.1
0.1	1.2	10	0.986	**0.5**	**0.8**

Table S3. Calibration details for the fluorescence spectrometer and detection limit (Exp 2)

c_{min} [µg/L]	c_{max} [µg/L]	N [1]	R^2 [-]	DL [µg/L]	QL [µg/L]
0.93	185.33	10	0.998	5.5	8.2
0.93	185.33	9	0.999	1.6	2.4
0.93	162.16	10	0.999	3.0	4.5
0.75	18.08	9	0.973	2.4	3.5
		mean	**0.992**	**3.1**	**4.7**

Table S4. Calibration details for the Fluorescence-Imaging-System and detection limit (Exp 3).

Movie S1. Infiltration of microplastics into the hyporheic zone (Exp 6).

8

7 Publications and manuscripts

Study 2: Assessing the Behavior of Microplastics in Fluvial Systems: Infiltration and Retention Dynamics in Streambed Sediments

Authors: **Jan-Pascal Boos**, Franz Dichgans, Jan H. Fleckenstein,
Benjamin-Silas Gilfedder, Sven Frei

Check for updates

AGU **ADVANCING EARTH AND SPACE SCIENCES**

Water Resources Research®

Assessing the Behavior of Microplastics in Fluvial Systems: Infiltration and Retention Dynamics in Streambed Sediments

Jan-Pascal Boos[1] ⓘ, Franz Dichgans[2] ⓘ, Jan H. Fleckenstein[2,3] ⓘ, Benjamin Silas Gilfedder[1,4] ⓘ, and Sven Frei[5] ⓘ

[1]Department of Hydrology, Bayreuth Center of Ecology and Environmental Research (BAYCEER), University of Bayreuth, Bayreuth, Germany, [2]Department of Hydrogeology, UFZ – Helmholtz Centre for Environmental Research, Leipzig, Germany, [3]Hydrologic Modeling Unit, Bayreuth Center of Ecology and Environmental Research (BAYCEER), University of Bayreuth, Bayreuth, Germany, [4]Limnological Research Station, Bayreuth Center of Ecology and Environmental Research (BAYCEER), University of Bayreuth, Bayreuth, Germany, [5]Wageningen University Research Centre, Department of Environmental Science, Aquatic Ecology and Water Quality Management Group, Wageningen, The Netherlands

Abstract Microplastics (MPs) have been detected ubiquitously in fluvial systems and advective transfer has been proposed as a potential mechanism for the transport of (sub-) pore-scale MPs from surface waters into streambed sediments. However, the influence of particle and sediment properties, as well as the hydrodynamic flow regime, on the infiltration behavior and mobility of MPs in streambed sediments remains unclear. In this study, we conducted a series of flume experiments to investigate the effect of particle size (1–10 µm), sediment type (fine and coarse sand), and flow regime (high/low flow) on particle infiltration dynamics in a rippled streambed. Quantification of particles in the flume compartments (surface flow, streambed interface, and in the streambed) was achieved using continuous fluorescence techniques. Results indicated that the maximum infiltration depth into the streambed decreased with increasing particle size (11, 10, and 7 cm for 1, 3, and 10 µm). The highest particle retardation was observed in the fine sediment experiment, where 22% of the particles were still in the streambed at the end of the experiment. Particle residence times were shortest under high flow conditions, suggesting that periods of increased discharge can effectively flush MPs from streambed sediments. This study provides novel insights into the complex dynamics of MP infiltration and retention in streambed sediments and contributes to a better understanding of MPs fate in fluvial ecosystems. Quantitative data from this study can improve existing modeling frameworks for MPs transport and assist in assessing the exposure risk of MPs ingestion by benthic organisms.

Plain Language Summary Microplastics (MPs) (small plastic particles) are present in river systems worldwide. The processes that lead to their transport and retention in rivers are not fully understood. Scientists have proposed that the infiltration of surface water into the streambed can carry MPs with it. In this study, we conducted experiments in a controlled environment that resembles a stream and its streambed. We investigated how different sizes of plastic particles (1, 3, and 10 µm), the types of sediment (fine and coarse sand), and water flow rates (low and high) affect how far particles travel in a streambed. We found that the size of MPs played a significant role in their depth of infiltration. Larger particles did not infiltrate as deeply as smaller particles, and were also retained in the streambed. Fine sand trapped particles for a longer time than coarse sand, and 22% of the particles remained in the streambed until the end of the experiment. Faster flowing water quickly removed MPs from the streambed. Our research helps understand how MPs spread in river systems and how long they remain in the streambed. The data can be used to improve transport models and assess the risk MPs pose to aquatic organisms.

1. Introduction

Plastic production has continuously increased over the last decades (PlasticsEurope, 2022). After usage, the majority of plastic waste is not properly managed (Lebreton & Andrady, 2019) and plastic pollution in the environment is now a global concern (Persson et al., 2022). Microplastics (MPs), small polymer compounds smaller than 5 mm (Frias & Nash, 2019) have been ubiquitously detected in marine (Gola et al., 2021), limnic (Yang et al., 2022) and riverine environments (Eerkes-Medrano et al., 2015). MPs can be incorporated by aquatic biota (Scherer et al., 2018) and trigger adverse effects on the organism (Brehm et al., 2022). Following bioaccumulation in higher trophic levels (Bhatt & Chauhan, 2023), MPs are reported to threaten aquatic ecosystems

(Anbumani & Kakkar, 2018), which makes it crucial to understand the transport mechanisms governing the fate of MPs in fluvial systems (Horton & Dixon, 2018).

Traditionally, rivers and streams were treated as pure transport vectors, where MPs are transported to the oceans and eventually buried in deep sea sediments (Kumar, Sharma, Manna, & Jain, 2021; Meijer et al., 2021; Woodall et al., 2014). In recent literature, fluvial systems are also discussed as potential accumulation areas for MPs (van Emmerik et al., 2022), which can be retained by instream vegetation (Shi et al., 2022), on floodplains (Rolf et al., 2022), river banks (Liong et al., 2021) and in streambed sediments (Frei et al., 2019; Yang et al., 2021). MPs in rivers and streams are subject to a variety of transport processes (Kumar, Sharma, Verma et al., 2021) and exhibit unique transport characteristics (Waldschläger & Schüttrumpf, 2019) and transport modes compared to natural particles such as mineral sediments (Valero et al., 2022). Flow conditions (Haberstroh et al., 2020), channel characteristics (Mostefaoui et al., 2022) and particle properties (Ahmadi et al., 2022; Elagami et al., 2022) are the major controls for the hydrodynamic transport behavior of MPs in fluvial systems. Surface flow velocity has a direct effect on the abundance of MPs in streambed sediments (Eibes & Gabel, 2022): Low flow velocities, such as found in pool structures or near river banks, facilitate gravitational settling, and can lead to a temporal accumulation of MPs in streambed sediments (Hübner et al., 2020) which can be reversed during flooding (Ockelford et al., 2020).

The mechanisms controlling the transfer of MPs between the surface flow domain and the streambed sediments, as well as the factors influencing their mobility within porous media, remain only poorly understood. Similar to solutes, the transport of (sub-) pore-scale MPs into streambed sediments can be driven by hyporheic exchange (Boos et al., 2021; Frei et al., 2019). Instead of being transported conservatively through bedform structures and being released back into the stream (Brunke, 1999), MPs were found to infiltrate into shallow layers of the hyporheic zone, where they can be temporally or permanently immobilized (Harvey et al., 2012). Simulations from headwater streams suggest that characteristic MPs residence times within streambed sediments can vary across different temporal scales, ranging from a few hours to several years (Drummond et al., 2022). Lower density MPs exhibited highest mobility within streambed sediments (He et al., 2021). In column experiments, retention of MPs was found to be strongly affected by sediment properties such as type and content of clay minerals (Lu, Gilfedder, Peng, Niu, & Frei, 2021), the presence of iron-oxides as well as pore water chemistry (Lu, Gilfedder, Peng, Peiffer et al., 2021). Retention mechanisms in porous media are primarily dependent on particle size, where larger particles (>30 µm) are prone to mechanical straining within the pore space and where the mobility of smaller particles (≈1 µm) is affected by heteroaggregation with sediments (Herzig et al., 1970). In the range of 3–30 µm, particles exhibit a high mobility within the porous media due to little mechanical straining and aggregation. For larger MPs (>100 µm) column experiments have shown that the infiltration depth into coarse sediments primarily depends on the particle/sediment grain size ratio $D = d_{MP} \, d_{Sediment}^{-1}$ (Waldschläger & Schüttrumpf, 2020). To deepen our understanding of the transport behavior of MPs in streambed sediments further research beyond the limitations of simplified one-dimensional column experiments is necessary. It is necessary to consider more realistic hydrodynamic conditions as well as different MPs properties (e.g., size, density, shape and surface properties) and sediment characteristics (e.g., grain size distribution, permeability and mineral composition) (Waldschläger et al., 2022).

Recently, a quantitative method was developed for the spatiotemporal analysis of transport mechanisms of MPs in an experimental flume environment (Boos et al., 2021). Experiments have shown that (sub-) pore scale MPs are advectively transferred into streambed sediments through infiltrating stream water along defined flow paths, supporting the hypothesis that hyporheic exchange is a significant mechanism for the transfer of small MPs into streambed sediments (Boos et al., 2021). In these experiments, propagation of 1 µm polystyrene beads through the streambed resembled a pattern commonly encountered for solutes (Elliott & Brooks, 1997; Thibodeaux & Boyle, 1987): Particles infiltrated at the upstream stoss side of ripple structures, propagated through the sediment following the hydraulic head gradient and were released at the downstream lee side. Although the experimental setup was limited to a specific combination of MPs (1 µm polystyrene beads), sediment types (mean diameter 1 mm) and hydrodynamic forcing (mean velocity 0.17 m s^{-1}) important insights into the complex behavior of MPs in fluvial systems were gained.

Building on previous work by Boos et al. (2021), we utilized quantitative methods to further explore the transport behavior of MPs in the surface water, at the streambed interface and within streambed sediments. The objective of this study is to investigate the influence of particle size (1–10 µm) on the infiltration dynamics and

65
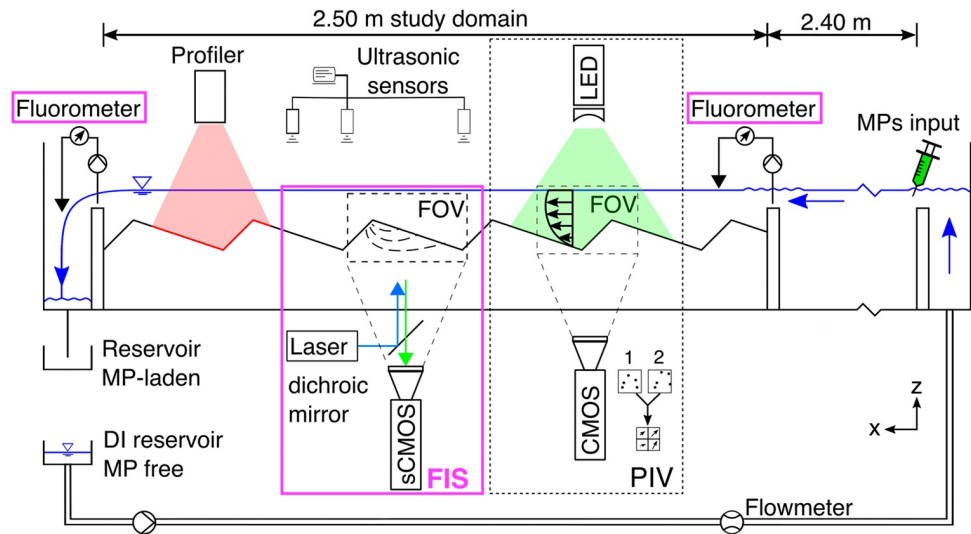
Figure 1. Schematics of the experimental flume setup: Tracking of Microplastics in the surface water (fluorometers) and within the streambed sediments Fluorescence-Imaging-System (FIS), and hydrodynamic measurements with Particle-Image-Velocimetry (PIV), complemented by water level measurements with ultrasonic sensors and bedform elevation measurement with a laser profiler. Note that FIS and PIV were consecutively applied at the same bedform. Modified after Boos et al. (2021).

penetration depths of MPs in different streambed sediments (fine/coarse sand) under varying hydrodynamic conditions (low/high flow). For this purpose, we performed a set of experiments using fluorescent MPs in an experimental flume environment in combination with sediments to represent typical rippled bedform structures found in fluvial systems. The experiments provided quantitative data that was used to estimate particle retardation capacities in streambed sediments as well as spatially distributed information about the particle mobility in rippled bedform structures. Computational Fluid Dynamics (CFD) simulations were used for the characterization of the hydrodynamic forcing at the streambed interface that controls hyporheic exchange and to better understand the flow conditions in the streambed sediments.

2. Materials and Methods

2.1. Flume Setup and Hydrodynamic Measurements

Transport experiments were carried out in an open-circuit flume (5 • 0.086 • 0.30 m, HM 160, G.U.N.T. GmbH), with an elevation gradient of 3 mm/m (Figure 1). The discharge in the flume (1–2 m^3 hr^{-1}) was continuously monitored using an electromagnetic flowmeter (flowTRANS MAG S01, Jumo GmbH) and resulted in surface flow velocities of approximately 0.07–0.11 m s^{-1}. The flume was operated using deionized water to avoid MPs aggregation. Water temperature was monitored using a temperature logger (Model 3001, Solinst Canada Ltd). A study domain within the flume was defined using a weir plate at $x = 2.40$ m distance from the flume inlet and a V-notch weir at $x = 4.90$ m, both were 15 cm high. An additional weir plate was positioned at the inlet ($x = 0$ m) to provide a homogeneous inflow.

Within the study domain, the streambed was manually formed from unimodal sands of two different types for the different experiments, characterized by a mean diameter of 1.0 mm (coarse) and 0.4 mm (fine). The streambed consisted of a series of 9 consecutive ripple structures, closely resembling a geometry commonly found in natural streams (Haque & Mahmood, 1985), with a height of 2.8 cm and a length of 20 cm of which 58% corresponded to the stoss side. The bedform morphology was measured along a 50 cm transect (including multiple ripple structures) using a 2D laser profile sensor (MLSL226, wenglor sensoric GmbH), which allowed us to monitor bedform stability during the experiments (Figure S1 in Supporting Information S1). After the experiment, the entire streambed elevation profile in the flume was measured using the laser profiler (measurement resolution of 4 mm^{-1}).

The water surface elevation was measured using 6 ultrasonic sensors (UFP 200, WayCon GmbH), providing information on the local water surface slope and an estimate of the discharge from the weir head, using Thompson

Table 1
Characteristics of the Experiments.

ID [-]	d_{MP} [μm]	d_S [μm]	$D = d_{MP} \ d_S^{-1}$ [1]	Q [m³h⁻¹]	$\bar{v}_x$ [ms⁻¹]	m_0 [mg]
1 μm	1	1032	0.0010	1.09	0.076	54
3 μm	3	1032	0.0029	1.09	0.070	98
10 μm	10	1032	0.0097	1.00	0.079	78
Fine sand	1	357	0.0028	1.05	0.066	53
High flow	1	1032	0.0010	2.15	0.114	28

Note. d_{MP} refers to the microplastic (MP) diameter, d_S to the mean sediment diameter, $D = d_{MP} \ d_S^{-1}$ the particle/sediment grain size ratio, Q is the discharge, $\bar{v}_{x,}$ is the mean longitudinal velocity in the surface flow (calculated from Particle-Image-Velocimetry measurements) and m_0 is the total input mass of MPs.

overflow coefficients. The 2D surface flow velocities along the longitudinal and vertical axis (x-z-plane) were measured using Particle-Image-Velocimetry (PIV). An LED sheet ($\lambda \approx 520$ nm, LPS3, iLA_5150 GmbH) illuminated a flow section along the flume centerline and images were acquired with a CMOS camera (UI3370, iDS Imaging GmbH), mounted on an optical rail. The flow field was measured over a selected bedform, between $x = 3.65$ m and $x = 3.85$ m, as well as its two adjacent ripples. 9 individual PIV measurements were merged, each using time averages of 1000 frames acquired at 40 Hz with a spatial resolution of 136 μm/pixel.

2.2. Experimental Procedure

Five different experiments were carried out to investigate the influence of (a) particle sizes (1, 3 and 10 μm beads), (b) sediment types (fine and coarse sand), and (c) hydrodynamic flow conditions (low/high flow) on the particle infiltration patterns and dynamics (characteristics of the experiments are provided in Table 1). The experiment using 1 μm particles, low flow conditions and coarse sediment was used as a reference case. Prior to all experiments, the measurement systems were calibrated, and the flume including the sediments were cleaned with deionized water to remove any residual MPs from previous work. A rippled streambed was formed and before the experiments started, the flume was run in a closed circuit for 2 h, and until optical inspection assured bedform stability. For the experiments, the water circuit was opened, and a concentrated MPs suspension was injected as a pulse into the surface flow at the inlet of the flume. Experiments were terminated after 30 min, after which concentrations in the outflow were below the detection limit, and optical inspection suggested no major change in MPs abundances in the monitored bedform. The input mass of MPs was chosen based on the particle size, flume discharge, and logistical constraints, to achieve ideal conditions to record the concentrations in the experiments. Importantly, the differences in initial masses are highly unlikely to significantly impact transport processes in both the surface water and the streambed. This is due to the fact that (a) the MPs were coated with a surfactant to prevent homoaggregation and (b) the overall mass of applied MPs (approximately 50 mg) is orders of magnitude lower than the sediment mass within the flume (approximately 50 kg), effectively ruling out any substantial streambed clogging processes.

2.3. Microplastic Detection and Quantification

The experiments were carried out with polystyrene microbeads with diameters of 1, 3 and 10 μm and a density of 1050 kg m⁻³ (Fluoresbrite® Plain YG Microspheres, PolySciences Inc.). The particles were internally coated with a fluorophore characterized by a maximum excitation and emission wavelength of 441 and 486 nm, respectively. Details about the coating process are considered confidential by the manufacturer. MPs monitoring is based on novel fluorometric techniques presented in Boos et al. (2021): Continuous detection of MPs-concentrations in the in- and outflow of the study domain of the flume was achieved by using portable fluorometers (GGUN FL-24, Albillia Co.) which were positioned at the weir overflows at $x = 2.40$ m and $x = 4.90$ m, measuring at 0.5 Hz (Figure 1). At the bedform structure selected for detailed study, between $x = 3.65$ m and $x = 3.85$ m, a Fluorescence-Imaging-System (FIS) was used to analyze MPs transport in the surface flow, at the streambed interface and in the streambed sediments near the glass interface of the flume. Two continuous-wave diode-pumped solid-state lasers (MBL-F-457, CNI Ltd) were used to excite the fluorescent particles and a scientific complementary metal-oxide-semiconductor (sCMOS) camera (Andor Zyla 5.5, Oxford Instruments) captured fluorescence images with a spatial resolution of 170 μm/pixel, using an exposure time of 100 ms and a frame rate of 8 Hz.

The MPs mass concentrations at the in- and outflow location of the surface water were normalized according to Equation 1 to allow for a comparison between the individual experiments. A normalized mass transfer (NMT) $\dot{m}$ [T⁻¹] was calculated using c [ML⁻³] the measured particle concentration, Q [L³T⁻¹] the observed discharge in the flume and m_0 [M] the mass of MPs input.

$$\dot{m}_{in,out}(t) = \frac{c_{in,out}(t) \cdot Q(t)}{m_0} \tag{1}$$

For any time t, integration of the NMT yields the total mass of MPs that has entered respectively left the study domain. The difference between the in- and outflow mass was normalized by the inflow mass, and this mass fraction was interpreted as MPs present in the study domain. At the end of each experiment the integration of the NMT at the in- and outlet yields a MPs recovery rate that was used to compare MPs retention for the different experimental scenarios.

MPs abundances in the control bedform were continuously quantified using the method outlined in Boos et al. (2021), where abundances were estimated by systematically analyzing the spatially averaged light intensities of the FIS images (Text S1 in Supporting Information S1). Detection limits for MPs in the streambed sediments were estimated from the calibration curve (Funk et al., 1985) and normalized using Equation 1. Spatial infiltration dynamics of MPs into the monitored bedform were estimated by extracting breakthrough curves at different depths (1–11 cm) below the ripple crest from the FIS monitoring (averaging depth for each breakthrough curve was 1 cm). Depth-specific breakthroughs were additionally filtered by rejecting the earliest and latest 5% of MPs detection in order to exclude outliers and reduce experimental artifacts. The start of MPs detection in each layer represented the arrival of the plume front and from the slope $\partial z/\partial t$, depth-specific vertical propagation velocities were calculated.

Due to the limited resolution of the FIS, it was not possible to track individual 1 and 3 µm particles within the monitored streambed. Resolution was however sufficient for the larger 10 µm particles, allowing to monitor their positions in a 2D plane of the bedform by using "blob" detection algorithms (The MathWorks Inc, 2019). Here, a pre-defined mask was used to differentiate between particles that infiltrated at the stoss side and particles which deposited from the surface water on the lee side of the bedform. Only images with more than 20 detected particles were used in the analysis. Infiltration dynamics was assessed using two aggregated metrics: (a) The center of mass of the particle cloud was calculated by averaging the individual positions and (b) the front of the infiltration plume was obtained by connecting the outermost particles.

2.4. Integrated Simulation of Surface and Porous Media Flow

To gather additional insight on the hydraulic conditions in the flume, a numerical model was built using the computational fluid dynamics toolbox OpenFOAM. The 3D integral model of surface and subsurface flow was solved using the multiphase solver interFoam. To accurately resolve the turbulent flow, specifically on the lee side of each ripple, turbulence was modeled using Large-Eddy-Simulation algorithms. The numerical model was built as direct representation of the geometries of the flume and the bedforms and used the measured information on hydrodynamical characteristics of the flow for model calibration. Additional details about the numerical model are given in Text S2 in Supporting Information S1. The methodology is also described and validated in Dichgans et al. (2023). By employing the integrated hydro-numerical model, the data set gained through the laboratory equipment can be augmented specifically in regard of the subsurface flow field and the hydrodynamic forcing at the streambed interface, which cannot be captured accurately through a physical recording in the laboratory.

3. Results

3.1. Hydrodynamic Characterization of the Flow

In the surface water compartment, the flow regime is separated into a fast-flowing upper region and a slower bottom-near region (Figures 2a–2d). This flow separation was observed for both low flow, and high flow regimes. For the low flow experiments, the mean horizontal velocity was $\bar{v}_{x,\text{top}} = 0.11$ m s^{-1} in the upper flow regime and $\bar{v}_{x,\text{bottom}} = 0.03$ m s^{-1} in the lower regime. Figures 2e and 2f show the 2D distribution of vertical velocity components in the surface water above the monitored bedform within the study domain of the flume. In all experiments, low-velocity recirculation eddies developed in the valley areas of the bedforms with flow components directed downwards for the stoss sides and upwards for the lee sides (Figures 2e and 2f).

The numerical model reproduced the surface flow field accurately (Figures 3a and 3b). Minor differences were observed in direct proximity to the overflow section of the ripple crest (0.01–0.02 m s^{-1}). This deviation was acceptable, given the turbulent flow conditions in the surface water, and a non-uniform flow field that varied over
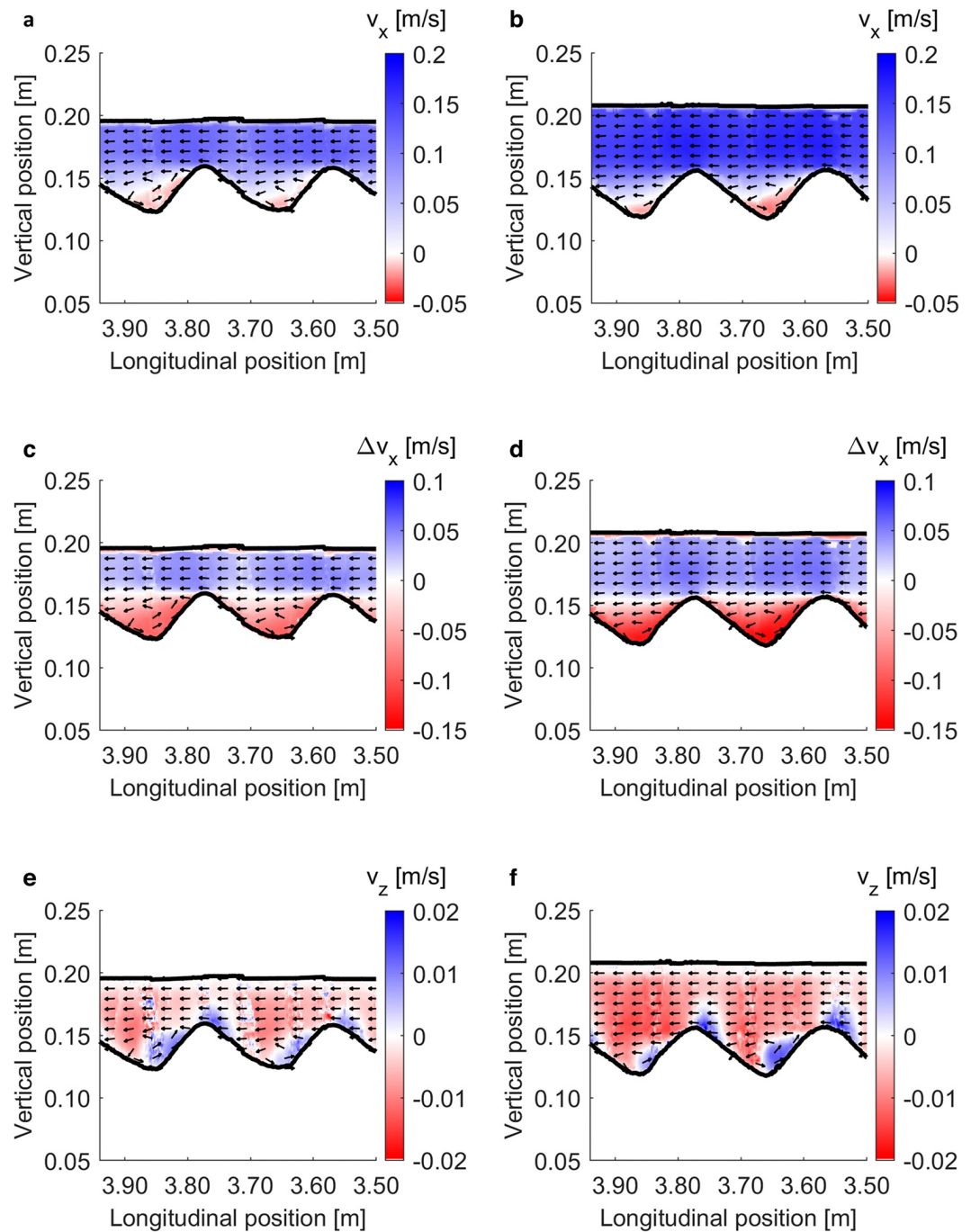
Figure 2. Hydrodynamic characterization of the surface flow field at the monitored bedform. First column (a,c,e): low-flow (reference) experiment, second column (b,d,f): high-flow experiment. (a) and (b): Horizontal velocity components, mean flow direction was from right to left. (c) and (d): Difference between local velocity and mean velocity in longitudinal direction, indicating a separation into a rapidly flowing upper region and a low-flow area in proximity to the ripples. (e) and (f): Vertical velocity components, red colors indicate downward flow, blue colors upward flow.

the flume width. Within the subsurface, individual flow cells developed under the ripples (Figure 3c). Beneath the flow cells, a continuous underflow layer was forming. Hyporheic flow depended on surface flow, and water entered at the upstream stoss side, and left at the downstream lee side, in proximity to the ripple crest. Subsurface flow velocities ranged between 0.01–2 mm s^{-1}.
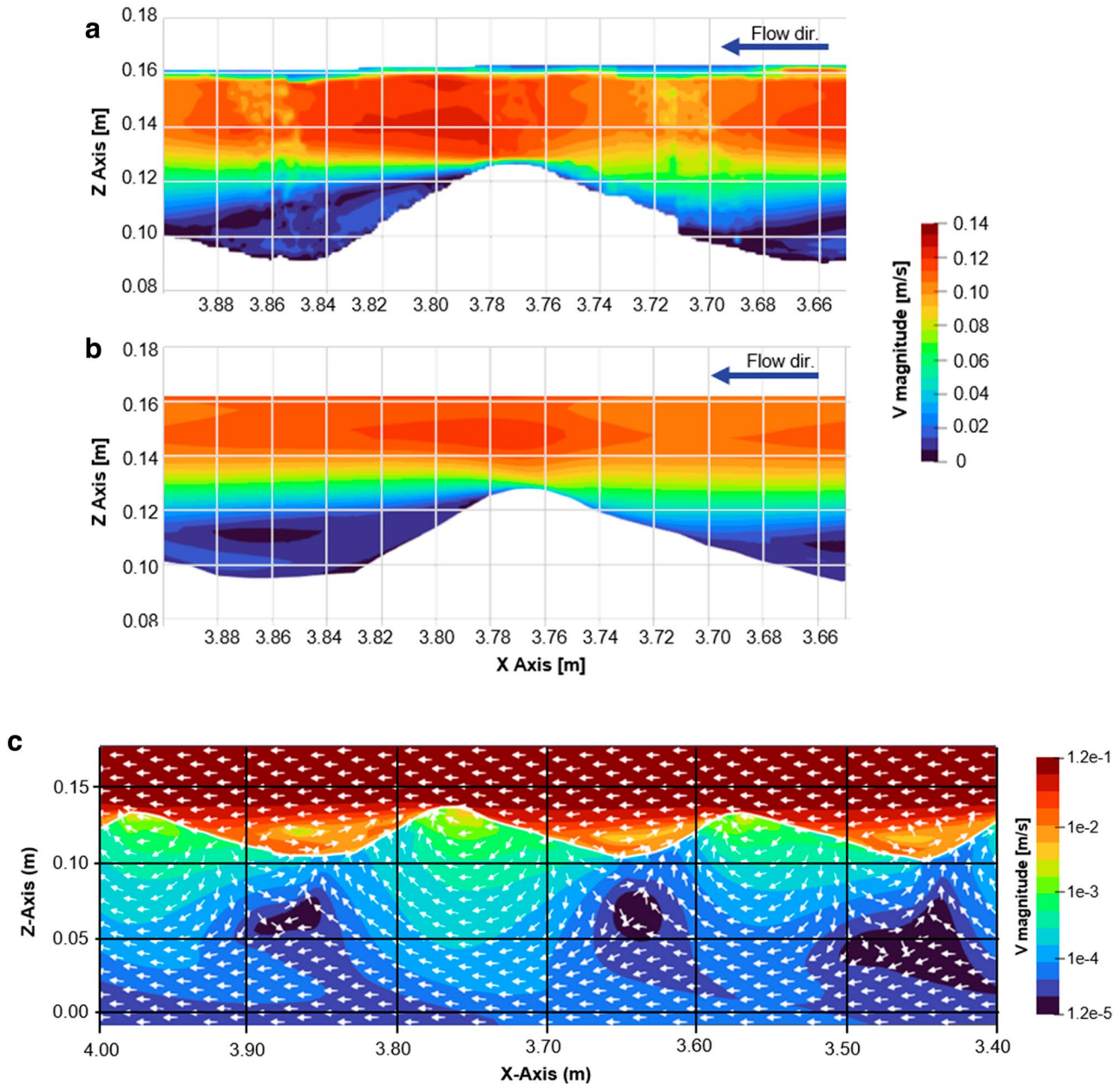
Figure 3. Velocity magnitudes in the low-flow (reference) experiment. Results for the surface flow obtained from (a) Particle-Image-Velocimetry, and (b) the openFOAM model show a close correlation. The numerical model additionally yields information on the subsurface flow domain (c).

3.2. Quantification of Particle Breakthrough and Retention

Figure 4a shows the NMT breakthrough curves for the different experiments which were measured in the surface water, using the fluorometer installed at the outflow location of the study domain. Initial timing of the particle breakthrough was similar for all experiments using low flow conditions and coarse sediments (Figure 4a). Here peak arrival times at the outflow were almost identical for the 1, 3 and 10 μm particles (136–146 s). In comparison to the reference experiment with 1 μm particles, peak NMT was higher for both 3 μm particles (+17%) and 10 μm particles (+9%). In the experiment with fine sediments, migration of the particle plume in the study domain was slowest as indicated by the longer peak arrival time of 168 s and peak mass 14% lower than the reference. In the high flow experiment, peak NMT was 77% higher than in the reference experiment and the peak was observed after 89 s, which was the fastest peak arrival time among all experiments.
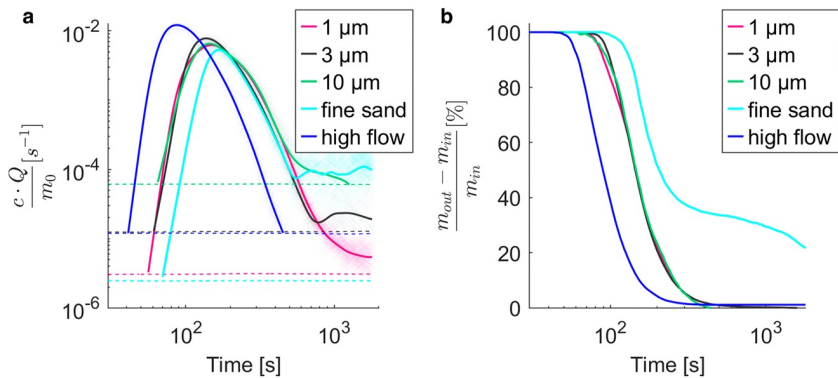
Figure 4. Results of surface water concentration measurements. (a) Normalized microplastics (MPs) mass transfer rates for the experiments measured at the outflow location of the study domain. Dashed lines indicate size-dependent, individual quantification limits, obtained from the calibration procedure, and normalized with Equation 1. (b) Temporal evolution of MPs mass stored in the study domain for the different experiments. The 1 µm run was the reference experiment.

NMTs for the 3 and 10 µm particles decreased more slowly during the receding limb of the breakthrough curves compared to the 1 µm particles, indicating a higher particle residence time in the study domain (Figure 4a). Higher residence times for the 3 µm particles are further supported by the presence of a secondary peak in the tail of the breakthrough curve. This secondary peak indicates a late increase in particle concentration in surface flow and we attributed this to the release of particles from the streambed sediments. Multiple secondary peaks can also be observed in the tail of the breakthrough curve for the experiment with fine sediments (Figure 4a). This experiment shows the highest particle concentrations in surface flow at the end of the experiment, indicating high particle residence times in the study domain. Particle concentrations for the high flow experiment fell below the detection limit after 450 s, which precluded any meaningful characterization of the tailing behavior and dynamics of particle retention.

MPs storage in the study domain was comparable for the different MPs sizes and was <5% after 304–307 s (Figure 4b). Stored mass fractions showed the most rapid decrease in the high flow experiment, with 95% of the total particle mass being flushed out from the study domain after 191 s. For the fine sediment experiment, 60% of the total mass was rapidly flushed (within 266 s) from the study domain through the surface flow. Afterward, MPs was slowly released over time, suggesting particle release from the streambed sediments. At the end of the fine sediment experiment, a significant mass of particles (22%) was still present in the study domain.

3.3. Particle Infiltration Dynamics and Penetration Depths

For all experiments the central bedform in the study domain was continuously monitored using the FIS to both visualize and estimate particle concentrations in the streambed sediments. Figure 5 presents different frames of the FIS monitoring sequence ($t = 300, 600, 1200,$ and 1800 s) containing the NMT. Movie S1 additionally shows the progress of the individual experiments. FIS monitoring indicated that particles entered the streambed at the upstream stoss side of a ripple and exited at the downstream lee side near the crest. This spatial infiltration pattern was consistent for the 1 and 3 µm particles. In contrast, the 10 µm particles only infiltrated into the most superficial layers of the sediment before becoming immobilized for the remaining duration of the experiment (Figures 5, 10 µm sequence). In the experiment using fine sediments, particles only infiltrated into the shallowest areas below the streambed interface at the stoss side of the ripple structure (Figure 5, fine sand sequence). Similar to the 10 µm experiment, a high fraction of particles that infiltrated into the fine sediments remained in the bedform, as indicated by frames taken at the end of the experiments, $t = 1800$ s. In the high flow experiment, particles were more efficiently flushed from the bedform structure as indicated by the low residual concentrations at the final monitoring FIS frame.

Detectable particle infiltration for the 1 µm particles (reference experiment) began at $t = 154$ s, and particles reached a maximum depth of 11 cm below the streambed interface after 1477 s (Figures 6a and 6b). The onset of detectable infiltration for the 3 µm particles was similar to the reference experiment ($t = 152$ s), but the maximum infiltration depth of 10 cm was slightly lower compared to the 1 µm particles. For the 10 µm particles detectable

71
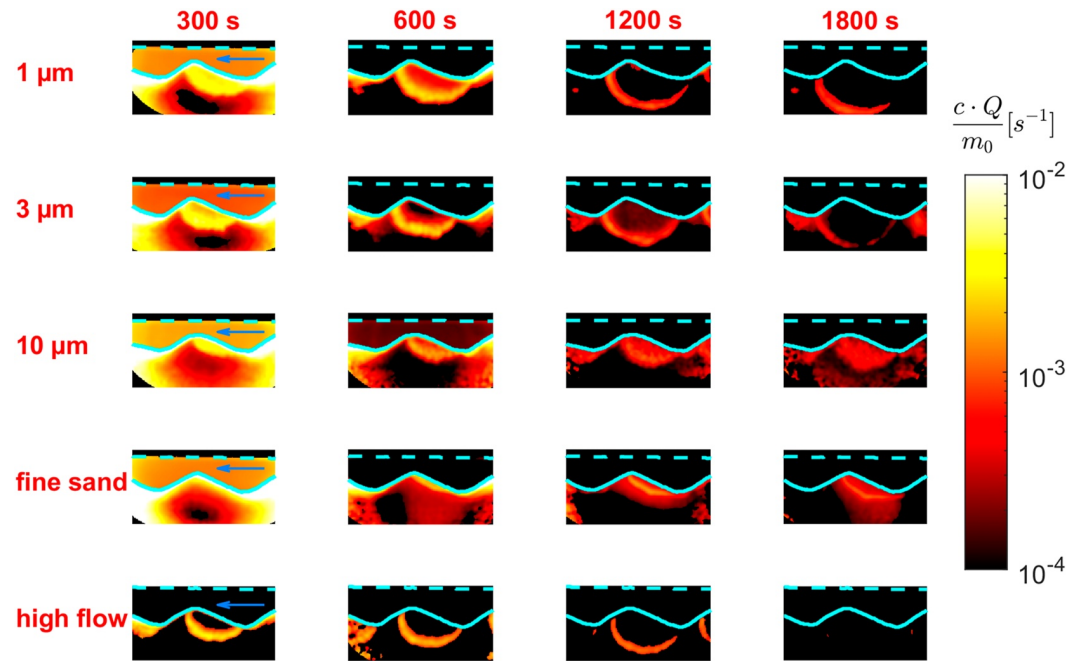
Figure 5. Planar normalized microplastic mass transfer rates for the 5 different experiments at 4 times, showing particle infiltration into the streambed sediments. The streambed interface is shown as solid line, the air-water-interface as dashed line, both in cyan color. The main direction of surface flow is from right to left, as indicated by a blue arrow at $t = 300$ s. Concentrations below the limits of quantification are discarded.

infiltration into the streambed occurred at $t = 449$ s, showing a high time delay (+294 s) compared to the reference experiment. Here particles only reached a maximum depth of 7 cm below the streambed interface. For the high flow experiment, the onset of detectable infiltration was the fastest among all experiments ($t = 121$ s), and particles reached a maximum depth of 10 cm after 1504 s. In the experiment using fine sediments, onset of particle infiltration was significantly delayed, occurring at $t = 547$ s and the maximum penetration depth of 5 cm was the lowest of all experiments. However, detection of MPs in the first 5 cm of the subsurface was nearly simultaneous for this experiment, and the data showed implausible gradients in layers deeper than 5 cm. All other experiments demonstrated consistent infiltration dynamics (Figures 6c and 6d), with high vertical propagation velocities occurring in the uppermost layers ($\sim$4 cm) below the ripple crest and an approximately exponentially decreasing trend in vertical propagation velocities with depth.

The resolution of the FIS camera was sufficient to track the fluorescent signal of individual particles through the bedform structure during the 10 μm experiment (Figure 7b). The peak of the particle count in the streambed was reached after 305 s where in total 937 particles were detected below the monitored bedform at the glass interface. During the experiment, the particle plume's center of mass moved along a trajectory approximately perpendicular to the stoss side of the ripple (Figure 7a). Propagation velocity for both, the center of mass and the plume front, initially was higher compared to later stages of the experiment, as indicated by the distance between consecutive crosses and solid lines in Figure 7a. After approximately 1500 s, both the center of mass and the plume front reached their final position, suggesting temporary or permanent immobilization of the 10 μm particles within the bedform (Figure S4 in Supporting Information S1). At the end of the experiment at $t = 1800$ s, still around 300 particles (Figure 7c) were located in the observable part of the bedform.

4. Discussion

Characterization of hydrodynamic flow conditions in the surface flow by combining PIV measurements and CFD modeling showed the presence of flow separation and the formation of recirculating eddies downstream of the rippled bedforms. The eddies and the streambed topography were responsible for an irregular distribution of dynamic and hydrostatic pressure heads over the streambed interface, driving hyporheic exchange. The hyporheic
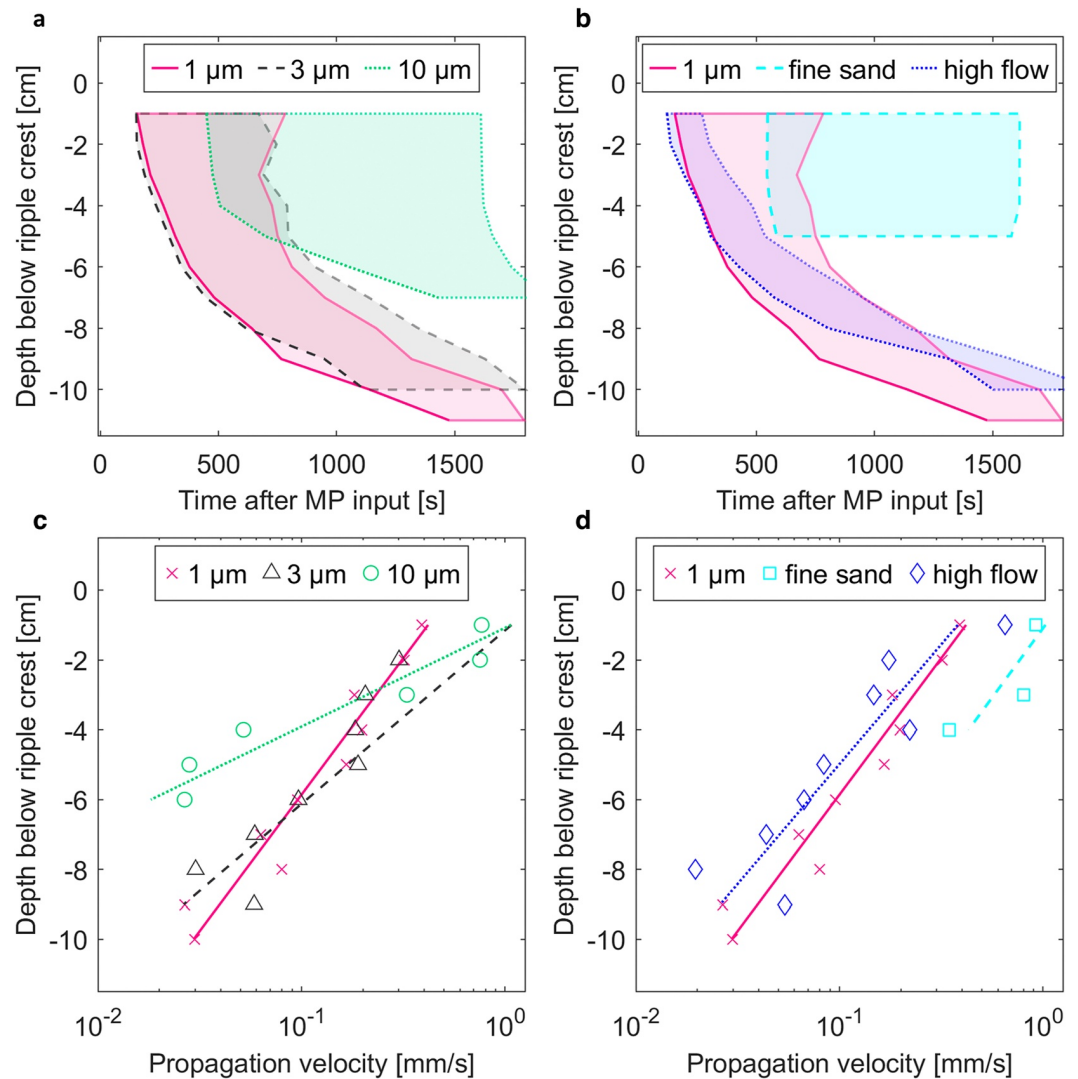
Figure 6. Particle infiltration dynamics below the ripple crest. (a–b): Infiltration depth as a function of time: Shaded areas correspond to the areas of variation based on the 5%–95% particle breakthrough criterium, highlighting the arrival of the plume front. (c–d): Vertical propagation velocities, calculated from the plume front arrival times, fitted to an exponential trendline.

flow field exhibited spatial patterns that are commonly described in literature for bedform-induced hyporheic exchange, where infiltration occurs at the stoss side and exfiltration at the lee side of the bedform structure (e.g., Elliott and Brooks (1997); Frei et al. (2018); Janssen et al. (2012); Trauth et al. (2014)). The FIS monitoring demonstrated that MPs between 1 and 10 µm were advectively transferred across the streambed interface with the preferential infiltration location at the stoss side of the bedform. While pore-scale MPs (<100 µm) have been found in high abundances in streambed sediments (Frei et al., 2019; Hurley et al., 2018), particles in this size class do not settle easily under the turbulent flow regimes found in rivers and streams. Our findings provide clear evidence that hyporheic exchange is the dominant mechanism for the transfer of small (sub-) pore-scale MPs into streambed sediments as was suggested before by Drummond et al. (2020, 2022).

Although the general patterns of MPs infiltration into the bedform structure were similar for all particles, there were differences in the infiltration dynamics, in particular the timing of the onset of detectable infiltration and the maximum penetration depth. Based on the arrival of the MPs plume below the ripple crest, all particles propagated rapidly into the first few centimeters of the bedform, and vertical propagation velocity decreased approximately exponentially with depth. This behavior matched the hyporheic flow field as expected from the

73
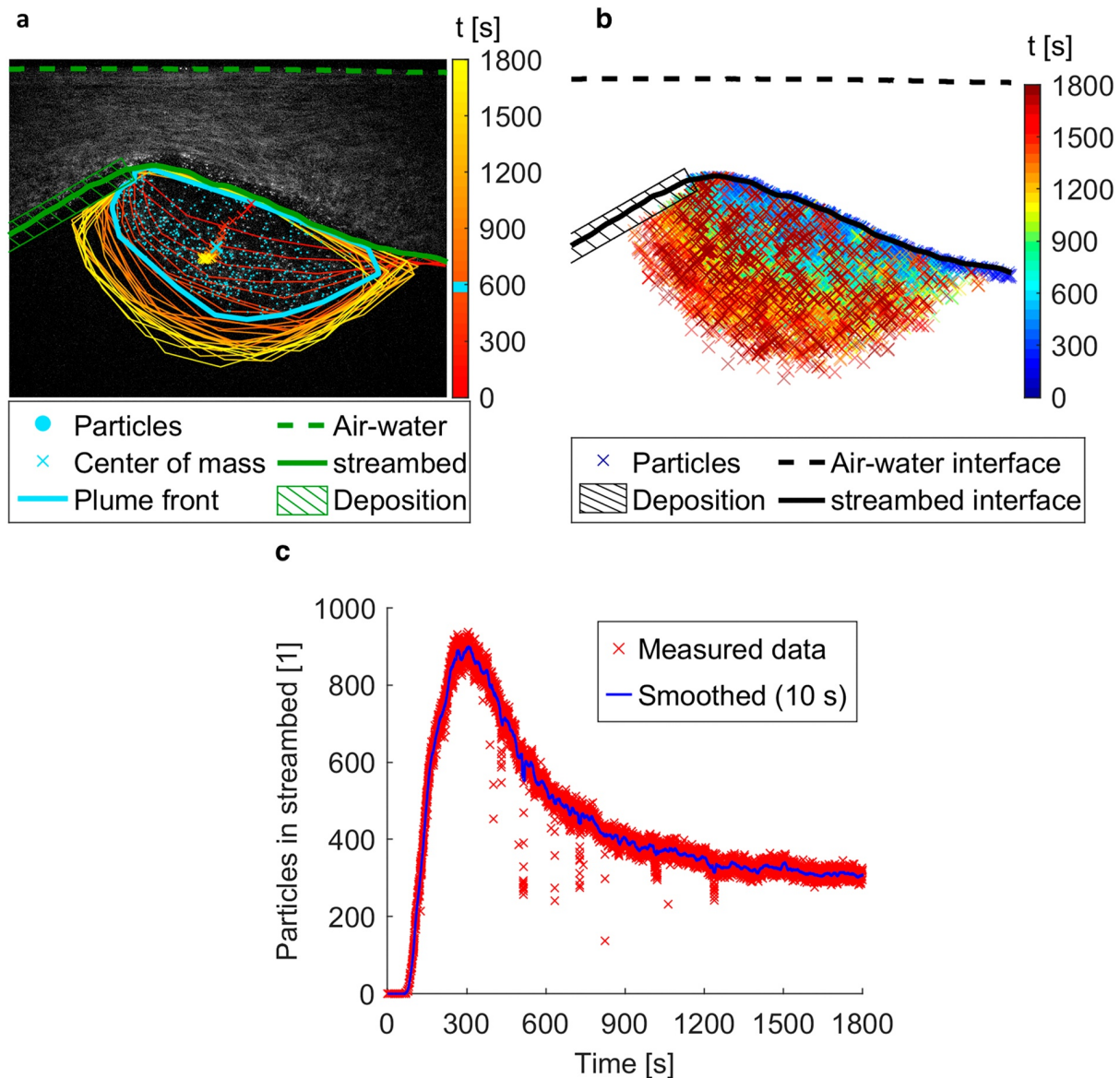
Figure 7. Infiltration experiment with 10 μm particles, analyzed by single particle tracking. (a) Particle center of mass (crosses) and plume fronts (solid lines) over time. The results are shown in 60 s-intervals during the experiment and highlighted after 600 s (cyan color), at which time also the background image was acquired, additionally indicating the detected particles (blobs). (b) Superposition of individual particle positions in the streambed, shown in 60 s-intervals during the experiment, and color-coded (blue to red), indicating the time since the start of the experiment. The air-water and streambed interfaces as well as the mask used to differentiate between infiltrated and deposited particles are shown in black. (c) Number of all particles detected in the monitored streambed section over time (red crosses), complemented by rolling mean over 10 s (blue solid line).

advective pumping model that is often used to describe bedform induced hyporheic exchange (Elliott, 1991; Grant et al., 2020; Saenger, 2000; Zhou & Mendoza, 1993). The CFD model supported this finding and additionally indicated that particle retardation in the streambed sediment increased with flow path length (Dichgans et al., 2023).

Waldschläger and Schüttrumpf (2020) used the particle/sediment grain size ratio $D = d_{MP} \, d_{S}^{-1}$ as a reliable indicator for the penetration depths of MPs into sediments. Column experiments showed that infiltration did not occur for $D > 0.32$ and penetration depths were highest for $D < 0.11$. Although the number of experiments performed in our study was limited, we also observed that higher particle/sediment grain size ratios tended to result in lower penetration depths and delayed onset of infiltration. For example, we observed the highest penetration depth of 11 cm for lowest $D = 0.001$ (1 μm particles) and a lower penetration depth of 7 cm for highest $D = 0.01$ (10 μm

particles). However, it is important to note that the 3 μm particles in coarse sediment ($D = 0.0029$) infiltrated deeper into the sediment (10 cm), than the 1 μm particles in fine sediment ($D = 0.0028$), where a maximum depth of 5 cm was observed. Although the particle/sediment grain size ratio has been identified as a reliable indicator for the infiltration depths of MPs into sediments, the relationship between D and penetration depths for bedform-induced hyporheic exchange may not be as straightforward as in one-dimensional column experiments where infiltration occurs vertically. While column studies indicate that mechanical straining becomes relevant for $D > 0.002$ (Bradford et al., 2002; Lu, Gilfedder, Peng, Niu, & Frei, 2021), the specific mechanism of particle entrainment in the streambed cannot be elucidated with the present data set. Various mechanisms influence particle transport in porous media, such as mechanical straining in the pore throats and attachment to the streambed sediments (Molnar et al., 2015). The impact of straining reduces with infiltration depth, and small particles (1–3 μm) retained deeper within the streambed may be affected more by colloid attachment (Bradford et al., 2003), which can lead to reversible as well as irreversible filtration (Chu et al., 2019). The quick decrease in concentrations of MPs and their low residuals at the end of the experiment for the 1 μm, 3 μm and high-flow experiment suggested that particle retention in the streambed was caused by reversible processes potentially facilitated by the use of deionized water in the experiment (Torkzaban et al., 2010). The retention of 10 μm particles in the streambed however suggests that mechanical straining is the dominant retention mechanism that prevents the deeper propagation of the particles into the streambed sediments.

Our experiments indicate that (sub-) pore-scale MPs exhibit high mobility in streambed sediments. In natural fluvial systems, infiltration depth is likely to exceed the depths observed in our controlled flume experiments. Bedform-driven hyporheic exchange and stream/groundwater interactions occur at various spatial and temporal scales and are influenced by multiple factors (Boano et al., 2014). Deeper hyporheic flow cells induced by head gradient variations over larger bedform structures, such as pool-riffle sequences (Frei et al., 2018), have the potential to transport particles deeper into hyporheic sediments. Also, under losing conditions where stream water infiltrates into the aquifer, mobile pore-scale MPs can be transferred into groundwater as suggested by Frei et al. (2019). In addition, hyporheic exchange is influenced by heterogeneous streambed conductivities (Laube et al., 2018; Marion et al., 2008), affecting the transport of MPs from the surface water into the streambed.

For most experiments, mass fractions of particles that entered the streambed sediments in the study domain of the flume were relatively low in comparison to particle transport in the surface water. In addition to particle size and sediment properties, particle retardation in the streambed sediments was influenced by the hydrodynamic forcing. This controls the magnitudes of advective flow velocities and volumes in the streambed sediments during hyporheic exchange. An increase in the surface flow velocity (high flow experiment) resulted in the fastest observed MPs breakthrough, and almost no residual particles were detected in the bedform at the end of the experiment, unlike in the low flow experiments. Flooding events have been recognized as significant drivers of MPs remobilization from streambed sediments, with reductions in MPs loads stored in sediments of up to 70% as reported by Hurley et al. (2018). During flooding, shear forces acting at the streambed interface lead to erosion of the bedform structures. This results in the suspension of river sediments and associated MPs and its transport through the river network. Results from our study suggest that in addition to flooding events, streambed sediments may be effectively flushed of pore-scale MPs during periods of increased discharge, under conditions when bedform structures remain stable.

In the fine sediment experiment, mass balance calculations based on the surface breakthrough curves indicated that a significant fraction of the inflowing particles (22%) was present in the study domain at the end of the experiment. Although particles can be retained in surface flow, for example, due to entrapment in recirculation eddies and at the streambed interface due to heteroaggregation, this effect was not observed in the other experiments given similar hydrodynamic conditions. This suggests that surface retention was of minor importance in the flume experiments and that most particles were retarded in the streambed sediments. This conclusion is supported by the FIS monitoring, which did not detect any trend in increasing particle concentrations in the areas where eddies are present or at the streambed interface.

Based on our experiments, we have found that fine sediment areas in streambeds have the potential to accumulate (sub-) pore-scale MPs where mechanical straining reduces particle mobility. While the duration of our flume experiments was insufficient to determine whether the particles were immobilized permanently or temporarily, results from particle tracking of 10 μm MPs suggest that a considerable portion of infiltrated particles showed a prolonged residence time. Pore-scale MPs that become immobile in fine sediment areas of streambeds pose an

75

increased risk for uptake by benthic organisms, since longer exposure times increase the likelihood of ingestion. Under these conditions, hyporheic sediments are especially vulnerable to MPs accumulation and can represent a primary entry point for MPs into riverine food webs (Huang et al., 2021; Wagner et al., 2014). Fine sediment loadings in many rivers and streams have been observed to exceed background levels, primarily due to changes in land cover, land use, and management practices (Collins & Zhang, 2016; Farnsworth & Milliman, 2003; Foster et al., 2011; Owens et al., 2005). It is anticipated that the trend of increasing fine sediment loadings in rivers and streams will persist in the future, due to the effects of climate change on rainfall and runoff regimes (Burt et al., 2016; Walling & Collins, 2016). This may also lead to a further accumulation of MPs in streambed sediments, exacerbating the existing issue.

This study analyzed the transport of almost neutrally buoyant MPs. Density is a key factor controlling particle transport, which can be transported floating, suspended or as bedload (Waldschläger et al., 2022). For larger particles between 1–3 mm, the location of MPs in the water column is similar to mineral sediments (Born et al., 2023), indicating that higher density MPs are more likely to be transported near the streambed. Conversely, turbulent mixing, such as caused by the weir overflow in our experiment, can also transport low density MPs to the streambed interface (Shamskhany & Karimpour, 2022). Within streambed sediments, low-density MPs, such as polyethylene and polypropylene, exhibit higher mobility, whereas high-density MPs, auch as polyamide and polyethylene terephthalate, are retained (He et al., 2021). The hydrodynamic behavior is influenced by additional processes under real environmental conditions. Biofilms on the surface of MPs facilitate the formation of heteroaggregates, as particles become "sticky" due to attached extracellular polymeric substances (Hossain et al., 2019; Long et al., 2015; Michels et al., 2018). While the formation of biofilms is typically more prevalent in lentic systems, it has been reported to be relevant in rivers and streams (Weig et al., 2021). Biofilms may form on MPs prior to entering fluvial systems, for example, due to their passage through wastewater treatment plants or in soils (Martínez-Campos et al., 2021; Zhang et al., 2019). The adhesive properties of biofilms may enhance the likelihood of particle heteroaggregation on the streambed, rather than being transported into the sediment via hyporheic exchange. Also, larger heteroaggregates containing both MPs and natural particles are not able to infiltrate into the streambed sediments as readily as individual, pristine particles.

Our experiments focused on the infiltration of microplastics into a stationary rippled streambed. Under natural conditions, bedform structures are rarely stable long-term. Small-scale hydrodynamical conditions create highly dynamic areas of erosion and sedimentation. As a result, bedform structures such as ripples or dunes migrate as "moving bedforms" in the direction of streamflow (Southard, 1991). The exchange of solutes and colloids between surface flow and streambed can be significantly higher for moving bedforms compared to stable bedform structures (Packman & Brooks, 2001). Recent flume experiments have demonstrated that dynamic sedimentation and erosion processes result in the preferential accumulation of clay particles within streambed sediments (Teitelbaum et al., 2021). Future research must address whether the accumulation of MPs within moving bedforms occurs similarly to that of clay particles and whether the erosion and sedimentation cycles associated with moving bedforms enhance the transfer of MPs into streambed sediments, as compared to stable bedforms where MPs exchange is purely driven by bedform-induced hyporheic exchange.

5. Conclusion

In analogy to solute transport, advective transport has been suggested as one potential mechanism driving the exchange of (sub-) pore-scale MPs between surface water and the streambed. This study confirms this hypothesis, as we were able to detect MPs migration between surface flow and streambed sediments and additionally link particle transport to the hydrodynamic characteristics of the flow. Smaller particles (1–3 μm) showed higher mobility and infiltrated into deeper areas of the sediment, while larger particles (10 μm) were retained in shallower parts of the streambed. Streambed sediment grain size had a major influence on the pattern of particle infiltration and retardation in the streambed.

Our results suggest that MPs are concentrated in the upper sediment layers in natural streams and show enhanced residence times within finer sediments. A prolonged immobilization near the streambed interface enhances the potential of particle uptake by benthic organisms and subsequent transfer within the aquatic food chain, possibly threatening local ecosystems. More work is needed to transfer the mechanistic understanding of MPs transport processes from laboratory experiments to real-world scenarios in order to improve our understanding of the fate of MPs in rivers and streams.

76

Conflict of Interest

The authors declare no conflicts of interest relevant to this study.

Data Availability Statement

The data sets as well as the developed MATLAB scripts are published in Zenodo (Boos et al., 2023a; 2023b).

References

Ahmadi, P., Elagami, H., Dichgans, F., Schmidt, C., Gilfedder, B. S., Frei, S., et al. (2022). Systematic evaluation of physical parameters affecting the terminal settling velocity of microplastic particles in lakes using CFD. *Frontiers in Environmental Science*, *10*. https://doi.org/10.3389/fenvs.2022.875220

Anbumani, S., & Kakkar, P. (2018). Ecotoxicological effects of microplastics on biota: A review. *Environmental Science and Pollution Research International*, *25*(15), 14373–14396. https://doi.org/10.1007/s11356-018-1999-x

Bhatt, V., & Chauhan, J. S. (2023). Microplastic in freshwater ecosystem: Bioaccumulation, trophic transfer, and biomagnification. *Environmental Science and Pollution Research International*, *30*(4), 9389–9400. https://doi.org/10.1007/s11356-022-24529-w

Boano, F., Harvey, J. W., Marion, A., Packman, A. I., Revelli, R., Ridolfi, L., & Wörman, A. (2014). Hyporheic flow and transport processes: Mechanisms, models, and biogeochemical implications. *Reviews of Geophysics*, *52*(4), 603–679. https://doi.org/10.1002/2012RG000417

Boos, J.-P., Dichgans, F., Fleckenstein, J. H., Gilfedder, B. S., & Frei, S. (2023). Data and code for the publication "Assessing the behavior of microplastics in fluvial systems: Infiltration and retention dynamics in streambed sediments" - Part 1. https://doi.org/10.5281/zenodo.10083568

Boos, J.-P., Dichgans, F., Fleckenstein, J. H., Gilfedder, B. S., & Frei, S. (2023). Data and code for the publication "Assessing the behavior of microplastics in fluvial systems: Infiltration and retention dynamics in streambed sediments" - Part 2. https://doi.org/10.5281/zenodo.10081788

Boos, J.-P., Gilfedder, B. S., & Frei, S. (2021). Tracking microplastics across the streambed interface: Using laser-induced-fluorescence to quantitatively analyze microplastic transport in an experimental flume. *Water Resources Research*, *57*(12). https://doi.org/10.1029/2021WR031064

Born, M. P., Brüll, C., Schaefer, D., Hillebrand, G., & Schüttrumpf, H. (2023). Determination of microplastics' vertical concentration transport (Rouse) profiles in flumes. *Environmental Science & Technology*, *57*(14), 5569–5579. https://doi.org/10.1021/acs.est.2c06885

Bradford, S. A., Simunek, J., Bettahar, M., van Genuchten, M. T., & Yates, S. R. (2003). Modeling colloid attachment, straining, and exclusion in saturated porous media. *Environmental Science & Technology*, *37*(10), 2242–2250. https://doi.org/10.1021/es025899u

Bradford, S. A., Yates, S. R., Bettahar, M., & Simunek, J. (2002). Physical factors affecting the transport and fate of colloids in saturated porous media. *Water Resources Research*, *38*(12), 63-1–63-12. https://doi.org/10.1029/2002WR001340

Brehm, J., Wilde, M. V., Reiche, L., Leitner, L.-C., Petran, B., Meinhart, M., et al. (2022). In-depth characterization revealed polymer type and chemical content specific effects of microplastic on Dreissena bugensis. *Journal of Hazardous Materials*, *437*, 129351. https://doi.org/10.1016/j.jhazmat.2022.129351

Brunke, M. (1999). Colmation and depth filtration within streambeds: Retention of particles in hyporheic interstices. *International Review of Hydrobiology*, *84*(2), 99–117. https://doi.org/10.1002/iroh.199900014

Burt, T., Boardman, J., Foster, I., & Howden, N. (2016). More rain, less soil: Long-term changes in rainfall intensity with climate change. *Earth Surface Processes and Landforms*, *41*(4), 563–566. https://doi.org/10.1002/esp.3868

Chu, X., Li, T., Li, Z., Yan, A., & Shen, C. (2019). Transport of microplastic particles in saturated porous media. *Water*, *11*(12), 2474. https://doi.org/10.3390/w11122474

Collins, A. L., & Zhang, Y. (2016). Exceedance of modern 'background' fine-grained sediment delivery to rivers due to current agricultural land use and uptake of water pollution mitigation options across England and Wales. *Environmental Science & Policy*, *61*, 61–73. https://doi.org/10.1016/j.envsci.2016.03.017

Dichgans, F., Boos, J.-P., Ahmadi, P., Frei, S., & Fleckenstein, J. H. (2023). Integrated numerical modeling to quantify transport and fate of microplastics in the hyporheic zone. *Water Research*, *243*, 120349. https://doi.org/10.1016/j.watres.2023.120349

Drummond, J. D., Nel, H. A., Packman, A. I., & Krause, S. (2020). Significance of hyporheic exchange for predicting microplastic fate in rivers. *Environmental Science and Technology Letters*, *7*(10), 727–732. https://doi.org/10.1021/acs.estlett.0c00595

Drummond, J. D., Schneidewind, U., Li, A., Hoellein, T. J., Krause, S., & Packman, A. I. (2022). Microplastic accumulation in riverbed sediment via hyporheic exchange from headwaters to mainstems. *Science Advances*, *8*(2), eabi9305. https://doi.org/10.1126/sciadv.abi9305

Eerkes-Medrano, D., Thompson, R. C., & Aldridge, D. C. (2015). Microplastics in freshwater systems: A review of the emerging threats, identification of knowledge gaps and prioritisation of research needs. *Water Research*, *75*, 63–82. https://doi.org/10.1016/j.watres.2015.02.012

Eibes, P. M., & Gabel, F. (2022). Floating microplastic debris in a rural river in Germany: Distribution, types and potential sources and sinks. *The Science of the Total Environment*, *816*, 151641. https://doi.org/10.1016/j.scitotenv.2021.151641

Elagami, H., Ahmadi, P., Fleckenstein, J. H., Frei, S., Obst, M., Agarwal, S., & Gilfedder, B. S. (2022). Measurement of microplastic settling velocities and implications for residence times in thermally stratified lakes. *Limnology & Oceanography*, *67*(4), 934–945. https://doi.org/10.1002/lno.12046

Elliott, A. H. (1991). *Transfer of solutes into and out of streambeds*. California Institute of Technology.

Elliott, A. H., & Brooks, N. H. (1997). Transfer of nonsorbing solutes to a streambed with bed forms: Laboratory experiments. *Water Resources Research*, *33*(1), 137–151. https://doi.org/10.1029/96WR02783

Farnsworth, K. L., & Milliman, J. D. (2003). Effects of climatic and anthropogenic change on small mountainous rivers: The Salinas river example. *Global and Planetary Change*, *39*(1–2), 53–64. https://doi.org/10.1016/S0921-8181(03)00017-1

Foster, I., Collins, A. L., Naden, P. S., Sear, D. A., Jones, J. I., & Zhang, Y. (2011). The potential for paleolimnology to determine historic sediment delivery to rivers. *Journal of Paleolimnology*, *45*(2), 287–306. https://doi.org/10.1007/s10933-011-9498-9

Frei, S., Azizian, M., Grant, S. B., Zlotnik, V. A., & Toundykov, D. (2018). Analytical modeling of hyporheic flow for in-stream bedforms: Perturbation method and implementation. *Environmental Modelling & Software*. (111), 375–385. https://doi.org/10.1016/j.envsoft.2018.09.015

Frei, S., Piehl, S., Gilfedder, B. S., Löder, M. G. J., Krutzke, J., Wilhelm, L., & Laforsch, C. (2019). Occurrence of microplastics in the hyporheic zone of rivers. *Scientific Reports*, *9*(1), 15256. https://doi.org/10.1038/s41598-019-51741-5

Frias, J. P. G. L., & Nash, R. (2019). Microplastics: Finding a consensus on the definition. *Marine Pollution Bulletin*, *138*, 145–147. https://doi.org/10.1016/j.marpolbul.2018.11.022

Funk, W., Dammann, V., Vonderheid, C., & Oehlmann, G. (Eds.) (1985). *Statistische Methoden in der Wasseranalytik: Begriffe, Strategien, Anwendungen*. VCH.

Gola, D., Kumar Tyagi, P., Arya, A., Chauhan, N., Agarwal, M., Singh, S. K., & Gola, S. (2021). The impact of microplastics on marine environment: A review. *Environmental Nanotechnology, Monitoring & Management*, 16, 100552. https://doi.org/10.1016/j.enmm.2021.100552

Grant, S. B., Monofy, A., Boano, F., Gomez-Velez, J. D., Guymer, I., Harvey, J. W., & Ghisalberti, M. (2020). Unifying advective and diffusive descriptions of bedform pumping in the benthic biolayer of streams. *Water Resources Research*, 56(11). https://doi.org/10.1029/2020WR027967

Haberstroh, C. J., Arias, M. E., Yin, Z., & Wang, M. C. (2020). Effects of hydrodynamics on the cross-sectional distribution and transport of plastic in an urban coastal river. *Water Environment Research*, 93(2), 186–200. https://doi.org/10.1002/wer.1386

Haque, M. I., & Mahmood, K. (1985). Geometry of ripples and dunes. *Journal of Hydraulic Engineering*, 111(1), 48–63. https://doi.org/10.1061/(ASCE)0733-9429(1985)111:1(48)

Harvey, J. W., Drummond, J. D., Martin, R. L., McPhillips, L. E., Packman, A. I., Jerolmack, D. J., et al. (2012). Hydrogeomorphology of the hyporheic zone: Stream solute and fine particle interactions with a dynamic streambed. *Journal of Geophysical Research*, 117(G4). https://doi.org/10.1029/2012JG002043

He, B., Smith, M., Egodawatta, P., Ayoko, G. A., Rintoul, L., & Goonetilleke, A. (2021). Dispersal and transport of microplastics in river sediments. *Environmental Pollution*, 279, 116884. https://doi.org/10.1016/j.envpol.2021.116884

Herzig, J. P., Leclerc, D. M., & Goff, P. L. (1970). Flow of suspensions through porous media—Application to deep filtration. *Industrial & Engineering Chemistry*, 62(5), 8–35. https://doi.org/10.1021/ie50725a003

Horton, A. A., & Dixon, S. J. (2018). Microplastics: An introduction to environmental transport processes. *Wiley Interdisciplinary Reviews: Water*, 5(2), e1268. https://doi.org/10.1002/wat2.1268

Hossain, M. R., Jiang, M., Wei, Q., & Leff, L. G. (2019). Microplastic surface properties affect bacterial colonization in freshwater. *Journal of Basic Microbiology*, 59(1), 54–61. https://doi.org/10.1002/jobm.201800174

Huang, W., Song, B., Liang, J., Niu, Q., Zeng, G., Shen, M., et al. (2021). Microplastics and associated contaminants in the aquatic environment: A review on their ecotoxicological effects, trophic transfer, and potential impacts to human health. *Journal of Hazardous Materials*, 405, 124187. https://doi.org/10.1016/j.jhazmat.2020.124187

Hübner, M. K., Michler-Kozma, D. N., & Gabel, F. (2020). Microplastic concentrations at the water surface are reduced by decreasing flow velocities caused by a reservoir. *Fundamental and Applied Limnology*, 194(1), 49–56. https://doi.org/10.1127/fal/2020/1307

Hurley, R., Woodward, J., & Rothwell, J. J. (2018). Microplastic contamination of river beds significantly reduced by catchment-wide flooding. *Nature Geoscience*, 11(4), 251–257. https://doi.org/10.1038/s41561-018-0080-1

Janssen, F., Cardenas, M. B., Sawyer, A. H., Dammrich, T., Krietsch, J., & de Beer, D. (2012). A comparative experimental and multiphysics computational fluid dynamics study of coupled surface-subsurface flow in bed forms. *Water Resources Research*, 48(8). https://doi.org/10.1029/2012WR011982

Kumar, R., Sharma, P., Manna, C., & Jain, M. (2021). Abundance, interaction, ingestion, ecological concerns, and mitigation policies of microplastic pollution in riverine ecosystem: A review. *Science of the Total Environment*, 782, 146695. https://doi.org/10.1016/j.scitotenv.2021.146695

Kumar, R., Sharma, P., Verma, A., Jha, P. K., Singh, P., Gupta, P. K., et al. (2021). Effect of physical characteristics and hydrodynamic conditions on transport and deposition of microplastics in riverine ecosystem. *Water*, 13(19), 2710. https://doi.org/10.3390/w13192710

Laube, G., Schmidt, C., & Fleckenstein, J. H. (2018). The systematic effect of streambed conductivity heterogeneity on hyporheic flux and residence time. *Advances in Water Resources*, 122, 60–69. https://doi.org/10.1016/j.advwatres.2018.10.003

Lebreton, L., & Andrady, A. (2019). Future scenarios of global plastic waste generation and disposal. *Palgrave Communications*, 5(1), 6. https://doi.org/10.1057/s41599-018-0212-7

Liong, R. M. Y., Hadibarata, T., Yuniarto, A., Tang, K. H. D., & Khamidun, M. H. (2021). Microplastic occurrence in the water and sediment of Miri river estuary, Borneo island. *Water, Air, & Soil Pollution*, 232(8), 342. https://doi.org/10.1007/s11270-021-05297-8

Long, M., Moriceau, B., Gallinari, M., Lambert, C., Huvet, A., Raffray, J., & Soudant, P. (2015). Interactions between microplastics and phytoplankton aggregates: Impact on their respective fates. *Marine Chemistry*, 175, 39–46. https://doi.org/10.1016/j.marchem.2015.04.003

Lu, T., Gilfedder, B. S., Peng, H., Niu, G., & Frei, S. (2021). Effects of clay minerals on the transport of nanoplastics through water-saturated porous media. *The Science of the Total Environment*, 796, 148982. https://doi.org/10.1016/j.scitotenv.2021.148982

Lu, T., Gilfedder, B. S., Peng, H., Peiffer, S., Papastavrou, G., Ottermann, K., & Frei, S. (2021). Relevance of iron oxyhydroxide and pore water chemistry on the mobility of nanoplastic particles in water-saturated porous media environments. *Water, Air, & Soil Pollution*, 232(5), 168. https://doi.org/10.1007/s11270-021-05125-z

Marion, A., Packman, A. I., Zaramella, M., & Bottacin-Busolin, A. (2008). Hyporheic flows in stratified beds. *Water Resources Research*, 44(9). https://doi.org/10.1029/2007WR006079

Martínez-Campos, S., González-Pleiter, M., Fernández-Piñas, F., Rosal, R., & Leganés, F. (2021). Early and differential bacterial colonization on microplastics deployed into the effluents of wastewater treatment plants. *The Science of the Total Environment*, 757, 143832. https://doi.org/10.1016/j.scitotenv.2020.143832

Meijer, L. J. J., van Emmerik, T., van der Ent, R., Schmidt, C., & Lebreton, L. (2021). More than 1000 rivers account for 80% of global riverine plastic emissions into the ocean. *Science Advances*, 7(18). https://doi.org/10.1126/sciadv.aaz5803

Michels, J., Stippkugel, A., Lenz, M., Wirtz, K., & Engel, A. (2018). Rapid aggregation of biofilm-covered microplastics with marine biogenic particles. *Proceedings of the Royal Society: Biological Sciences*, 285(1885), 20181203. https://doi.org/10.1098/rspb.2018.1203

Molnar, I. L., Johnson, W. P., Gerhard, J. I., Willson, C. S., & O'Carroll, D. M. (2015). Predicting colloid transport through saturated porous media: A critical review. *Water Resources Research*, 51(9), 6804–6845. https://doi.org/10.1002/2015WR017318

Mostefaoui, O., Lopez, D., Mignot, E., & Massardier-Nageotte, V. (2022). Extended Abstract CFTL 2022.

Ockelford, A., Cundy, A., & Ebdon, J. E. (2020). Storm response of fluvial sedimentary microplastics. *Scientific Reports*, 10(1), 1865. https://doi.org/10.1038/s41598-020-58765-2

Owens, P. N., Batalla, R. J., Collins, A. J., Gomez, B., Hicks, D. M., Horowitz, A. J., et al. (2005). Fine-grained sediment in river systems: Environmental significance and management issues. *River Research and Applications*, 21(7), 693–717. https://doi.org/10.1002/rra.878

Packman, A. I., & Brooks, N. H. (2001). Hyporheic exchange of solutes and colloids with moving bed forms. *Water Resources Research*, 37(10), 2591–2605. https://doi.org/10.1029/2001WR000477

Persson, L., Carney Almroth, B. M., Collins, C. D., Cornell, S., de Wit, C. A., Diamond, M. L., et al. (2022). Outside the safe operating space of the planetary boundary for novel entities. *Environmental Science & Technology*, 56(3), 1510–1521. https://doi.org/10.1021/acs.est.1c04158

PlasticsEurope. (2022). Plastics—The facts 2022.

Rolf, M., Laermanns, H., Kienzler, L., Pohl, C., Möller, J. N., Laforsch, C., et al. (2022). Flooding frequency and floodplain topography determine abundance of microplastics in an alluvial Rhine soil. *The Science of the Total Environment*, 836, 155141. https://doi.org/10.1016/j.scitotenv.2022.155141

78

Saenger, N. (2000). *Identifikation von Austauschprozessen zwischen Fließgewässer und hyporheischer Zone* (Vol. 115). Technische Universität Darmstadt.

Scherer, C., Weber, A., Lambert, S., & Wagner, M. (2018). Interactions of microplastics with freshwater biota. In M. Wagner & S. Lambert (Eds.), *The handbook of environmental chemistry, Freshwater microplastics* (Vol. 58, pp. 153–180). Springer International Publishing. https://doi.org/10.1007/978-3-319-61615-5_8

Shamskhany, A., & Karimpour, S. (2022). Entrainment and vertical mixing of aquatic microplastics in turbulent flow: The coupled role of particle size and density. *Marine Pollution Bulletin*, *184*, 114160. https://doi.org/10.1016/j.marpolbul.2022.114160

Shi, W., Peruzzo, P., & Defina, A. (2022). Transient retention of floating particles captured by emergent vegetation through capillarity. *Water Resources Research*, *58*(6). https://doi.org/10.1029/2022WR031964

Southard, J. B. (1991). Experimental determination of bed-form stability. *Annual Review of Earth and Planetary Sciences*, *19*(1), 423–455. https://doi.org/10.1146/annurev.ea.19.050191.002231

Teitelbaum, Y., Dallmann, J., Phillips, C. B., Packman, A. I., Schumer, R., Sund, N. L., et al. (2021). Dynamics of hyporheic exchange flux and fine particle deposition under moving bedforms. *Water Resources Research*, *57*(4). https://doi.org/10.1029/2020WR028541

The MathWorks Inc. (2019). MATLAB and image processing toolbox R2019b.

Thibodeaux, L. J., & Boyle, J. D. (1987). Bedform-generated convective transport in bottom sediment. *Nature*, *325*(6102), 341–343. https://doi.org/10.1038/325341a0

Torkzaban, S., Kim, H. N., Simunek, J., & Bradford, S. A. (2010). Hysteresis of colloid retention and release in saturated porous media during transients in solution chemistry. *Environmental Science & Technology*, *44*(5), 1662–1669. https://doi.org/10.1021/es903277p

Trauth, N., Schmidt, C., Vieweg, M., Maier, U., & Fleckenstein, J. H. (2014). Hyporheic transport and biogeochemical reactions in pool-riffle systems under varying ambient groundwater flow conditions. *Journal of Geophysical Research: Biogeosciences*, *119*(5), 910–928. https://doi.org/10.1002/2013JG002586

Valero, D., Belay, B. S., Moreno-Rodenas, A., Kramer, M., & Franca, M. J. (2022). The key role of surface tension in the transport and quantification of plastic pollution in rivers. *Water Research*, *226*, 119078. https://doi.org/10.1016/j.watres.2022.119078

Van Emmerik, T., Mellink, Y., Hauk, R., Waldschläger, K., & Schreyers, L. (2022). Rivers as plastic reservoirs. *Frontiers in Water*, *3*. https://doi.org/10.3389/frwa.2021.786936

Wagner, M., Scherer, C., Alvarez-Muñoz, D., Brennholt, N., Bourrain, X., Buchinger, S., et al. (2014). Microplastics in freshwater ecosystems: What we know and what we need to know. *Environmental Sciences Europe*, *26*(1), 12. https://doi.org/10.1186/s12302-014-0012-7

Waldschläger, K., Brückner, M. Z., Carney Almroth, B., Hackney, C. R., Adyel, T. M., Alimi, O. S., et al. (2022). Learning from natural sediments to tackle microplastics challenges: A multidisciplinary perspective. *Earth-Science Reviews*, *228*, 104021. https://doi.org/10.1016/j.earscirev.2022.104021

Waldschläger, K., & Schüttrumpf, H. (2019). Erosion behavior of different microplastic particles in comparison to natural sediments. *Environmental Science & Technology*, *53*(22), 13219–13227. https://doi.org/10.1021/acs.est.9b05394

Waldschläger, K., & Schüttrumpf, H. (2020). Infiltration behavior of microplastic particles with different densities, sizes, and shapes-from glass spheres to natural sediments. *Environmental Science & Technology*, *54*(15), 9366–9373. https://doi.org/10.1021/acs.est.0c01722

Walling, D. E., & Collins, A. L. (2016). Fine sediment transport and management. In D. J. Gilvear, M. T. Greenwood, M. C. Thoms, & P. J. Wood (Eds.), *River science* (pp. 37–60). John Wiley & Sons, Ltd. https://doi.org/10.1002/9781118643525.ch3

Weig, A. R., Löder, M. G. J., Ramsperger, A. F. R. M., & Laforsch, C. (2021). In situ prokaryotic and eukaryotic communities on microplastic particles in a small headwater stream in Germany. *Frontiers in Microbiology*, *12*, 660024. https://doi.org/10.3389/fmicb.2021.660024

Woodall, L. C., Sanchez-Vidal, A., Canals, M., Paterson, G. L. J., Coppock, R., Sleight, V., et al. (2014). The deep sea is a major sink for microplastic debris. *Royal Society Open Science*, *1*(4), 140317. https://doi.org/10.1098/rsos.140317

Yang, L., Zhang, Y., Kang, S., Wang, Z., & Wu, C. (2021). Microplastics in freshwater sediment: A review on methods, occurrence, and sources. *The Science of the Total Environment*, *754*, 141948. https://doi.org/10.1016/j.scitotenv.2020.141948

Yang, S., Zhou, M., Chen, X., Hu, L., Xu, Y., Fu, W., & Li, C. (2022). A comparative review of microplastics in lake systems from different countries and regions. *Chemosphere*, *286*(2), 131806. https://doi.org/10.1016/j.chemosphere.2021.131806

Zhang, M., Zhao, Y., Qin, X., Jia, W., Chai, L., Huang, M., & Huang, Y. (2019). Microplastics from mulching film is a distinct habitat for bacteria in farmland soil. *The Science of the Total Environment*, *688*, 470–478. https://doi.org/10.1016/j.scitotenv.2019.06.108

Zhou, D., & Mendoza, C. (1993). Flow through porous bed of turbulent stream. *Journal of Engineering Mechanics*, *119*(2), 365–383. https://doi.org/10.1061/(ASCE)0733-9399(1993)119:2(365)

79

AGU PUBLICATIONS

Water Resources Research

Supporting Information for

**Assessing the Behavior of Microplastics in Fluvial Systems:
Infiltration and Retention Dynamics in Streambed Sediments**

Jan-Pascal Boos *[1], Franz Dichgans[2], Jan H. Fleckenstein[2,3], Benjamin Silas Gilfedder [1,4], Sven Frei [5]

[1] Department of Hydrology, Bayreuth Center of Ecology and Environmental Research (BAYCEER), University of Bayreuth, Universitätsstraße 30, 95440, Bayreuth, Germany

[2] Department of Hydrogeology, UFZ – Helmholtz Centre for Environmental Research, Permoserstr. 15, 04318, Leipzig, Germany

[3] Hydrologic Modeling Unit, Bayreuth Center of Ecology and Environmental Research (BAYCEER), University of Bayreuth, Universitätsstraße 30, 95440, Bayreuth, Germany

[4] Limnological Research Station, Bayreuth Center of Ecology and Environmental Research (BAYCEER), University of Bayreuth, Universitätsstraße 30, 95440, Bayreuth, Germany

[5] Wageningen University Research Centre, Department of Environmental Science, Aquatic Ecology and Water Quality Management Group, P.O. Box 47, 6700 AA Wageningen, The Netherlands

* Corresponding author: Jan-Pascal Boos (Jan-Pascal.Boos@uni-bayreuth.de)

Contents of this file

> Text S1 to S4
> Figures S1 to S4
> Table S1

Additional Supporting Information (Files uploaded separately)

> Caption for Movie S1

1

Introduction

This document provides additional details to describe the following topics:

- Short description of calibration of Fluorescence-Imaging-System (Text S1)
- Boundary conditions used in the numerical model (Text S2)
- Bedform stability during the experiment (Text S3, Figure S1)
- Hydrodynamical characterization of the flow (Text S4, Figure S2)
- Breakthrough curves of Microplastics in the streambed (Figure S3)
- Individual particle detection in the streambed (Figure S4)
- Overview of the presented experiments (Table S1)

2

Text S1.

The Fluorescence-Imaging system was calibrated using suspensions of MPs in both surface water and pore space of the streambed sediments. Local regressions were performed by averaging squares of 10 x 10 pixels, and the resulting calibration slopes were filtered with a 2d Gaussian filter to achieve a homogeneous distribution. The two resulting slope fields were merged according to the position of the sediment-water-interface during the experiment, which was identified using an edge detection algorithm (The MathWorks Inc., 2019). A detailed discussion of the quantification technique has been presented in (Boos et al., 2021).

Text S2.

The numerical model was built as an exact representation of the flume, including the initial section of the flume (similar to Figure 1 in Dichgans et al. (2023)). Thus, the boundary conditions have been chosen accordingly. For the velocity field U, we selected flowRateInletVelocity at the inlet (U governed by prescribed discharge), pressureInletOutletVelocity at the outlet and "atmosphere" patches (U prescribed through pressure boundary), noSlip at the walls. As turbulence was represented using large eddy simulation (LES), only boundary conditions for the parameter nut (ν_t = turbulent viscosity) are required. We applied the nutUSpaldingWallFunction for the walls (Spalding's wall function), while the remaining patches (inlet, outlet, atmosphere) are set to the type "calculated" (set via field assignment). The sediment bed was represented with a conductivity of $k_s = 3.44 \cdot 10^{-4}$ m s^{-1}. A porosity value has not been defined, as the energy loss in the porous medium was computed using the Darcy law.

Text S3.

The bedforms were formed manually according to a fixed pattern. Minor changes in bedform morphology were observed between experiments, but were negligible for our analysis (Table S1). In addition, the profiles acquired during the experiment and after experiment completion were sufficiently close (Figure S1), such that the bedform was considered stable throughout the experiment.

3

Text S4.

The surface water levels in the control volume section were affected by both weirs, installed at the in- and outlet boundary (Figure S2). The V-notch weir at the outlet caused an increase of the water level with a head gradient of (3.1 ± 0.2) mm/m, (Figure S2), which matched the flume slope of 3.0 mm/m. This implies that the local velocity field at the investigated section in the middle of the study domain is not significantly influenced by the downstream weir and the infiltration pattern reflects the local bedform morphology. Water levels decreased in the immediate vicinity of the V-notch weir. Spatial variations of surface water levels were similar for all low flow experiments. The maximum overflow height in front of the weir was 39 mm during low flow, and 52 mm for the high flow experiment. Calculated discharge for the outflow weir was 6 % lower than the values obtained from direct MID measurements (0.29 L/s and 0.60 L/s).

4
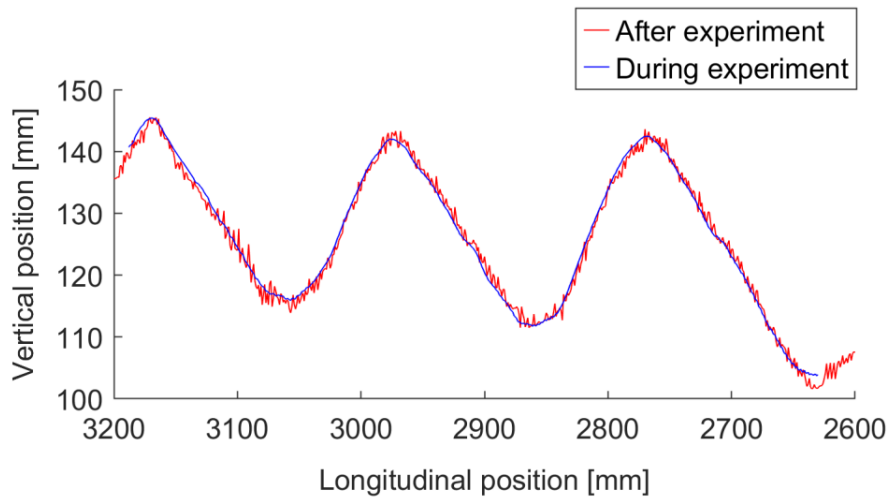
Figure S1. Comparison of bedform morphology near the upstream end of the study domain, measured during and after the experiment (fine sand).
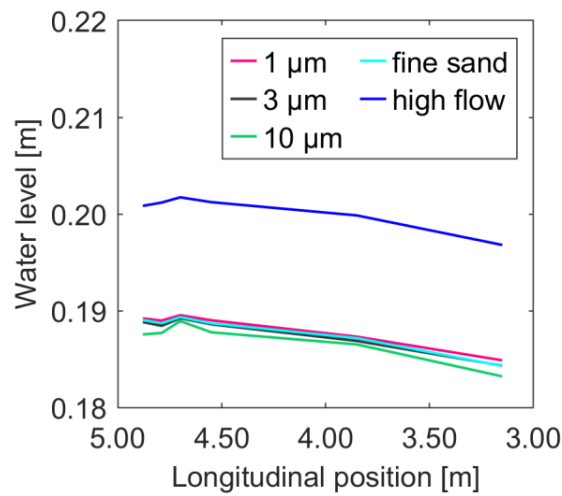
Figure S2. Surface water level profiles along the study domain, measured at 6 locations between 3.15 m and 4.88 m. Water level is influenced by the inflow and outflow weirs (located at 240 cm, and 489 cm, each 15 cm high).

5
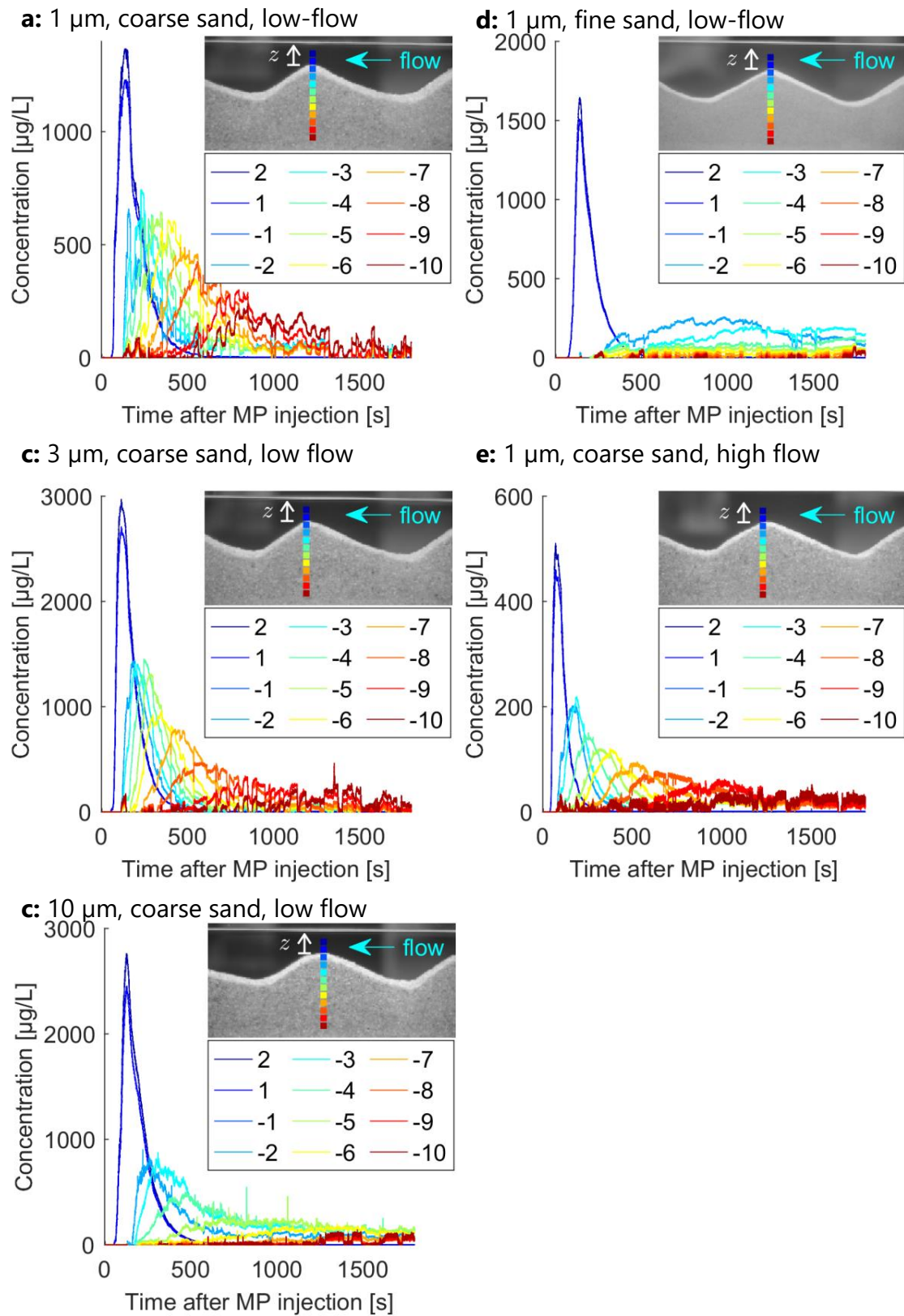
Figure S3. Breakthrough curves in the streambed below the ripple crest
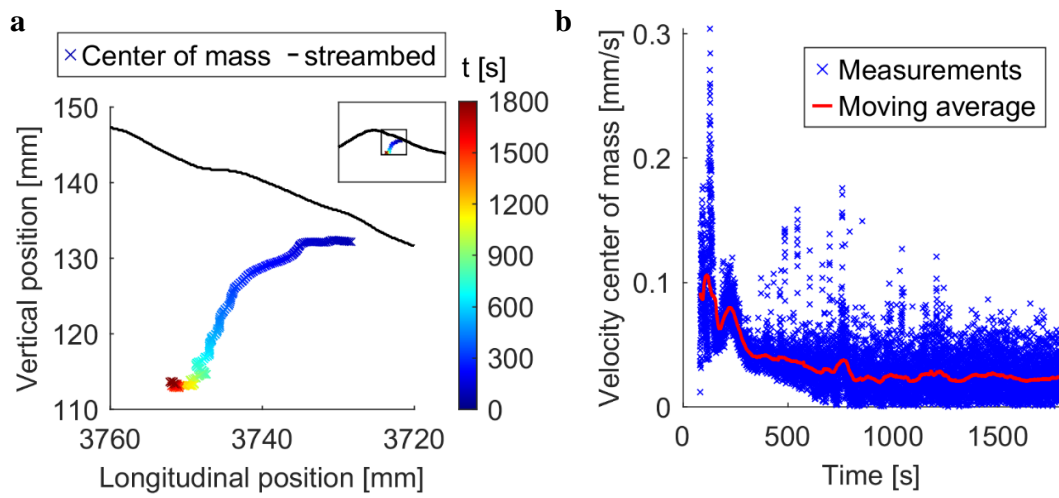
Figure S4. Results from individual particle detection (10 µm experiment), averaging particle positions by a 60 s moving average.
(a): Position of particle center of mass over time. After ~ 1500 s, the position changes only slightly. **(b)**: Propagation velocity of the center of mass, additionally filtered by 60 s moving average. Infiltration is rapid in the beginning and becomes slower over time.

7

Characteristic	Unit	1 μm	3 μm	10 μm	Fine sand	High flow
d_{MP}	[μm]	1	3	10	1	1
d_{Sand}	[μm]	1032	1032	1032	357	1032
$D = d_{MP}\,d_{Sand}^{-1}$	[-]	0.0010	0.0029	0.0097	0.0028	0.0010
Q	[m^3 h^{-1}]	1.09	1.09	1.00	1.05	2.15
$\bar{v}_x$	[m s^{-1}]	0.076	0.070	0.079	0.066	0.114
m_0	[mg]	54	98	78	53	28
$m_{r,in}$	[m-%]	96.4	98.7	97.2	97.7	95.3
$m_{r,out}$	[m-%]	97.9	98.8	99.4	76.5	94.2
a	[mm]	27	29	28	29	27
λ	[mm]	199	200	201	201	201
η	[%]	60	58	60	55	55

Table S1. Characteristics of the experiments: d_{MP} refers to the MP diameter, d_{Sand} to the median sediment diameter, $D = d_{MP}\,d_{Sand}^{-1}$ the particle/grain ratio, Q is the discharge; $\bar{v}_x$ is the mean longitudinal velocity and m_0 is the total injected MP mass. Additionally, the recovered MP mass at the inlet and outlet of the measurement area are denoted by $m_{r,in}$ and $m_{r,out}$. The bedform was characterized by the ripple amplitude a, the ripple length λ and the relative length of the stoss side η. Additionally, the recovered MP mass at the inlet and outlet of the measurement area are denoted by $m_{r,in}$ and $m_{r,out}$.

Movie S1. Comparison of microplastics infiltration into the streambed sediments

References From the Supporting Information

Boos, J.-P., Gilfedder, B. S., & Frei, S. (2021). Tracking Microplastics Across the Streambed Interface: Using Laser-Induced-Fluorescence to Quantitatively Analyze Microplastic Transport in an Experimental Flume. *Water Resources Research*, *57*(12). https://doi.org/10.1029/2021WR031064

Dichgans, F., Boos, J.-P., Ahmadi, P., Frei, S., & Fleckenstein, J. H. (2023). Integrated numerical modeling to quantify transport and fate of microplastics in the hyporheic zone. *Water Research*, *243*, 120349. https://doi.org/10.1016/j.watres.2023.120349

The MathWorks Inc. (2019). MATLAB and Image Processing Toolbox R2019b. Natick, Massachusetts.

7 Publications and manuscripts

Study 3: Integrated Numerical Modelling to Quantify Transport and Fate of Microplastics in the Hyporheic Zone

Authors: Franz Dichgans, **Jan-Pascal Boos**, Pouyan Ahmadi, Sven Frei,
Jan H. Fleckenstein

Integrated numerical modeling to quantify transport and fate of microplastics in the hyporheic zone

Franz Dichgans [a,*], Jan-Pascal Boos [b], Pouyan Ahmadi [a], Sven Frei [b], Jan H. Fleckenstein [a,c]

[a] *Helmholtz Centre for Environmental Research - UFZ, Department Hydrogeology, Permoserstr. 15, 04318 Leipzig, Germany*
[b] *Department of Hydrology, Bayreuth Center of Ecology and Environmental Research (BayCEER), University of Bayreuth, 95440 Bayreuth, Germany*
[c] *Hydrologic Modeling Unit, Bayreuth Center of Ecology and Environmental Research (BayCEER), University of Bayreuth, 95440 Bayreuth, Germany*

ARTICLE INFO

ABSTRACT

Despite the significance of rivers and streams as pathways for microplastics (MP) entering the marine environment, limited research has been conducted on the behavior of MP within fluvial systems. Specifically, there is a lack of understanding regarding the infiltration and transport dynamics of MP across the streambed interface and within the hyporheic sediments. In this study, transport and retention of MP are investigated using a new numerical modeling approach. The model is built as a digital twin of accompanying flume experiments, which are used to validate the simulation results. The model accurately represents particle transport in turbulent water flow and within the hyporheic zone (HZ). Simulations for transport and infiltration of 1 μm MP particles into a sandy streambed demonstrate that the advection-dispersion equation can be used to adequately represent particle transport for pore-scale sized MP within the HZ. To assess the applicability of the modeling framework for larger MP, the experiment was repeated using 10 μm particles. The larger particles exhibited delayed infiltration and transport behavior, and while the model successfully represented the spatial extent of particle transport through the HZ, it was unable to fully replicate hyporheic transit times. This study is the first to combine explicit validation against experimental data, encompassing qualitative observations of MP concentration patterns and quantification of fluxes. By that, it significantly contributes to our understanding of MP transport processes in fluvial systems. The study also highlights the advantages and limitations of employing a fully integrated modeling approach to investigate the transport and retention behavior of MP in rivers and streams.

1. Introduction

In recent years, microplastics (MP) have been identified as a global environmental micropollutant (Andrady, 2011; Napper and Thompson, 2020). Since the term was coined by marine researchers (Thompson et al., 2004), research has long been focusing on marine environments (D'Avignon et al., 2022). MP are synthetic particles with a size range from 1 μm to 5 mm (Frias and Nash, 2019). The widespread use of plastic products has also led to an increase in plastic pollution. Abrasion during use as well as improper disposal leads to fragmentation of larger plastic debris into smaller particles that ubiquitously can be found in the environment (Horton and Dixon, 2018; Koelmans et al., 2014; Petersen and Hubbart, 2021; Ahmadi et al., 2022). As the vast majority of polymers released into the environment are not biodegradable, MP pollution is a long-lasting problem (Laforsch et al., 2021). The effects of MP pollution on aquatic organisms (pelagic, benthic and hyporheic),

specifically under environmental conditions are still largely unknown and subject of current research (Besseling et al., 2017a; Burns and Boxall, 2018; Windsor et al., 2019), though initial works indicate adverse effects (Choi et al., 2021; Laforsch et al., 2021).

Pollutants, including MP, are transported from terrestrial sources via rivers and streams into marine environments. As a major transport pathway, streams and rivers play a key role in understanding the fate of MP in the environment (Mani et al., 2016; Meijer et al., 2021; Schmidt et al., 2017). Rivers are not only transport corridors, but also retain considerable amounts of MP in their sediments (Castañeda et al., 2014; Constant et al., 2021; Frei et al., 2019; Laermanns et al., 2021; Mani et al., 2019; Nizzetto et al., 2016). However, most studies on MP transport in fluvial systems have mainly focused on identifying dominant transport pathways from source areas to marine systems, neglecting the impact of MP pollution on the riverine environment and small-scale transport phenomena. These coarser-scaled approaches,

F. Dichgans et al.

frequently rely on often not well tested analogies from sediment transport in fluvial environments (Besseling et al., 2017b; Lebreton et al., 2017; Nizzetto et al., 2016; Siegfried et al., 2017) or are simplifying the mechanistic processes in riverine environments (Domercq et al., 2022; Drummond et al., 2022, 2020). First laboratory studies with MP particles of approximately neutral buoyancy suggest that these particles are conservatively transported in the surface flow similar to solutes (Cook et al., 2020; Stride et al., 2023).

The hyporheic zone (HZ), occupying the uppermost sediment layers in a river and the interface between the river and its adjoining aquifer is provider of many ecosystem services (Lewandowski et al., 2019). It can be defined as comprising saturated streambed sediments with flow paths originating from and subsequently returning to the surface water (Harvey and Bencala, 1993; Lewandowski et al., 2019). Studies have shown high abundances of different MP particles in the HZ without specifically investigating the associated transport and retention mechanisms leading to the observed accumulation (Frei et al., 2019). However, a mechanistic understanding of processes resulting in the accumulation of MP in streambed sediments is essential for understanding the impact of MP in the HZ.

The effects of pollutants on organisms are strongly linked to the exposure time (Amoatey and Baawain, 2019), which is in turn correlated with the transport time scales. Besides hazardous effects after ingestion (von Moos et al., 2012), MP particles also can leach potentially harmful substances (Schrank et al., 2019) and are known as vectors for pathogens (Kirstein et al., 2016; McCormick et al., 2014), further highlighting the importance to estimate hyporheic transit times for MP. Transfer of MP from surface flow into the hyporheic sediments and mobility within porous media needs to be studied to accurately predict hyporheic transit times and retention quantities in fluvial systems (Drummond et al., 2020). The retention of MP in stream networks in turn affects the transfer of MP from the terrestrial to the marine system (Besseling et al., 2017b) and hence controls MP loadings to the sea. Laboratory studies have been performed to specifically investigate the hydrodynamic controls on MP transport processes relevant to fluvial systems, but results from these studies have not been extrapolated to larger scales (Hoellein et al., 2019; Waldschläger and Schüttrumpf, 2020). This gap can be closed through calibrated hydro-numerical models, which allow extrapolation of small-scale findings to larger scales such as river reaches or entire catchments.

Process based modeling of surface-groundwater interactions as well as hyporheic exchange is often carried out using weakly (sequentially) coupled models: Here, the river hydrodynamics are simulated without accounting for advective exchange of water with the HZ and where the pressure distribution along the streambed interface is used as a boundary condition for a separate HZ model (Dudunake et al., 2020; Ren and Zhao, 2020; Trauth et al., 2013; Xiao et al., 2022). Other studies have focused on conservative and reactive solute transport and the resulting concentration patterns in the HZ in fully-coupled versus weakly-coupled models (Li et al., 2020). It has been suggested to use integral modeling for a detailed analysis of hyporheic exchange processes, which can improve the accuracy of simulation results (Broecker et al., 2019). These integrated approaches have been used mostly for the validated investigation of solute transport in streambeds and were a significant advance in the modeling of hyporheic exchange processes (Broecker et al., 2019, 2018; Sobhi Gollo et al., 2021; Sobhi Gollo et al., 2022a, Sobhi Gollo et al., 2022b). These works mostly focused on solute transport and not on particle transport and were focused more on capturing the overall spatiotemporal distribution of a dye tracer in the hyporheic sediments, while locally occurring concentrations could not be fully validated due to the lack of a respective dataset.

In this paper we address this gap and present a novel numerical modeling scheme based on the OpenFOAM toolbox, which allows an integrated hydrodynamic simulation of the interactions between the surface water and the HZ. The numerical modeling is based on data from laboratory flume experiments where a novel tracking method was used

to investigate and quantify the transfer of MP between surface flow and streambed sediments (Boos et al., 2021). By building a digital twin model of the laboratory setup, the results of the numerical model can be directly validated. This specific combination of integrated modeling and a reference flume experiment with a full quantification of MP transport in the open water and in the hyporheic sediments enables us to investigate the following research questions on MP transport in fluvial systems with unprecedented rigor:

- Can the proposed integrated mechanistic CFD methodology adequately reproduce the transport behavior of very small MP particles, as investigated in the accompanying laboratory experiments qualitatively as well as quantitatively?
- Are sufficiently small MP particles transported in the HZ in a similar manner as a conservative solute tracer?
- How does particle behavior in the flume and HZ change with increasing particle size?
- Can commonly-used concepts to simulate solute transport in porous media be adapted to account for deviating behavior of larger particles?

2. Methodology

2.1. Model overview

To investigate the transport mechanisms for MP particles at the streambed interface, a two-fold approach has been developed. A numerical model was set up using the open-source C++ suite of computational fluid dynamics (CFD) solvers OpenFOAM (Weller et al., 1998). The model was set up as a digital twin of accompanying laboratory experiments. In the experiments MP transport was tracked in a flume and across a model streambed interface using novel optical methods (Boos et al., 2021). The experimental results were used to validate the numerical model.

2.2. Case description

The flume experiments (Fig. 1) were performed using sand (with a median grain size $d_{50} = 1.04$ mm and a hydraulic conductivity range of $k_s = 3.44^{-4}$ m/s) to mimic naturally occurring streambeds (Haque and Mahmood, 1985). Prior to each experiment, the sand was carefully sculpted into rippled bedforms, adhering to geometrical properties representative for natural bedforms. The flume was inclined by 0.003 m/m and operated with deionized water at a constant discharge of 0.27 L/s.

Sediments were stabilized by using plates at the up- and downstream sides of the flume (Fig. 1A). A V-notch weir located at the downstream plate was used for the quantification of flume discharge. The experiments were carried out using fluorescent 1 μm and 10 μm polystyrene (PS, density 1050 kg/m³) microbeads.

Prior to the MP application, deionized water was pumped through the flume and recirculated for 120 min until a quasi-steady state (a condition where bedforms were stable and surface water flow was perceived as quasi steady and uniform based on optical inspection) was reached. After opening the water circuit, the MP sample was injected at the inlet of the flume in a single pulse and the MP propagation in the flume was monitored for a total duration of 2000 s. During the MP experiments the flume was operated in a non-recirculating setup to allow for an accurate monitoring of the entire MP breakthrough without refeeding the particles back into the flume.

The experimental methods which were used in the experiments carried out for this work are described in detail in (Boos et al., 2021). The MP concentration in the streambed sediments was continuously measured for a monitoring window (Fig. 1B) using a Fluorescence-Imaging-System (FIS) through the glass sidewall of the flume (Fig. 2, Table 1). Fluorometers continuously monitored the MP

F. Dichgans et al.
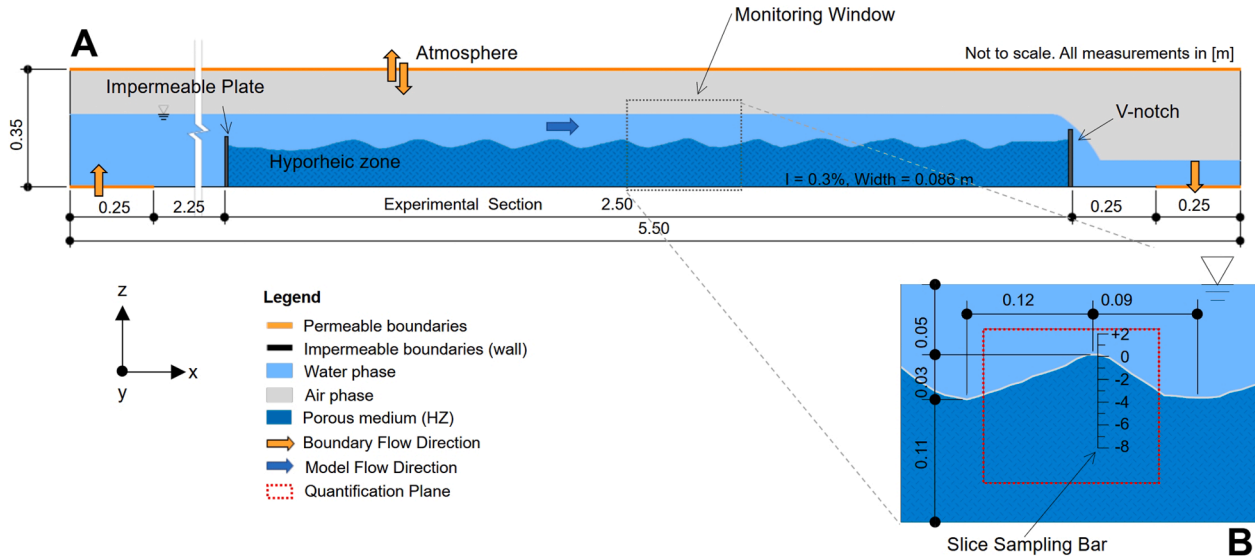
Fig. 1. Model setup: (A) Longitudinal section of the model setup and monitoring locations, (B) Detailed view of the monitoring window.
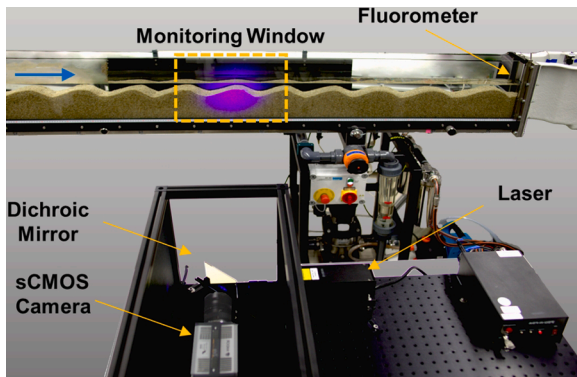
Fig. 2. MP monitoring setup in the hydraulic laboratory.

Table 1
Monitoring setup for the laboratory flume.

#	Parameter	Instrument	Monitoring location
1	Water surface elevation	Ultrasonic sensors	Six point measurements along the experimental section/control volume
2	Discharge	Electromagnetic flow meter + v-Notch	Feeder pipe/Downstream end
3	Bedform geometry	2D X-Z laser profiler	Complete bedform
4	2D (X-Z) velocity field	Particle-Image-Velocimetry (PIV)	Reference monitoring window
5	MP concentration in surface water	Fluorometer	Inlet and outlet of the experimental section
6	MP concentration in surface water and HZ	Fluorescence-Imaging-System (FIS)	Reference monitoring window
7	Temperature	Levelogger	Inlet tank

concentrations in the surface water at the up- and downstream ends of the experimental section. The setup was supplemented with a 2D laser profiler to digitize the bedform geometry and continuously monitor a representative subset of the bedform during the experiments to ensure bedform stability.

The water level was monitored continuously at six locations along the flume centerline with ultrasonic water level sensors, mounted on top of the flume. 2D surface flow velocities in the flume were measured using Particle-Image-Velocimetry (PIV) (Boos et al., 2022). The velocity

field was acquired at three adjoining ripples in the monitoring window to validate the numerical model.

2.3. Turbulent flow and transport modeling

2.3.1. Governing equations

To model microplastic transport in the open water (stream) and in the sediments (HZ), an integrated hydrodynamic model has been set up using the numerical toolbox OpenFOAM (version v2112). The model is solved using InterFoam, a solver for the computation of two-phase flows with immiscible, isothermal, and incompressible fluids. It solves the three-dimensional Navier-Stokes equations based on the finite volume method. The phase interface is tracked using the volume of fluid (VoF) method (Hirt and Nichols, 1981).

The HZ has been defined as a porous continuum with the hydraulic losses being calculated based on the Darcy-Forchheimer equation (Eq. (1)). The computed losses are applied to the momentum equation as a sink term S:

$$S = -\left(\mu D + \frac{\rho |U|}{2} F\right) U \qquad (1)$$

Where μ is the dynamic viscosity of the fluid [kg/m/s], ρ the density of the fluid [kg/m³], D the Darcy coefficient [1/m²], F the Forchheimer coefficient [1/m] and U the flow velocity vector [m/s]. The Darcy coefficient D accounts for the viscous flow losses in the porous medium. In the present case, it is set to $D = 4.995 \times 10^{-7}$ 1/m², based on the laboratory analysis of the utilized bedform material as well as validation runs with the numerical model. The Forchheimer coefficient F accounts for the inertial losses within the porous medium, which are relevant in turbulent flow regimes. In the investigated case, the porous flow regime within the HZ is generally laminar with Reynolds numbers < 10, with only singular areas within the first 2 cm below the bed surface on the upstream ripple crest being located in the lower region of the transitional regime with Reynolds numbers < 50 (Dybbs and Edwards, 1984). Therefore, the coefficient is set to $F = 0$.

Transport of MP particles is simulated using the scalarTransport function object, which solves the advection-dispersion (ADE) equation for the non-reactive transport of a conservative solute at the end of each time step. The use of the ADE to simulate the transport of 1 μm MP particles in the hyporheic sediments was motivated by recent evidence that MP particles in this size range show transport behavior in groundwater similar to that of conservative solutes (Goeppert and Goldscheider, 2021). To be able to account for possible particle retention and

3

remobilization in the pore space due to a variety of processes, such as physical clogging and heteroaggregation, a dimensionless advective retardation factor R has been added to the scalar transport function object, resulting in the following transport equation:

$$\frac{\partial}{\partial t}(C) + \frac{1}{R}\nabla\cdot(uC) - \nabla\cdot(D_T\nabla C) = S_C \tag{2}$$

where C represents the scalar, U the flow velocity vector [m/s], D_C the dispersivity of the scalar [m²/s], R the dimensionless retardation factor and S_C the source term. In accordance with our own observations and the findings of (Broecker et al., 2021), the scalar dispersivity is set to $D_C = 2 \times 10^{-9}$ m²/s, accounting for the molecular diffusivity only. By considering the particle cloud as a conservative scalar tracer, the transport processes at the subgrid scale such as particle collision, homo- or heteroaggregation processes are not explicitly resolved. Furthermore, this assumes a largely uniform distribution of particles in the particle cloud. Possible influences of the particle on the surrounding flow field are not considered as well.

In natural flow over streamed ripples, complex turbulent structures can evolve at the lee side of each ripple, which can either be directly modeled numerically with a very fine mesh or indirectly approximated with a turbulence model (Janssen et al., 2012). For the present case, a large eddy simulation (LES) model was utilized to resolve turbulent patterns. This model separates smaller turbulent structures and approximates them algebraically, while larger eddies are directly solved (Ferziger et al., 2020). For the representation of the subgrid-scale, the Smagorinsky subgrid-scale model was used.

Different commonly used and computationally less expensive methods for representing turbulence patterns (such as k-ε or k- ω SST) were tested, but resulted in less accurate flow fields, especially regarding the representation of secondary currents as well as the flow separation and eddy zone at the lee side of each stream ripple. As these inaccuracies lead to an underestimation of the hyporheic exchange rate, these turbulence modeling schemes were not applied. This is also matching the findings of (Broecker et al., 2021; Sobhi Gollo et al., 2022b).

2.3.2. Discretization

Discretization of the model domain was done using different meshing algorithms of the OpenFOAM suite. To allow for a clear separation of the HZ from the surface flow domain, the mesh cell boundaries have to be adapted to the bedform geometry. This is achieved by using the algorithm MoveDynamicMesh, which deforms the hexahedral base mesh to given geometry constraints. The weir plates in the flume are implemented using SnappyHexMesh. The developed approach ensures that the mesh is dominated by hexahedral and split-hexahedral mesh cells, minimizing non-orthogonality (e.g. in comparison to prismatic meshes) and allowing for an efficient and accurate representation of the geometry in the mesh. The final computational mesh consists of 912,164 cells, of which >99% are hexahedral. Refinements are implemented along the sediment-water-interface and to the upstream/downstream weir plates.

LES modeling has strict requirements for the mesh resolution at the mesh boundaries (Ferziger et al., 2020). To relax these requirements, wall functions are commonly used. Instead of resolving the viscous sublayer along the walls in the mesh, they implement the physics of the near-wall flow in empirical equations. In the presented case, functions based on Spalding's law (nutUSpaldingWallFunction) were applied to the wall boundaries.

2.3.3. Boundary and initial conditions

Boundary conditions for key variables of the model are listed in Table 2. The inflow is realized as a fully submerged inflow boundary. The outflow boundary is defined with a fixed water level of 0.10 m. Therefore, the digital twin model does not require dynamic boundary conditions for the phase fraction variable alpha.water and can be operated with fixed Value boundary conditions for the alpha.water variable at the inlet and outlet patches. The top of the virtual flume is modeled to allow the air phase to move freely. Along the flume walls, as well as along the weir plates at the inlet/outlet of the experimental section, noSlip conditions are applied. The MP tracer has been injected in the model through a cell zone at the location of the upstream fluorometer in the laboratory model. The injected particle concentration could therefore be prescribed from the lab-measured concentrations at this point.

3. Results

3.1. Hydrodynamic characterization of the flow

The surface water flow field in the monitoring section showed a typical pattern for the given bedform geometry as observed in the seminal experimental work by Elliott and Brooks (Elliott and Brooks, 1997). At the specified discharge of 0.27 L/s, the water depth ranged between approx. 0.04 m over the ripple crests to 0.07 m at the inter-ripple troughs. The water elevations showed a close match between the physical and numerical models, without significant deviations (< 1 mm).

In the upper ~ 3 cm of the surface water flow, the main flow passes over the ripple crests, with a zone of maximum velocities at and downstream of the ripple crests (Fig. 3). At the lee side of each ripple, a single eddy is forming, rotating around the Y-Axis (Fig. 5). The flow shows a clear separation between the eddy zone and the main flow zone as shown in Fig. 3. The flow velocities in the centerline of the flume approximately range from 0.08 to 0.14 m/s in the main flow and 0 to 0.08 m/s in the eddy zone.

Simulated surface flow velocities for the monitored ripple segment in general are matching the observed ones (Figs. 3 and 4). Shape and magnitude of relevant features of the flow velocity field, such as the general flow direction, peak over the ripple crest, and eddy zone in the ripple valley are accurately represented in the digital twin (Fig. 3). Simulated and observed velocity magnitudes for surface flow are differing by only ~0.01…0.02 m/s between the PIV and CFD results. Largest differences mostly occur within the upper flow regime, whereas the velocity magnitudes in the ripple valleys are matching closely. Towards the air-water interface, the measured flow velocities are dropping sharply, whereas the modeled velocity field does not show such a sharp drop (Fig. 4).

The flow conditions in the flume can be characterized as narrow open channel flow, with an aspect ratio of flow depth to channel width

Table 2
Boundary conditions for key parameters.

Boundary	p_rgh (Pressure)	U (Velocity)	alpha.water (Phase fraction)
Inlet	**fixedFluxPressure:** Pressure gradient set to fulfill the prescribed U boundary condition	**flowRateInletVelocity:** Uniform velocity field to match the prescribed flow rate	**fixedValue:**Value is fixed, in this case water only
Outlet	**fixedValue:** Value is fixed to maintain an approximately constant water level over the outlet patch	**pressureInletOutletVelocity:** Governed by the pressure boundary condition	**fixedValue:**Value is fixed, in this case water only
Atmosphere	**totalPressure:** Patch pressure described by subtracting the dynamic pressure from the reference pressure	**pressureInletOutletVelocity:** Governed by the pressure boundary condition	**inletOutlet:**Zero Gradient, no return flow
Walls	**fixedFluxPressure:** Pressure gradient set to fulfill the prescribed U boundary condition	**noSlip:**$U = 0$ at the wall	**zeroGradient:**Zero gradient condition
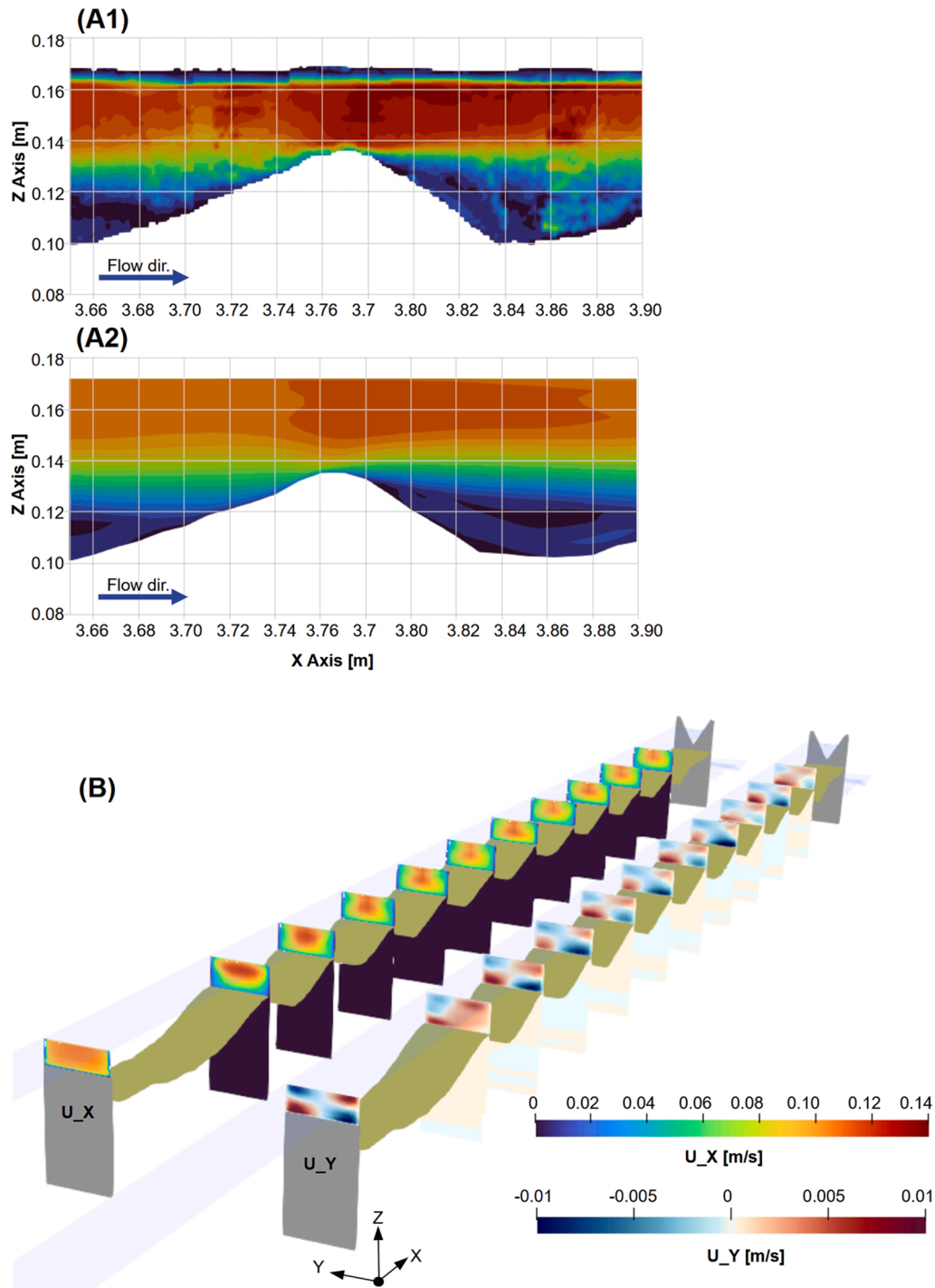
Fig. 3. Velocity field in the flume: (A) Observed (A1) vs simulated (A2) velocity magnitudes in the flume centerline (B) Velocity component magnitudes in the main flow direction (U_X) and in lateral direction (U_Y) at the ripple crests, showing the friction-induced secondary currents in the narrow flume.

of ~1.25...1.5 (Jing et al., 2019). This results in pronounced secondary currents (Nikitin et al., 2021; Yang et al., 2012), which were also represented in the CFD model and are one of the reasons for using a 3D model. The PIV data did not feature cross-sectional velocity field measurements as the laboratory setup only allowed PIV recordings in the XZ plane. Hence a direct comparison of the simulated lateral flow components (Fig. 3B) with experimental data was not possible.

In the hyporheic zone, the typical hyporheic flow cells as illustrated in the seminal work by (Elliott and Brooks, 1997) develop between the ripple surfaces (Fig. 5). An underflow section is forming due to the inclination of the flume. Due to slight variations of the ripple geometries,

the flow patterns slightly differ for consecutive ripples, but the hyporheic flow field for the ripples is independent from each other, since local infiltration patterns did not expand over more than one bedform.

3.2. Fully integrated simulation of open water and HZ

A key feature of this work is the integration of subsurface and surface water flow and interactions between both flow domains into a single integrated model. Calculations of the hyporheic flow conditions are based on the Navier-Stokes equations, with the energy losses through the porous medium being calculated based on the Darcy-Forchheimer
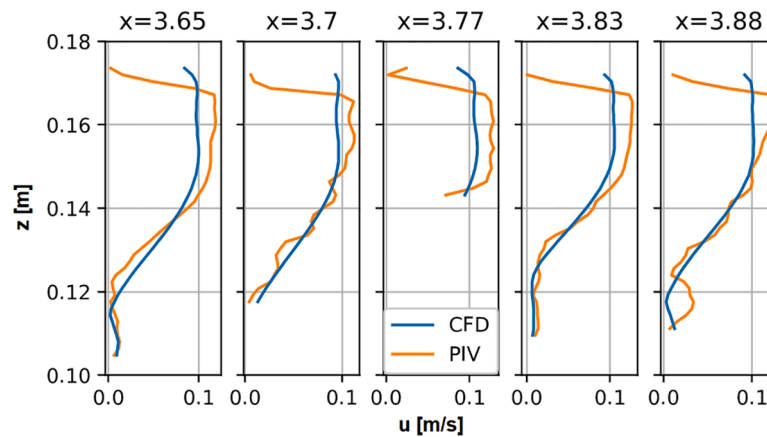
Fig. 4. Comparison of measured (orange) and modeled (blue) flow velocities: Velocity profiles at select x-locations at the foot of the luv slope ($x = 3.65$), on the luv slope ($x = 3.70$), at the ripple crest ($x = 3.77$), on the lee slope ($x = 3.83$) and at the foot of the lee ripple slope ($x = 3.88$). (For interpretation of the references to color in this figure legend, the reader is referred to the web version of this article.)
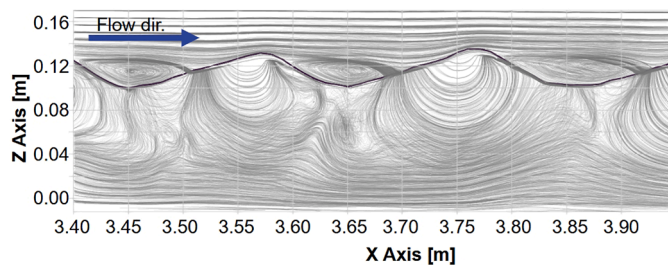
Fig. 5. Flow pattern (streamlines) within the monitoring window, showing surface flow with developing eddies at the ripples' lee sides and the hyporheic flow cells with the underflow.

equation. This allowed for an accurate representation of the hyporheic exchange processes, since hyporheic flow is not only influenced by hydrostatic pressure-differences, but also by dynamic pressure variations over the bedform resulting from the turbulent flow regime in the surface water (Broecker et al., 2019). Furthermore, the permeable streambed allowed for bidirectional exchange flows across the open-water-sediment interface, which fed back into the flow processes in the surface water. To illustrate this interrelationship, we showcase results from a simulation with an impermeable streambed in comparison to our fully integrated simulation in Fig. 6. The velocity fields are distinctly different (Fig. 6A1 and Fig. 6A2). In particular, the shape, size, and magnitude of the eddies on the lee side of each ripple are significantly different, as backward-facing eddies are only forming when the HZ is included in the simulations. This also results in slightly different water levels in the model. Due to these differences, the pressure field differs between a fully integrated and a quasi-non-coupled computation, as shown in Fig. 6B. The plot shows the pressure difference without the hydrostatic component (p_rgh) between the cases with and without a coupled HZ at the interface between surface water and HZ. As indicated by the velocity fields, the pressure differences in the ripple valleys are significant, which is caused by lack of pronounced eddy formation in the quasi non-coupled case.

3.3. Transport of 1 μm MP particles

A qualitative, visual assessment of the MP infiltration into the streambed sediments showed that the complex flow patterns in the open water resulting from the narrow flume setup lead to asymmetries in particle infiltration into the HZ. These asymmetries were observed between the left and right sides of the flume, as shown also in Fig. SI4. Therefore, the following comparisons between the laboratory

experiment and the digital twin were carried out at the left wall of the flume, as the optical measurements of MP concentrations are taken through the left sidewall of the flume and hence reflect concentrations on that side of the flume.

The simulated and observed MP propagation through the streambed sediments in the monitoring window are compared in Fig. 7. It is shown that the MP particles followed the hyporheic flow paths (Fig. 5) and propagated according to the velocity field in the HZ. This led to a sickle-shaped infiltration front, which propagated through each ripple, with the majority of the MP particles exiting the ripple surface in the lower third of the lee side. Infiltration of MP took place preferentially on the upstream and downstream faces of each ripple, with an infiltration zone on the lower half of the upstream face and the main exfiltration zone on the lower third of the downstream face. Due to small variations in the ripple shapes, in- and exfiltration areas varied slightly in their location and spatial extent for each ripple sequence. Due to the flow separation between individual hyporheic flow cells (Fig. 5), flow in one cell did not directly influence flows in the downstream cells. The MP front itself appeared more spatially defined in the CFD results than in the FIS dataset, specifically during the initial 800 s of the experiment.

The blanked areas visible in Fig. 7 result from limitations in the optical measuring approach and inaccuracies in the conversion of the fluorescent intensity recordings to MP concentrations. In the post-processing of the FIS data, we blanked areas where the recorded concentrations were outside of the observed local concentration range of $0\ldots1500$ mg/m³. Furthermore, around the bedform interface, implausibly large MP concentrations occur before $t = 500$ s. These are attributed to a mismatch of the calibration slopes for surface and subsurface area in the transition zone around the bedform interface and subsequently blanked as well.

The comparison of the hyporheic MP-concentration patterns between the flume experiment and the digital twin model generally shows a close match. The propagation speed of the infiltration front through the HZ as well as its shape are fairly well matched by the model as illustrated in Fig. 7. In the simulations the early MP concentrations in the surface water (at 400 s in Fig. 7) were slightly elevated in the ripple valleys, while the FIS recorded a more uniform MP concentration field. A comparison of the infiltration patterns in Fig. 7 also suggests that the application of a retardation factor is not required to model the propagation of the 1 μm MP particles. It was therefore set to $R = 1$ (equivalent to no retardation) for the modeling of 1 μm MP particle transport.

To quantitatively assess the propagation speed of the concentration front through the streambed ripple, the concentration over a vertical section at $x = 3.77$ m was extracted from the physical and numerical models (Fig. 1B slice sampling bar). To compare the propagation speed,
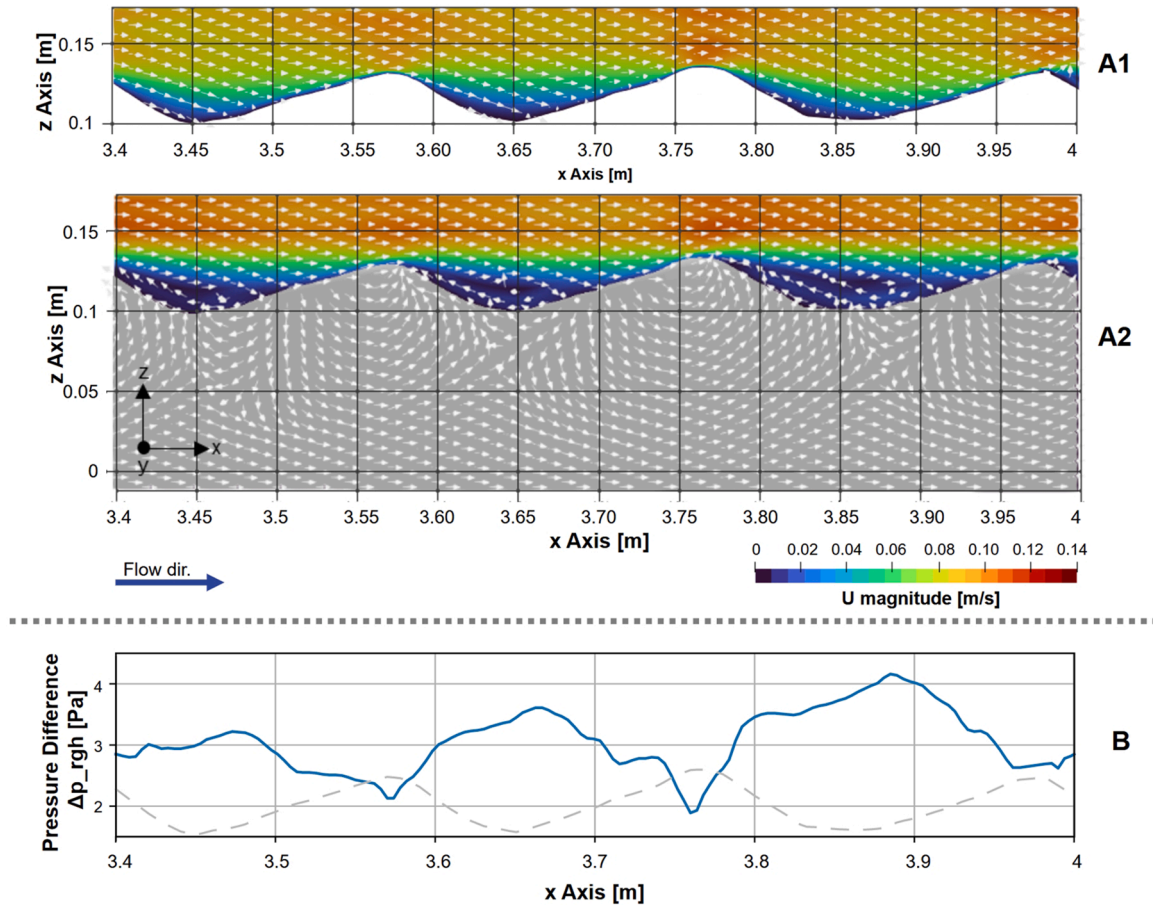
Fig. 6. Velocity field in longitudinal section along the flume centerline without (A1) and with (A2) integrated modeling of a HZ. The pressure difference without the hydrostatic components (p_rgh) between the two cases is shown in (B), with the bedform shown as a dashed line.

the time when the peak concentration passed through the section at different depths is analyzed in Fig. 8. Additionally, for each sampling point the interval of presence of the respective highest 5% of the measured MP concentrations is shown. With an average relative error of 13.1% in the surface water section and 5.3% in the streambed, the exact peak arrival times are predicted satisfactorily by the model. Additionally, the interval, where the largest 5% of the MP concentration passes over the monitoring points has been extracted and shown in the figure. The comparison shows a close match of these intervals between the two datasets, as they coincide for all sampled points. When comparing the mean time of these intervals, the relative error within the surface water section is reduced to 8.3% in the surface water and to 4.7% in the HZ. These intervals furthermore highlight the previously mentioned spatial variability of the infiltration fronts within the porous medium. While the CFD results show a monotonically increasing interval length with depth, the interval width of the lab-measured data is overall increasing with depth, but not monotonically.

Due to the overexposure of the FIS data for the HZ in the boundary layer (blanked areas in Fig. 7), the propagation curves had to be reconstructed partially through curve fitting. The parameters are given in the supplementary material S2. The quantitative assessment of the MP transport is carried out via comparison between the simulated and observed MP breakthroughs at the up- and downstream ends of the flume as well as within the monitoring window. The concentration peak passes through the experimental section within 75 s. Fig. 9 indicates the breakthrough curves resulting from the inflow and outflow concentrations in the experimental section for the initial 750 s of the experiment. As the in- and outflow concentrations reach the lower quantification limit of the fluorometers (0.36 mg/m^3) at around 700 s and 750 s

respectively, the mass balance cannot be fully closed based on the fluorometer data. The dataset extracted from the digital twin model is matching the fluorometer data from the laboratory experiment. As the upstream fluorometer serves as the inflow boundary condition for the MP particles in the CFD model, both time series are identical (Fig. 9A). The injection starts at $t = 40$ s. 50% of the mass is injected before $t = 144$ s, and 99% by $t = 430$ s. The downstream fluorometer model results correlate closely with the laboratory measurements at a determination coefficient of $R^2 = 0.9943$ and show a normalized root mean square error (NRMSE) of 0.0148. In regard to the passed mass (i.e. the curve integral of the display concentration curve), 50% of the injected MP mass passed within 199 s and 200 s for laboratory and model respectively. 90% of the particle mass passed through the experimental section after 384 s and 367 s respectively. Upon reaching the quantification limit of the lab fluorometers at 750 s, 95.11% of the injected particles exited the laboratory model, while 98.67% have been discharged in the CFD model.

With the CFD model, the mass fraction of MP particles in the streambed sediment and surface water compartments can be tracked separately as well as globally without relying only on the in- and outflow measurements. After 504 s, the total particle mass present in the streambed sediments surpassed the one in the surface water compartment. At this point, the fluorometer data indicates that 96.9% of the MP particles have passed through the laboratory flume, compared to 96.6% obtained from the CFD results data indicates that 96.6% of the particles have been transported through the digital twin (Fig. 9A). Both results indicate that the majority of the particles are transported through the surface water section of the flume. The injection of MP into the model stops at 529 s. With the aforementioned passing time of 75 s, the
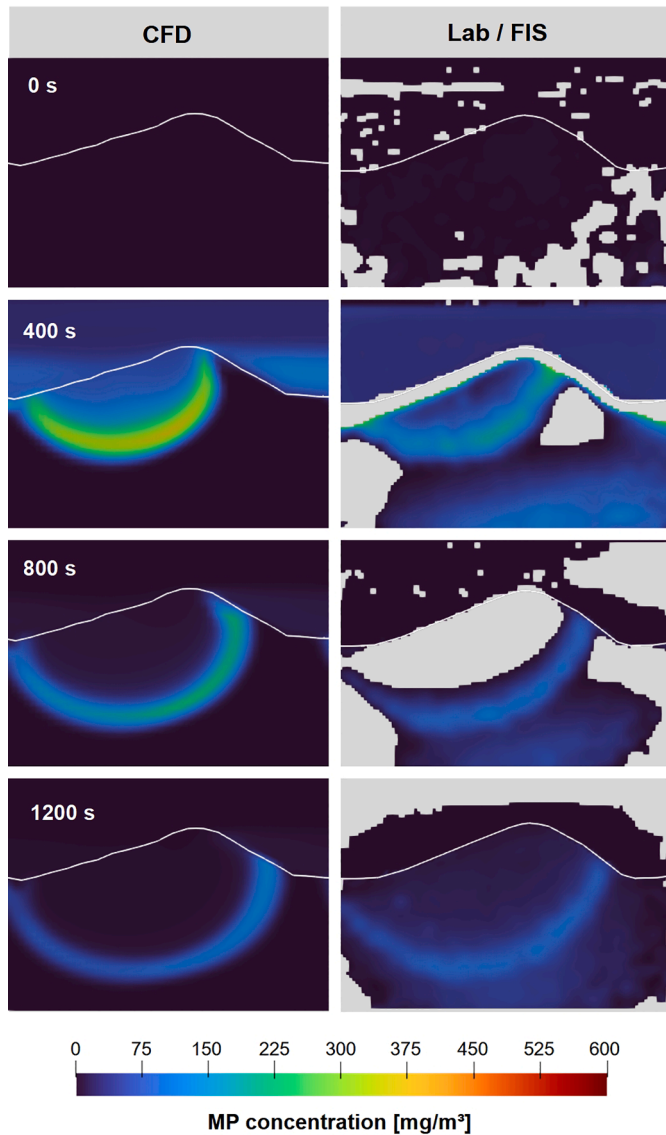
Fig. 7. MP infiltration into the reference ripple.

presence of MP in the surface water after 604 s must predominantly result from releases from the HZ.

Apart from the global quantifications, MP infiltration can be analyzed numerically within the monitoring window. The laboratory measurement of the MP concentration in the HZ is taken through the sidewall of the flume, resulting in the monitoring of a quasi-2D plane due to the opacity of the sediment. For the surface water section, the FIS is also detecting the concentrations behind the HZ monitoring plane, as the water is not blocking the fluorescent signal from the particles. The CFD-equivalent for the surface water section is therefore the average over the complete flume width rather than only the 2D section at the outer wall.

To analyze the MP quantities in the surface flow and the HZ, the monitoring window is reduced to the quantification plane (Fig. 1B), which comprises a single ripple without fringe areas, minimizing the areas of lower data quality along the outer edges of the monitoring window (Fig. 1). On the quantification plane, the average concentration of MP is calculated for the surface water and HZ over time as shown in Fig. 9B. The modeled distribution shows a good match to the laboratory measurements, with a coefficient of determination $R^2 = 0.9912$. The peak is slightly over-predicted with a relative error of 5.9%, while the overall NRMSE is at 0.0213.

The data shows that the average concentration in the surface and subsurface are matching between laboratory and CFD, with the CFD model resulting in slightly reduced (≤ 20 mg/m^3) concentrations in the decay period of the subsurface MP concentration. After 550 s runtime, the concentrations in laboratory and CFD model are closely matching.

3.4. Transport of 10 μm MP particles

Due to physical limitations of the sensor equipment, laboratory comparison data for the 10 μm experiment is only available within the monitoring window. As the physical particle size is close to the size of a sensor pixel, the recording of the quantities is not as reliable as for smaller particles and results in noisier datasets. Despite these limitations, the data can be compared to the simulation data.

While the infiltration patterns as well as the transport flow paths through the HZ are controlled by the hyporheic flow cells as in the case of the smaller 1 μm particles, the propagation speed of the concentration front (the "sickle") is reduced in comparison to the experiment with 1 μm particles. This is not only noticeable in the qualitative comparison (Fig. 10), but also in the comparison of the peak transit times (Fig. 11). As the retarded transport is evident, the retardation factor introduced in Eq. (2) has been utilized in an attempt to account for this. The retardation factor is used in the transport equation of the HZ only, so that the
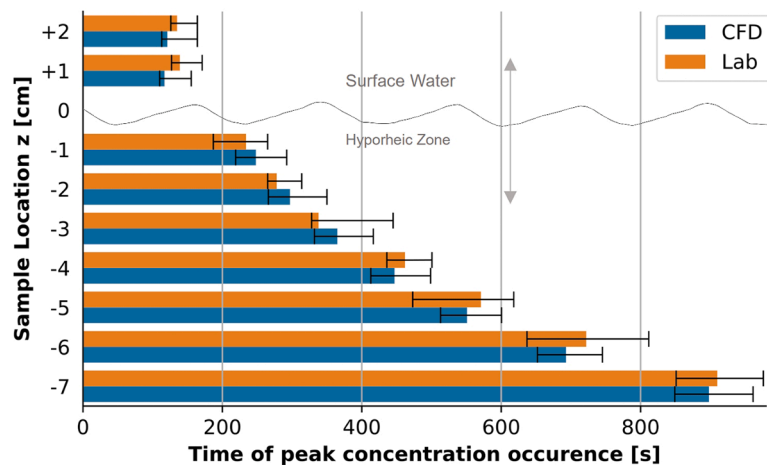
Fig. 8. Arrival time of peak concentration at the slice sampling bar below the ripple crest at $x = 3.77$ m. The interval markers depict the times where 95% of the respective maximum concentration is reached at the respective sampling point.
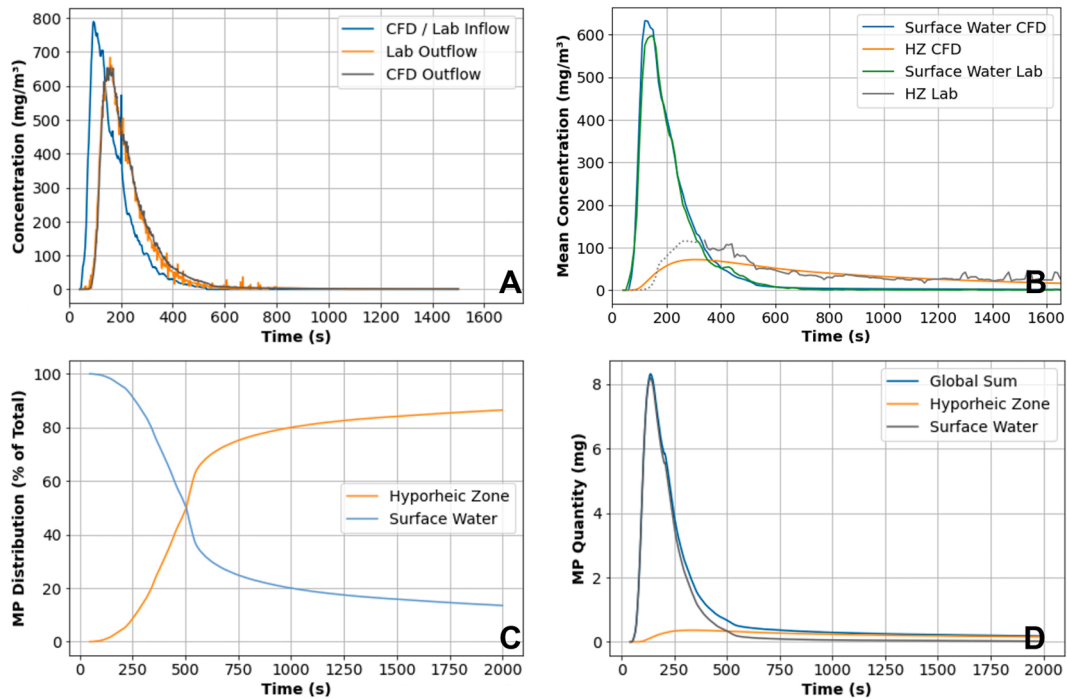
Fig. 9. Volumetric MP transport validation in the model: (A) Upstream and downstream MP concentration measurements in the surface flow (B) Average of MP concentration in the quantification plane (dotted line shows extrapolated data) (C) Distribution of MP particles between surface water and HZ (from CFD) (D) Temporal distribution of MP in the model (from CFD).
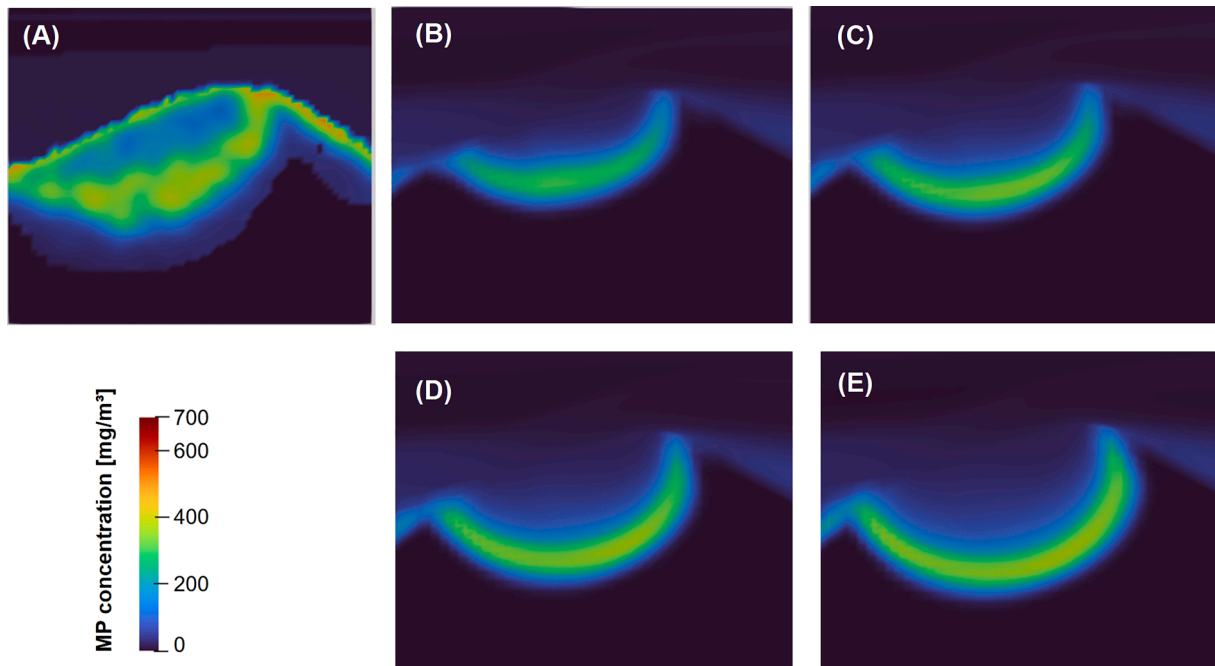
Fig. 10. Comparison of infiltration pattern at t = 400 s. Experimental data (A) and simulated patterns for different retardation factors: 5 (B), 4 (C), 2 (D), 1.25 (E).

surface water transport is not retarded.

Comparison of the experimental and simulated peak transit times for 10 μm particles reveals that the use of a single retardation factor can improve model fit either for the upper or the lower segments of the HZ, but not for both at the same time. This indicates that retardation is not steady and increases with flow path length and time. The quantification in the reference plane also reveals that the model overestimates the magnitude of particle infiltration into the HZ for all retardation options

(Fig. 12), but replicates the particle behavior in the surface water compartment closely.

4. Discussion

4.1. Hydraulic conditions

The hydraulic conditions in the flume were adequately represented

98
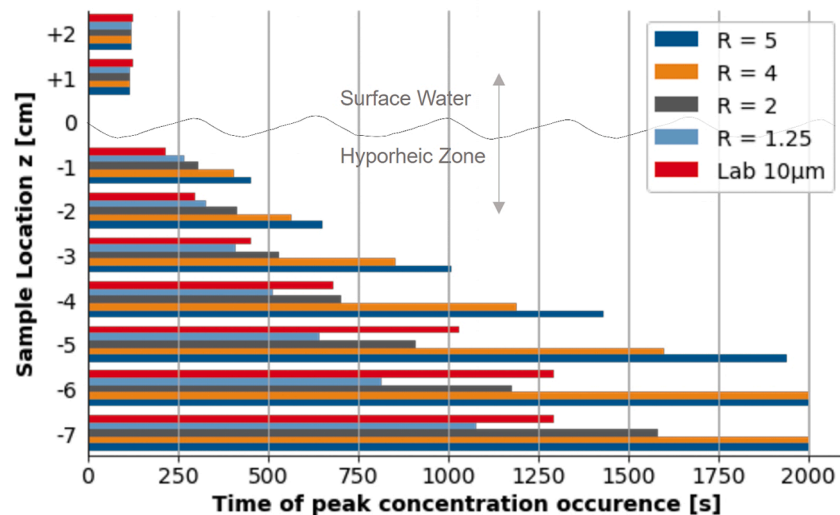
Fig. 11. Propagation time of Peak concentration at $x = 3.77$ m, 10 μm MP particles and CFD runs with different retardation factors.
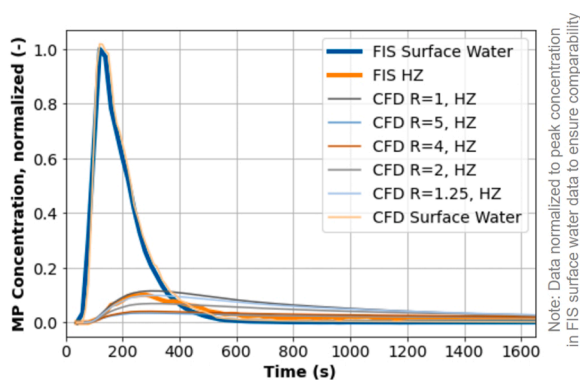
Fig. 12. MP concentrations in monitoring section, 10 μm PS beads.

in the CFD model lending credibility to the chosen model setup. The general features of the flow field, as well as the velocity magnitudes computed in the model matched the PIV records closely. Specifically flow conditions close to the streambed interface, where infiltration into the sediment bed occurred, the model provided accurate results. Towards the air-water interface, the model results deviated by up to 0.07 m/s, as the lab-recorded velocity dropped significantly towards the interface. This can be explained by deficiencies of the PIV records towards the surface. The simulation results indicated significant secondary flow in the narrow channel, which was expected given the channel geometry and low water depth. Due to the complex hydraulics of narrow flumes as well as the pronounced ripple structure, high-order turbulence modeling, e.g., using LES, is required to compute the flow conditions in the flume with a sufficient level of detail. Test runs with RANS models also resulted in reduced hyporheic exchange rates, leading to MP concentrations and MP distributions in the HZ that differed significantly from the laboratory results. This suggests that for flume channels, which are commonly narrow relative to the flow depth the hyporheic flow and transport problem might not be adequately approximated with a 2D model and the modeling strategy should be selected with care.

It could be shown that the fully integrated simulation is significantly increasing the accuracy of the modeling results in the present case. The lack of eddy formation in the ripple valleys leads to inaccurate pressure values on the streambed interface in the simulated non-coupled test case with no hyporheic zone. This would result in inaccurate estimates of the hyporheic exchange flux in a weakly (consecutively) coupled model, which would use the independently simulated pressure field over the

streambed as the coupling boundary condition for the hyporheic flow model. These differences will be specifically relevant in cases with pronounced bedform structures, where the surface water flow field is strongly influenced by the shape of the ripples and the influence of the underlying bedform on the overall flow field is significant (Zhou and Endreny, 2013).

This is also in line with the findings presented in (Sobhi Gollo et al., 2022b). In this comparative study, a rippled streambed has been modeled using an integrated and a coupled approach. Their investigated case features a slightly different and more conductive streambed geometry and larger flow velocities than in our case. Furthermore, the set of equations used to compute the hydraulic losses in the porous medium differs. The reported qualitative pressure differences over the ripple, with larger differences over the ripple crest and a decline in the valley, as well as the differences in the velocity magnitude are in general agreement with our findings. This is further highlighting the importance of integrated modeling approaches for the investigation of rippled streambeds.

The computation of the flow conditions in the HZ relies on a Darcy-based loss term. The Darcy equation is valid in groundwater flows for laminar flow conditions only, which are present at Reynolds numbers of up to 300 (Dybbs and Edwards, 1984). In the presented study, Reynolds numbers in the sediments did not exceed the value of 50, placing the flow problem in a laminar flow regime and the Darcy loss term has shown to produce an accurate flow field. If coarser sediments were to be used, which may facilitate more prominent non-laminar flows in the uppermost sediment layers, additional validation experiments would be needed to confirm the applicability of the utilized equations, or to calibrate additional Forchheimer or other loss coefficients as for example presented in (Broecker et al., 2019).

4.2. MP particle transport

Simulation results indicate that the transport of the 1 μm MP particles in a sandy HZ can reasonably be modeled using the advection-dispersion equation in a fully integrated hydrodynamic model (i.e. flow in the open water and sediments is solved with one set of equations simultaneously) that accurately accounts for the hydrodynamic feedbacks and exchange flows between the open water and hyporheic domains. The model could adequately reproduce the shape and temporal evolution of the particle concentration fronts in the HZ (Fig. 7) and the experimental breakthrough curves for 1 μm MP particles in the open water and in the sediment were matched very well (Fig. 9). The trajectory of the particle peak concentrations with depth in the HZ could also

be captured well (Fig. 8). Due to the limitations of the MP detection in the laboratory, the concentration fields obtained from the CFD simulations are more refined, showing a more sharply defined spatial extent than the results obtained from the laboratory (Fig. 7). The quantitative comparison of the results shows nonetheless that the model is accurately predicting the transport quantities and locations (Fig. 9). The deviations between observed and simulated MP concentrations in the HZ between 400 and 500 s, as shown in Fig. 9B fall within the period where the MP transport is still predominantly located within the surface water compartment and are related to large areas in the detection window with non-plausible concentrations, which were present in the FIS records during this period. However, the overall MP outflow record at the downstream end of the experimental stretch was closely matched by the model, indicating that the temporary deviation between experiment and model can be attributed to detection artefacts.

It cannot be ruled out that in the experiment single particles were trapped in the pore spaces and bound to the surrounding mineral particles, e.g. by electrochemical bonds (Lu et al., 2021). Also, physical retention of individual particles in the pore space is theoretically possible, but our observed and simulated breakthrough curves suggest that there is no significant retention of the 1 μm particles in the sediments and that they appear to move through the HZ more or less uninhibited like a non-adsorbing, conservative solute. As single particles of 1 μm size are not detectable in the sediments with the utilized online methods, we could not further corroborate this statement experimentally. However, this finding is backed by the results reported in (Goeppert and Goldscheider, 2021), who showed similar, unretarded transport of small, similar size MP particles (1, 2 and 5 μm) in a sandy alluvial aquifer.

In contrast, for larger particles, our results suggest that retention processes will play a more crucial role. We attribute the delayed transport of the 10 μm particles through the HZ to temporary retention of the particles in the sediments as they, due to their size, cannot move as smoothly through the pore spaces as the 1 μm particles. As shown in Fig. 12, the infiltration quantity of 10 μm compared to the 1 μm particles is reduced, with the concentration in the HZ being approximately halved. This also highlights the requirement of a differentiated treatment of the different MP size ranges in transport modeling.

The comparison case with 10 μm MP particles reveals the limitations of the presented approach for larger MP particles. While the surface water transport is modeled accurately, the infiltration into the HZ is overestimated, particularly during the later phase of the experiment, and the general transport pattern is not matched accurately (Fig. 12). The particle propagation within the HZ is furthermore delayed (Figs. 10 and 11). Our analyses showed that the retardation factor required to compensate for the mismatch between laboratory observation and modeling results is increasing with depth, suggesting that the particles are getting increasingly retarded with growing flow path length. This transport behavior with non-steady retardation cannot easily be implemented in the Eulerian approach used here and may require the use of an adapted Lagrangian particle tracking approach. Furthermore, the presented experimental approach needs to be refined to deliver accurate validation data for more complex numerical setups, e.g. by employing optical particle tracking within the FIS.

4.3. Limitations and future challenges

As Dong et al. (2022) have shown, the transport behavior of MP particles in partly and fully saturated porous media also depends on the polymer type and the biogeochemical conditions of the surrounding medium. Such effects could not be fully addressed in this study. To test a broader, more general applicability of our modeling approach, additional experiments with different particles and under different biogeochemical regimes in the sediments need to be carried out. However, the market availability of suitable particles is a limiting factor for the laboratory work, as only a relatively small range of polymer types and

particle shapes is available with the required fluorescent properties.

Given experimental limitations, studies usually work with high non-realistic MP concentrations, which are significantly higher compared to what is usually observed in streams. To what degree this affects the transfer of experimental results to natural systems remains to be tested in future work.

Using opaque sediment, the MP concentrations can only be monitored along the glass interface of the flume, if the hyporheic continuum should not be disturbed. To our knowledge, there are also no suitable methods to continuously monitor MP concentrations within 2D sections in sediment bodies. Hence, only singular measurements after the experimental runs could be taken either by extracting sediment cores and analyzing them manually or by using more involved non-destructive methods (Tötzke et al., 2021). This approach will, however, not yield information on the infiltration dynamics and is therefore not suited to improve our mechanistic understanding of MP transport. This leads to uncertainties regarding MP transport in the HZ away from the flume wall. However, the accurate representation of the hydraulic conditions in the flume and of the transport in the surface water and in the sediment along the sidewalls in the 3D digital twin model, suggest that the concentrations simulated in the digital twin are in fact a good representation of the actual transport of MP particles in the laboratory flume experiment.

Our results show that the transport and infiltration behavior of particles of 1 μm and 10 μm varies within the same sediment type. We hypothesized that the behavior is dependent on the relation between pore and particle size, but additional experimental investigations are needed to further corroborate this. Furthermore, the effects of different biogeochemical regimes in sediments on particle transport within the HZ are not considered in our study and should be addressed in future work.

Long-term retention cannot be adequately analyzed with the modeling approach or the laboratory setup. The spatial averaging method employed for the laboratory data does not allow detecting single particles within the sediments. Therefore, the retention by processes such as heteroaggregation of MP with mineral particles, or physical retention in the pore space, e.g. by size-exclusion, cannot be detected and therefore also not be reliably implemented in the used numerical model at this stage. Here pore-scale models would be needed.

4.4. Specific utility of the digital twin model

In the previous paragraph we discussed some of the limitations of the experimental design with regard to a seamless detection of MP concentrations throughout the flume system. The calibrated digital twin model of the flume experiment can overcome some of the limitations of the laboratory experiment, at least for the small particles. The successful calibration of the model to the hydraulics in the flume as well as to the propagation of MP concentration fronts at the sidewalls of the flume, lends credibility to the consistency of the model in terms of an accurate representation of the true 3D flows in the HZ in the flume. While in the flume experiment hyporheic MP concentrations can only be measured and monitored through the sidewall of the flume, i.e. at the outer boundary of the flow field, the numerical approach allows the user to look inside the porous continuum and investigate the flow and transport patterns in all three dimensions. Furthermore, the numerical model resolves the flow over the entire domain, so that the analyses are not limited to a fixed monitoring window resulting from limited viewing angles of monitoring equipment. All physical parameters can be directly derived from the CFD output data, while in the laboratory flume, each parameter (set) requires specific instrumentation. Physical limitations, such as the size of the laboratory, the limited ability to recirculate particle-laden flows or detection limits can be overcome with the numerical model. Also, the implementation of scenarios is easily facilitated with a numerical model, as materials and geometries can be changed efficiently digitally and different virtual particles would not require

different monitoring setups as long as they generally adhere to the same general transport mechanisms identified for the original particles.

However, to produce reliable results, a numerical model has to be validated, which is usually done through laboratory experiments. Hydraulic conditions can be reliably predicted by standalone numerical models, as they have been studied extensively. In the relatively new and evolving field of MP transport in fluvial systems, however, the governing transport processes are still poorly understood and subject to current research. Therefore, reliable transport modeling of MP in fluvial systems needs to be backed up by physical studies confirming the applied transport models. In any case, an integral numerical model can be used to explore hydraulic effects for a given flume or field site geometry to inform an appropriate study design.

As the online particle detection is currently limited to a quasi-2D section at the flume wall, the overall width of the flume is not relevant for the laboratory measurements beyond the general hydraulic conditions. The narrow flume also is reducing the amount of MP particles required to generate detectable MP concentrations in the monitoring window. To this end, the narrow flume presents an efficient way of carrying out the validation experiments for the digital twin.

In comparison, more conceptual, stochastic approaches, such as the model utilized in Drummond et al. (2020), can usually represent mass balances well at larger scales. However, local effects, such as more complex hydrodynamic conditions or specific infiltration behavior of differently sized particles can only indirectly be implemented in those more aggregated approaches. The presented integral, mechanistic modeling approach in turn allows us to analyze the spatiotemporal transport behavior in more detail, which could inform parameterizations in simpler models. It is thus complementing the conceptual modeling approaches towards the smaller scales, which provides additional insights, e.g. with respect to the spatiotemporal particle distributions or transit times. This is required not only for a deeper mechanistic understanding of MP pollution in fluvial systems, but can also provide feedback to the larger-scale approaches to improve the overall modeling accuracy.

5. Summary and conclusions

In this study we could show that the investigated 1 μm MP particles are transported through the hyporheic zone like a solute tracer. Our simulations indicate that the majority (96.6%) of the MP particle pulse is transported in the surface water section and only a very small fraction (3.4%) infiltrates into the HZ. Within the HZ the concentration peak of the 1 μm particles is following the advective transport of the water as it has been shown for solute transport in the HZ (Broecker et al., 2021). For larger particles, such as the investigated 10 μm PS particles, the physical and numerical investigations show that particle transport is delayed in comparison to the 1 μm particles. We attributed this to additional physicochemical processes, which cannot be mechanistically elucidated with the experimental and modeling setups in this study. Instead we proposed and tested an effective description using a constant retardation factor as commonly used to describe retardation of solutes undergoing adsorption and desorption. While a constant retardation factor could not account for the delays of the particle breakthroughs at all depths, formulations with a time-variant retardation factor, which increases with flow path length, are theoretically conceivable, but would require a Lagrangian modeling approach.

In a conceptual modeling study Drummond et al. (2020) concluded that MP particles, ranging in size from 1 to 100 μm, are advectively transported through the HZ with around half of the particles being retained temporarily. Our findings suggest that the transport of larger particles (10 μm) through the HZ is retarded indicating a temporary retention. While the investigated 1 μm particles appear to be transported in the investigated system like a conservative, non-adsorbing, solute tracer, retardation effects are detected for the larger particles. Using a constant retardation factor the match between observed and modeled

breakthrough of the concentration peak at different depth could be improved, but not at the same rate over the entire depth range. For a good match at shallower depth retardation at deeper depth was underestimated while a good match at deeper depth was accompanied with an overestimation of retardation at shallow depth. This suggests that retardation may increase with flow path length, illustrating that further investigations are required to improve our mechanistic understanding of the dominant transport processes for MP particles within the size range of 1–100 μm in the pore space of hyporheic sediments. As our study is closely focusing on small-scale effects in the transport of MP particles in the HZ, the differences in transport behavior between seemingly similar MP particles will be more apparent (and relevant), than in coarser, larger-scale models, which represent a diverse particle mixture with a wide variability of size, density and polymer types as a particle distribution. The modeling approach proposed here, which uses scalar transport equations to model MP transport in the HZ might therefore be a viable and practical complement to the simpler, coarser models, to simulate spatial infiltration patterns, as successfully demonstrated in this study.

The application of a fully integrated digital twin model revealed the peculiarities of the laboratory flume experiment and could further provide new insights into potential limitations of commonly used coupled, numerical modeling approaches. The results show that both the narrow laboratory flume as well as the CFD model produce valid results for MP transport investigations in and into the HZ, but effects such as secondary currents or hydraulic feedbacks from the HZ to the surface water have to be individually assessed and considered.

To our knowledge, the presented approach for mechanistic modeling of integral open-water and hyporheic flow and transport of MP is the first to be explicitly validated against experimental (flume) data not only in terms of qualitative observations of concentration patterns, but also in terms of the quantification of fluxes. The very good agreement between the model and the observational data suggests that the hydraulic conditions and the transport behavior for 1 μm MP particles are accurately replicated by the model. This makes the presented modeling approach not only amenable to analyses of small MP particle transport in the HZ, but with additional validation also to other research questions involving hyporheic exchange flows and transport processes. Our results further suggest that the retardation of larger 10 μm particles could be accounted for using a dynamic retardation factor. Additional processes acting on even larger particles, causing further retardation or even permanent retention in the sediments, need to be investigated in future pore-scale studies.

Author contribution statement

FD co-developed the research idea, developed the numerical modeling setup, assisted with the flume experiment setup, carried out the numerical modeling and validation, processed, analyzed and interpreted the numerical and laboratory datasets, and wrote the initial draft of the manuscript. JPB developed the laboratory setup and carried out the flume experiment, processed the experimental dataset and assisted in the data interpretation. PA assisted in data interpretation. SF supported the laboratory experiments. JHF conceived the project, co-developed the research idea, and assisted in the data interpretation. All authors contributed to reviewing and editing the manuscript.

Declaration of Competing Interest

The authors declare that they have no known competing financial interests or personal relationships that could have appeared to influence the work reported in this paper.

Data availability

Data will be made available on request.

7 Publications and manuscripts

F. Dichgans et al.

Water Research 243 (2023) 120349

Acknowledgment

This study was funded by the Deutsche Forschungsgemeinschaft (DFG, German Research Foundation) – Project Number 391977956 – SFB 1357. Additional funding was provided by the Helmholtz-Centre for Environmental Research (Topic 5, subtopic 5.2).

Supplementary materials

Supplementary material associated with this article can be found, in the online version, at doi:10.1016/j.watres.2023.120349.

References

Ahmadi, P., Elagami, H., Dichgans, F., Schmidt, C., Gilfedder, B.S., Frei, S., Peiffer, S., Fleckenstein, J.H., 2022. Systematic evaluation of physical parameters affecting the terminal settling velocity of microplastic particles in lakes using CFD. Front. Environ. Sci. 10, 875220 https://doi.org/10.3389/fenvs.2022.875220.

Amoatey, P., Baawain, M.S., 2019. Effects of pollution on freshwater aquatic organisms. Water Environ. Res. 91, 1272–1287. https://doi.org/10.1002/wer.1221.

Andrady, A.L., 2011. Microplastics in the marine environment. Mar. Pollut. Bull. 62, 1596–1605. https://doi.org/10.1016/j.marpolbul.2011.05.030.

Besseling, E., Foekema, E.M., van den Heuvel-Greve, M.J., Koelmans, A.A., 2017a. The effect of microplastic on the uptake of chemicals by the lugworm *Arenicola marina* (L.) under environmentally relevant exposure conditions. Environ. Sci. Technol. 51, 8795–8804. https://doi.org/10.1021/acs.est.7b02286.

Besseling, E., Quik, J.T.K., Sun, M., Koelmans, A.A., 2017b. Fate of nano- and microplastic in freshwater systems: a modeling study. Environ. Pollut. (Barking, Essex : 1987) 220, 540–548. https://doi.org/10.1016/j.envpol.2016.10.001.

Boos, J., Gilfedder, B.S., Frei, S., 2021. Tracking microplastics across the streambed interface: using laser-induced-fluorescence to quantitatively analyze microplastic transport in an experimental flume. Water Resour. Res. 57, 1–10. https://doi.org/10.1029/2021WR031064.

Boos, J.-P., Dichgans, F., Gilfedder, B.-S., Frei, S., 2022. An experimental method to quantitatively assess the transport of microplastic particles in fluvial systems. In: Proceedings of the 39th IAHR World Congress. Presented at the 39th IAHR World Congress From Snow to Sea. International Association for Hydro-Environment Engineering and Research (IAHR), pp. 5030–5034. https://doi.org/10.3850/IAHR-39WC252171192022487.

Broecker, T., Elsesser, W., Teuber, K., Özgen, I., Nützmann, G., Hinkelmann, R., 2018. High-resolution simulation of free-surface flow and tracer retention over streambeds with ripples. Limnologica 68, 46–58. https://doi.org/10.1016/j.limno.2017.06.005.

Broecker, T., Sobhi Gollo, V., Fox, A., Lewandowski, J., Nützmann, G., Arnon, S., Hinkelmann, R., 2021. High-resolution integrated transport model for studying surface water–groundwater interaction. Groundwater 59, 488–502. https://doi.org/10.1111/gwat.13071.

Broecker, T., Teuber, K., Sobhi Gollo, V., Nützmann, G., Lewandowski, J., Hinkelmann, R., 2019. Integral flow modelling approach for surface water-groundwater interactions along a rippled streambed. Water (Basel) 11, 1517. https://doi.org/10.3390/w11071517.

Burns, E.E., Boxall, A.B.A., 2018. Microplastics in the aquatic environment: evidence for or against adverse impacts and major knowledge gaps: microplastics in the environment. Environ. Toxicol. Chem. 37, 2776–2796. https://doi.org/10.1002/etc.4268.

Castañeda, R.A., Avlijas, S., Simard, M.A., Ricciardi, A., 2014. Microplastic pollution in St. Lawrence River sediments. Can. J. Fish. Aquat. Sci. 71, 1767–1771. https://doi.org/10.1139/cjfas-2014-0281.

Choi, J.S., Kim, K., Hong, S.H., Park, K.-I., Park, J.-W., 2021. Impact of polyethylene terephthalate microfiber length on cellular responses in the Mediterranean mussel Mytilus galloprovincialis. Mar. Environ. Res. 168, 105320 https://doi.org/10.1016/j.marenvres.2021.105320.

Constant, M., Alary, C., De Waele, I., Dumoulin, D., Breton, N., Billon, G., 2021. To what extent can micro- and macroplastics be trapped in sedimentary particles? A case study investigating dredged sediments. Environ. Sci. Technol. 55, 5898–5905. https://doi.org/10.1021/acs.est.0c08386.

Cook, S., Chan, H.-L., Abolfathi, S., Bending, G.D., Schäfer, H., Pearson, J.M., 2020. Longitudinal dispersion of microplastics in aquatic flows using fluorometric techniques. Water Res. 170, 115337 https://doi.org/10.1016/j.watres.2019.115337.

D'Avignon, G., Gregory-Eaves, I., Ricciardi, A., 2022. Microplastics in lakes and rivers: an issue of emerging significance to limnology. Environ. Rev. 30, 228–244. https://doi.org/10.1139/er-2021-0048.

Domercq, P., Praetorius, A., MacLeod, M., 2022. The full multi: an open-source framework for modelling the transport and fate of nano- and microplastics in aquatic systems. Environ. Modell. Softw. 148, 105291 https://doi.org/10.1016/j.envsoft.2021.105291.

Dong, S., Zhou, M., Su, X., Xia, J., Wang, L., Wu, H., Suakollie, E.B., Wang, D., 2022. Transport and retention patterns of fragmental microplastics in saturated and unsaturated porous media: a real-time pore-scale visualization. Water Res. 214, 118195 https://doi.org/10.1016/j.watres.2022.118195.

Drummond, J.D., Nel, H.A., Packman, A.I., Krause, S., 2020. Significance of hyporheic exchange for predicting microplastic fate in rivers. Environ. Sci. Technol. Lett. 7, 727–732. https://doi.org/10.1021/acs.estlett.0c00595.

Drummond, J.D., Schneidewind, U., Li, A., Hoellein, T.J., Krause, S., Packman, A.I., 2022. Microplastic accumulation in riverbed sediment via hyporheic exchange from headwaters to mainstems. Sci. Adv. 8, eabi9305. https://doi.org/10.1126/sciadv.abi9305.

Dudunake, T., Tonina, D., Reeder, W.J., Monsalve, A., 2020. Local and reach-scale hyporheic flow response from boulder-induced geomorphic changes. Water Resour. Res. 56 https://doi.org/10.1029/2020WR027719.

Dybbs, A., Edwards, R.V., 1984. A new look at porous media fluid mechanics — darcy to turbulent. Eds.. In: Bear, J., Corapcioglu, M.Y. (Eds.), Fundamentals of Transport Phenomena in Porous Media. Springer Netherlands, Dordrecht, pp. 199–256. https://doi.org/10.1007/978-94-009-6175-3_4.

Elliott, A.H., Brooks, N.H., 1997. Transfer of nonsorbing solutes to a streambed with bed forms: laboratory experiments. Water Resour. Res. 33, 137–151. https://doi.org/10.1029/96WR02783.

Ferziger, J.H., Perić, M., Street, R.L., 2020. Computational Methods for Fluid Dynamics. Springer International Publishing, Cham. https://doi.org/10.1007/978-3-319-99693-6.

Frei, S., Piehl, S., Gilfedder, B.S., Löder, M.G.J., Krutzke, J., Wilhelm, L., Laforsch, C., 2019. Occurence of microplastics in the hyporheic zone of rivers. Sci. Rep. 9, 15256. https://doi.org/10.1038/s41598-019-51741-5.

Frias, J.P.G.L., Nash, R., 2019. Microplastics: finding a consensus on the definition. Mar. Pollut. Bull. 138, 145–147. https://doi.org/10.1016/j.marpolbul.2018.11.022.

Goeppert, N., Goldscheider, N., 2021. Experimental field evidence for transport of microplastic tracers over large distances in an alluvial aquifer. J. Hazard. Mater. 408, 124841 https://doi.org/10.1016/j.jhazmat.2020.124844.

Haque, M.I., Mahmood, K., 1985. Geometry of Ripples and Dunes. J. Hydraul. Eng. 111, 48–63. https://doi.org/10.1061/(ASCE)0733-9429(1985)111:1(48).

Harvey, J.W., Bencala, K.E., 1993. The effect of streambed topography on surface-subsurface water exchange in mountain catchments. Water Resour. Res. 29, 89–98. https://doi.org/10.1029/92WR01960.

Hirt, C.W., Nichols, B.D., 1981. Volume of fluid (VOF) method for the dynamics of free boundaries. J. Comput. Phys. 39, 201–225. https://doi.org/10.1016/0021-9991(81)90145-5.

Hoellein, T.J., Shogren, A.J., Tank, J.L., Risteca, P., Kelly, J.J., 2019. Microplastic deposition velocity in streams follows patterns for naturally occurring allochthonous particles. Sci. Rep. 9, 3740. https://doi.org/10.1038/s41598-019-40126-3.

Horton, A.A., Dixon, S.J., 2018. Microplastics: an introduction to environmental transport processes. WIREs Water 5. https://doi.org/10.1002/wat2.1268.

Janssen, F., Cardenas, M.B., Sawyer, A.H., Dammrich, T., Krietsch, J., de Beer, D., 2012. A comparative experimental and multiphysics computational fluid dynamics study of coupled surface-subsurface flow in bed forms. Water Resour. Res. 48 https://doi.org/10.1029/2012WR011982.

Jing, S., Yang, W., Chen, Y., 2019. Smooth open channel with increasing aspect ratio: influence on secondary flow. Water (Basel) 11, 1872. https://doi.org/10.3390/w11091872.

Kirstein, I.V., Kirmizi, S., Wichels, A., Garin-Fernandez, A., Erler, R., Löder, M., Gerdts, G., 2016. Dangerous hitchhikers? Evidence for potentially pathogenic Vibrio spp. on microplastic particles. Mar. Environ. Res. 120, 1–8. https://doi.org/10.1016/j.marenvres.2016.07.004.

Koelmans, A.A., Gouin, T., Thompson, R., Wallace, N., Arthur, C., 2014. Plastics in the marine environment. Environ. Toxicol. Chem. 33, 5–10. https://doi.org/10.1002/etc.2426.

Laermanns, H., Reifferscheid, G., Kruse, J., Földi, C., Dierkes, G., Schaefer, D., Scherer, C., Bogner, C., Stock, F., 2021. Microplastic in water and sediments at the confluence of the Elbe and Mulde rivers in Germany. Front. Environ. Sci. 9, 794895 https://doi.org/10.3389/fenvs.2021.794895.

Laforsch, C., Ramsperger, A.F.R.M., Mondellini, S., Galloway, T.S., 2021. Microplastics: a novel suite of environmental contaminants but present for decades. Eds.. In: Reichl, F.-X., Schwenk, M. (Eds.), Regulatory Toxicology. Springer Berlin Heidelberg, Berlin, Heidelberg, pp. 1–26. https://doi.org/10.1007/978-3-642-36206-4_138-1.

Lebreton, L.C.M., van der Zwet, J., Damsteeg, J.-W., Slat, B., Andrady, A., Reisser, J., 2017. River plastic emissions to the world's oceans. Nat. Commun. 8, 15611. https://doi.org/10.1038/ncomms15611.

Lewandowski, J., Arnon, S., Banks, E., Batelaan, O., Betterle, A., Broecker, T., Coll, C., Drummond, J., Gaona Garcia, J., Galloway, J., Gomez-Velez, J., Grabowski, R., Herzog, S., Hinkelmann, R., Höhne, A., Hollender, J., Horn, M., Jaeger, A., Krause, S., Löchner Prats, A., Magliozzi, C., Meinikmann, K., Mojarrad, B., Mueller, B., Peralta-Maraver, I., Popp, A., Posselt, M., Putschew, A., Radke, M., Raza, M., Riml, J., Robertson, A., Rutere, C., Schaper, J., Schirmer, M., Schulz, H., Shanafield, M., Singh, T., Ward, A., Wolke, P., Wörman, A., Wu, L., 2019. Is the hyporheic zone relevant beyond the scientific community? Water (Basel) 11, 2230. https://doi.org/10.3390/w11112230.

Li, B., Liu, X., Kaufman, M.H., Turetcaia, A., Chen, X., Cardenas, M.B., 2020. Flexible and modular simultaneous modeling of flow and reactive transport in rivers and hyporheic zones. Water Resour. Res. 56 https://doi.org/10.1029/2019WR026528.

Lu, T., Gilfedder, B.S., Peng, H., Peiffer, S., Papastavrou, G., Ottermann, K., Frei, S., 2021. Relevance of iron oxyhydroxide and pore water chemistry on the mobility of nanoplastic particles in water-saturated porous media environments. Water Air Soil Pollut. 232, 168. https://doi.org/10.1007/s11270-021-05125-z.

Mani, T., Hauk, A., Walter, U., Burkhardt-Holm, P., 2016. Microplastics profile along the Rhine River. Sci. Rep. 5, 17988. https://doi.org/10.1038/srep17988.

13

Mani, T., Primpke, S., Lorenz, C., Gerdts, G., Burkhardt-Holm, P., 2019. Microplastic pollution in benthic midstream sediments of the Rhine river. Environ. Sci. Technol. 53, 6053–6062. https://doi.org/10.1021/acs.est.9b01363.

McCormick, A., Hoellein, T.J., Mason, S.A., Schluep, J., Kelly, J.J., 2014. Microplastic is an abundant and distinct microbial habitat in an urban river. Environ. Sci. Technol. 48, 11863–11871. https://doi.org/10.1021/es503610r.

Meijer, L.J.J., van Emmerik, T., van der Ent, R., Schmidt, C., Lebreton, L., 2021. More than 1000 rivers account for 80% of global riverine plastic emissions into the ocean. Sci. Adv. 7, eaaz5803. https://doi.org/10.1126/sciadv.aaz5803.

Napper, I.E., Thompson, R.C., 2020. Plastic Debris in the marine environment: history and future challenges. Global Chall. 4, 1900081 https://doi.org/10.1002/gch2.201900081.

Nikitin, N.V., Popelenskaya, N.V., Stroh, A., 2021. Prandtl's secondary flows of the second kind. Problems of description, prediction, and simulation. Fluid Dyn. 56, 513–538. https://doi.org/10.1134/S0015462821040091.

Nizzetto, L., Bussi, G., Futter, M.N., Butterfield, D., Whitehead, P.G., 2016. A theoretical assessment of microplastic transport in river catchments and their retention by soils and river sediments. Environ. Sci.: Processes Impacts 18, 1050–1059. https://doi.org/10.1039/C6EM00206D.

Petersen, F., Hubbart, J.A., 2021. The occurrence and transport of microplastics: the state of the science. Sci. Total Environ. 758, 143936 https://doi.org/10.1016/j.scitotenv.2020.143936.

Ren, J., Zhao, B., 2020. Model-based analysis of the effects of rippled bed morphologies on hyporheic exchange. J. Hydrol. Eng. 25, 04020023 https://doi.org/10.1061/(ASCE)HE.1943-5584.0001931.

Schmidt, C., Krauth, T., Wagner, S., 2017. Export of plastic debris by rivers into the sea. Environ. Sci. Technol. 51, 12246–12253. https://doi.org/10.1021/acs.est.7b02368.

Schrank, I., Trotter, B., Dummert, J., Scholz-Böttcher, B.M., Löder, M.G.J., Laforsch, C., 2019. Effects of microplastic particles and leaching additive on the life history and morphology of Daphnia magna. Environ. Pollut. 255, 113233 https://doi.org/10.1016/j.envpol.2019.113233.

Siegfried, M., Koelmans, A.A., Besseling, E., Kroeze, C., 2017. Export of microplastics from land to sea. A modelling approach. Water Res. 127, 249–257. https://doi.org/10.1016/j.watres.2017.10.011.

Sobhi Gollo, V., Broecker, T., Lewandowski, J., Nützmann, G., Hinkelmann, R., 2022a. Flow and transport modeling in heterogeneous sediments using an integral approach. Groundwater gwat 13275. https://doi.org/10.1111/gwat.13275.

Sobhi Gollo, V., Broecker, T., Lewandowski, J., Nützmann, G., Hinkelmann, R., 2021. An integral approach to simulate three-dimensional flow in and around a ventilated U-shaped chironomid dwelled burrow. J. Ecohydraul. 1–11. https://doi.org/10.1080/24705357.2021.1938258. Ahead of Print.

Sobhi Gollo, V., Broecker, T., Marx, C., Lewandowski, J., Nützmann, G., Hinkelmann, R., 2022b. A comparative study of integral and coupled approaches for modeling hydraulic exchange processes across a rippled streambed. Int. J. Geomath. 13, 16. https://doi.org/10.1007/s13137-022-00206-5.

Stride, B., Abolfathi, S., Odara, M.G.N., Bending, G.D., Pearson, J., 2023. Modeling microplastic and solute transport in vegetated flows. Water Resour. Res. 59, e2023WR034653 https://doi.org/10.1029/2023WR034653.

Thompson, R.C., Olsen, Y., Mitchell, R.P., Davis, A., Rowland, S.J., John, A.W.G., McGonigle, D., Russell, A.E., 2004. Lost at sea: where is all the plastic? Science 304, 838. https://doi.org/10.1126/science.1094559. –838.

Tötzke, C., Oswald, S.E., Hilger, A., Kardjilov, N., 2021. Non-invasive detection and localization of microplastic particles in a sandy sediment by complementary neutron and X-ray tomography. J. Soils Sediments 21, 1476–1487. https://doi.org/10.1007/s11368-021-02882-6.

Trauth, N., Schmidt, C., Maier, U., Vieweg, M., Fleckenstein, J.H., 2013. Coupled 3-D stream flow and hyporheic flow model under varying stream and ambient groundwater flow conditions in a pool-riffle system. Water Resour. Res. 49, 5834–5850. https://doi.org/10.1002/wrcr.20442.

von Moos, N., Burkhardt-Holm, P., Köhler, A., 2012. Uptake and effects of microplastics on cells and tissue of the blue Mussel *Mytilus edulis* L. after an experimental exposure. Environ. Sci. Technol. 46, 11327–11335. https://doi.org/10.1021/es302332w.

Waldschläger, K., Schüttrumpf, H., 2020. Infiltration behavior of microplastic particles with different densities, sizes, and shapes—from glass spheres to natural sediments. Environ. Sci. Technol. acs.est.0c01722. https://doi.org/10.1021/acs.est.0c01722.

Weller, H.G., Tabor, G., Jasak, H., Fureby, C., 1998. A tensorial approach to computational continuum mechanics using object-oriented techniques. Comput. Phys. 12, 620. https://doi.org/10.1063/1.168744.

Windsor, F.M., Tilley, R.M., Tyler, C.R., Ormerod, S.J., 2019. Microplastic ingestion by riverine macroinvertebrates. Sci. Total Environ. 646, 68–74. https://doi.org/10.1016/j.scitotenv.2018.07.271.

Xiao, Y., Liu, J., Wang, N., Gualtieri, C., Zhang, T., Liu, J., Fu, J., Zhou, J., 2022. Numerical simulation of overbank hyporheic transport and biogeochemical reactions in a compound channel. Hydrol. Process 36. https://doi.org/10.1002/hyp.14670.

Yang, S.-Q., Tan, S.K., Wang, X.-K., 2012. Mechanism of secondary currents in open channel flows: secondary currents, sand ridges, flows. J. Geophys. Res. 117 https://doi.org/10.1029/2012JF002510 n/a-n/a.

Zhou, T., Endreny, T.A., 2013. Reshaping of the hyporheic zone beneath river restoration structures. Water Resour. Res. 49, 5009–5020. https://doi.org/10.1002/wrcr.20384.

SUPPLEMENTARY MATERIAL

S1 COMPUTATIONAL MESH
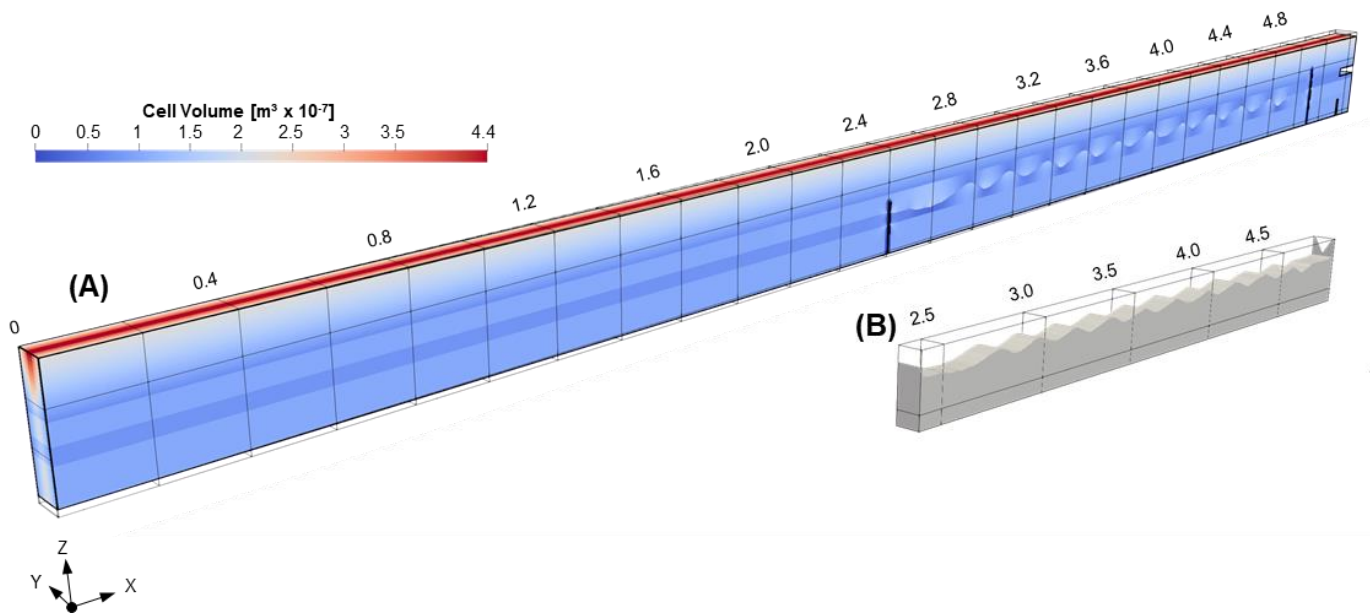
Figure S1.1 View of the computational mesh with cell size coloring (A) and digitized bedform geometry (B)
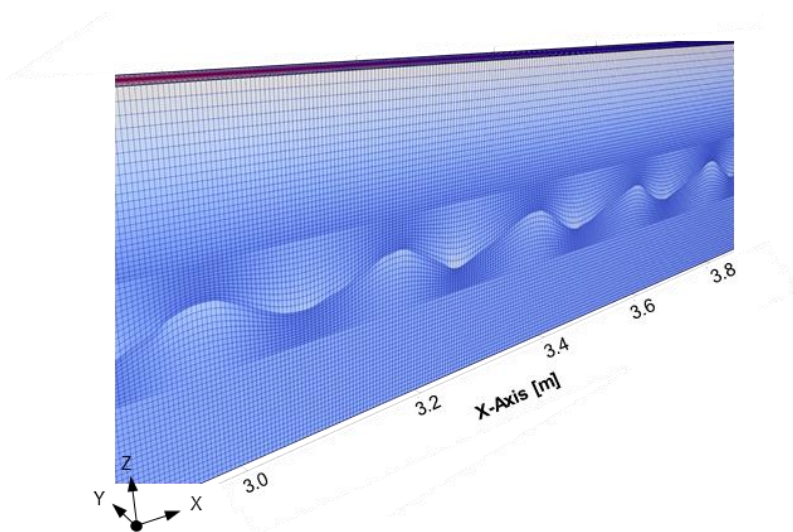
Figure S1.2 Excerpt from computational mesh view

S2. CURVE FITTING FOR FIS CURVES

Due to overexposure, the concentration curves sampled at the slice sampling line in the HZ had to be partially reconstructed due to the overexposure of the sensor during the passing of the particle cloud through the surface water section. The exponential Gaussian fit is given by the following equation:

$$y = \sum_{i=1}^{3} a_i e^{\left[-\left(\frac{x-b_i}{c_i}\right)^2\right]}$$

Table S2.1. Fit parameters for reconstruction of 1µm particle concentrations at the slice sampling line

	+2	+1	0	-1	-2	-3	-4	-5	-6	-7	-8
a1	552.855	483.213	0	431.718	222.121	93.007	136.072	131.160	98.633	13.397	0.000
b1	127.956	125.805	0	228.028	310.646	510.625	443.603	571.375	750.000	572.497	460.235
c1	35.389	59.251	0	50.994	54.617	118.930	96.439	132.469	244.849	128.586	-10249.921
a2	399.758	294.935	0	290.495	199.381	133.702	-62.673	68.588	35.849	75.027	109.822
b2	184.048	204.519	0	181.288	261.039	329.813	505.250	453.660	1251.845	867.938	1338.911
c2	61.963	114.906	0	24.260	34.951	32.723	2.841	65.339	468.929	205.259	471.501
a3	144.830	-283.903	0	279.659	151.523	146.435	98.693	45.366	27.097	78.407	18.618
b3	272.898	78.256	0	305.426	397.258	404.972	562.137	790.635	586.478	1286.766	798.021
c3	111.324	-34.951	0	101.171	113.677	69.702	161.938	262.055	115.574	457.020	236.632
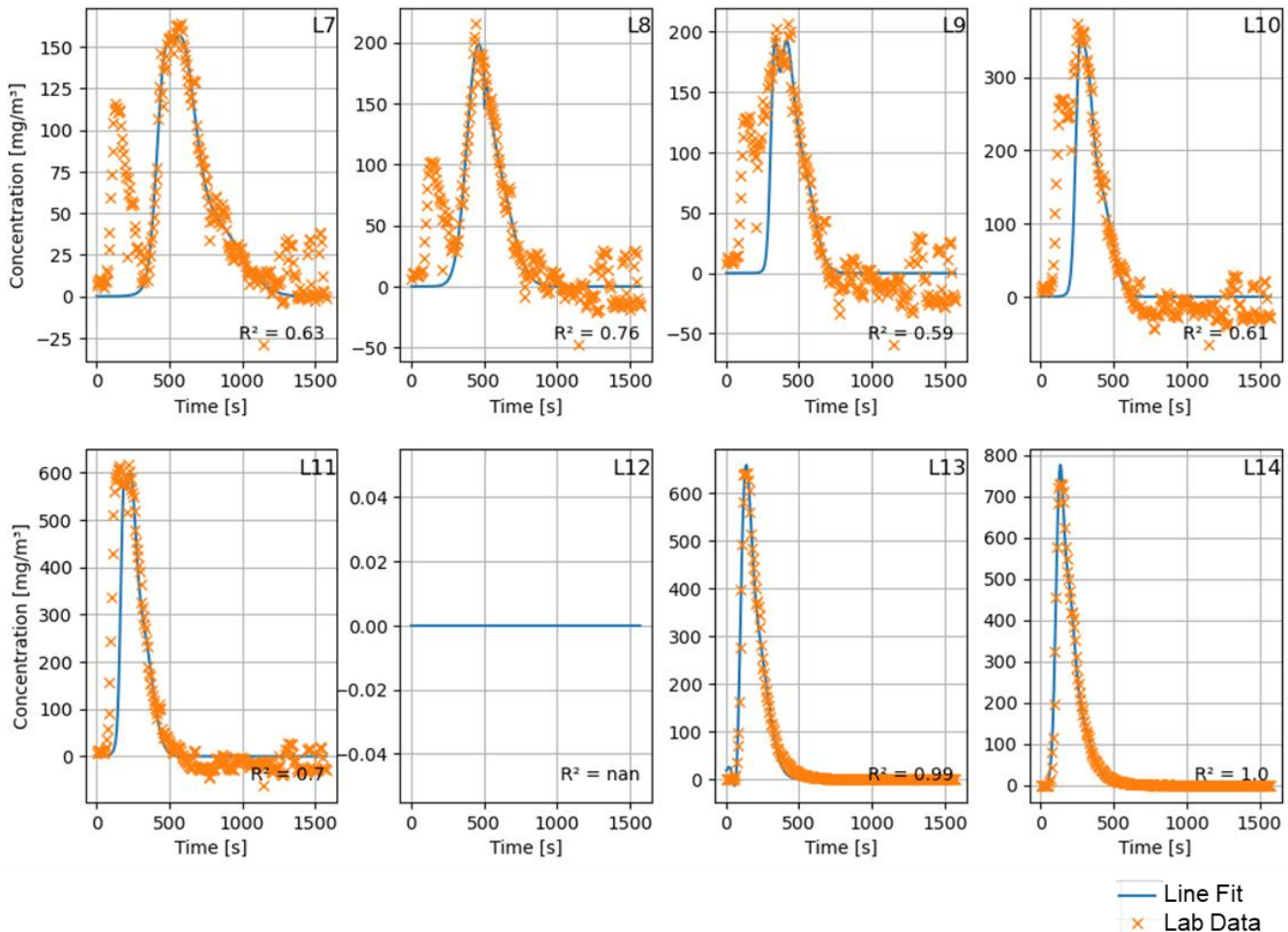
Figure S2.1. Raw laboratory records and line fits for the 1µm particle concentrations at the slice sampling line

S3. OPENFOAM MODEL SETUP: TECHNICAL DETAILS

The following table provides an overview over the OpenFOAM key functions utilized for the presented digital twin model, which allows interested researchers to replicate the results. The required boundary conditions for the various model variables are given in the model description.

OpenFOAM Version	v2112
Solver	interFoam
Turbulence Modelling	simulationType: LES LESmodel: Smagorinsky delta: vanDriest
Subsurface Flow Modelling	explicitPorositySource Type: DarcyForchheimer
Meshing	BlockMesh (Basemesh) MoveDynamicMesh (HZ, general setup) SnappyHexMesh (weir plates, details)
Transport of Conservative Scalar	Scalar Transport (Function Object) Phase: alpha.water D: 2e-9 Injection of MP through a scalarSemiImplicitSource

S4. INFILTRATION PATTERNS

The figure below shows the infiltration of 1μm particles into the HZ at different time steps (200, 600, 1200 s) for the complete experimental section. The lateral sections are located at the ripple crests.
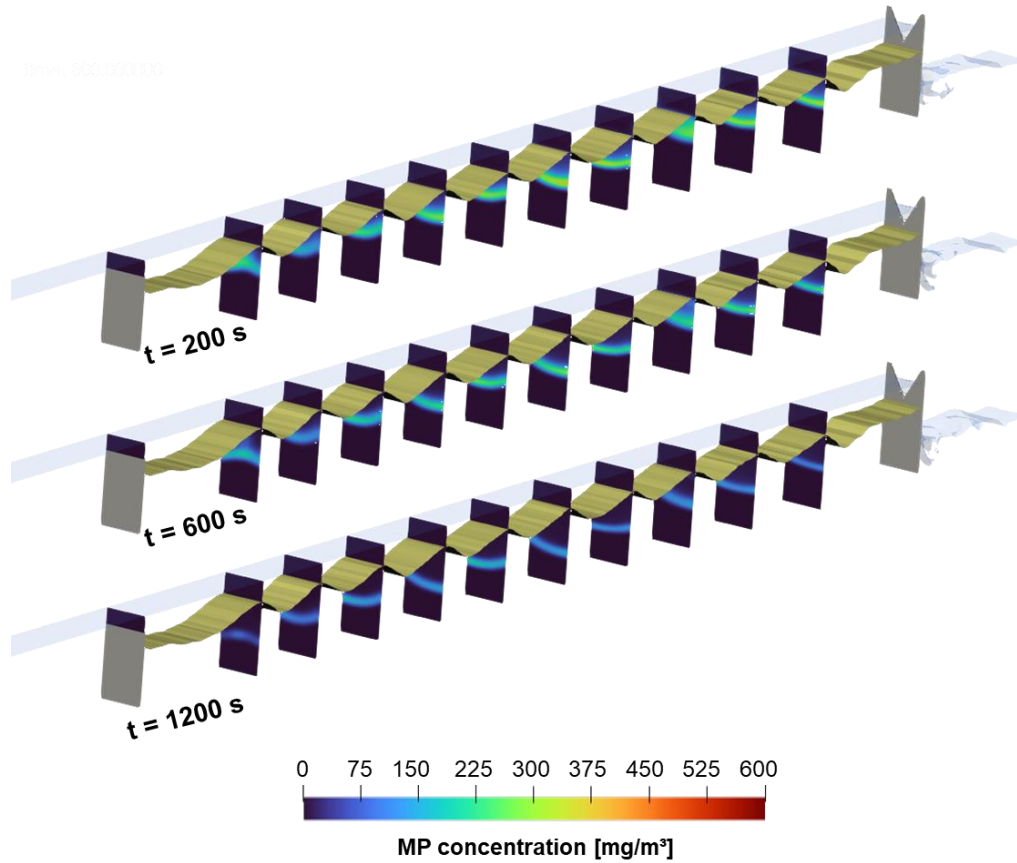
Figure S4: Infiltration of 1μm particles into the HZ below the ripple crests at 200, 600 and 1200s.

7 Publications and manuscripts

Study 4: Quantifying microplastic residence times in lakes using meso-cosm experiments and transport modelling

Authors: Hassan Elagami, Sven Frei, **Jan-Pascal Boos**, Gabriele Trommer, Benjamin-Silas Gilfedder

Quantifying microplastic residence times in lakes using mesocosm experiments and transport modelling

Hassan Elagami [a,b,*], Sven Frei [b], Jan-Pascal Boos [b], Gabriele Trommer [c], Benjamin S. Gilfedder [a,b]

[a] *Limnological Research Station, Bayreuth Center of Ecology and Environmental Research (BayCEER), University of Bayreuth, Bayreuth, Germany*
[b] *Department of Hydrology, Bayreuth Center of Ecology and Environmental Research (BayCEER), University of Bayreuth, Bayreuth, Germany*
[c] *Water Management Office, Ansbach, Germany*

ABSTRACT

The microplastic residence time in lakes is a key factor controlling its uptake by lake organisms. In this work we have, for the first time, conducted a series of microplastic addition experiments in a 12×3 m lake mesocosm and traced its transport through the lake water column. This was combined with a 1D physically based random walk model of microplastic transport. Four experiments were conducted using three microplastic size ranges (1–5, 28–48, and 53–63 μm) over one year during thermal stratification and lake turnover. The results showed that the residence time in the water column largely depended on particle size and lake hydrodynamics, although the smallest particles were poorly represented by the model. Residence times in the mesocosm ranged between ~1 day for the largest particles to 24 days for the small particles during summer. The modeled residence time were similar to the measured values of the 28–48 μm and 53–63 μm particles, but for the smallest particles residence times were calculated to be >200 d. The discrepancy is likely due to aggregation between the small microplastic particles and natural lake particles, which increases the microplastic settling velocity. Aggregation is favored for the small particles due their large surface area to volume ratio. In contrast, density instabilities in the water column during autumn likely led to turbulent convective mixing and rapid microplastic transport within the water column. This work shows that microplastic transport within lakes is complex and not fully understood, especially for the smallest sizes, and involves interactions between physical, physicochemical and biological processes.

1. Introduction

Continual technological advances in polymer engineering have reduced the costs of plastic production, allowing it to be used in a wide range of applications (D'Avignon et al., 2022). The majority of the global plastic volume produced is typically made for single-use, particularly as packaging (D'Avignon et al., 2022). Ideally, after use, the polymer is recycled and reenters the production stream. However, evidence from life cycle studies shows that improper disposal of plastic is significant (Lavoie et al., 2021; Woods et al., 2021). This has led to migration and accumulation of plastic debris in the environment (e.g., in inland waters) before it reaches the ocean (Cai et al., 2021). During the transport of plastic debris in the environment, it is exposed to various physical, chemical, and biological degradation processes (Meides et al.,

2021). The fragmentation and degradation processes in natural environments transform the large plastic debris (> 5 mm) into 'secondary' microplastic (5 mm to 100 nm) and nanoplastics (< 100 nm). While secondary microplastic results from the breakdown of macroplastic, primary microplastic is plastic pellets designed for commercial purposes such as in cosmetics (Arthur et al., 2009). These particles can reach lake systems predominantly from terrestrial sources such as effluents from sewage treatment plants (Sun et al., 2019), surface runoff (Wang et al., 2022), agriculture (Bigalke et al., 2022), and improper disposal of plastic waste close to the shoreline.

Since non-buoyant pristine microplastic particles are small in size and have polymer densities close to that of water, they are expected to have significant residence times in lake systems (Elagami et al., 2022). During their residence in the lake water column, they are exposed to a

H. Elagami et al.

wide range of lake organisms (e.g., zooplankton, fish). This results in a high likelihood of uptake by lake organisms before the plastic reaches the lake sediment, or before they are flushed from the lake via outlets (Canniff and Hoang, 2018; D'Avignon et al., 2022). Recent studies have shown that lake organisms such as zooplankton have a limited ability to distinguish between their food, which is usually composed of natural particulate organic carbon either from the lake or its catchment, and microplastic particles (Aljaibachi and Callaghan, 2018). Once microplastic particles have entered the food web, they can migrate to higher trophic levels through direct ingestion or indirect ingestion of microplastic containing organisms by predators (D'Avignon et al., 2022; Nelms et al., 2018).

The settling velocity of microplastic is controlled by key physical particle properties such as density and size (Ahmadi et al., 2022; Elagami et al., 2022; Khatmullina and Isachenko, 2017; Waldschläger and Schüttrumpf, 2019). Physical-chemical factors such as hydrophobic adhesion between pristine particles and fine air bubbles, formation of aggregates with natural particles existing in lake water column (Schmidtmann et al., 2022), as well as biofouling can affect the buoyancy of the microplastic, modify its settling velocity and thus also influence its residence time in lakes (Elagami et al., 2022; Leiser et al., 2020; Renner et al., 2020).

Lake hydrodynamics can also influence the residence times of microplastic within the water column. For instance, turbulent mixing in the epilimnion during summer is expected to cause a significant increase in the residence times of sinking particles compared to particles in the laminar metalimnion (Elagami et al., 2022; Kirillin et al., 2012; Reynolds and Wiseman, 1982). However, the behavior of microplastic during lake turnover is expected to be very different from that during the stratification period. This is due to the instability of the lake water column which leads to the onset of natural (turbulent) convective mixing (Cannon et al., 2021). The role that such complex hydrodynamic processes play in determining microplastic residence time is currently poorly understood.

Despite the growing number of studies investigating microplastic transport in lake systems, it is still a poorly understood process. All results from previous research are based on controlled laboratory settings (Elagami et al., 2022; Waldschläger and Schüttrumpf, 2019) and modeling (Ahmadi et al., 2022) and are unlikely to represent the complex microplastic behavior in a real lake . This is attributed to the fact that microplastic behavior in lake systems incorporates various interrelated biological, chemical, and hydrodynamic processes that are not yet well understood, especially at the whole-lake scale. Such processes and their associated impacts on residence time can only be captured by experiments directly in a lake water column.

In this work, we have performed microplastic addition experiments in a 3 × 12 m in-lake mesocosm located in lake Großer Brombachsee, Germany. The experiments were conducted over one year capturing the complexities of real lake settings during thermal stratification and lake turnover. Fluorescence techniques were used to quantify microplastic concentrations and infer residence times in the mesocosm during complex hydrodynamic conditions in the lake water column. The results from the mesocosm experiments were compared with results from a physically based random walk model that included turbulent and gravitational transport. The primary aims were to (i) develop a quantitative understanding of the primary processes influencing microplastic transport in the lake water column (e.g. particle size and lake hydrodynamics), (ii) investigate how well physical transport processes can explain observations in a complex in-lake mesocosm , and (iii) understand how the complex processes in the lake water column influence the exposure of organisms to this emerging pollutant.

2. Methodology

2.1. Study region

All field experiments were conducted at lake Großer Brombachsee in the German federal state of Bavaria. The Großer Brombachsee is a 5.1 km long and 2.0 km wide water reservoir with a maximum depth of 32.5 m covering an area of ~8.50 km^2. According to the long term monitoring data of the Water Management Authority Office Ansbach, the thermal stratification period extends from May until the end of October. Lake turnover typically begins in November. The lake has an intermediate level of productivity and is classified as mesotrophic. The average annual total nitrogen and phosphorus concentrations over lake depth are ∼ 0.95 and 0.025 mg l^{-1} respectively. The experimental site was situated at the border of a nature reserve, located on the southwestern side of the lake (Fig. 1). The water depth at the mesocosm site varied between 10 and 12 m depending on the season and extraction for water supply.

2.2. Mesocosm setup

The mesocosm setup (Aquatic Research Instruments, USA) consisted of a round 12 m deep and 3 m diameter impermeable polyethylene plastic enclosure with 80 % light transmittance, reinforced with nylon fibers (Figs. 2 and S1). The enclosure was fitted with side loops at 3 m intervals to stabilize the mesocosm. The upper end of the mesocosm was fitted with a 3 m diameter ring buoy constructed from a foam-filled corrugated drain pipe. The bottom of the enclosure was fixed to the sediment layer using 5 × 20 kg concrete ballasts. The enclosure was freely open from the top, but partially sealed from the bottom with a mesh. The mesocosm was lowered slowly into the lake before the mesh was installed shortly after the mesocosm. No filling (pumping) was required. A U-shaped pontoon was fixed around the mesocosm and adopted as a platform for fixing the instruments. The whole setup was anchored to the lake bed with 4 anchors and the ropes were tensioned to prevent the setup from drifting and rotating. The mesocosm was deployed in May 2021 and left for two months to allow the water column to equilibrate with the surrounding lake water before conducting the first experiment.

2.3. Microplastic particles

In this work we exclusively used microspheres due to the limited availability of fluorescent microplastic with irregular or fibrous forms. All microspheres were supplied by Cospheric LLC in green fluorescence dry powder. The fluorescent dye had maximum excitation and emission wave lengths of 414 and 514 nm respectively. Table 1 shows the polymers, their densities, particle sizes and the amounts of the microplastic used in each experiment. The 1–5 μm particles were composed of a propriety polymer of unknown chemical structure, whereas the larger particles were polyethylene with custom specific gravities. Aqueous microplastic solutions with concentrations of 1.0 g l^{-1} were prepared in the laboratory prior to each experiment. Due to the hydrophobic nature of Cospheric particles, the stock solutions were prepared using distilled water mixed with 0.1 g of surfactant (Tween 20) per 100 ml of stock solution. This also prevented the microplastic from agglomerating or floating on the surface of the water while preparing the solution. The solutions were then preserved in clean sealed buckets in a cool room before transportation to the lake.

Four microplastic addition experiments were conducted in the mesocosm over one year (from July 2021 to June 2022). The experimental dates were chosen carefully to capture lake stratification in summer as well as lake turnover in autumn. Three experiments were conducted during summer using 1–5, 28–48, and 53–63 μm spherical fluorescence particles. The summer experiments were aimed at investigating the effect of particle size and surface area to volume ratio on the
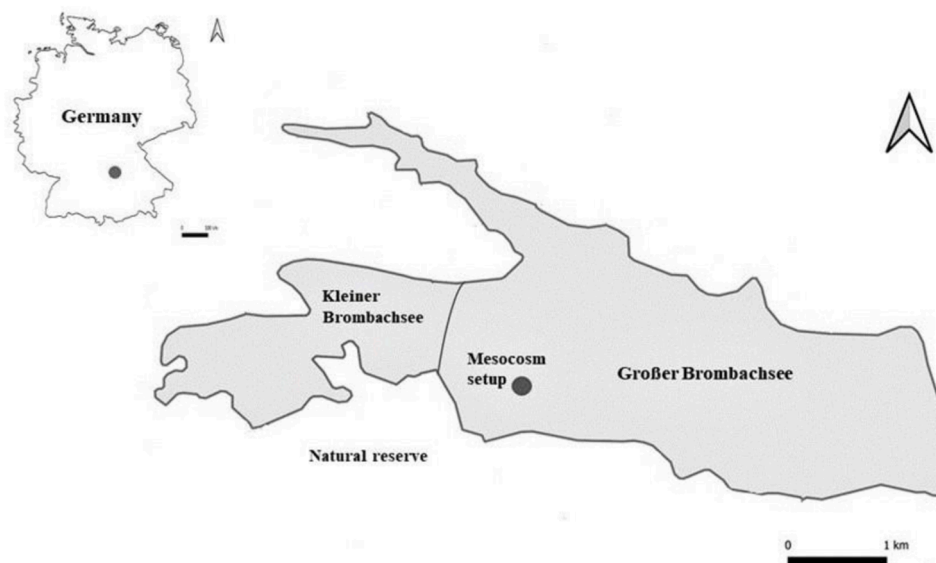
Fig. 1. A map showing the location of the experimental setup at lake Großer Brombachsee in Bavaria, Germany.
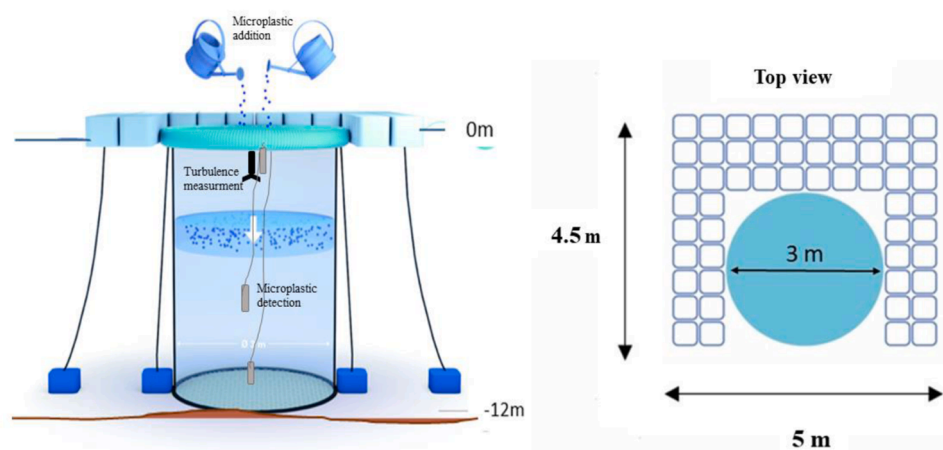
Fig. 2. A sketch of the mesocosm setup at lake Großer Brombachsee.

Table 1
A list of polymer names, particle densities, amount, and sizes of the microplastic microspheres used in the experiments.

Polymer	Density (g cm^{-3})	Amount (g)	Diameter (μm)	Time of experiment
Polyethylene	1.10	20	53–63	Summer 2021
Polyethylene	1.10	20	28–48	Summer 2021
Unknown (Proprietary Polymer)	1.30	5	1–5	Summer 2022
Unknown (Proprietary Polymer)	1.30	5	1–5	Autumn 2021

residence time of the particles during thermal stratification. The autumn experiment conducted using the 1–5 μm particles was aimed at quantifying the effect of lake turnover (convection) on the residence time of the particles in the mesocosm.

2.4. Microplastic addition to the mesocosm

Prior to each experiment, the surface of the water inside the mesocosm was cleaned using fine nets. The stock solutions were stirred in the buckets until all settled particles were resuspended and uniformly distributed in the solution. The particles were then added as a pulse from the top of the mesocosm simultaneously by two persons using two metal watering cans fitted with wide sprinklers to ensure a uniform distribution of the microplastic at the surface of the mesocosm (Fig. S2). The watering cans and sprinklers were carefully rinsed using lake water to ensure that all microplastic were flushed into the mesocosm. The particle additions are estimated to have lasted a maximum of five minutes.

2.5. Field measurements

Water temperatures were measured in the center of the mesocosm for the duration of the experiments using Hobo TidbiT temperature loggers at 1 m intervals and with a sampling resolution of 30 min. Temperature profiles were also taken outside the mesocosm before the start of each experiment and compared with the temperatures in the mesocosm. The temperature data were used to infer the stability and stratification of the water column, and to define the epilimnion and metalimnion.

3

H. Elagami et al.

A 3D acoustic doppler velocimeter (ADV, Nortek vector 300) was used to measure 3D water velocities inside the mesocosm, and infer turbulent kinetic energy and turbulent diffusion. The ADV was fixed in the center of the mesocosm at 1 m below the water surface. The instrument was set to sample at burst intervals of 600 s with 100 samples per burst at 8 Hz. The ADV was set to detect flow velocities in the East-North-Up (ENU) directions in a sampling volume of $\sim$ 1.5 cm^3. The instrument is equipped with a magnetometer and tilt sensors to correct measured velocities for movement of the instrument in the water column.

The fluorescent microplastic was measured in the center of the mesocosm using submersible field fluorometers (GGUN-FL24) from Albillia (Bailly-Comte et al., 2018). The fluorometers used an excitation wavelength of 470 nm to excite the green microplastic particles and the fluorescent intensity was measured in the 'uranine' channel. The fluorometers were calibrated in the laboratory following the same procedures as presented in Boos et al. (2021). At least 8 calibration points were used. The only difference to Boos et al. (2021) is that calibration solutions were prepared using filtered lake water rather than distilled water. The calibrations are presented in Fig. S3. The minimum detection limits of the 1–5, 28–48, and 53–63 μm particles were approximately 2, 100, and 200 μg l^{-1} respectively. The fluorometers were less sensitive to the 28–48 and 53–63 μm microspheres due to the lower particle numbers per gram microplastic and higher scattering in the measuring cell (Fig. S3). The measurement frequency of the fluorometers in the mesocosm was selected according to the expected residence times of the particles based on their laminar settling velocities. Thus, the sampling interval was fixed at 2 and 120 s for the large (fast) and the small (slow) particles, respectively. During lake stratification, the fluorometers were positioned at 0.5 m below the water surface, the epilimnion-metalimnion interface, and 1 m from the bottom of the mesocosm. During lake turnover in autumn, the fluorometers were only positioned at 0.5 m below the water surface and 1 m over lake sediment.

2.6. Microplastic settling velocity

In this work we have used three characteristic settling velocities for the microplastic particles. Firstly, the settling velocities of the 28–48 and 53–63 μm particles were measured in the laboratory under laminar conditions using particle image velocimetry system (PIV). The measured velocities were then corrected to the water temperature of each lake compartment in the mesocosm. The corrected settling velocities were denoted as v_{s_PIV} [L T^{-1}]. Secondly, due to the limitations of our PIV system, it was not possible to measure the settling velocity of the particles in the range of 1 μm in the laboratory. Here we used Stokes equation to calculate the settling velocity of the 1–5 μm particles as these particles were large enough that the Brownian motion will not affect their settling, but also small enough that the Reynolds number would be $<<$1, and so laminar conditions around the particle can be assumed (i.e. in Stokes range). Stokes velocity was denoted (v_{s_Stokes}) [L T^{-1}]. Finally, effective settling velocities for all microplastic particles were calculated using the experimental data from the mesocosm (v_{s_eff}) [L T^{-1}].

The settling velocities of the large 28–48 and 53–63 μm microspheres were measured in the laboratory using the same two-dimensional iLa 5051 PIV system used by Elagami et al. (2022). The system consists of a high-speed camera (40 frames per second) and a light source (high-power light-emitting diodes) with a wavelength of 530 nm. The settling velocities were measured in a 10 cm x10 cm x 40 cm glass column filled with filtered lake water based on the design of Khatmullina and Isachenko (2017). The room temperature was kept constant at 20 °C. Approximately 1 ml of the stock microplastic solution was added carefully at the top of the column as a pulse (cloud) . The average settling velocity of each particle cloud was calculated based on the PIV images. The v_{s_PIV} were corrected as in Ghawi and Kris (2012) using the water temperature of each lake compartment using Eq. (S4).

Stokes settling velocities were calculated as:

$$v_{s\_Stokes} = \frac{2}{9} \frac{(\rho_p - \rho_w)}{\mu} g R^2 \tag{1}$$

Where ρ_p [M L^{-3}] is the density of the particle, ρ_w [M L^{-3}] is the density of the lake water, R [L] is the radius of the particle, g [L T^{-2}] is the acceleration due to gravity, and μ [M L^{-1} T^{-1}] is the dynamic viscosity of the water.

The effective settling velocities from the mesocosm experiments were calculated for all microplastic sizes by dividing the depth of each compartment (i.e. epilimnion or metalimnion) by the time required until 50% of the particles were lost from the compartment (median particle breakthrough at the bottom of the compartment):

$$v_{s\_eff} = \frac{z}{\tau_{50\%}} \tag{2}$$

Where z [L] is the depth of the compartment, and $\tau_{50\%}$ [T] is the time elapsed until 50% of particles was lost from that compartment (median residence time).

2.7. Hydrodynamic calculations

The temperature data inside the mesocosm was used to calculate the Rayleigh number to elucidate if natural convection occurred in the water column during the autumn experiment. The Rayleigh number was calculated according to Eq. (3) (Weeraratne and Manga, 1998):

$$Ra = \frac{\alpha g \Delta T z^3}{\nu \beta} \tag{3}$$

where α is the thermal expansion coefficient of water (210×10^{-6} C^{-1}), g is the acceleration due to gravity, ΔT (°C) is the temperature difference between the bottom and top boundaries, z is the thickness of the compartment, ν [L^2 T^{-1}] is the kinematic viscosity of water, and β [L^2 T^{-1}] is thermal diffusivity of water.

The 3D water velocity data were used to calculate the turbulence kinetic energy (TKE) [L^2 T^{-2}] in the mesocosm. The time series for TKE of each burst was calculated using Eq. (4) as in Wüest and Lorke (2003):

$$TKE = \frac{1}{2} \left(\sigma_{East}^2 + \sigma_{North}^2 + \sigma_{Up}^2 \right) \tag{4}$$

Where, σ_{East}, σ_{North}, and σ_{up} [L T^{-1}], are the standard deviations of the fluctuations in velocity components during each burst.

The vertical component of the velocity data was also used to calculate the vertical eddy diffusivity (D) [L^2 T^{-1}] for each burst. Since velocities were measured in the Eulerian frame of reference, where the flow moves past the velocity sensor fixed at 1 m below the water surface, D can be estimated from Taylor's approach using (Holtappels and Lorke, 2011)

$$D = w' . L_E \tag{5}$$

$$L_E = \int_0^\infty E_r . dr \tag{6}$$

Where, w' is the standard deviation of the vertical velocities [L T^{-1}], L_E [L] is the Eulerian integral length scale, E_r [-] is the spatial correlation coefficient, and r [L] is the spatial distance. For simplification, L_E [L] was assumed to be equal to the Lagrangian length scale (L_L) [L] as also done by Holtappels and Lorke (2011). Hence, D [L^{2}T^{-1}] was calculated as follows:

$$D = w' . L_L \tag{7}$$

$$L_L = w' . T_L \tag{8}$$

$$T_L = \int_0^\infty R_L . d\tau \tag{9}$$

Where T_L [T] is the Lagrangian time scale, R_L [-] is the Lagrangian velocity autocorrelation, and τ [T] is the time interval between two velocity measurements (0.125 s).

2.8. Calculation of residence times in the mesocosm

The residence time of the microplastic in each compartment was calculated as the delay between the time required for 95% of the microplastics to be lost from the compartment and the time of microplastic input to that compartment. For instance, the residence time in the epilimnion (τ_{epi}) [T] was calculated as the difference between the time required until 95% of the particles were lost from the epilimnion and the time when the microplastic was added to the mesocosm. The residence time in the metalimnion (τ_{meta}) [T] was calculated as the delay between the time where 95% of the particles was lost from the metalimnion and the start of the pulse detected by the fluorometer positioned at the epilimnion-metalimnion interface. During lake turnover in the autumn, the mesocosm was treated as one mixed compartment and thus the residence time was calculated for the whole mesocosm (τ_{tot}) [T]. The total residence times in the mesocosm during autumn and summer experiments were calculated as the difference between the time required until 95% of the particles passed the deepest fluorescence detector and the time of adding the microplastic to the mesocosm.

2.9. Modeling of microplastic sinking trajectories and residence times

Particle sinking trajectories and residence times in the mesocosm were modeled using a Lagrangian particle tracking technique based on the Huret et al. (2007), Visser (1997) scheme which was later modified and applied by Rowe et al. (2016) and Ross (2006) to simulate the vertical distribution of bacteria and plankton under turbulent conditions in lakes. The effect of turbulent motion on particle trajectories and residence times in the water column is represented by a 1D random walk assuming a vertically heterogeneous turbulence field:

$$z(t + \Delta t) = z(t) + v_s \Delta t + D'(z(t))\Delta t + R\sqrt{\frac{2D(\widetilde{z})\Delta t}{r}} \tag{10}$$

where the vertical particle trajectory $z(t+\Delta t)$ [L] for a time increment Δt [T] can be estimated based on the current particle location $z(t)$ [L], the depth specific particle settling velocity v_s [L T^{-1}], the depth gradient of the turbulent diffusivity $D' = \frac{dD}{dz}$ [L T^{-1}], a normally distributed random number R [-] in the range of $R \epsilon [-1, 1]$ with zero mean and a variance of $r = 1/3$ and the turbulent diffusivity $D(\widetilde{z})$ [L^2 T^{-1}] at an intermediate location $\widetilde{z} = z(t) + 0.5\frac{dD(z(t))}{dz} \Delta t$.

For representation of the vertical turbulent diffusivity, a power law model similar to Kirillin et al. (2012) was used:

$$K(z) = \begin{cases} D_s^{(1-z/H_E)} D_M^{z/H_E} & at \ z \leq H_E \\ D_M & at \ H_E < z < H_M \\ D_M^{(H-z/H_H)} D_H^{z-(H_M+H_E)/H_H} & H_M < z < H_H \end{cases} \tag{11}$$

Where D_S, D_M and D_H [L^2 T^{-1}] are the turbulent diffusivities at the lake surface, the interface to the metalimnion and the lake bottom respectively. H_E, H_M and H_H [L] denote the thickness of the epilimnion, the metalimnion and the total depth of the lake respectively. Turbulent diffusivity at the lake surface D_s was estimated using the Taylor's approach based on the ADV data. Diffusivities at the interface to the metalimnion and the lake bottom were estimated by fitting the measured particle curves at each depth to an Advection-Dispersion-Model (A-D). The A-D model represents an analytical solution to the one-dimensional advection dispersion equation for a semi-infinite system with an instantaneous injection of a tracer (in our case microplastic

particles) in the fluid flux (Kreft and Zuber, 1978; Małoszewski and Zuber, 1982). From the A-D fitting, the depth specific Peclet number $Pe = v_s z/D$ [-] can be derived, relating the effect of gravitational settling and turbulent diffusion for a specific depths z where microplastic concentrations were measured (Ross 2006). D values can then be derived from the Pe-number using the settling velocity (i.e. v_{s_Stokes}, v_{s_PIV}, v_{s_eff}). A detailed description of the A-D fitting procedure is provided as part of the supplementary information. Each breakthrough experiment was represented using 2500 particles in the random walk simulations. All parameters used to run the random walk model are provided in the supplementary information S5.

3. Results

3.1. Mesocosm temperature profiles

The measurements at the start of the experiments showed that the water column inside and outside the mesocosm were near to identical and during summer was thermally stratified and divided into an epilimnion and metalimnion (Fig. S6). The water temperatures inside the mesocosm for the duration of the experiments are shown in Fig. 3. The thickness of the epilimnion inside the mesocosm over the extent of the experiments were ~8, 9, and 6 m for the first, second and third summer experiment, respectively (Fig. 3). The thickness of the metalimnion during the three summer experiments were ~ 3, 2, and 4 m. The water temperatures varied between 18 and 25°C for the epilimnion and 12 to 14°C for the metalimnion.

Prior to and during the autumn experiment, the temperature tended to be warmer at depth than at the surface (Figs. 3d and S6). The differences between the lower (the warmer) and the upper (the cooler) layer inside and outside the mesocosm at the start of the experiment were ~ 0.8 and 0.85°C respectively (Fig. S6). Also, the average temperature difference between the lower and the upper layer inside the mesocosm during the whole autumn experiment was ~ 0.8°C (over an extent of 11 m). The Rayleigh number (Eq. (3)) was calculated to investigate the propensity for natural convection in the mesocosm. The time series for the Rayleigh numbers is presented in Fig. S7. The minimum Rayleigh number was ~ 4 × 10^{12}, considerably exceeding the critical value of ~1700 (Reid and Harris, 1958). The Rayleigh number also indicated that the convection was turbulent (Ra>10^9).

3.2. Turbulence kinetic energy

There were substantial fluctuations in the TKE in the epilimnion during summer experiments, especially for the experiment with the 1–5 μm particles (Fig. 4). The maximum values for TKE during the summer experiments were ~ 2.7 × 10^{-3}, 5 × 10^{-3}, and 6.6 × 10^{-3} m^2 s^{-2} for the first, second, and third experiments respectively. The average TKE values were 3.5 × 10^{-4}, 5 × 10^{-4}, and 1 × 10^{-4} m^2 s^{-2}. During autumn, however, the fluctuations in the TKE values were much lower, showing much flatter TKE time series than that during summer experiments. The maximum and the average TKE values during autumn were 1.8 × 10^{-4} and 2 × 10^{-5} m^2 s^{-2} respectively.

3.3. Microplastic concentrations in the mesocosm

Fig. 5a, b, and c show the abundance and distribution of the microplastic in the mesocosm during the summer experiments. The maximum microplastic concentrations measured at 0.5 m were approximately 15, 11 mg l^{-1}, and 400 μg l^{-1} during the first (53–60 μm), second (28–48 μm), and third (1–5 μm) experiments, respectively. The maximum concentrations at the epilimnion-metalimnion interface were approximately 10, 5 mg l^{-1}, and 200 μg l^{-1} during the first, second, and third experiments . At the bottom of the metalimnion, the maximum microplastic concentrations were approximately 2, 7 mg l^{-1}, and 50 μg l^{-1} for the first, second, and third experiments. The time required until

H. Elagami et al.
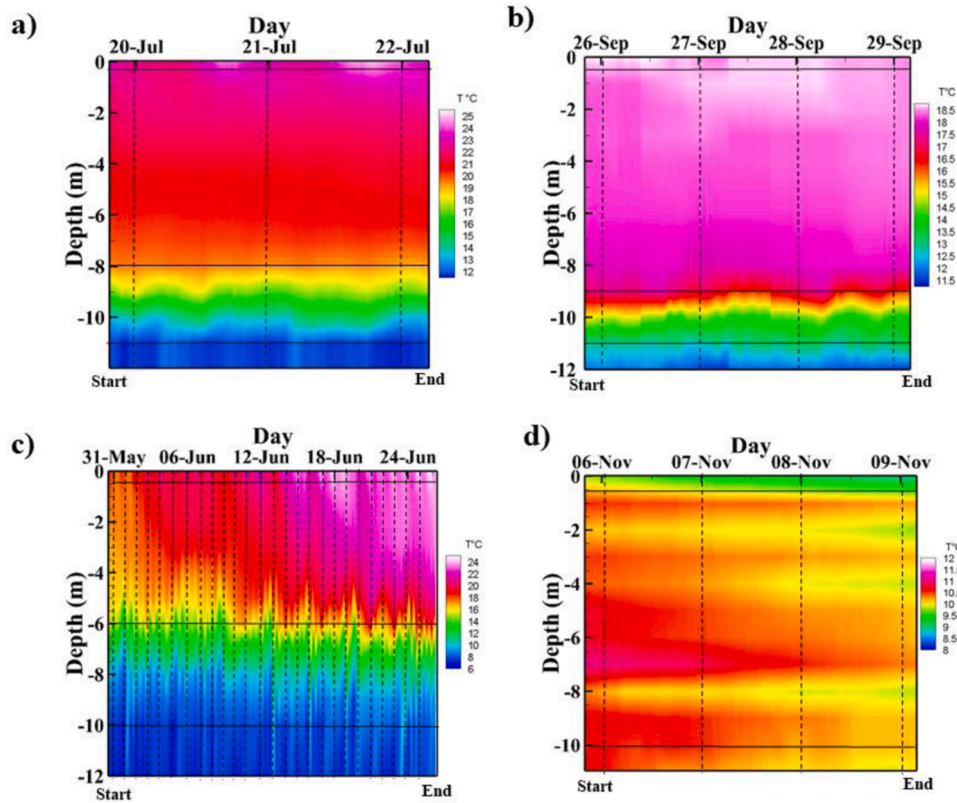
Fig. 3. Temperature profiles inside the mesocosm for the duration of each experiment. Figures (a), (b), and (c) show the temperature profiles during summer while figure (d) shows the temperature profile during autumn. The horizontal lines show the location of the fluorometers which also define the lake epilimnion and metalimnion. The vertical dashed lines represent midnight.
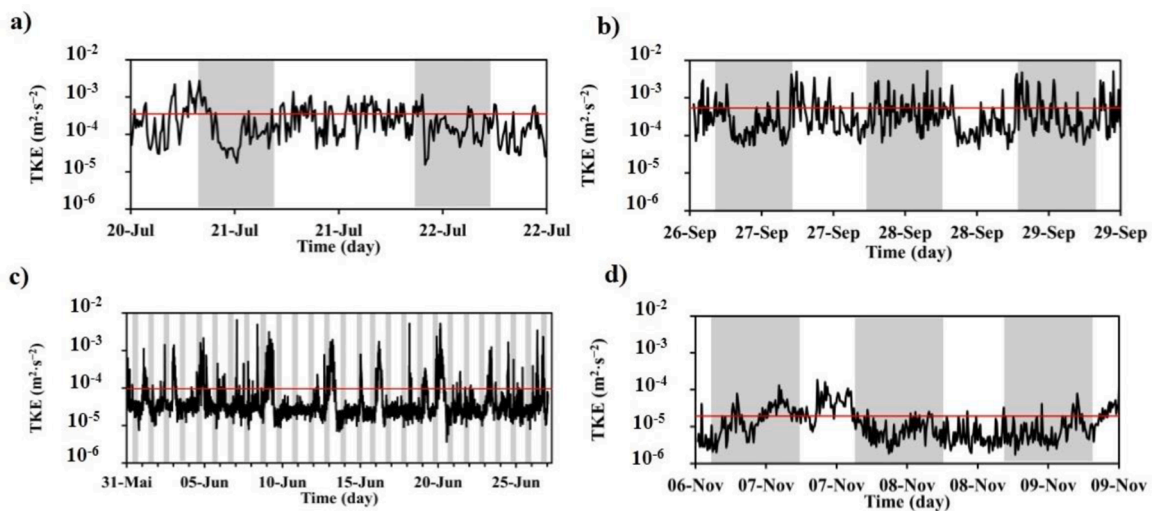
Fig. 4. Time series of TKE for all experiments. Figures (a), (b), and (c) present TKE during summer for the 53–63, 28–48, and 1–5 μm particles respectively. Figure (d) shows TKE during autumn for the 1–5 μm microspheres. The gray intervals represent the night times. The red lines show the average TKE values. Note the logarithmic scale.

95% of the particles was lost from the epilimnion (τ_{epi}) was 0.8, 1.9, and 19.5 days for the first, second, and third summer experiments (Fig. 5). For the metalimnion, τ_{meta} was 0.6, 1.4, and 22 days for the first, second, and third experiments (Fig. 5). The total residence times in the mesocosm were 1, 2.5, and 24.7 days.

The measured particle concentrations during autumn are presented in Fig. 5d. Surprisingly, the upper and the lower pulses showed an overlap of ~ 1 day. The maximum microplastic concentration detected by the upper fluorometer was ~ 80 μg l^{-1}. The lower pulse was divided into large initial and small subsequent pulses with maximum concentrations of ~ 55 and 25 μg l^{-1} respectively. The time until 95% of the particles had passed the lowest detector 1 m over lake sediment (τ_{tot}) 1.9 days.

H. Elagami et al.
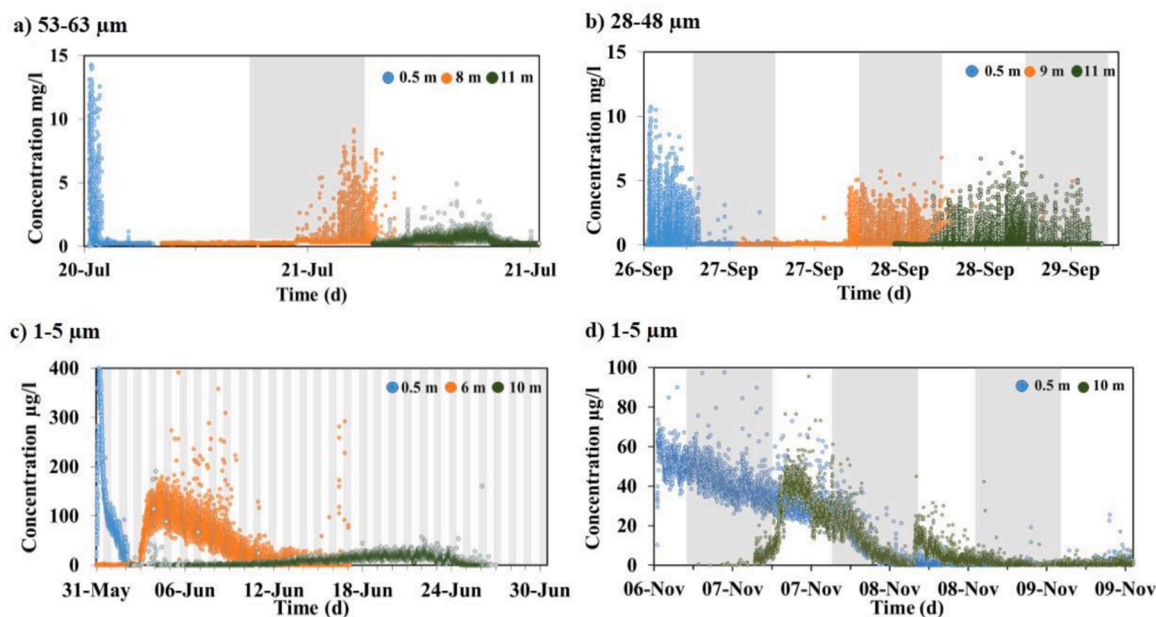
Fig. 5. The measured concentrations of microplastic in the mesocosm. Figures (a), (b), and (c) show particle concentrations during summer experiments. Figure (d) shows particle concentrations during autumn. The gray intervals represent the night times. The blue, orange and green pulses represent the microplastic concentrations at 0.5 m below the water surface, epilimnion-metalimnion interface (in summer), and deepest fluorometer (bottom of the metalimnion in summer) respectively.

3.4. Settling velocity

Table 2 shows the values of the characteristic settling velocities (v_{s_Stokes}, v_{s_PIV}, and v_{s_eff}) used in the random walk model. For the 1–5 µm particles, the lowest velocities were estimated using Stokes Law (0.079 m d^{-1}) while the highest settling velocities were the $vs_{\_eff}$ (1.09 m d^{-1}). Also, for the 53–63 µm particles, vs$_{\_eff}$ was the highest (50 m d^{-1}), while v_{s_PIV} was the lowest (17 m d^{-1}). In contrast, for the 28–48 µm particles v_{s_PIV} was the highest (8.7 m d^{-1}) while v_{s_eff} was the lowest (0.16 m d^{-1}).

3.5. Eddy diffusivity

The A-D fitting routine provided estimates for the turbulent diffusivities that were comparable to those derived using Taylor's approach and the ADV data for the summer experiments using the 1–5 µm particles (Supplementary information S8). The turbulent diffusivities ranged between $D_H =1.12 \times 10^{-6}$ and $D_s = 6.7 \times 10^{-6}$ m^2 s^{-1} (Table S9). For the summer experiments using 28–48 and 53–63 µm the A-D fitting was less successful so that the random walk modeling relied primarily on D values derived from Taylors approach. This ranged from 3×10^{-6} to 1×10^{-5} m^2 s^{-1} depending on experiment and depth (Table S9). During

autumn, our modeling depended exclusively on the D values calculated from Taylor's approach.

3.6. Random walk model

The random walk model was run using the three different settling velocities $v_{s\,Stokes}$, v_{s_PIV} and v_{s_eff} depending on the experiment being simulated. The distribution in residence times of the individual simulated particles (i.e. microplastic residence time distribution) where then used to calculate the time until 95% of particles had passed a specified depth in the water column. This is defined as the virtual microplastic residence time. The simulations using $v_{s\,Stokes}$ (summer experiment 1–5 µm) are shown in Fig. 6, and have a rapid rise as the particle pulse reaches the measurement depth, and then a long tail as particles are transported by a combination of settling and turbulence from the water column. The simulated residence times were considerably longer than the measured values, with ~ 135 days for the first 0.5 m, 225 days for the epilimnion (6 m) and 239 days for the whole mesocosm water column (10 m).

When using $v_{s\,eff}$ for the same model run, the simulated microplastic residence times of the 1–5 µm particles in summer were similar to that inferred from microplastic concentrations in the mesocosm (Fig. 7). All distributions showed the characteristic shape of the A-D model with a fast increase, a local maxima and a slowly decaying tail. The only parts that could not accurately be represented by the random walk model were the initial peak in particle concentrations at 0.5 m and the rapidly decaying tails at 0.5 and 10 m depth (Fig. 7). Using $v_{s\,eff}$, the residence times were 4 days for 0.5 m, 11 days for the epilimnion (6 m) and 32 days for the whole 10 m water column.

Results from simulations for the 28–48 and 53–63 µm particles in summer and the 1–5 µm particles in autumn experiment are summarized in Table 3. As the $v_{s\,eff}$ method did not work well for the larger particle sizes (28–48 µm) due to a noisy signal from the detectors, the random walk simulations for this size class were parameterized using $v_{s\,PIV}$. The results show that while the random walk model can reproduce the measured residence times for the larger particles relatively well (e.g. 0.8 vs. 0.62 days for the 53–63 µm particles), it significantly overestimated the residence times for the small particles in the autumn experiments

Table 2
A comparison between the characteristic settling velocities.

Experiment	Settling velocity Epi. (m d^{-1})	Settling velocity Meta. (m d^{-1})	Settling velocity Hypo. (m d^{-1})
1–5 µm Summer	0.098[1]	0.086[1]	0.079[1]
	1.09[2]	0.5[2]	0.5[2]
1–5 µm Autumn	0.077[1]	0.077[1]	0.077[1]
	0.78[2]	0.78[2]	0.78[2]
28–48 µm Summer	0.16[2]	4.11[2]	5.15[2]
	8.7[3]	8.0[3]	8.0[3]
53–63 µm Summer	50.0[2]	50.0[2]	50.0[2]
	19.0[3]	17.0[3]	17.0[3]

[1] v_{s_Stokes} [2] v_{s_eff} [3] v_{s_PIV}.

H. Elagami et al.

Fig. 6. Simulated residence time distribution (RT) at 0.5, 6 and 10 m depth for the 1–5 μm particles of the summer experiment using Stokes velocity.
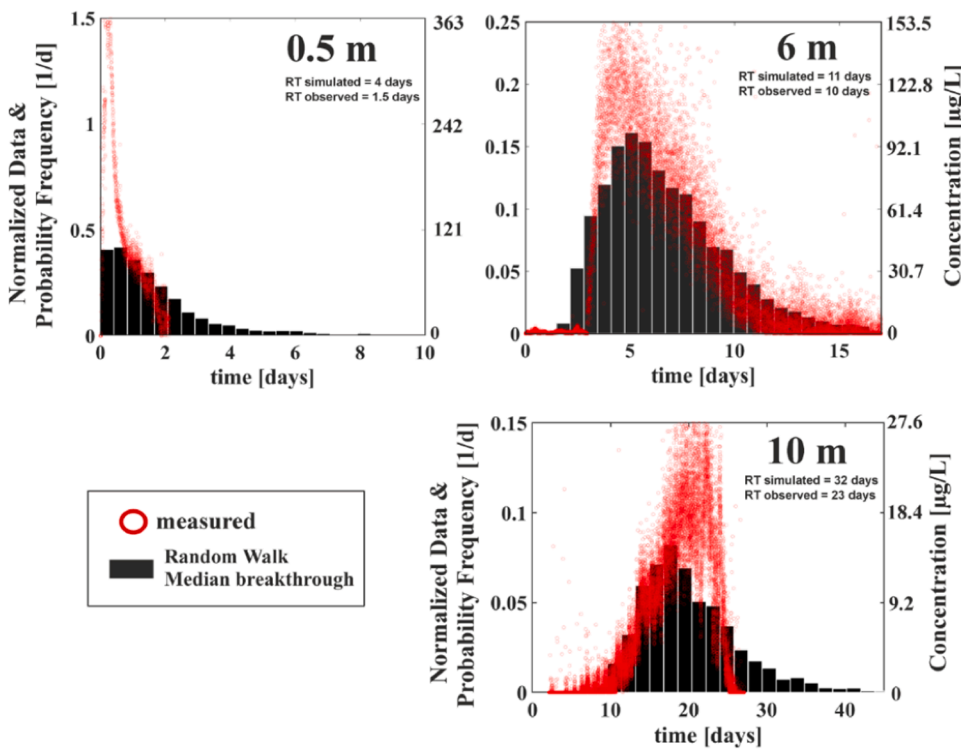
Fig. 7. Simulated and measured particle breakthroughs at 0.5, 6 and 10 m depth. Shown are the residence time distribution (RT) for the 1–5 μm particles in the summer experiment using the random walk model in combination with v_{s_eff}. The measured particle concentrations are presented as a concentration (secondary Y-axis) and as normalized data (primary Y-axis). Data normalization (described in detail as part of the supplement) was necessary to compare the output of the random walk model to the measured particle breakthrough curves.

Table 3

A comparison between actual residence times in the mesocosm and simulated residence times using vs $_{Stokes}$, v$_{s\_PIV}$ v$_{s\_eff}$.

Experiment	Depth (m)	Residence time in days calculated from		
		Mesocosm (actual)	$v_{s\,Stokes}$	$v_{s\,PIV}$	$v_{s\,eff.}$
Summer 53–63 μm	11	0.9	–	0.62	–
Summer 28–48μm	11	2.5	–	1.39	–
Summer 1–5μm	10	24	239	–	32
Autumn 1–5μm	10	2	225	–	17

independent of the settling velocity used (2 vs. 17–225 days).

4. Discussions

Microplastic abundance in lake systems is associated with negative impacts on lake organisms and ecosystem functioning (Aljaibachi and Callaghan, 2018; D'Avignon et al., 2022). Uptake from the water column by organisms such as filter feeders is highly dependent on the residence time in the water column, and particularly in the epilimnion where most organisms reside. Several factors such as particle size, polymer density, water temperature, and lake hydrodynamics affect the residence times of microplastic (Waldschläger and Schüttrumpf 2019; Elagami et al., 2022; Ahmadi et al., 2022). These factors coupled with the abundance of microplastic in lakes control the uptake probability of microplastic by lake organisms and their potential transfer through the food web (D'Avignon et al., 2022; Nelms et al., 2018).

The temperature gradient, and thus the strong density gradient during lake stratification, formed a very stable water column inside the mesocosm. The water column was divided into a turbulent epilimnion and a more-or-less laminar metalimnion. This shows maximum TKE values at the 1 m below the water surface (top of the epilimnion) of $\sim 2.7 \times 10^{-3}$, 5×10^{-3}, and 6.6×10^{-3} m^2 s^{-2} for the first, second and third experiments respectively. The major source of the high TKE in the surface layer during turbulent mixing is likely to be the wind (Cannon et al., 2021; Singh et al., 2019). The waves in the lake impacting directly on the mesocosm walls and the platform could also have contributed to the relatively high TKE in the surface layer. The D values calculated from the A-D fitting for the 1–5 μm particles during summer experiments (Table S10) were similar to those calculated from ADV data and Taylor's approach ($\sim 10^{-6}$ m^2 s^{-1}). The calculated D_S, D_M, and D_H values were in a similar range, but at the lower end of typical D values in stratified lakes (10^{-7} to 10^{-2} m^2 s^{-2}) (Wüest and Lorke, 2009)

In contrast to the summer experiments, the average temperature difference between the bottom part of the mesocosm and the water surface was $\sim 0.8°$C. This temperature difference and subsequently the density difference, combined with the 11 m depth of the water column and the temperature fluctuations in the water column resulted in a highly unstable water column. This instability resulted in Rayleigh numbers ($>10^{12}$) which were significantly higher than the critical values for convection, suggesting that the water column was mixed by turbulent convection. The maximum TKE values at 1 m below the water surface during this period was one order of magnitude lower than that during summer ($\sim 1.8 \times 10^{-4}$ m^2 s^{-2}). The major source of TKE is convection during autumn which results in the sinking of the upper (cool) water parcels. Finally, the calculated D values in autumn (in the range of 10^{-7} m^2 s^{-1}) were considerably lower than during the summer and at the lower end of the compilation of D values in Wüest and Lorke (2009).

Microplastic concentrations were affected by the hydrodynamic conditions in the mesocosm. For instance, the maximum microplastic concentrations in the mesocosm water column during summer were ~5 times higher than that in autumn for the same 1–5 μm particles (Fig. 5c and d). The distribution of microplastic inside the mesocosm was also affected by season. Unlike the summer experiment, the upper pulse at 0.5 m below water surface and the lower pulse at 1 m over the sediment

during autumn experiment had an overlap of ~1day (Fig. 5c and d). Furthermore, the fluorometer at 1 m over the lake sediment detected two subsequent microplastic pulses during the autumn experiment. The maximum concentration of the two pulses at 1 m over sediment were 55 and 25 μg l^{-1}. Surprisingly however, the measurements suggest that turbulent convection seemed to be not strong enough to start resuspension of the settled microplastic, as neither fluorometer detected any microplastic after the end of the pulse. These differences between microplastic behaviors during summer and autumn experiments are to be attributed to the instability in the water column that likely led to turbulent convective mixing and rapid microplastic transport within the mesocosm.

As also found by Elagami et al. (2022), the microplastic residence times were significantly affected by the size of the particles in the stratified water column. When increasing the particle size from 28-48 to 53–63, the residence time in the whole column decreased by ~2.5 times. By comparing the residence times in the mesocosm for the particle group 1–5 μm during summer (thermal stratification) with that during autumn (lake turnover), the total residence time in summer was $\sim$ 13 times longer than that during autumn. We suspect that the instability of the lake water column during lake turnover which resulted in the onset of lake convection and fast transport of the microplastic to the lake sediment. Also during lake turnover, organic materials, cyanobacteria, and iron particles could resuspend and attach to the microplastic particles either increasing their density or building aggregates, both of which would increasing their settling velocity and reducing residence time in the mesocosm (D'Avignon et al., 2022). This shows that, in addition to size, complex lake hydrodynamics can play a critical role in microplastic transport, especially for the smallest particle sizes.

The simulated residence times using the random walk model differed from the actual residence times in the mesocosm, especially for the simulations using $v_{s\,Stokes}$ for the smallest particle sizes (Tables 2 and 3). The simulated residence time of the 1–5 μm particles in summer using $v_{s\,Stokes}$ was $\sim$ 10 times higher than the actual residence time in the mesocosm (Table 3). This could be due to the interaction with natural particles existing in the lake (Schmidtmann et al., 2022) or the agglomeration of the microplastic particles in the mesocosm caused by the large surface area to volume ratio and the surface charge of the small microplastic particles. Such aggregates are large and likely to have higher settling velocities compared to the individual pristine microplastic particles used in Stokes model.

The simulated residence times during summer of the 1–5 μm particles using $v_{s\,eff.}$ (32 days) were very close to the actual residence times in the mesocosm (24 days). This is due to $v_{s\,eff.}$ and D being derived directly from the mesocosm data. As such $v_{s\,eff}$ implicitly incorporates processes influencing settling velocities in the mesocosm such as particle-microplastic interactions and hydrodynamic conditions. Such processes are not included in the laminar settling velocities in $v_{s\,Stokes}$ or $v_{\_PIV}$. The only part of the measured data that could not be represented by the random walk model for the 1–5 μm particles during summer using $v_{s\,eff.}$ were the peak height and the rapidly decaying tail of the pulse at 0.5 m below the water surface as well as the width of the pulse at the bottom of the metalimnion (Fig. 7). This is likely due to the simplified way the random walk represents the complexities of real-world microplastic transport particularly that the model assumes one dimensional transport and uses predefined and stationary D values. In reality the TKE time series shows that the turbulent strength is transient and likely depends many interrelated factors such as winds, currents and waves that impact on the mesocosm.

For the summer experiments using the large 28–48 and 53–63 μm particles, the simulated residence times using $v_{s\,PIV}$ values were comparable to the actual residence times in the mesocosm with a difference of $\sim$ 1.4 and 1.9 times. This is likely to be attributed to the faster sinking velocities and relatively lower surface area of the large particles which subsequently reduces the potential particle-microplastic interactions and aggregation formation with organic matter (e.g. live and dead

phytoplankton) inside the mesocosm.

During autumn, the modeled residence times of the 1–5 μm particles were considerably longer than those derived from the mesocosm. The simulation results using $v_{s\_Stokes.}$ and $v_{s\_eff.}$ were ~113 and 8.8 times higher than the actual residence time, respectively. These significant differences are likely due to the complex hydrodynamic conditions caused by the high instability in the lake water column, and particularly the initiation of natural convection which cannot be represented by the simplified lake physics used in the random walk model. Also, the complex biological, and chemical processes occurring in the lake water during lake turnover (D'Avignon et al., 2022) are not included in the model. This shows that the processes controlling microplastic settling velocities and residence times in lake systems during highly unstable hydrodynamic conditions need to be more deeply studied in future research.

The residence times calculated from the mesocosm experiments are considered more realistic than residence times calculated based on previous modeling or laboratory experiments, as mesocosm experiments more closely represent the complexities existing in lake systems. However, the conditions in the mesocosm are still likely to be quite different from a real lake. This could be due to several factors such as the boundary effect of the mesocosm walls, the small surface area of the mesocosm exposed to wind (~7 m²), and the isolation of the water inside the mesocosm from the rest of the lake. This will limit the size of turbulent eddies that can develop in the water column and the influence of other hydrodynamic processes such as seiches and currents that only develop in lake basins. We also noticed that the productivity in the mesocosm was higher than in the surrounding lake, making the likelihood and effect of interactions with plankton larger than in the Große Brombachsee. Also, there were some limitations caused by the field instruments. For example, microplastic concentrations and residence times were calculated depending solely on the signals detected in the measuring cells of the fluorometers, with the best case being measurements at three depths. This resulted in a lack of knowledge about the behavior of the microplastic particles over the extent of the entire water column. In addition, our understanding of the hydrodynamics inside the water column depended largely on the velocity measurements by the ADV at a single point fixed at 1 m below the water surface. This also limits our understanding of the hydrodynamic conditions over the entire extent of the water column. Finally, we exclusively used microspheres and only two polymer types in all experiments. We believe that irregular particles would have longer residence time than perfect spheres due to the increase in the drag forces exerted on the irregular particles compared to spheres. However, we think that particle shape and roundness would have less effect on the residence time of microplastic than that of density and size (Ahmadi et al., 2022). We also believe that the polymer type can affect the residence time. For instance, particles from biodegradable polymers may attach fine air bubbles in the lake water column, increasing buoyancy and thus having a longer residence time compared to non-biodegradable polymers (Elagami et al., 2022).

5. Conclusion

Previous studies investigating microplastic behavior in lake systems have used simplified laboratory settings to estimate microplastic transport. Here we have attempted to address the real complexity of transport in lakes by adopting a combination of complex in-lake mesocosm experiments with random walk modeling to quantify microplastic residence times and understand the underlying processes controlling microplastic transport in the lake water column. The experiments were conducted over of one year capturing thermal stratification and lake turnover and the associated complex chemical, biological, and hydrodynamic conditions. High-end techniques were used to infer microplastic residence times and lake hydrodynamics. Our results quantified for the first time the effect of particle size and lake hydrodynamics on the residence time in conditions close to that in real lake systems. The limitations of the model have highlighted where real lake microplastic transport processes are more complex than pure physical transport based on sinking and turbulent diffusion.

Our field experiments have confirmed that particle size has a significant impact on the residence time during stratified summer conditions. The small microplastic particles had considerably longer mesocosm residence times than large particles. However, the residence times of these small particles were still 1 to 2 orders of magnitude shorter than predicted by a random walk model parameterized using the Stokes sinking velocities and turbulent dispersivities from the mesocosm. This was thought to be due to complex processes such as aggregation of the microplastic with existing lake particulate matter, agglomeration and potentially the interactions with biota.

Lake hydrodynamics driven by seasonal temperature changes affected the residence time and distribution of microplastic in the mesocosm in autumn. The microplastic residence times during lake turnover were significantly shorter than during the summer experiment and the random walk simulations using the velocities calculated from the mesocosm data and Stokes calculations. It is thought that this was induced by the initiation of turbulent convection and associated complex biological, chemical, and hydrodynamic conditions in the water column. This shows that the behavior of microplastic in real lake systems and the uptake probability by lake biota such as zooplankton is still poorly understood. Future work needs to quantitatively incorporate processes such as heteroaggregation, biofouling, and uptake by lake organisms as well as lake hydrodynamics to quantitatively understand microplastic residence times and associated ecological effects of microplastic in these sensitive environments.

Author contribution statement

HE built the mesocosm setup, performed all experiments, worked on data analysis and interpretation, and wrote the manuscript. SF built the mesocosm, helped with conducting the experiments, assisted in data interpretation, built the random walk model, did all simulations, and worked on writing and editing the manuscript. JPB assisted in data interpretation and worked on writing and editing the manuscript. GT assisted with planning the experiments and provided lake monitoring data and logistics. BSG conceived the project, built the mesocosm, helped with conducting the experiments, assisted in data interpretation, and worked on writing and editing the manuscript.

Declaration of Competing Interest

The authors declare that they have no known competing financial interests or personal relationships that could have appeared to influence the work reported in this paper.

Data availability

Data will be made available on request.

7 Publications and manuscripts

Supplementary materials

Supplementary material associated with this article can be found, in the online version, at doi:10.1016/j.watres.2022.119463.

References

Ahmadi, P., Elagami, H., Dichgans, F., Schmidt, C., Gilfedder, B.S., Frei, S., Peiffer, S., Fleckenstein, J.H., 2022. Systematic evaluation of physical parameters affecting the terminal settling velocity of microplastic particles in lakes using CFD. Front. Environ. Sci. 10.

Aljaibachi, R., Callaghan, A., 2018. Impact of polystyrene microplastics on Daphnia magna mortality and reproduction in relation to food availability. PeerJ 6, e4601.

1959- Arthur, C., Baker, J.E., Bamford, H.A., 2009. In: Proceedings of the International Research Workshop on the Occurrence, Effects, and Fate of Microplastic Marine Debris. Tacoma, WA, USA. University of Washington Tacoma. September 9-11, 2008NOAA technical memorandum NOS-OR&R 30.

Bailly-Comte, V., Durepaire, X., Batiot-Guilhe, C., Schnegg, P.A., 2018. *In situ* monitoring of tracer tests: how to distinguish tracer recovery from natural background. Hydrogeol. J. 26 (6), 2057–2069.

Bigalke, M., Fieber, M., Foetisch, A., Reynes, J., Tollan, P., 2022. Microplastics in agricultural drainage water: a link between terrestrial and aquatic microplastic pollution. Sci. Total Environ. 806 (Pt 4), 150709.

Boos, J.P., Gilfedder, B.S., Frei, S., 2021. Tracking microplastics across the streambed interface: using laser-induced-fluorescence to quantitatively analyze microplastic transport in an experimental flume. Water Resour. Res. 57 (12).

Cai, Y., Li, C., Zhao, Y., 2021. A review of the migration and transformation of microplastics in inland water systems. Int. J. Environ. Res. Public Health 19 (1).

Canniff, P.M., Hoang, T.C., 2018. Microplastic ingestion by Daphnia magna and its enhancement on algal growth. Sci. Total Environ. 633, 500–507.

Cannon, D.J., Troy, C., Bootsma, H., Liao, Q., MacLellan-Hurd, R.A., 2021. Characterizing the seasonal variability of hypolimnetic mixing in a large. Deep Lake. JGR Oceans 126 (11).

D'Avignon, G., Gregory-Eaves, I., Ricciardi, A., 2022. Microplastics in lakes and rivers: an issue of emerging significance to limnology. Environ. Rev. 30 (2), 228–244.

Elagami, H., Ahmadi, P., Fleckenstein, J.H., Frei, S., Obst, M., Agarwal, S., Gilfedder, B. S., 2022. Measurement of microplastic settling velocities and implications for residence times in thermally stratified lakes. Limnol. Oceanogr. 67 (4), 934–945.

Ghawi, A.H., Kris, J., 2012. A computational fluid dynamics model of flow and settling in sedimentation tanks. Woo Oh, H. Applied Computational Fluid Dynamics. IntechOpen. Erscheinungsort nicht ermittelbar.

Holtappels, M., Lorke, A., 2011. Estimating turbulent diffusion in a benthic boundary layer. Limnol. Oceanogr. Methods 9 (1), 29–41.

Huret, M., Runge, J.A., Chen, C., Cowles, G., Xu, Q., Pringle, J.M., 2007. Dispersal modeling of fish early life stages: sensitivity with application to Atlantic cod in the western Gulf of Maine. Mar. Ecol. Prog. Ser. 347, 261–274.

Khatmullina, L., Isachenko, I., 2017. Settling velocity of microplastic particles of regular shapes. Mar. Pollut. Bull. 114 (2), 871–880.

Kirillin, G., Grossart, H.P., Tang, K.W., 2012. Modeling sinking rate of zooplankton carcasses: effects of stratification and mixing. Limnol. Oceanogr. 57 (3), 881–894.

Kreft, A., Zuber, A., 1978. On the physical meaning of the dispersion equation and its solutions for different initial and boundary conditions. Chem. Eng. Sci. 33 (11), 1471–1480.

Lavoie, J., Boulay, A.M., Bulle, C., 2021. Aquatic micro- and nano-plastics in life cycle assessment: development of an effect factor for the quantification of their physical impact on biota. J. Ind. Ecol.

Leiser, R., Wu, G.M., Neu, T.R., Wendt-Potthoff, K., 2020. Biofouling, metal sorption and aggregation are related to sinking of microplastics in a stratified reservoir. Water Res. 176, 115748.

Małoszewski, P., Zuber, A., 1982. Determining the turnover time of groundwater systems with the aid of environmental tracers. J. Hydrol. 57 (3–4), 207–231 (Amst).

Meides, N., Menzel, T., Poetzschner, B., Löder, M.G.J., Mansfeld, U., Strohriegl, P., Altstaedt, V., Senker, J., 2021. Reconstructing the environmental degradation of polystyrene by accelerated weathering. Environ. Sci. Technol. 55 (12), 7930–7938.

Nelms, S.E., Galloway, T.S., Godley, B.J., Jarvis, D.S., Lindeque, P.K., 2018. Investigating microplastic trophic transfer in marine top predators. Environmental Pollution (Barking, Essex: 1987) 238, 999–1007.

Reid, W.H., Harris, D.L., 1958. Some further results on the bénard problem. Phys. Fluids 1 (2), 102.

Renner, G., Nellessen, A., Schwiers, A., Wenzel, M., Schmidt, T.C., Schram, J., 2020. Hydrophobicity-water/air-based enrichment cell for microplastics analysis within environmental samples: a proof of concept. MethodsX 7, 100732.

Reynolds, C.S., Wiseman, S.W., 1982. Sinking losses of phytoplankton in closed limnetic systems. J. Plankton Res. 4 (3), 489–522.

Ross, O.N., 2006. Particles in motion: how turbulence affects plankton sedimentation from an oceanic mixed layer. Geophys. Res. Lett. 33 (10) n/a-n/a.

Rowe, M.D., Anderson, E.J., Wynne, T.T., Stumpf, R.P., Fanslow, D.L., Kijanka, K., Vanderploeg, H.A., Strickler, J.R., Davis, T.W., 2016. Vertical distribution of buoyant Microcystis blooms in a Lagrangian particle tracking model for short-term forecasts in Lake Erie. JGR Oceans 121 (7), 5296–5314.

Schmidtmann, J., Elagami, H., Gilfedder, B.S., Fleckenstein, J.H., Papastavrou, G., Mansfeld, U., Peiffer, S., 2022. Heteroaggregation of PS microplastic with ferrihydrite leads to rapid removal of microplastic particles from the water column. Environ. Sci. Process. Impacts 24 (10), 1782–1789.

Singh, P., Bagrania, J., Haritash, A.K., 2019. Seasonal behaviour of thermal stratification and trophic status in a sub-tropical Palustrine water body. Appl. Water Sci. 9 (5).

Sun, J., Dai, X., Wang, Q., van Loosdrecht, M.C.M., Ni, B.J., 2019. Microplastics in wastewater treatment plants: detection, occurrence and removal. Water Res. 152, 21–37.

Visser, A.W., 1997. Using random walk models to simulate the vertical distribution of particles in a turbulent water column. Mar. Ecol. Prog. Ser. 158, 275–281.

Waldschläger, K., Schüttrumpf, H., 2019. Effects of particle properties on the settling and rise velocities of microplastics in freshwater under laboratory conditions. Environ. Sci. Technol. 53 (4), 1958–1966.

Wang, C., O'Connor, D., Wang, L., Wu, W.M., Luo, J., Hou, D., 2022. Microplastics in urban runoff: global occurrence and fate. Water Res., 119129

Weeraratne, D., Manga, M., 1998. Transitions in the style of mantle convection at high Rayleigh numbers. Earth Planet. Sci. Lett. 160 (3–4), 563–568.

Woods, J.S., Verones, F., Jolliet, O., Vázquez-Rowe, I., Boulay, A.M., 2021. A framework for the assessment of marine litter impacts in life cycle impact assessment. Ecol. Indic. 129, 107918.

Wüest, A., Lorke, A., 2003. Small -scale hydrodynamics in lakes. Annu. Rev. Fluid Mech. 35 (1), 373–412.

Wüest, A., Lorke, A., 2009. Small-Scale Turbulence and Mixing: Energy Fluxes in Stratified Lakes. Encyclopedia of Inland Waters. Elsevier, pp. 628–635.

1   **Quantifying microplastic residence times in lakes using mesocosm experiments and**

2   **transport modelling**

3   **Hassan Elagami[1,2]*, Sven Frei[2], Jan-Pascal Boos[2], Gabriele Trommer[3], Benjamin S.**

4   **Gilfedder[1,2]**

5   [1]Limnological Research Station, Bayreuth Center of Ecology and Environmental Research

6   (BayCEER), University of Bayreuth, Bayreuth, Germany

7   [2]Department of Hydrology, Bayreuth Center of Ecology and Environmental Research

8   (BayCEER), University of Bayreuth, Bayreuth, Germany

9   [3]Water Management Office, Ansbach, Germany

10

11   **Corresponding Author:**

12   **Hassan Elagami**: Limnological Research Station, & Department of Hydrology, Bayreuth

13   Center of Ecology and Environmental Research (BayCEER), University of Bayreuth,

14   Bayreuth, Germany; **orcid.org/0000-0002-2919-5230**; **Email: hassan.elagami@uni-**

15   **bayreuth.de**

16

17   **Keywords: microplastic, settling velocity, residence time, turbulent mixing, lake**

18   **turnover, random walk modeling.**

19   **Supplementary information**

20   **S1) Mesocosm enclosure and mesocosm setup**

21

22   *Figure S1: The mesocosm enclousure and the mesocosm setup used for all experiments.*

23   **S2) Adding microplastics to the lake**

24

25   *Figure S2: Adding microplastics to the mesocosm using watering cans.*

26 **S3) Calibration lines**
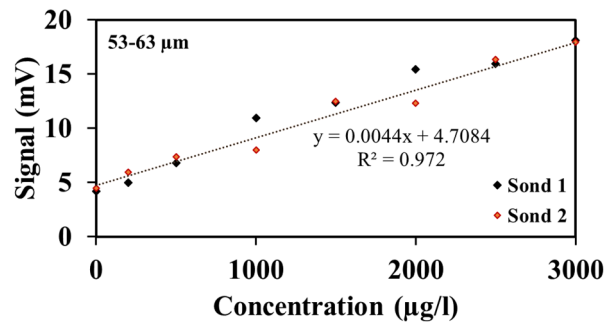
27
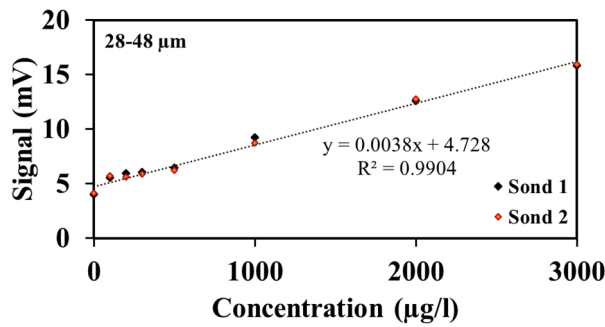
28
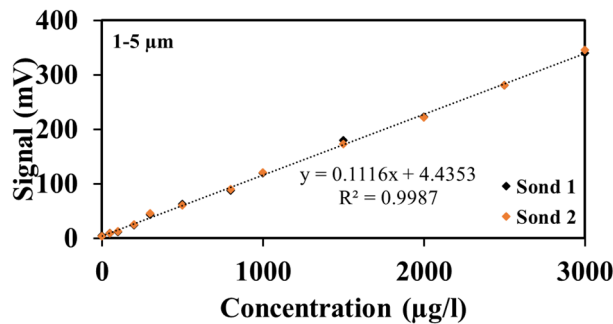
29

30 *Figure S3: Calibration lines of the fluricence detectors.*

31 **S4) Corrected settling velocities**

$$V_{S\_PIV} = V_{ST_1} \left(\frac{10^{\left[\frac{247.8}{T1+133.15} \right]}}{10^{\left[\frac{247.8}{T2+133.15} \right]}} \right)$$

32 where V_{ST_1} $[LT^{-1}]$, V_{S_PIV} $[LT^{-1}]$, T_1 $[^0C]$, and T_2 $[^0C]$ are the settling velocity measured in the

33 laboratory at 20^0C, the corrected settling velocity for the lake compartments, water

34 temperature in the laboratory, and the temperature of the lake compartment respectively.

35   **S5) Advection-Dispersion-Model**

$$pdf_{AD}(t-a) = \cfrac{1}{\tau_s \sqrt{4\pi Pe^{-\frac{t-a}{\tau_s}}}} e^{-\cfrac{\left(1-\frac{t-a}{\tau_s}\right)^2}{4Pe^{-\frac{t-a}{\tau_s}}}}$$

36   where *pdf* $_{AD}$*(t-a)* [T-1] is the A-D probability density function, *a* [T] is a time delay parameter,

37   τ_s [T] is the mean residence time of microplastic and *Pe=v$_s$z/D* [-] the Peclet-Number, relating

38   vertical settling of particles *v$_s$* [LT-1] for a given length scale *z* [L] (in our case the observation

39   depths in the mesocosm) to the turbulent diffusivity *D*. Assuming that the vertical particle

40   settling velocities *vs* are known, *Pe* from a fitted A-D Model can be used to estimate the

41   corresponding turbulent diffusivity *D*. For fitting the observed particle concentrations *c(t)* [ML-

42   ³] to the A-D Model, the concentrations first have to be transformed into a corresponding

43   probability frequency *f(t)* [T-1]:

$$f(t) = \frac{c(t)}{\sum c(t)\Delta t}$$

44   Where $\sum c(t)$ [ML-3] is the sum of all measured concentrations belonging to a breakthrough

45   experiment and Δt [T] is the corresponding measurement resolution.

46 **S6) Temperature profiles inside and outside the mesocosm**
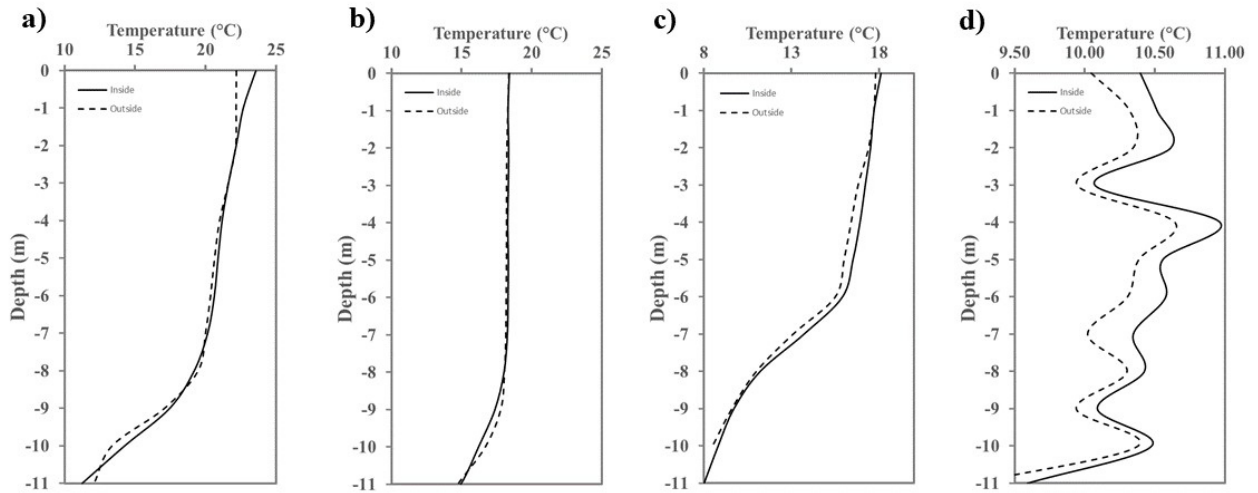
47

48 *Figure S6: temperature profiles inside and outside the mesocosm before the start of each experiment. Figures*

49 *5a, b, and c represent the remperature profiles during summer,for the 53-63 and 28-48, and 1-5 µm while figure*

50 *d repredsents the tepmeratue profile during autumn for the 1-5 µm.*

51 **S7) Calculated reyliegh numbers during autumn experiemnt**

52

53 *Figure S7:* Calculated Reyleigh numbers during autumn experiemnt at 30 minutes resolution.

54   S8) A detailed description of the A-D fitting procedure

55   *a) Summer 1-5 µm*

depth	Pe^{-1}	a	τ_s
[m]	[-]	[days]	[days]
0.5	0.63	0.028	0.29
6	0.22	2.10	3.19
10	0.019	0	19.37

56

57

58

126

59

60
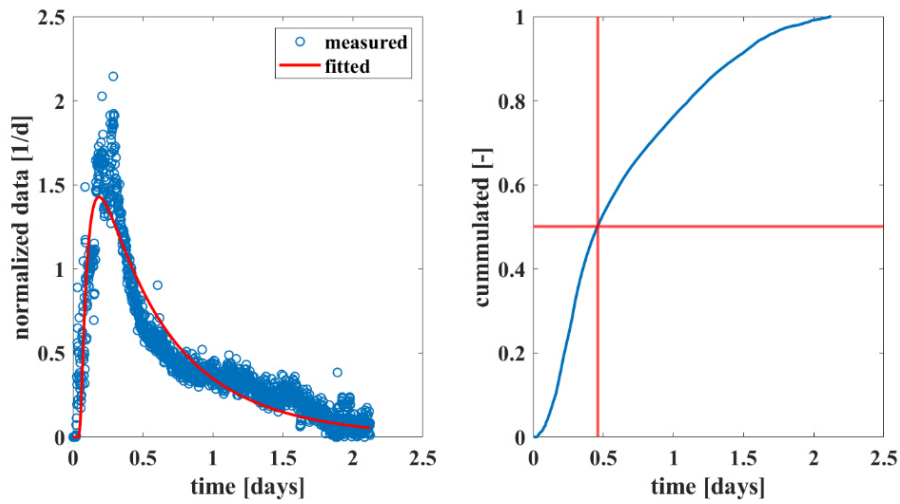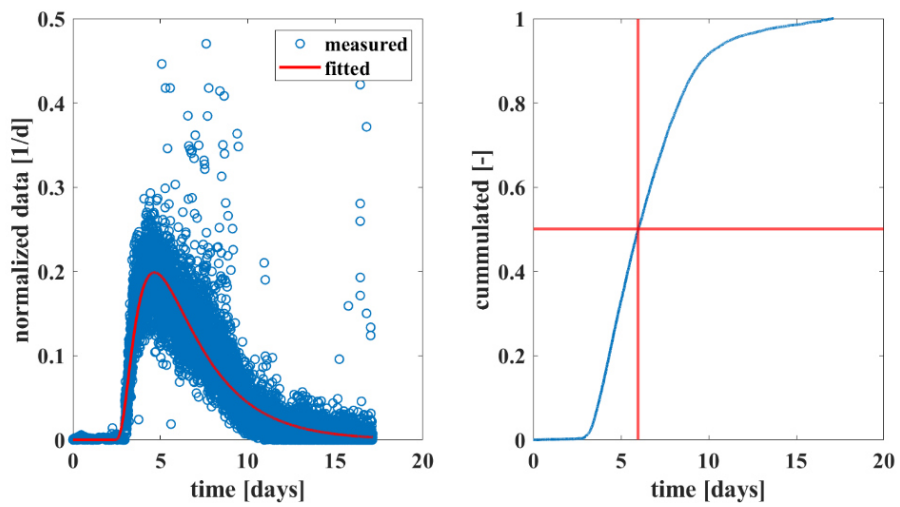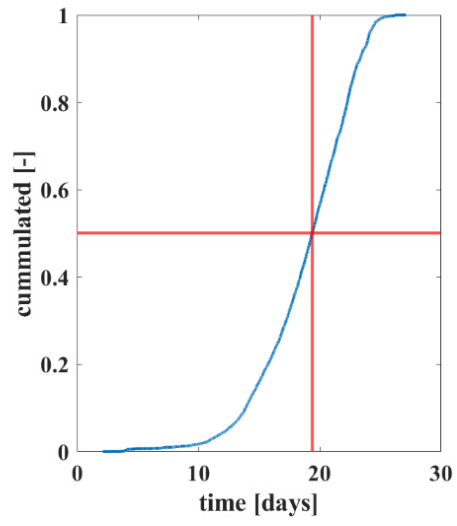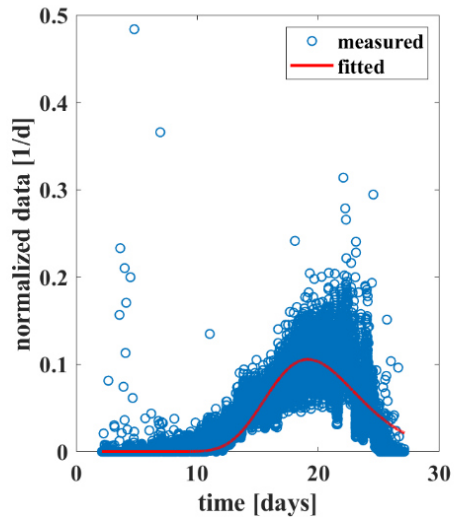
61   *b)   Autumn 1- 5µm*

depth	Pe^{-1}	a	τ_s
[m]	[-]	[days]	[days]
0.5	1.27	0	0.31
6	0.5	0.72	0.24
10	-	-	-

62
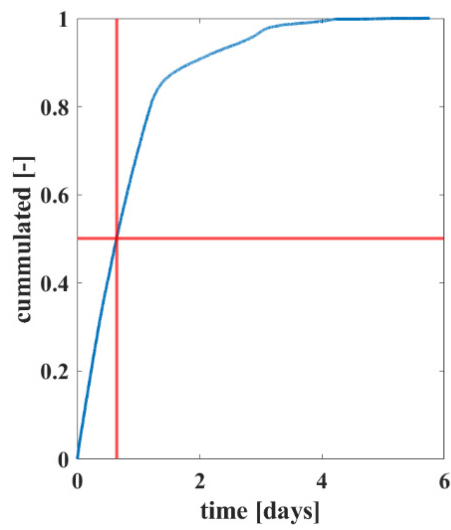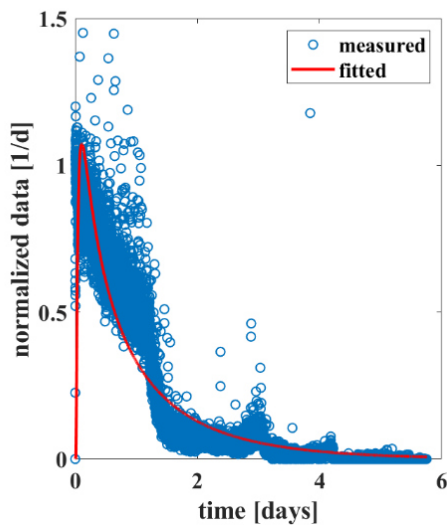
63

64

65
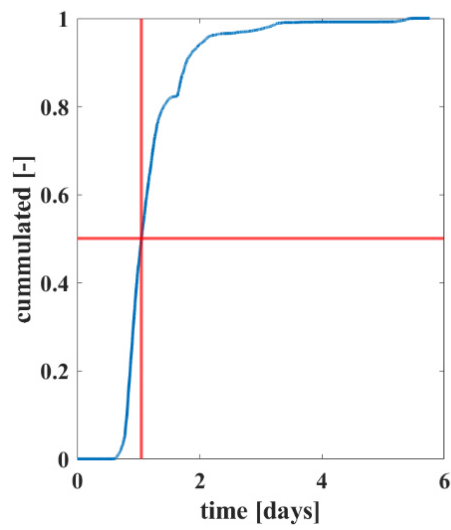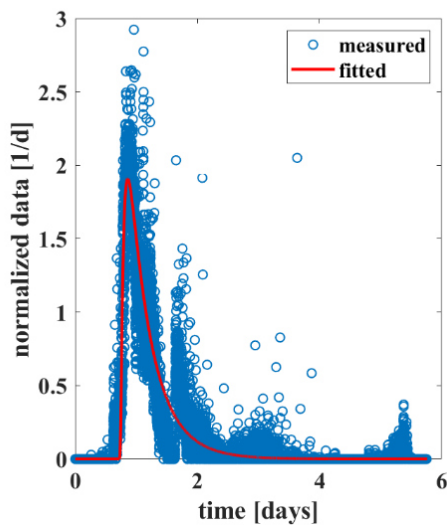
66   *c) Summer 28-48μm*

depth	Pe^{-1}	a	τ_s
[m]	[-]	[days]	[days]
0.5	5.762	0.34	0.37
6	1.68	1.16	0.24
11	0.0102	0	2.14
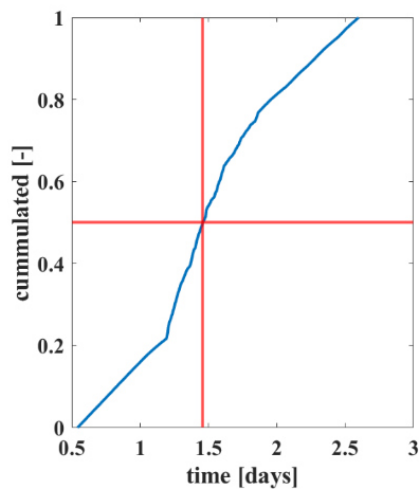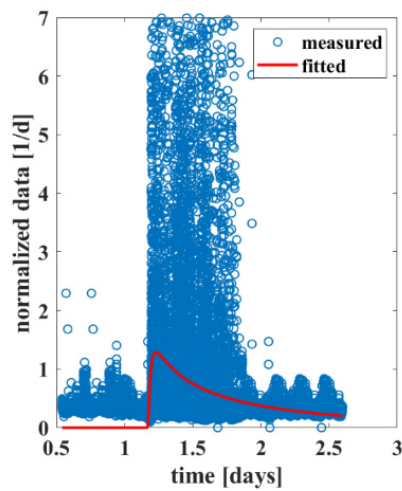
67

68
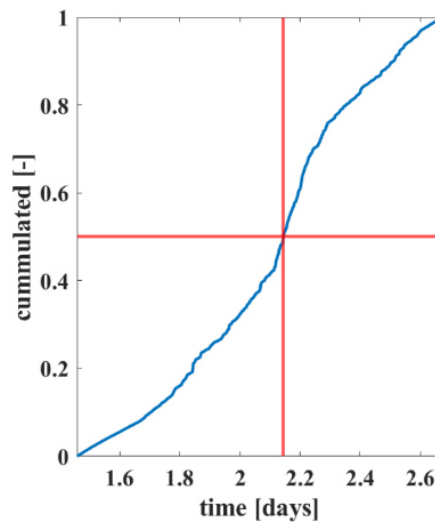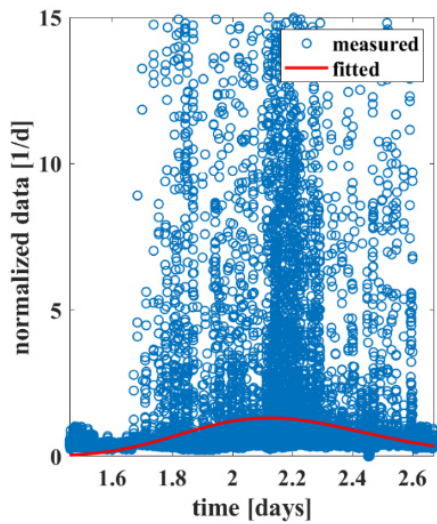
69   *d) Summer 53-63µm*

depth	Pe^{-1}	a	τ_s
[m]	[-]	[days]	[days]
0.5	1.41	0.0021	0.0048
6			
11			

70

71   **S9) Random Walk Model Parametrization**

Experiment	H_E	H_M	H_H	D_s	D_M	D_H
	[m]	[m]	[m]	[m²/s]	[m²/s]	[m²/s]
1-5 µm Summer	8	2	11	6.7x10-6[1]	6.7x10-6[1]	1.12x10-6[2]
1-5 µm Autumn	9	1	11	9.2x10-7[1]	9.2x10-7[1]	9.2x10-7[1]
28-48 µm Summer	8	3	11	1.07x10-5[1]	3x10-6[2]	3x10-6[2]
53-63 µm Summer	8	3	11	4.6x10-6[1]	4.6x10-6[1]	4.6x10-6[1]

72   Taylor's approach[1], AD fitting[2]

Study 5: Filter feeders are key to small microplastic residence times in stratified lakes: A virtual experiment

Authors: Benjamin-Silas Gilfedder, Hassan Elagami, **Jan-Pascal Boos**, Julian Brehm, Matthias Schott, Lorenz Witt, Christian Laforsch, Sven Frei

Filter feeders are key to small microplastic residence times in stratified lakes: A virtual experiment

B.S. Gilfedder [a,b,*], H. Elagami [a,b], J.P. Boos [b], J. Brehm [c], M. Schott [c], L. Witt [c], C. Laforsch [c], S. Frei [b]

[a] Limnological Research Station, Bayreuth Centre of Ecology and Environmental Research (BayCEER), University of Bayreuth, Bayreuth, Germany
[b] Department of Hydrology, Bayreuth Center of Ecology and Environmental Research (BayCEER), University of Bayreuth, Bayreuth, Germany
[c] Department of Animal Ecology I, Bayreuth Centre of Ecology and Environmental Research (BayCEER), University of Bayreuth, Bayreuth, Germany

HIGHLIGHTS

- Model suggests MP residence time in lakes controlled by zooplankton uptake.
- MP imbedded in zooplankton faeces sink much faster than individual particles.
- Lake residence times of small MP shorted from 15 years to <1 year
- Small MP will cycle through the ecosystem before reaching the sediments.
- Sinking also important for large particles (>15 μm)

GRAPHICAL ABSTRACT
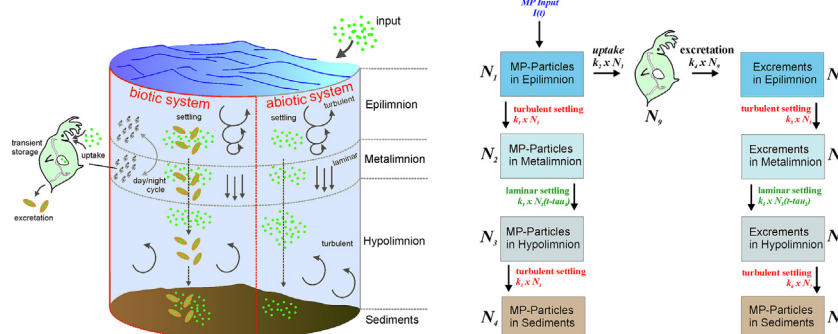
ARTICLE INFO

ABSTRACT

Microplastic (MP) is potentially harmful to lake ecosystems, with its uptake into the food web largely controlled by its residence time in the lake water column. Here we combine laboratory and virtual experiments to quantify residence times of small MP (<15 μm) in two contrasting model lakes; Lake Constance (large lake) and Esthwaite Water (a small lake). We compare MP residence times in a purely physical system with MP transport controlled by sinking and mixing to a model where, in addition to physical processes, zooplankton package MP into faecal pellets that are then egested into the water column. The laboratory experiments showed that MP settling velocities increased from $\sim 5 \times 10^{-6}$–10^{-3} mm s^{-1} for pristine MP to ~ 1 mm s^{-1} for MP embedded faeces. Modeled lake residence times for the 0.5 and 5 μm particles were >15 years in the abiotic models, while in the biotic simulations they were reduced to ~ 1 year. There was little difference between abiotic and biotic simulations for the 15 μm particles. The ratio of the MP zooplankton uptake velocity to the sinking velocity (v_{up}/v_{s_epi}) was used to classify biological vs. physical transport pathways. For the 0.5 and 5 μm particles v_{up}/v_{s_epi} was $\gg 1$ in all cases for both lakes, while for the 15 μm MP there was a transition between biological and physical processes dominating residence times depending on zooplankton numbers. Our results suggest that packaging of small MP in faecal pellets by zooplankton will control its residence time in lakes. Moreover, the majority of small MP will cycle through organisms before reaching the sediment, increasing the likelihood of negative ecological effects and transfer in the food web.

1. Introduction

Microplastic (MP) is of growing concern for lake ecosystems. MP cycling in lakes involves a number of complex interrelated processes such as transport within the water column, sedimentation to the lake sediments, uptake

by biota, transfer within the food chain, and potentially degradation and colonisation by biofilms (D'Avignon et al., 2022). Organisms can consume MP particles at all ecological levels and transfer it within the food chain, with only poorly understood effects that potentially range from individuals to populations (Elizalde-Velázquez et al., 2020; Schwarzer et al., 2022; Trotter et al., 2021). There is a growing body of literature that has documented the quantity and characteristics of MP polymers found in lake water (D'Avignon et al., 2022; Tamminga and Fischer, 2020), lake sediments (Su et al., 2016) as well as within lake organisms (Michler-Kozma et al., 2022; Yıldız et al., 2022). Although it is difficult to generalise MP numbers in lakes due to the large diversity of lake types and geographical settings as well as differing sampling and quantification techniques (e.g., lower MP size cut-off often differs between studies, (Stock et al., 2019)), recent reviews have estimated that MP numbers in the water column typically vary between 0.1 and 10 MP particles m^{-3} (D'Avignon et al., 2022; Tanentzap et al., 2021). While the highest MP numbers are usually found in highly populated industrialised areas (e.g. 15,000 MP particles m^{-3} in the water column of Lake Tai Hu, China (Su et al., 2016)), MP can also be found in regional (Tamminga and Fischer, 2020) and remote areas in remarkably high numbers (e.g. Negrete Velasco et al. (2020) identified ~2600 MP particles m^{-3} in the water column and outlet of a frozen Swiss mountain lake), demonstrating the importance of long-range transport and local sources far from industrialised areas (Dong et al., 2021). Microplastic numbers in freshwater organisms can be considerably higher than the water column, with estimates ranging from 100 to 10,000 particles per kg body mass (dry weight), showing a tendency for organisms to ingest and accumulate plastic particles (D'Avignon et al., 2022).

Lakes are often considered as MP sinks, as MP numbers in the sediment are typically significantly higher than the water column (see data compilation in D'Avignon et al., 2022). A lake serves as a permanent sink if MP is buried long-term in the sediments. It may also be a transitory storage if MP is resuspended back into the water column by bottom currents or waves in the littoral zone, or if it has a long residence time in the water column. Large dense particles (>10's of μm) tend to sink rapidly, and thus are expected to have short residence times within the water column and accumulate in the lake sediments (Ahmadi et al., 2022; Khatmullina and Isachenko, 2017; Waldschläger and Schüttrumpf, 2019). In contrast small, low density particles (<few μm) have slower settling velocities, longer residence times, and are more likely to be flushed through the lake before they can enter long-term storage in the sediments (Elagami et al., 2022). Despite this, recent lake mesocosm experiments cannot explain MP residence time in the water column, with transport to the sediments being faster than expected based on purely physical transport processes such as sinking and turbulent diffusion (Elagami et al., 2023).

Lakes host a range of organisms from various trophic levels, with the potential for uptake either directly via filter-feeding (Scherer et al., 2017) or ingestion of MP-containing prey (Chae et al., 2018) with subsequent transfer within the aquatic food web (Yıldız et al., 2022). The MP residence time in the water column, and especially in the epilimnion, is an important parameter for evaluating the probability of ingestion by lake organisms. Long residence times in the epilimnion leads to a higher likelihood of uptake, especially by planktonic filter feeders such as the zooplankton *Daphnia*. In contrast, short residence times will give organisms a limited time to ingest MP particles. Uptake will also be influenced by MP size, as larger particles cannot pass the feeding apparatus (Ebert, 2005). Filter feeders, and especially zooplankton that are non-specific in their feeding habits, are central for MP entering into the food web, as they feed by consuming particulate organic carbon (POC) from the water column. This POC is typically phytoplankton, live or dead, and bacteria but also includes other POC sources such as allochthonous detritus (Bell and Ward, 1970; McMahon and Rigler, 1965). At the population maximum zooplankton can remove most of the POC from the epilimnion (e.g. during the clear water phase), where most, if not all, water in the epilimnion passes through these organisms (Effler et al., 2015).

There is still very little known about how MP uptake affects freshwater aquatic organisms at concentrations relevant for real lake systems

(O'Connor et al., 2020). However, there are numerous studies that have shown detrimental effects of MP on lake biota at elevated MP concentrations and also transfer of MP within the lake food web (O'Connor et al., 2020). There is little known about what uptake and release of MP embedded in faeces means for MP transport and residence times within the water column. It seems reasonable to assume that once embedded in zooplankton faeces the hydrodynamic properties of the MP should be governed largely by the faeces properties rather than by those of the individual plastic particles, as has been observed in the ocean (Cole et al., 2016; Pérez-Guevara et al., 2021).Thus, the role of filter feeders in the lake MP cycle may be critical, particularly in determining microplastic residence times within the lake water column and thus availability for uptake by lake organisms.

In this work we use a series of generic virtual lake experiments to quantitatively study the role of the zooplankton *Daphnia*, and how the egestion of MP as part of *Daphnia* faeces, influences the MP settling velocities and residence times in lakes. The simulations are parametrised using data from a large (Lake Constance, Germany) and a small lake (Esthwaite Water, UK) as well as from existing literature and our own laboratory experiments. The aim is to elucidate how lake size and *Daphnia* population dynamics affect MP residence times in the lake water column.

2. Materials and methods

2.1. Model Lake system

The transport and accumulation of MP particles with and without *Daphnia* was studied using an array of generic virtual experiments, using Lake Constance, Germany, to represent large lakes and Esthwaite Water, UK, to represent small lakes. Microplastic has been identified in both the water column and fish gut in Lake Constance, with the dominant particles being fragments composed on polyethylene and polypropylene (Roch et al., 2019). There is currently no data on MP numbers and polymer type in Esthwaite Water. The full mathematical description of the model can be found in the supplement. In the following we give a description of the most pertinent aspects of the models. Each model represents a stratified lake with a well-mixed (fully turbulent) epilimnion and hypolimnion and a laminar metalimnion similar to that described in Elagami et al. (2022) (Fig. 1). Model parameters such as lake area, water residence time, mean depth and temperature for each lake layer are based on literature data (Achterberg et al., 1997; ISF, 2016) (Table 1).

The abiotic model system includes an exponential RT distribution in the epilimnion and hypolimnion and one unique RT in the metalimnion based on its depth and the MP sinking velocity v_s (i.e. t = depth/v_s) to simulate sinking in a laminar water column. The biotic model was based on the abiotic model but also included a *Daphnia* ingestion rate in the epilimnion, the MP residence time in the intestinal tract, the egestion rate of MP in faeces, the settling velocity of these faeces and the *Daphnia* population numbers in the lake during the year. While we do not explicitly model ecosystem processes such as grazing or predator-prey relationships, these processes are implicitly included due to the use of measured population data from the two lakes.

Due to the lack of literature data for individual *Daphnia* species, we were required to pool data from various species for each model parameter. For example, only the total numbers of Cladocera were available from monthly monitoring at Lake Constance (ISF, 2016) and Esthwaite Water (Talling, 2003), while the *Daphnia* MP ingestion rates were specifically for *Daphnia magna* (Scherer et al., 2017). This mix of parameters introduces an inherent uncertainty in the model results as each species is likely to have a characteristic set of representative parameters that may even change with life stage and season. This was addressed using an uncertainty analysis described in Section 2.6. Each model lake system was run in two ways: 1) by exclusively simulating physical MP transport within the water column (abiotic system, Fig. 1B), and 2) by accounting for physical MP transport and ingestion, storage and egestion by *Daphnia* (biotic system, Fig. 1A). Uptake of MP by *Daphnia* was assumed to occur only during night in the epilimnion as part of the diel vertical migration, with the model using a 12 h day-night
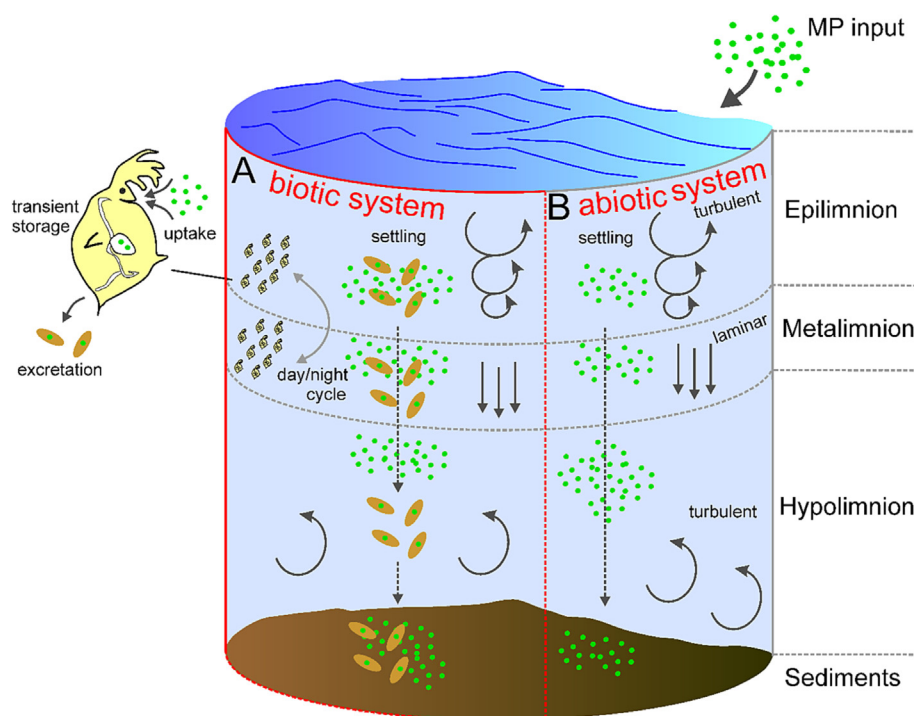
Fig. 1. Conceptual model of the primary processes effecting MP transport and residence times in a stratified lake as implemented in the model. A) a model containing biological ingestion, storage and egestion by *Daphnia* plus physical transport, B) purely physical transport in the water column represented as a series of transfer functions.

cycle. This is another simplification of reality, as real lakes are populated with an array of *Daphnia* species with individual migration patterns that are often responding to predator (fish) behaviour and day length (Ringelberg, 1999). However, this seems to be the most realistic way of simply representing the most important aspects of *Daphnia* feeding habits into the model. MP particles are released as part of *Daphnia* faeces into the epilimnion which then sink with a characteristic sinking velocity. Once the MP particles reach the lake sediments they were assumed to be permanently immobilized. For both model systems we further assume 1) both lakes are perpetually stratified and 2) once particles enter the lake they are uniformly distributed in the epilimnion. These are necessary simplifications, as simulating the full hydrodynamics of the two lakes is not possible with our simplistic representation of the lake system as a series of transfer functions.

2.2. Settling velocities for MP particles

Microplastic settling velocities for the different lake compartments were estimated using Stokes law for polystyrene (PS; $\rho = 1.050 \, \text{kg m}^{-3}$) spheres with particle diameters of 0.5 μm, 5 μm and 15 μm. Settling velocities of the particles were corrected for water temperature based on mean annual temperatures in each of the lake compartments by applying an empirical relationship that is dependent water density and dynamic viscosity (Elagami et al., 2022).

Table 1
Lake parameters used in the virtual experiments.

	Lake constance	Esthwaite water
Lake area [km^2]	472	1.0
Water residence time	4 years	13 weeks
Depth [m]		
Epilimnion	15	6
Metalimnion	10	2
Hypolimnion	65	4
Mean temperature [°C]		
Epilimnion	15	15
Metalimnion	10	11
Hypolimnion	4.5	8

2.3. Uptake and egestion of MP by Daphnia

Ingestion of particles into the digestive tract of *Daphnia* was represented by assuming proportionality between the particle uptake rate and MP numbers in the epilimnion (Eq. (S1)). The parameter $k_2(t)$ represents the time dependent MP uptake rate for the entire population of *Daphnia* and essentially represents the proportion of the epilimnic water that passes through the *Daphnia* population per day. It requires 1) a representative filtration rate for a single daphnid individual m, 2) the total volume of the epilimnion V_{epi}, 3) the *Daphnia* population per lake area P as a function of time and 4) the corresponding lake area A. Data used to derive the filtration rate (Supplementary Fig. S1A) were taken from MP feeding experiments presented in Scherer et al. (2017) while the population densities of Cladocera for Lake Constance and Esthwaite Water are based on ISF (2016) and Talling (2003) respectively (Supplementary Fig. S1B).

$$k_2(t) = \frac{m}{V_{epi}} A \, P(t) \tag{3}$$

The faeces egestion rate (supplementary Eq. (S1)) controlling the release of MP from the *Daphnia* into the epilimnion, was estimated from feeding experiments using *D. magna* presented in Rosenkranz et al. (2009). An exponential model was used to represent the experimental data shown in Supplementary Fig. 1C. The exponential model showed a very good fit ($r^2 = 0.99$), providing an estimate for the excretion rate of 14.5 d^{-1} which translates to a RT in the *Daphnia* of about 5 h for 95 % of particles to leave the organism.

2.4. Faeces sinking velocities

There is currently no data available on the sinking velocities of *Daphnia* faeces containing MP from fresh water lakes. To quantify the sinking velocities of these MP imbedded faeces, experiments were conducted using the *D. magna* clone BL2.2 (Imhof et al., 2017). Prior to the experiment, female *D. magna* were cultured in 1.5 l jars containing 1 l artificial M4 medium at 20 ± 0.5 °C and a 16 h:8 h light:dark regime with half an hour dusk and dawn respectively (Elendt and Bias, 1990). *Daphnia* were fed ad libitum

3

with the unicellular green algae *Acutodesmus obliquus* three times a week. To avoid crowding effects, neonates of the first and second broods were removed within 24 h after release.

Microplastic used in the feeding experiments were wet ground PS fragments (diameter ~ 17.7 μm, PS158N/L; INEOS Styrolution Group GmbH, Germany) and red PS spheres (diameter ~ 3 μm; Polybead®, Polysciences, Inc.; USA). Additionally, spray dried fluorescent labelled (rhodamine B) PS (Ø 10.4 μm; Europäisches Zentrum für Dispersionstechnologien, Germany) was used to analyze the degree of MP incorporation into the faeces. Stock suspensions of PS particles were prepared following the protocol of Schür et al. (2020) ensuring that particles were well dispersed. Approximately 50 mg of the respective particles were suspended in 50 ml autoclaved M4 medium and shaken for 48 h at 100 rpm. Stock suspensions were then stored at 4 °C and continuously stirred before dilution. Finally, the particle concentration of stock suspensions was evaluated using a hemocytometer (Brand GmbH) prior to the experiments.

Third brood age synchronized primiparous *D. magna* were separated in 150 ml beakers containing 50 ml of the M4 medium, 2 mg C 1^{-1} of *A. obliquus* and 5000 particles ml^{-1} of the respective MP particles. After 24 h of exposure to the particles, *Daphnia* faeces were collected from the bottom of the beakers and gently transferred with 5 ml plastic pipettes to a plexiglass chamber ($3 \times 3 \times 12$ cm) filled with M4 medium for settling velocity measurements. Faeces settling velocities were measured using particle image velocimetry (PIV) (Elagami et al., 2022). Sinking velocities were subsequently determined using the TrackMate plugin (Ershov et al., 2021) in ImageJ (Schindelin et al., 2012).

To determine if the MP were incorporated into the *Daphnia* faeces, the animals were exposed to the rhodamine B labelled PS as described above. After 24 h, faecal pellets were collected, gently washed three times in ultrapure water, transferred to microscope slides, dried in a desiccator and imaged using a Leica M205 FCA fluorescence stereo microscope (excitation: 553 nm; emission: 627 nm; Leica Microsystems; Germany).

2.5. Physical sinking vs biological uptake

The ratio between the mean MP residence time in the epilimnion τ_{epi}, and a characteristic *Daphnia* ingestion time τ_{up} was used to quantitatively compare abiotic vs. biotic transport processes in the lake epilimnion (Eq. (4)). τ_{up} is the inverse of $k_2(t)$, while v_{up} is $m\,P(t)$. By using the definition of the mean residence time in the epilimnion (Supplementary Eq. (2a)), the ratio in Eq. (4) can also be expressed in terms of the particle sinking and uptake velocities v_{up}/v_{s_epi}. When v_{up}/v_{s_epi} ratio is ~1 both ingestion/egestion by *Daphnia* and physical sinking are equally important for MP residence times, while for $v_{up}/v_{s\_epi} \gg 1$ biological uptake dominates, and for $v_{up}/v_{s\_epi} \ll 1$ physical transport dominates.

$$\frac{\tau_{epi}}{\tau_{up}} = \frac{m\,P(t)}{v_{s\_epi}} = \frac{v_{up}}{v_{s\_epi}} \tag{4}$$

2.6. Parameter uncertainty

Data on MP uptake and egestion rates of MP by filter feeding organisms such as *Daphnia* are sparse, especially at the species level. We have been restricted to data from a limited number of sources and usually to one single *Daphnia* species, which also varies from parameter to parameter. To account for the uncertainty this introduced into the simulation we performed an sensitivity analysis using a bootstrapping method. Egestion, filtration rates and *Daphnia* population dynamics were randomly selected as model input from a range of ±50 % of the original values, assuming the original values represent the mean of a normal distribution. This changes the absolute numbers of each parameter, but not the temporal development of the population. In total 200 unique parameter sets for each lake system were generated and run through the model. All simulations were evaluated for the time it takes for 95 % of the MP particles to reach the lake sediments, which is referred to as the lake residence time.

3. Results

The settling velocities of *Daphnia* faeces had a mean and standard error of 1.13 ± 0.10 ($n = 8$), 1.04 ± 0.07 ($n = 14$) and 0.93 ± 0.13 mm s^{-1} ($n = 13$) for the control, 17.4 μm and 3 μm MP particles, respectively (Fig. 2). There was no significant difference in sinking velocities between the control and MP containing faeces or between faeces containing MP of different sizes (*t*-test, $p < 0.05$). In comparison, the Stokes sinking rates of pristine MP spheres of the same size were 7.5×10^{-3} and 2.2×10^{-4} mm s^{-1}. The MP particles were clearly imbedded in the *Daphnia* faecal pellets (Fig. 2). A sinking velocity of 1 mm s^{-1} was used for all subsequent simulations of faecal pellet sinking velocities, except for the sensitivity analysis where it was varied by ±50 %, as described above.

Initially the model MP flux to both lakes was kept constant for one full year at 10^7 particles per day, which amounted to a total MP input to both lakes of 3.65×10^9 particles per year (Figs. 3 & 4). Thereafter MP particle numbers in the epi-, meta-, and hypolimnion were solely controlled by in-lake processes. During the first year MP numbers increased rapidly in the epilimnion of both lakes. In the Lake Constance abiotic model MP numbers in the water column reached ~3.6×10^9 particles for the 0.5 μm MP, 2.1×10^9 particles for the 5 μm MP, and 0.3×10^9 particles for the 15 μm MP (Fig. 3). In the biotic system containing *Daphnia* the number of particles in the epilimnion were only 5–10 % of the abiotic system, with a maximum of 0.4×10^9 particles for both the 0.5 and 5 μm MP and ~0.2×10^9 particles for the 15 μm MP. The maximum in MP numbers were not found at the end of the first year as in the abiotic system, but shortly before the maximum in *Daphnia* populations. MP numbers in the epilimnion of Esthwaite Water were similar to Lake Constance for the 0.5 μm particles during the abiotic simulations, but where considerably lower for the 5 μm (~1.1×10^9) and especially the 15 μm (~0.1×10^9) particles (Fig. 4). In the Esthwaite Water biotic model the highest MP numbers in the epilimnion were not found at the end of the first year, as also seen in Lake Constance, but slightly before the maximum in the *Daphnia* population, with ~0.5×10^9 particles for the 0.5 μm, 0.4×10^9 for the 5 μm particles, and 0.1×10^9 for the 15 μm particles. This is 14 %, 45 % and ~100 % of the maximum particle numbers found in the abiotic system for the three particle sizes.

In the abiotic simulations, once the MP flux ceased the numbers of 0.5 μm particles decreased very slowly in the epilimnion of both lakes; ~95 % of the particles remained in the Lake Constance and ~87 % in the Esthwaite Water epilimnion after 5 years simulation time (Figs. 3 & 4). The 5 μm and especially the 15 μm particles exited the epilimnion considerably faster than the 0.5 μm particles in both lakes, with 95 % of these larger particles lost in <1–3.5 years.

In contrast to the epilimnion, the time required for 95 % of the particles to exit the entire lake water column and reach the sediments (MP lake residence time, τ) for the abiotic systems was in excess of 15 years for the 0.5 μm and 5 μm particles and ~2.4 years for the 15 μm particles for Lake Constance (Table 2). Similarly the 0.5 μm particles in Esthwaite Water were calculated to have a residence time of >15 years, with no noticeable flux to the sediments over the 15 year simulated period. In contrast the residence times for 5 μm and 15 μm particles in Esthwaite Water were only ~2.15 and 1.03 years due to the shallower lake depth.

Apart from the 15 μm particles for Esthwaite Water, the MP residence times for both lake systems were significantly shorter in the biotic than in the abiotic simulations (Table 2). The largest difference in residence times were observed for the 0.5 μm particles, where 95 % of the MP particles reached the sediments after ~1 year for both lakes. The difference in residence times between the biotic and abiotic models decreased with increasing particle size and decreasing lake depth to the point where there was little (a few %) difference between simulated residence times for the 15 μm particles in the shallow Esthwaite Water. Only a very small proportion of MP was found in the *Daphnia* biomass at any one time, with a maximum of 0.15 % of the total MP added to the lake, and usually around 0.05 % (Figs. 3 & 4). There were a larger number of the 0.5 μm and 5 μm particles stored in biomass than 15 μm particles. The temporal ´changes

4
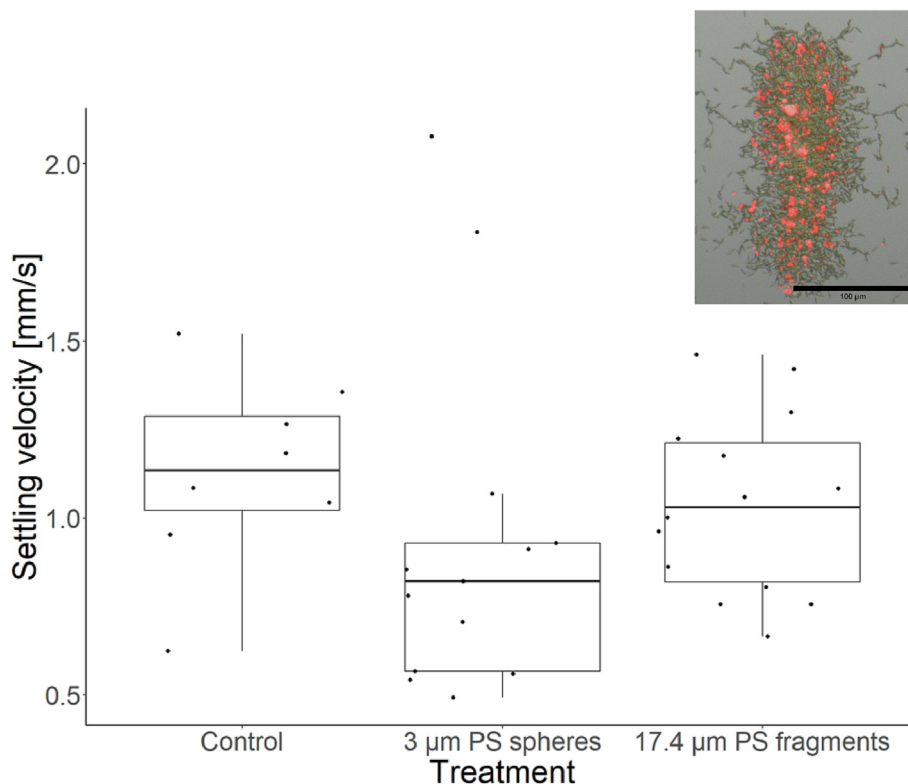
Fig. 2. Settling velocities of *Daphnia magna* faecal pellets containing polystyrene MP (control n = 8; fragments n = 14; spheres n = 13). Mean settling velocities (±SE): control 1.13 ± 0.10, fragments 1.04 ± 0.07 mm s^{-1}; spheres: 0.93 ± 0.13 mm s^{-1}. Inset is an image of *D. magna* faeces containing MP. Scale bar of inset faeces is 100 μm.

in particle numbers in both lakes was largely controlled by the *Daphnia* population dynamics, with the minimum MP numbers in the water column during the clear water phase when the *Daphnia* population was at its maximum. The highest numbers were in the winter months when there was nearly no *Daphnia* in both lakes. There was little noticeable effect of the dial feeding cycle on MP numbers.

The parameter uncertainty analysis for the biotic Lake Constance model indicated that the residence times of 0.5 μm and 15 μm particles were only minimally affected by parameters associated with ingestion and egestion of MP and *Daphnia* population dynamics (Table 2 & supplementary Fig. 3). The estimated 95 % confidence intervals for residence times ranged between 0.99-1.15 years for 0.5 μm and 1.33–1.9 years for 15 μm particles (Table 2). For the 5 μm particles the uncertainty was larger, with a range from 1.01 to 4.04 years. In the Esthwaite Water model parameter uncertainty had a significant effect for the 0.5 μm and 5 μm particles. The 95 % confidence intervals ranged between 0.98 and 1.26 (0.5 μm), 1.02–1.37 (5 μm) and 0.98–1.01 years (15 μm). As would be expected, the combined effect of the filtering rate and the total numbers of *Daphnia* in the lake had the largest influence on MP residence times in the simulations. The combination of these two parameters quantifies the total amount of water, and thus also number of particles, that passes through the *Daphnia* population. The egestion rate has less of an effect on the residence times but controls the amount of MP stored in the organisms. The parameters associated with particle settling were not subject to the bootstrapping analysis, as the model uncertainty is assumed to be primarily associated with the poorly constrained and often lumped biological parameters from the literature.

The ratio between the MP uptake rate by *Daphnia* and the sinking velocity of pristine MP in epilimnion ($v_{\_up}/v_{s\,epi}$) was used as a dimensionless number to characterize the importance of the biotic versus abiotic transport pathways for MP residence times in the lake water column. A $v_{\_up}/v_{s\,epi}$ ratio of 1 indicates that sinking and uptake are of equal importance, ≫1 indicates the biological pathway dominates while a value ≪1 indicates that the abiotic sinking dominates. We define the transition zone between 0.1 and 10. This analysis showed that $v_{\_up}/v_{s\,epi}$ scales with the *Daphnia*

population and particle size; and that the smaller the MP particle the more dominant is the biological pathway (Fig. 5). For the 0.5 μm particles the biological pathway is constantly the dominant way for MP to be removed from the lake water column and enter storage in the sediments (as faeces), while for the 5 μm and 15 μm particles the biological pathway becomes dominant (>10) at *Daphnia* populations of 10,000 and 100,000 individuals per m^2 respectively. The 5 μm particles remain >1 for *Daphnia* numbers >1000 individuals per m^2 and $v_{\_up}/v_{s\,epi}$ is never below 0.1 for the populations recorded in both lakes. Only the 15 μm particles produced a $v_{\_up}/v_{s\,epi}$ value smaller than 1 for the *Daphnia* populations measured in the lakes while the abiotic pathway becomes dominant (<0.1) at populations below 1000 individuals per m^2.

4. Discussion

Despite decades of plastic pollution research in the world's oceans, it is still in its infancy in limnic environments. Microplastic is of growing concern in these systems due to is ubiquitous presence, concentration and transfer within the food web and potentially adverse effects ranging from individual organisms to whole populations (D'Avignon et al., 2022; O'Connor et al., 2020). The amount of plastic, and MP in particular, entering the terrestrial environment is expected to increase in the future (Lebreton and Andrady, 2019), making it imperative to more deeply understand it's transport through and between terrestrial compartments.

Microplastic transport processes in the lentic water column control MP residence times, but these processes are poorly understood because of the complexity of various interacting factors (Elagami et al., 2023). Residence time is important to quantify, however, as it controls the probability of uptake by filter feeding organisms such as zooplankton. The longer such organisms are exposed to MP, the higher the probability that it will be ingested and enter the lentic food web, and possibly be transferred between trophic levels (Yıldız et al., 2022). Previous research has focused predominately on physical transport processes such as sinking velocities (Kaiser et al., 2019; Waldschläger and Schüttrumpf, 2019) and mixing (Elagami et al., 2022)

5
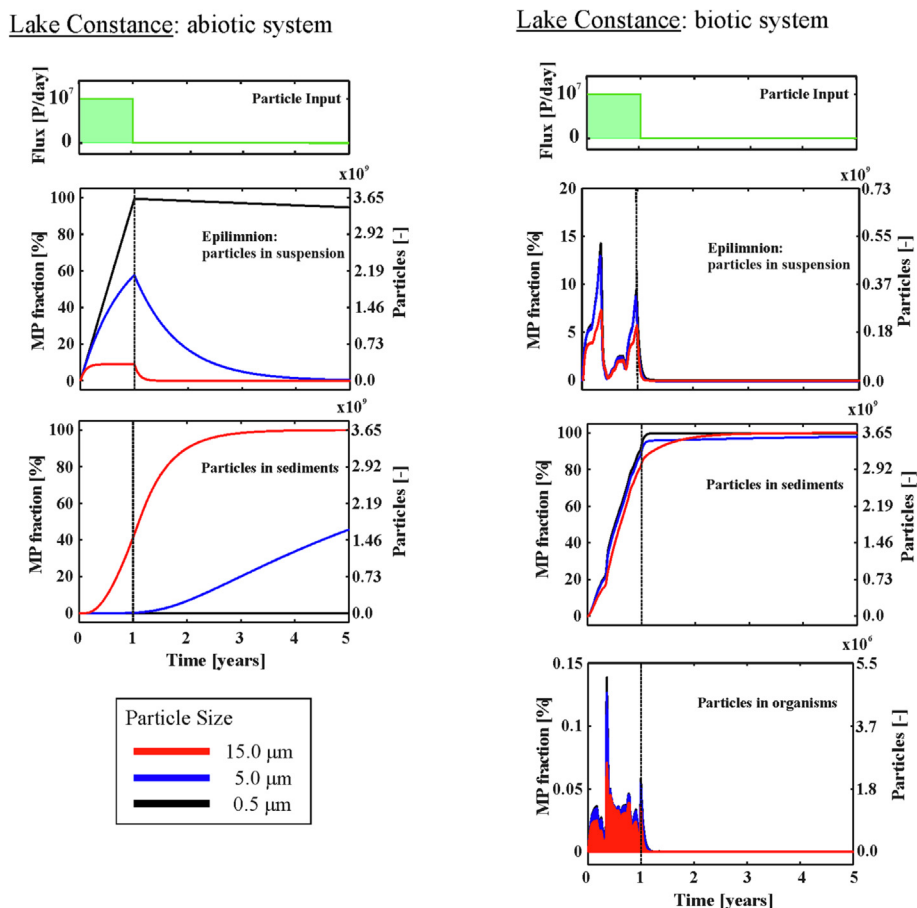
Fig. 3. Comparison between simulated abiotic and biotic MP numbers and the percent of total input for Lake Constance epilimnion, entering the sediments and stored in *Daphnia* biomass.

and how this is influenced by particle properties such as plastic polymer type, size and shape. There is currently little known about the role lake organisms play in determining MP residence times in lakes. Evidence from the marine environment suggests that MP packed into faeces can have a significant effect on settling velocities, but even these experiments assume laminar conditions in the water column (Pérez-Guevara et al., 2021).

The simulations performed here show that when neglecting the biological pathway residence times for small (0.5 and 5 μm) PS particles in Lake Constance are very long for both the epilimnion and the entire lake water column (both >15 years). The residence time for these particles was considerably longer than the lake flushing time (~4 years, defined as river discharge leaving lake divided by the lake volume), suggesting that MP will be transported conservatively through the lake rather than deposited in the sediments. This is similar for the Esthwaite Water, with the MP residence time ranging between >60 (0.5 μm) and ~8 (5 μm) times the flushing time (13 weeks) despite shorter MP residence times in this small lake. These results suggest that lakes will not act as a sink for small MP particles unless additional processes, such as uptake by filter feeders or aggregation of MP with existing lake particles increases their settling velocities (Long et al., 2015; Schmidtmann et al., 2022). The 15 μm particles are expected to reach the sediments as their residence times are only a fraction of the lake flushing time for both lakes, with this being more evident in Esthwaite Water due to its shallow depth.

When MP ingestion and egestion by *Daphnia* was introduced into the model structure the residence times for the small particles were drastically reduced for both the epilimnion and the entire lake water column. More than 90 % of MP, regardless of particle size and lake size, reached the sediments in less than a year. The importance of the biological pathway is also demonstrated by particle numbers in the epilimnion being controlled

by the number of *Daphnia* present. During winter when *Daphnia* numbers are low MP numbers increased to their highest levels, while they sank to near-zero in the clear water phase when *Daphnia* filter a significant portion of the POC, including MP, out of the lake epilimnion.

The proportion of epilimnic water that passes through the *Daphnia* (k_2 in Eq. (3)) each day controls MP uptake. At the height of the clear water phase in Lake Constance (~10^6 *Daphnia* individuals m^{-2}), the whole of the epilimnic water volume passes through the organisms 2.5 times per day. This is a very high filtering capacity. To evaluate if this is plausible, we have conducted a simple calculation based on measured *Daphnia* filter rates from the literature (0.1–5 ml h^{-1} individual^{-1}, depending largely on *Daphnia* size (Burns, 1969)), the *Daphnia* numbers in Supplementary Fig. 1 (max. 10^6 individuals m^{-2}) and lake area and epilimnion depth given in Table 1. This calculation suggests that between 0.2 and 8 times the volume of the epilimnion can pass through the *Daphnia* population per day. While this calculation has several assumptions, such as uniform *Daphnia* numbers across the lake, our value for k_2 is in reasonable agreement with literature values. The sensitivity analysis supports this conclusion as it showed that the residence times are only minimally influenced by the selection of the biological parameters used, and the same interpretation would be made by varying the biological uptake rate, population density and excretion rate from 50 to 150 % of the original value.

The dominance of the biological pathway for the 0.5 μm and 5 μm MP particles is also clearly shown by the value of $v_{\_up}/v_{s\_epi}$. In all cases the biological pathway dominates (>10) for the 0.5 μm MP, while it is dominant for the 5 μm particles for all but the winter *Daphnia* populations (<10,000 individuals m^{-2}). For the largest particles, the value of $v_{\_up}/v_{s\_epi}$ is consistently in the transition zone (ratio 0.1–10) where both biologically mediated transport and physical transport are important for MP residence times in the epilimnion.
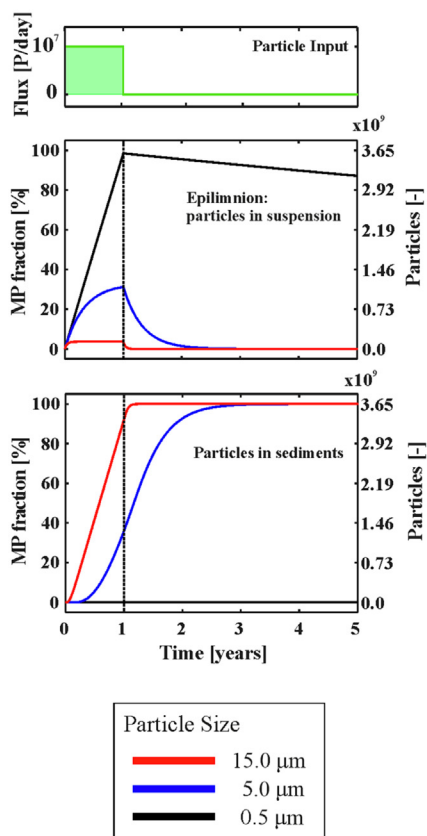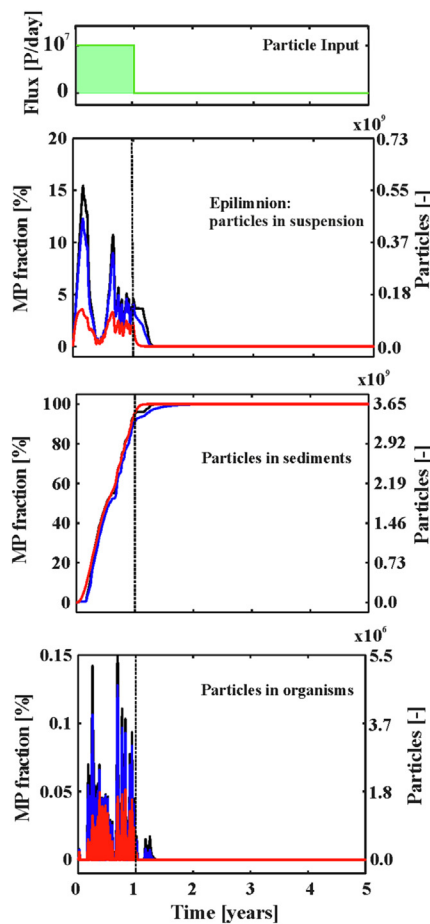
Fig. 4. Comparison between simulated abiotic and biotic MP numbers and percent of total input in the Esthwaite Water epilimnion, entering the sediments and stored in the *Daphnia* biomass.

4.1. Model uncertainties

The model presented here is a highly simplified representation of reality, both in terms of the data used and the model physics. Parameter uncertainty is addressed to some extend by the sensitivity analysis, so that the largest uncertainties probably stem from the simplified way the model represents lake physics. For example, the model assumes that the virtual lakes are permanently stratified rather than mixing one or more times per year as is typical for mid latitude lakes such as Lake Constance and Esthwaite Water. These simplifications were necessary to avoid a full simulation of

lake hydrodynamics, and coupling the hydrodynamic model to a biological module and a particle transport module, all of which is not trivial. In reality lake turnover would have distributed the MP throughout the lake water column, rather than it being confined to the individual compartments where

Table 2
Microplastic residence time and uncertainties (from the sensitivity analysis) in the two lakes, defined as the time for 95 % of the particles to leave the lake and enter the sediments.

	Lake constance Residence time [years] (Confidence interval)	Esthwaite water Residence time [years] (Confidence interval)
0.5 µm		
bitotic system	1.02 (0.99–1.15)	1.19 (0.98–1.26)
abiotic system	>15	>15
5.0 µm		
bitotic system	1.1 (1.01–4.04)	1.2 (1.02–1.37)
abiotic system	>15	2.15
15.0 µm		
bitotic system	1.58 (1.33–1.9)	1 (0.98–1.01)
abiotic system	2.4	1.03

Fig. 5. Ratio of *Daphnia* uptake vs. physical sediment as a function of the *Daphnia* population as an indicator of physically vs. biologically controlled MP removal from lake systems.

the residence time is controlled by the sinking velocity. It is difficult to predict what this mixing would imply for MP residence times, as MP from the epilimnion would be mixed into the hypolimnion, which may reduce the total residence time. Concurrently, MP from the hypolimnion would also be mixed back into the epilimnion, increasing the residence time, and leading to an enhanced exposure to organisms such as *Daphnia* with the potential for ingestion and egestion as faeces.

We also assumed that the sediments act as a permanent sink. Given the low density of many plastic polymers and shear forces acting on the lake bed, especially in large lakes or the littoral zone (Lorrai et al., 2011), it is possible that MP will be re-suspended back into the lake. This is expected to be enhanced during turnover due to the turbulent conditions induced by mixing events, even in the hypolimnion (Cannon et al., 2021). This would render these re-suspended particles available for uptake, effectively increasing their RT in the lake.

A potentially important biological assumption not directly related to transport is that the faecal pellets are assumed to undergo no changes while sinking to the sediments. It is known that *Daphnia* faecal pellets are fragile and are colonized by bacteria that can decompose the pellets in the water column (He and Wang, 2006; Pérez-Guevara et al., 2021). This mass-loss would reduce the sinking velocity of the pellets. Pellets can also form a food source for higher organisms such as fish, in which case the MP would likely end up in large faecial material and sink more rapidly than in the *Daphnia* pellets (Pérez-Guevara et al., 2021). Finally, we have only used *Daphnia* as our 'model' filter feeding organism. Lakes host an array of filter feeding zooplankton, such as Copepods and rotifers, meaning that there is a large potential for more MP to enter the food web than predicted by the model. This MP would also be packed in faecal pellets and sink to the sediments. Despite uptake likely being somewhat species specific (e.g. general vs. selective feeders) we believe that our uptake rates are at the lower end of the expected range in nature as we have concentrated exclusively on *Daphnia* as a representative filter feeding organism. Finally, we have used PS as the model MP polymer due to data availability, and its ubiquitous presence in aquatic environments (Schwarz et al., 2019). However, other polymers are also important, and often more dominant than PS in lakes (Schwarz et al., 2019). Due to zooplankton faeces being the dominant pathway for sedimentation of small MP in the lake, we believe the polymer type will not be critical when determining MP residence times. However dense polymers may be an important aspect for larger MP particles, as sinking is an important pathway to the sediments, especially in small lakes. Particle shape is another aspect that may influence settling and uptake dynamics. Fibers, in particular, are likely to behave differently to spheres and irregular shapes, both in the water column and the intestinal tract of lake organisms. Thus in the future it would be useful to obtain experimental data and preform residence time calculations of polymer types and shapes other than PS spheres. Despite these model uncertainties, we believe that our simplified model captures the most salient transport and uptake processes controlling the residence times of MP in lakes and that the results will be applicable to lakes across a spectrum of sizes and plastic types.

5. Conclusions

These virtual experiments highlight the importance of including lake ecology into calculations estimating MP transport processes and residence times. The model predicts that the residence time of small micrometer sized plastic particles imbedded in faecal pellets will be orders of magnitude shorter than single MP and will likely play a critical role in determining MP residence times and zooplankton uptake in lakes and ponds. It also shows that the vast of majority of small MP will cycle through lake organisms rather than sinking to the sediments via physical transport processes, with potential negative effects to these organisms and ecosystems. Microplastic has been found in an array of lake organsims (including in Lake Constance (Roch et al., 2019)) at different trophic levels, which highlights the need to better understand both transport in the lake water column and through the lake ecosystem, and how this influences residence time in these

environments (Elizalde-Velázquez et al., 2020). It will be vital in the future to test these first model predictions with experimental data; we hope these virtual experiments will stimulate both discussions and experiments to this effect.

CRediT authorship contribution statement

B.S. Gilfedder was responsible for the paper concept, writing the paper, and data analysis. H. Elagami was responsible for data assimilation from existing literature and paper revision and discussion of results. J.P. Boos conducted the PIV measurements to quantify the settling velocities of Daphnia faeces and editing of the paper. J. Brehm, M. Schott, L. Witt designed, conducted and analysed the data from the Daphnia faeces settling experiments, while C. Laforsch supervised these experiments and assisted with the data analysis. S. Frei designed and conducted the modelling, helped with the interpretation of the data and assisted in writing the paper.

Data availability

Data will be made available on request.

Declaration of competing interest

Benjamin S. Gilfedder reports financial support was provided by German Research Foundation.

Appendix A. Supplementary data

Supplementary data to this article can be found online at https://doi.org/10.1016/j.scitotenv.2023.164293.

References

Achterberg, E.P., van den Berg, C.M.G., Boussemart, M., Davison, W., 1997. Speciation and cycling of trace metals in Esthwaite Water: a productive English lake with seasonal deep-water anoxia. Geochim. Cosmochim. Acta 61, 5233–5253.

Ahmadi, P., Elagami, H., Dichgans, F., Schmidt, C., Gilfedder, B.S., Frei, S., et al., 2022. Systematic evaluation of physical parameters affecting the terminal settling velocity of microplastic particles in lakes using CFD. Front. Environ. Sci. 10.

Bell, R.K., Ward, F.J., 1970. Incorporation of organic carbon by Daphnia pulex. Limnol. Oceanogr. 15, 713–726.

Burns, C.W., 1969. Relation between filtering rate, temperature, and body size in four species of Daphnia. Limnol. Oceanogr. 14, 693–700.

Cannon, D.J., Troy, C., Bootsma, H., Liao, Q., MacLellan-Hurd, R.-A., 2021. Characterizing the seasonal variability of hypolimnetic mixing in a large, deep lake. J. Geophys. Res. Oceans 126, e2021JC017533.

Chae, Y., Kim, D., Kim, S.W., An, Y.-J., 2018. Trophic transfer and individual impact of nano-sized polystyrene in a four-species freshwater food chain. Sci. Rep. 8, 284.

Cole, M., Lindeque, P.K., Fileman, E., Clark, J., Lewis, C., Halsband, C., et al., 2016. Microplastics alter the properties and sinking rates of zooplankton faecal pellets. Environ. Sci. Technol. 50, 3239–3246.

D'Avignon, G., Gregory-Eaves, I., Ricciardi, A., 2022. Microplastics in lakes and rivers: an issue of emerging significance to limnology. Environ. Rev. 30, 228–244.

Dong, H., Wang, L., Wang, X., Xu, L., Chen, M., Gong, P., et al., 2021. Microplastics in a remote lake basin of the Tibetan Plateau: impacts of atmospheric transport and glacial melting. Environ. Sci. Technol. 55, 12951–12960.

Ebert, D., 2005. Ecology, Epidemiology, and Evolution of Parasitism in Daphnia. National Library of Medicine.

Effler, S.W., Spada, M.E., Gelda, R.K., Peng, F., Matthews, D.A., Kearns, C.M., et al., 2015. Daphnia grazing, the clear water phase, and implications of minerogenic particles in Onondaga Lake. Inland Waters 5, 317–330.

Elagami, H., Ahmadi, P., Fleckenstein, J.H., Frei, S., Obst, M., Agarwal, S., et al., 2022. Measurement of microplastic settling velocities and implications for residence times in thermally stratified lakes. Limnol. Oceanogr. 67, 934–945.

Elagami, H., Frei, S., Boos, J.-P., Trommer, G., Gilfedder, B.S., 2023. Quantifying microplastic residence times in lakes using mesocosm experiments and transport modelling. Water Res. 229, 119463.

Elendt, B.P., Bias, W.R., 1990. Trace nutrient deficiency in Daphnia magna cultured in standard medium for toxicity testing. Effects of the optimization of culture conditions on life history parameters of D. magna. Water Res. 24, 1157–1167.

7 Publications and manuscripts

Elizalde-Velázquez, A., Carcano, A.M., Crago, J., Green, M.J., Shah, S.A., Cañas-Carrell, J.E., 2020. Translocation, trophic transfer, accumulation and depuration of polystyrene microplastics in Daphnia magna and Pimephales promelas. Environ. Pollut. 259, 113937.

Ershov, D., Phan, M.-S., Pylvänäinen, J.W., Rigaud, S.U., Le Blanc, L., Charles-Orszag, A., et al., 2021. Bringing TrackMate in the era of machine-learning and deep-learning. bioRxiv 1–4 2021.09.03.458852.

He, X., Wang, W.-X., 2006. Relative importance of inefficient feeding and consumer excretion to organic carbon flux from Daphnia. Freshw. Biol. 51, 1911–1923.

Imhof, H.K., Rusek, J., Thiel, M., Wolinska, J., Laforsch, C., 2017. Do microplastic particles affect Daphnia magna at the morphological, life history and molecular level? PLoS One 12, e0187590.

ISF LfUB-W, 2016. Institut für Seenforschung, Arbeitsbericht 2016, Karlsruhe/Langenargen. https://pudi.lubw.de/detailseite/-/publication/87532.

Kaiser, D., Estelmann, A., Kowalski, N., Glockzin, M., Waniek, J.J., 2019. Sinking velocity of sub-millimeter microplastic. Mar. Pollut. Bull. 139, 214–220.

Khatmullina, L., Isachenko, I., 2017. Settling velocity of microplastic particles of regular shapes. Mar. Pollut. Bull. 114, 871–880. https://doi.org/10.1016/j.marpolbul.2016.11.024.

Lebreton, L., Andrady, A., 2019. Future scenarios of global plastic waste generation and disposal. Palgrave Commun. 5, 6.

Long, M., Moriceau, B., Gallinari, M., Lambert, C., Huvet, A., Raffray, J., et al., 2015. Interactions between microplastics and phytoplankton aggregates: impact on their respective fates. Mar. Chem. 175, 39–46.

Lorrai, C., Umlauf, L., Becherer, J.K., Lorke, A., Wüest, A., 2011. Boundary mixing in lakes: 2. Combined effects of shear- and convectively induced turbulence on basin-scale mixing. J. Geophys. Res. Oceans 116.

McMahon, J.W., Rigler, F.H., 1965. Feeding rate of daphnia magna straus in different foods labeled with radioactive phosphorus. Limnol. Oceanogr. 10, 105–113.

Michler-Kozma, D.N., Kruckenfellner, L., Heitkamp, A., Ebke, K.P., Gabel, F., 2022. Uptake and transfer of polyamide microplastics in a freshwater mesocosm study. Water 14, 887.

Negrete Velasco, AdJ, Rard, L., Blois, W., Lebrun, D., Lebrun, F., Pothe, F., et al., 2020. Microplastic and fibre contamination in a remote mountain lake in Switzerland. Water 12, 2410.

O'Connor, J.D., Mahon, A.M., Ramsperger, A.F.R.M., Trotter, B., Redondo-Hasselerharm, P.E., Koelmans, A.A., et al., 2020. Microplastics in freshwater biota: a critical review of isolation, characterization, and assessment methods. Global Chall. 4, 1800118.

Pérez-Guevara, F., Roy, P.D., Kutralam-Muniasamy, G., Shruti, V.C., 2021. A central role for fecal matter in the transport of microplastics: an updated analysis of new findings and persisting questions. J. Hazard. Mater. Adv. 4, 100021.

Ringelberg, J., 1999. The photobehaviour of Daphnia spp. as a model to explain diel vertical migration in zooplankton. Biol. Rev. 74, 397–423.

Roch, S., Walter, T., Ittner, L.D., Friedrich, C., Brinker, A., 2019. A systematic study of the microplastic burden in freshwater fishes of south-western Germany - are we searching at the right scale? Sci. Total Environ. 689, 1001–1011.

Rosenkranz, P., Chaudhry, Q., Stone, V., Fernandes, T.F., 2009. A comparison of nanoparticle and fine particle uptake by Daphnia magna. Environ. Toxicol. Chem. 28, 2142–2149.

Scherer, C., Brennholt, N., Reifferscheid, G., Wagner, M., 2017. Feeding type and development drive the ingestion of microplastics by freshwater invertebrates. Sci. Rep. 7, 17006.

Schindelin, J., Arganda-Carreras, I., Frise, E., Kaynig, V., Longair, M., Pietzsch, T., et al., 2012. Fiji: an open-source platform for biological-image analysis. Nat. Methods 9, 676–682.

Schmidtmann, J., Elagami, H., Gilfedder, B.S., Fleckenstein, J.H., Papastavrou, G., Mansfeld, U., et al., 2022. Heteroaggregation of PS microplastic with ferrihydrite leads to rapid removal of microplastic particles from the water column. Environ. Sci. Impacts 24, 1782–1789. https://doi.org/10.1039/D2EM00207H.

Schür, C., Zipp, S., Thalau, T., Wagner, M., 2020. Microplastics but not natural particles induce multigenerational effects in Daphnia magna. Environ. Pollut. 260, 113904.

Schwarz, A.E., Ligthart, T.N., Boukris, E., van Harmelen, T., 2019. Sources, transport, and accumulation of different types of plastic litter in aquatic environments: a review study. Mar. Pollut. Bull. 143, 92–100.

Schwarzer, M., Brehm, J., Vollmer, M., Jasinski, J., Xu, C., Zainuddin, S., et al., 2022. Shape, size, and polymer dependent effects of microplastics on Daphnia magna. J. Hazard. Mater. 426, 128136.

Stock, F., Kochleus, C., Bänsch-Baltruschat, B., Brennholt, N., Reifferscheid, G., 2019. Sampling techniques and preparation methods for microplastic analyses in the aquatic environment – a review. TrAC Trends Anal. Chem. 113, 84–92.

Su, L., Xue, Y., Li, L., Yang, D., Kolandhasamy, P., Li, D., et al., 2016. Microplastics in Taihu Lake, China. Environ. Pollut. 2016, 711–719. https://doi.org/10.1016/j.envpol.2016.06.036.

Talling, J.F., 2003. Phytoplankton–zooplankton seasonal timing and the 'clear-water phase' in some English lakes. Freshw. Biol. 48, 39–52.

Tamminga, M., Fischer, E.K., 2020. Microplastics in a deep, dimictic lake of the North German Plain with special regard to vertical distribution patterns. Environ. Pollut. 267, 115507.

Tanentzap, A.J., Cottingham, S., Fonvielle, J., Riley, I., Walker, L.M., Woodman, S.G., et al., 2021. Microplastics and anthropogenic fibre concentrations in lakes reflect surrounding land use. PLoS Biol. 19, e3001389.

Trotter, B., Wilde, M.V., Brehm, J., Dafni, E., Aliu, A., Arnold, G.J., et al., 2021. Long-term exposure of Daphnia magna to polystyrene microplastic (PS-MP) leads to alterations of the proteome, morphology and life-history. Sci. Total Environ. 795, 148822.

Waldschläger, K., Schüttrumpf, H., 2019. Effects of particle properties on the settling and rise velocities of microplastics in freshwater under laboratory conditions. Environ. Sci. Technol. 53, 1958–1966.

Yıldız, D., Yalçın, G., Jovanović, B., Boukal, D.S., Vebrová, L., Riha, D., et al., 2022. Effects of a microplastic mixture differ across trophic levels and taxa in a freshwater food web: in situ mesocosm experiment. Sci. Total Environ. 836, 155407.

Study 5: Filter feeders are key to small microplastic residence times in stratified lakes: …

Supplementary Information

Mathematical Transport Model

A dynamic lake model was developed to represent the transport behaviour of MP for the biotic and abiotic systems. Similarly to Elagami et al. (2022) the model represents a lumped parameter approach that uses transfer functions to represent the behaviour of MP-particles in each lake compartment. The transfer functions represent transport, mixing and uptake processes occurring in the two lake water columns (Figure 1B). Particle numbers N_i in free suspension (N_1 = epi- , N_2 = meta-, N_3 = hypolimnion) in lake sediment (N_4) and within zooplankton faeces (N_5 = epi- , N_6 = meta-, N_7 = hypolimnion and N_8 = lake sediments) were simulated for each of the lake compartments as well as within the digestive tract of the zooplankton (N_9) in the epilimnion. For the epi- and hypolimnion, the model assumes fully mixed (turbulent) conditions that are represented by exponential transfer functions (i.e., exponential residence time distributions). For the metalimnion, the model assumes laminar conditions, where particles have a single residence time, mathematically represented by a Delta-Dirac transfer function that is similar to a 'piston flow' type model. For all compartments the governing equations can be combined into a set of nine coupled ordinary differential equations:

$$\frac{d}{dt}\vec{N} = M \cdot \vec{N} + \vec{L} \quad (S1)$$

In Equation S1 $\frac{d}{dt}\vec{N}$ [particles T^{-1}] represents the change of MP numbers in time for each model compartment $\vec{N} = (N_1 \ ... \ N_9)$, M [T^{-1}] represents a matrix containing first order transfer coefficients k_1-k_6 [T^{-1}] defining the exponential transfer functions used to represent the effect of turbulent mixing for the epi- and hypolimnion as well as the uptake and excretion by Daphnia (Equation S2).

$$M = \begin{bmatrix} -k_1 - k_2(t) & 0 & 0 & 0 & 0 & 0 & 0 & 0 & 0 \\ k_1 & 0 & 0 & 0 & 0 & 0 & 0 & 0 & 0 \\ 0 & 0 & -k_3 & 0 & 0 & 0 & 0 & 0 & 0 \\ 0 & 0 & k_3 & 0 & 0 & 0 & 0 & 0 & 0 \\ 0 & 0 & 0 & 0 & -k_5 & 0 & 0 & 0 & k_4 \\ 0 & 0 & 0 & 0 & k_5 & 0 & 0 & 0 & 0 \\ 0 & 0 & 0 & 0 & 0 & 0 & -k_6 & 0 & 0 \\ 0 & 0 & 0 & 0 & 0 & 0 & k_6 & 0 & 0 \\ k_2(t) & 0 & 0 & 0 & 0 & 0 & 0 & 0 & -k_4 \end{bmatrix} \quad \text{(S2)}$$

$\vec{L}$ [particles T^{-1}] is a vector containing information about the input of MP into the epilimnion $I(t)$ [particles T^{-1}] and fluxes associated with the laminar settling of MP and MP containing faeces in the metalimnion (Equation S3).

$$\vec{L} = \begin{bmatrix} I(t) \\ -k_1 N_1(t - \tau_1) \\ k_1 N_1(t - \tau_1) \\ 0 \\ 0 \\ -k_5 N_5(t - \tau_2) \\ k_5 N_5(t - \tau_2) \\ 0 \\ 0 \end{bmatrix} \quad \text{(S3)}$$

The first order exchange coefficients for the epi- and hypolimnion were estimated according to the definition of the mean lifetime of an exponential function $k = \dfrac{1}{\tau_{epi,hypo}}$ where $\tau_{epi,hypo}$ [T] are mean residence times of MP and MP containing faeces in the turbulent epi- and hypolimnion. Values for the mean residence times τ_{epi}, τ_{meta} and τ_{hypo} were calculated using equation S4a-c, where v_s [LT^{-1}] represents the laminar settling velocities for MP in each lake compartment and z [L] is the corresponding thickness of the epi- meta- and hypolimnion. The final set of coupled differential equations (shown in Figure S2) was solved simultaneously for every timestep by using the SIMULINK toolbox in MATLAB. For both lake systems the model was run for a period of $t_{end} = 15$ years with variable time stepping.

Study 5: Filter feeders are key to small microplastic residence times in stratified lakes: …

$$\tau_{epi} = \frac{z_{epi}}{v_{s\_epi}} \quad \text{(S4a)}$$

$$\tau_{meta} = \frac{z_{meta}}{v_{s\_meta}} \quad \text{(S4b)}$$

$$\tau_{hypo} = \frac{z_{hypo}}{v_{s\_hypo}} \quad \text{(S4c)}$$
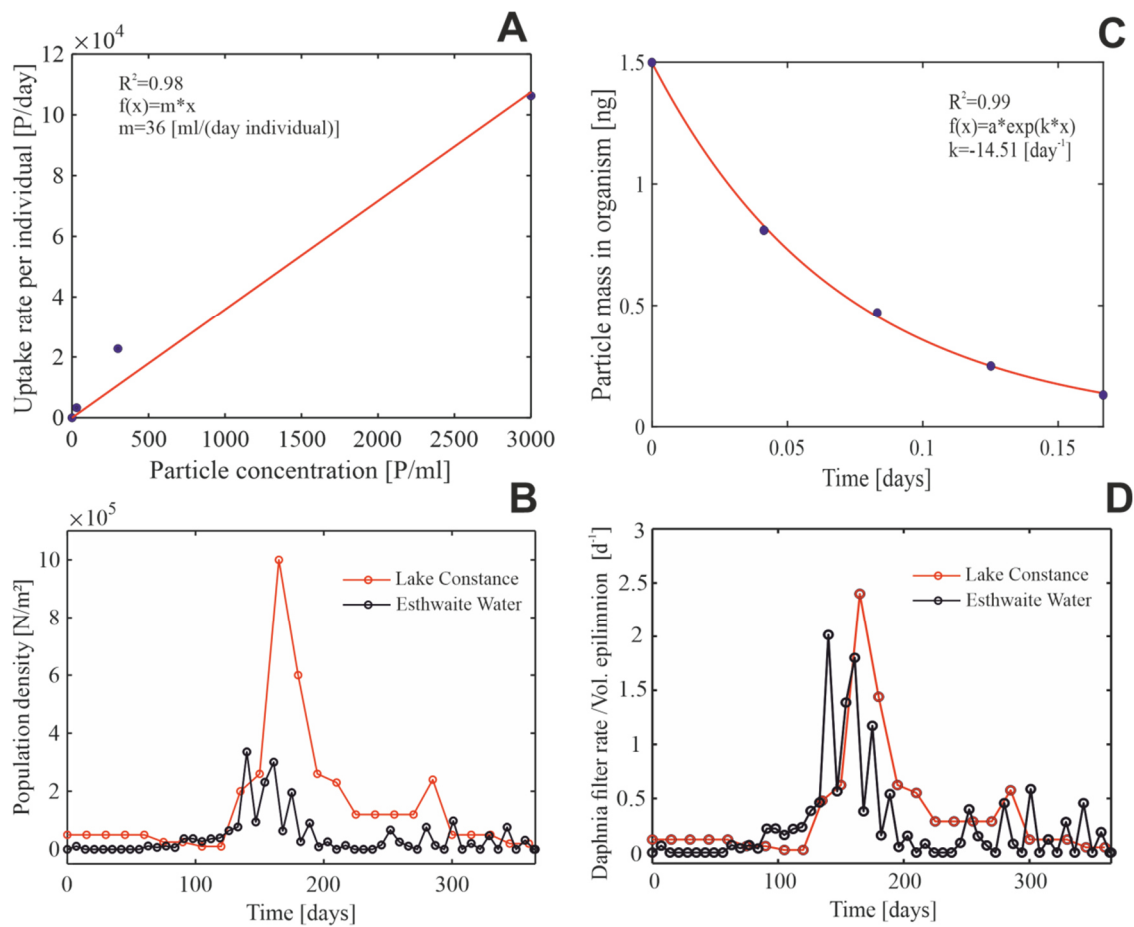
Supplementary S1: A) relationship between particle concentrations and uptake rate of MP for Daphnia Magna from Scherer et al. (2017). B) Daphnia population dynamics in Lake Constance and Esthwaite Water are from ISF (2016) and Achterberg et al. (1997), C) Data used to calculate MP excretion rates of Daphnia faeces, and D) Daphnia filtration rate as a proportion of the epilimnion water volume.
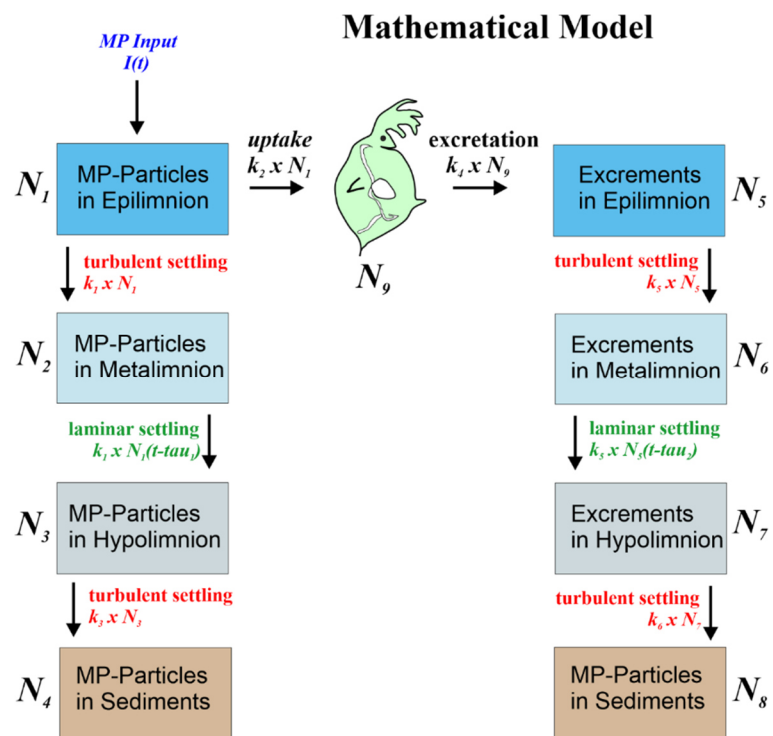
Supplementary Figure S2: Graphical representation of the mathematic lake model including the most important parameters used in the calculations.
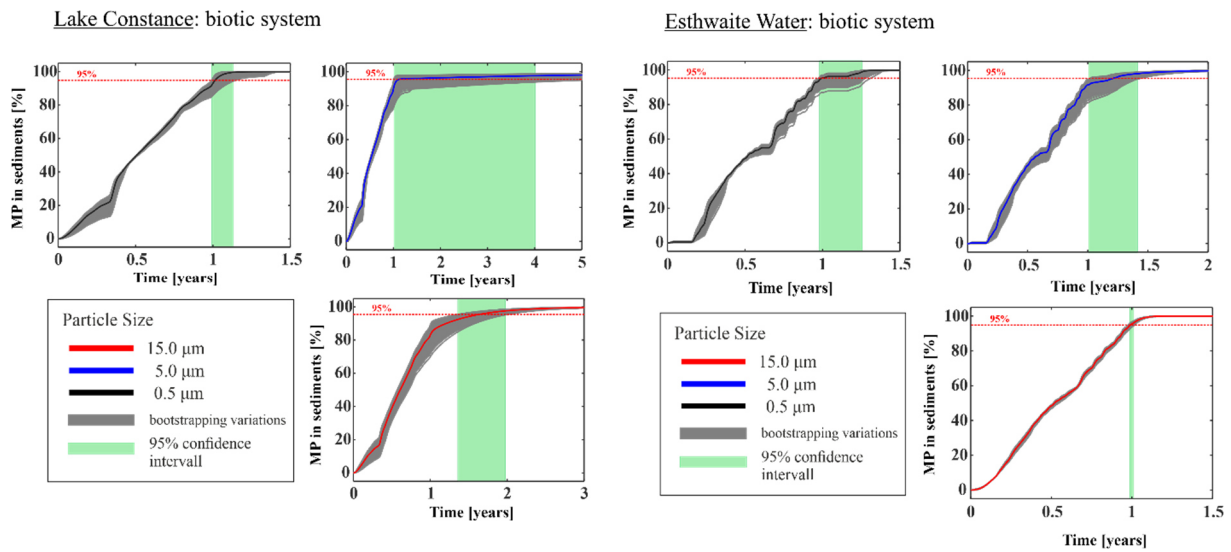
Supplementary Figure S3: Sensitivity analysis of the fraction of MP particles entering the sediments (residence times) in Lake Constance and Estwaite Water. Sedimentation rate, population density, egestion and filtration rates was varied from 50-150 % of their average values to quantify the effects of parameter selection on residence time estimates.

Achterberg, E.P., van den Berg, C.M.G., Boussemart, M., Davison, W., 1997. Speciation and cycling of trace metals in Esthwaite Water: A productive English lake with seasonal deep-water anoxia. Geochimica et Cosmochimica Acta, 61(24): 5233-5253.

Elagami, H. et al., 2022. Measurement of microplastic settling velocities and implications for residence times in thermally stratified lakes. Limnology and Oceanography, 67(4): 934-945.

ISF, L.f.U.B.-W., 2016. Institut für Seenforschung, Arbeitsbericht 2016, Karlsruhe / Langenargen.

Scherer, C., Brennholt, N., Reifferscheid, G., Wagner, M., 2017. Feeding type and development drive the ingestion of microplastics by freshwater invertebrates. Scientific Reports, 7(1): 17006.

7 Publications and manuscripts

Study 6: In-depth characterization revealed polymer type and chemical content specific effects of microplastic on *Dreissena bugensis*

Authors: Julian Brehm, Magdalena V. Wilde, Lukas Reiche, Lisa-Cathrin Leitner, Benedict Petran, Marcel Meinhart, Simon Wieland, Sven Ritschar, Matthias Schott, **Jan-Pascal Boos**, Sven Frei, Holger Kress, Jürgen Senker, Andreas Greiner, Thomas Fröhlich, Christian Laforsch

Research Paper

In-depth characterization revealed polymer type and chemical content specific effects of microplastic on *Dreissena bugensis*

Julian Brehm [a], Magdalena V. Wilde [b], Lukas Reiche [a], Lisa-Cathrin Leitner [c], Benedict Petran [c], Marcel Meinhart [d], Simon Wieland [a,e], Sven Ritschar [a], Matthias Schott [a], Jan-Pascal Boos [f], Sven Frei [f], Holger Kress [e], Jürgen Senker [d], Andreas Greiner [c], Thomas Fröhlich [b], Christian Laforsch [a,*]

[a] *University of Bayreuth, Animal Ecology I, Universitätsstraße 30, 95440 Bayreuth, Germany*
[b] *LMU Munich, Gene Center Munich, Laboratory for Functional Genome Analysis (LAFUGA), Feodor-Lynen Straße 25, 81377 Munich, Germany*
[c] *University of Bayreuth, Macromolecular Chemistry and Bavarian Polymer Institute, Universitätsstraße 30, 95440 Bayreuth, Germany*
[d] *University of Bayreuth, Inorganic Chemistry III and Northern Bavarian NMR Centre, Universitätsstraße 30, 95440 Bayreuth, Germany*
[e] *University of Bayreuth, Biological Physics, Universitätsstraße 30, 95440 Bayreuth, Germany*
[f] *University of Bayreuth, Department of Hydrology and Bayreuth Center of Ecology and Environmental Research (BAYCEER), Universitätsstraße 30, 95440 Bayreuth, Germany*

HIGHLIGHTS

- Mussels may not be able to distinguish between natural occurring particles and MP.
- Toxicity of MP is polymer-type dependent and linked to harmful chemicals in the MP.
- Recycled PET contained the most harmful chemicals.
- Recycled PET consequently caused the strongest adverse effects.

GRAPHICAL ABSTRACT
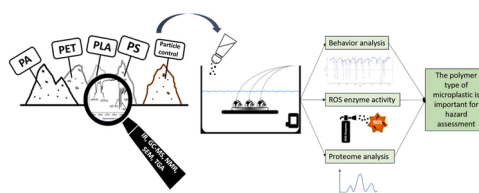
ARTICLE INFO

ABSTRACT

In aquatic ecosystems, filter feeders like mussels are particularly vulnerable to microplastics (MP). However, little is known about how the polymer type and the associated properties (like additives or remaining monomers) of MP impact organisms, as the predominant type of MP used for effect studies on the organismic level are micron grade polystyrene spheres, without considering their chemical composition. Therefore, we exposed the freshwater mussel *Dreissena bugensis* (*D. bugensis*) to in-depth characterized fragments in the same concentration and size range (20–120 μm): recycled polyethylene terephthalate from drinking bottles, polyamide, polystyrene, polylactic acid, and mussel shell fragments as natural particle control. Real-time valvometry, used to study behavioral responses via the movement of the mussels' valves, showed that mussels cannot distinguish between natural and MP particles, and therefore do not cease their filtration, as when exposed to dissolved pollutants. This unintentional ingestion led to polymer type-dependent adverse effects (activity of antioxidant enzymes and proteomic alterations), related to chemicals and residual monomers found in MP. Overall, recycled PET elicited the strongest negative effects, likely caused by anthranilamide, anthranilonitrile and butylated hydroxytoluene, contained in the fragments, which are toxic to aquatic organisms. As PET is among the most abundant MP in the

environment, sublethal effects may gradually manifest at the population level, leading to irreversible ecosystem changes.

1. Introduction

Sustainable life in modern society is impossible without the extensive and appropriate use of plastic materials. Plastic materials are cheap and have a range of unique property combinations (Andrady and Neal, 2009). Consequently, the consumption of plastic materials continually increases, reaching a worldwide demand of 367 million tons in 2020 (Plastics Europe, 2021). However, once plastics enter the environment due to inappropriate waste management, so-called secondary microplastics ((MP); plastic debris 1 to < 1000 µm (Hartmann et al., 2019)) are formed through mechanical forces or other degradation processes such as photooxidation (Galloway et al., 2017; Klemchuk, 1990). Next to these secondary MP, primary MP (intentionally produced in this size range (Hwang et al., 2020)) can enter the environment via many pathways. To date, MP are present in all environmental compartments (Cristaldi et al., 2020), including freshwater ecosystems (Anderson et al., 2017; Imhof et al., 2013).

Although freshwater habitats are vital as drinking water resources, they are severely affected by pollutants (Revenga et al., 2005), including MP (Dris et al., 2015a). Since an increase of MP in the environment is expected, there is a great need to investigate the impact of MP on these ecosystems. Once MP enters the environment, it can be encountered by various aquatic organisms, potentially causing adverse effects. Filter-feeding organisms are already known to ingest large amounts of MP (Moore, 2008) as they feed on particulate matter. Therefore, the necessity to elucidate the effects of MP on these filter feeding organisms arises. So far, reported negative effects include a reduced number of offspring in *Daphnia* (Ogonowski et al., 2016), changes of the proteomic profile in both *Daphnia* and the mussel *Dreissena* (Trotter et al., 2021; Magni et al., 2019) or changes in the antioxidative capacity in *Dreissena* (Weber et al., 2020).

In this context, specific physico-chemical properties of MP that could be responsible for these effects, such as size (An et al., 2021) and shape (Schwarzer et al., 2021) of the particles, or the adsorption of chemicals (Schür et al., 2021), are gaining more and more attention (Wieland et al., 2022), while other parameters like leakage of residual monomers or additives (Renzi et al., 2019) were rarely considered. Interestingly, even MP of the same polymer type and shape can differ tremendously in their properties, resulting in differing effects on organisms (Ramsperger et al., 2021). This, in turn, makes it very likely that the effects of MP from different polymer types will vary even more. However, to date, the scientific focus has been on only a few polymer types (such as polyethylene (PE) and polystyrene (PS)) to study the effects on organisms. Other polymer types with high production and consumption rates, such as polyethylene terephthalate (PET), are rarely investigated (71 out of 1054 MP used in studies) (Rozman and Kalčíková, 2022). Concerning polymer type effect studies, there is a discrepancy between laboratory studies and plastics found in nature, as bottles made of PET are the most common type of macroscopic debris in European rivers (Earth Watch Institute, 2018). An estimated 480 billion plastic drinking bottles are produced each year globally, with differing amounts of recycled material (e.g. in Germany every PET bottle consists of ~30 % recycled material (gvm Gesellschaft für Verpackungsmarktforschung, 2020)). Since a large fraction of them is not disposed properly (Ryan et al., 2019), for example via illegal dumping from ships (Ryan, 2020) or public littering (Sheavly and Register, 2007), the amount of PET waste in freshwater systems will continue to rise in a business-as-usual scenario.

Due to the different properties of microplastics, extrapolating ecotoxicological findings caused by one or two types of MP (i.e. petroleum-based MP like PS or bio-based MP like polylactic acid (PLA) (derived from renewable sources such as vegetable oil (Verschoor, 2015)) to the

entire spectrum of MP types may be misleading (Ogonowski et al., 2018). For a valid hazard assessment of MP, a preceding in-depth characterization of the MP particles is essential. This in combination with comparisons of different polymer types will allow a better understanding of the properties that cause detrimental effects in organisms.

We therefore exposed the limnic filter feeder *Dreissena bugensis* (*D. bugensis*) to three frequently used petroleum-based polymers (recycled PET, polyamide 66 (PA 66), PS), and one bio-based polymer (PLA). PET and PS are commonly found in freshwater bodies, respectively accounting for 11 % and 13 % of plastics found in freshwater samples (Li et al., 2020). Additionally, we used ground mussel shell fragments as natural control particles, which were not associated with adverse effects (Schwarzer et al., 2021). All MP and the control particles were irregular particles (fragments (mean sphericity ~0.80–0.91)) with a similar size range (~20–120 µm) and the suspension in water was proved using laser doppler velocimetry (LDV). Physico-chemical properties of MP particles were analyzed in-depth using differential scanning calorimetry (DSC), gas chromatography-mass spectrometry (GC-MS), infrared (IR) spectroscopy, laser diffraction (LD) / dynamic image analysis (DIA), nuclear magnetic resonance (NMR) spectroscopy, scanning electron microscopy (SEM), and thermogravimetric analysis (TGA).

The ingestion of MP by the mussels was shown using rhodamine B labelled PS fragments and cryosections in a companion experiment. In the main experiment the behavioral endpoints "filtration activity" (percentage of time the mussels are actively filtrating) and "transition frequency" (number of changes between open and closed behavior per day) of *D. bugensis* were recorded using the Hall sensor technology (Hartmann et al., 2016a). Further, to measure the overall stress level, the activities of oxidative stress biomarkers (activity of ROS detoxifying enzymes catalase (CAT), glutathione peroxidase (GPx), super-oxide dismutase (SOD, and glutathione-s-transferase (GST)) were analyzed, and proteomic profiling was performed to address underlying biochemical processes. Thus, we can link possible effects directly to the polymers and their specific properties. Additionally, we aim to rule out effects caused by particles per se by using ground mussel shell fragments that resemble naturally occurring particles.

2. Materials and methods

2.1. MP and control particles preparation

Four different synthetic polymer types and one natural control particle type (mussel shell fragments) were used in the experiment (see Table 1). The PET was obtained from recycled PET bottles, provided by Veolia (Paris, France). Additionally, fluorescently labelled PS was used to investigate the ingestion of MP particles.

The original plastic material was milled in a centrifugal mill (ZM 200, Retsch GmbH, Haan, Germany) and air jet sieved to gain fragments in a comparable size range (~ 20–120 µm).

Mussel shell fragments were prepared by mortaring thoroughly cleaned shells (using 70 % EtOH, demineralized water, brushes, and paper towels) and sieving them through 70 µm and 20 µm meshes (the middle fraction was then used) (pluriStrainer, pluriSelect, Leipzig, Germany).

Before the experiments, stock suspensions were prepared for all different fragment types, following the protocol by Schür et al. (2020). This protocol enables that the polymers are well dispersed in water. For that, 1 g of the respective fragments were suspended in 1 L autoclaved Achener *Daphnia* Medium (ADaM) (Klüttgen et al., 1994) in 1 L Schott DURAN borosilicate glass bottles and shaken for 48 h. Stock suspensions were then stored at 4 °C and continuously stirred before dilutions.

7 Publications and manuscripts

Finally, the particle concentration of stock suspensions was evaluated using a hemocytometer (Neubauer Improved, Brand GmbH & Co. KG., Wertheim, Germany). For these measurements and the preparation of test suspensions, particles were taken from the middle water layer of the stock suspensions after 48 h of shaking. Particle concentrations of stock suspensions can be found in the SI (Table S1).

2.2. MP and control particle characterization

To precisely characterize the used particles, the size/shape distribution and the chemical composition of the different particles were analyzed. The shell fragments' chemical composition was analyzed using attenuated total reflection (ATR) infrared spectroscopy (Alpha FT-IR Spectrometer, Bruker, Billerica, USA) and was confirmed to be aragonite. The chemical composition of MP used in the behavior and molecular experiment was additionally analyzed using NMR spectroscopy, IR spectroscopy, DSC measurements, GC-MS measurements, and TGA measurements.

2.2.1. Size and shape distribution

Particle size and shape analysis were performed using a particle size- and shape analyzer (FLOWSYNC, Microtrac MRB, Montgomeryville and York, USA) based on LD/DIA.

To investigate the morphology of the different particles, 10 µl of each stock suspension were pipetted to silicon wafers. These were mounted on aluminum stubs (Ø 12 mm, Plano GmbH, Wetzlar, Germany) using carbon conductive tabs (Ø 12 mm, Plano GmbH, Wetzlar, Germany) and dried in a desiccator. The samples were then coated with a 4 nm thick platinum layer (208HR sputter coater, Cressington, Watford, UK). Finally, they were analyzed with SEM (FEI Apreo VolumeScope, Hillsboro, USA) at 3 kV (PA 66, PET, PLA) and 5 kV (PS, mussel shell fragments) using an Everhart-Thornley detector.

2.2.2. Chemical composition of MP

First, a Bruker Advance (Billerica, USA; 300 MHz) was used to record NMR spectra, with the chemical shift given in parts per million (ppm) and the coupling constant (J) in Hz. Deuterated chloroform δ (CDCl$_3$) = 7.26 ppm was used as the solvent for PLA and PS. For PA 66 and recycled PET, a mixture of deuterated HFIP ((CF$_3$)$_2$CDOD) and deuterated chloroform δ was used. Approximately 10 mg of the sample were solved in 0.7 ml of deuterated solvent at room temperature.

Then, for acquiring high-resolution ^{1}H and ^{13}C liquid-state NMR spectra of recycled PET, approximately 5 mg dried particles were dissolved in 0.7 ml of a 3:1 (wt. ratio) mixture of deuterated chloroform-D and deuterated trifluoroacetic acid (TFA-D). The filled sample tubes were mounted in helium-cooled TCI-CryoProbe on an Avance III HD spectrometer (Bruker, Massachusetts, USA) with a B$_0$ field of 16.4 T. Quantitative ^{1}H NMR spectra (ν_0(^{1}H) = 700.2 MHz) were measured with single-pulse (SP) excitation using a recycle delay of 1 s and a pulse length of 3.0 µs corresponding to a 30° tip angle. The ^{13}C NMR spectra (ν_0(^{13}C) = 176.0 MHz) were also measured with SP excitation using a

recycle delay of 3 s and a pulse length of 6 µs corresponding to a 45° tip angle. For ^{1}H broadband decoupling, a WALTZ-16 sequence (v_{nut} = 3.6 kHz) was applied. The ^{1}H and ^{13}C NMR spectra are referenced with respect to tetramethylsilane (TMS).

The IR spectra were recorded with an Excalibur Series IR (Bio-Rad Laboratories, USA), and the wavenumber was given in cm^{-1}. DSC measurements, and therefore the thermal properties, were measured with a Netzsch DSC 204 F1 Phoenix (Selb, Germany) using aluminum crucibles (Thepro GbR, Heinsberg, Germany). The thermogravimetric data were generated using a TG 209 F1 Libra thermobalance from Netzsch (Selb, Germany). For DSC and TGA, evaluation was performed using Proteus 8.0 (Netzsch, Selb, Germany).

Thermal desorption was performed on a gas chromatograph (GC 8790B, Agilent Technologies, Santa Clara, USA) coupled with a quadrupole mass spectrometer (MSD 5977 A, Agilent Technologies). The GC-MS was equipped with a thermal desorption unit 2 (Gerstel GmbH, Mülheim an der Ruhr, Germany). Desorption glass tubes, closed with glass wool, have been conditioned for 1–4 h at 300 °C with a 300 ml/min helium flow. Blank measurements have been performed before and after every measurement to verify the absence of contamination. 20 ± 1 mg of powdered sample was charged into the conditioned glass desorption tube. Desorption was carried out by maintaining the temperature at 40 °C for 0.5 min before increasing the temperature to 100 °C with a rate of 10 K/min and holding this temperature for 20 min. The helium desorption flow was 100 ml/min in solvent vent mode. The analytes were cryocooled at a temperature of − 100 °C. After thermal desorption, the cold injection system (CIS 4 C, Gerstel GmbH) was heated with a rate of 10 K/s to 280 °C. This temperature was remained for 5 min. The GC oven was heated with 10 K/min from 40° to 300°C with a subsequent hold time of 5 min. The helium column carrier gas flow was 1 ml/min. Mass spectrometry was measured in TIC mode in a mass range between 40 and 550 *m/z*. The resulting spectra were analyzed with Masshunter software (version 10.0, Agilent) in combination with the NIST spectral library (version 20, National Institute of Standards and Technology, Gaithersburg, USA). Available Kovats indices in the literature verified suitable matches. Kovats indices are temperature program and device-independent, column type dependent constants based on the retention time of the analytes, which is a reliable indicator for GC measurements (Kovats, 1958). Therefore, a mixture of C7-C33 aliphatic hydrocarbons was measured with the method described above. Peaks of high interest (i.e. anthranilamide, BHT, 2-aminobenzonitrile (anthranilonitrile)) were additionally verified by measurements of synthetic standards (anthranilamide: Acros organics, 99 +%, BHT: Sigma-Aldrich, 99 +%, 2-Aminobenzonitrile (anthranilonitrile): Fluka, 98 %) (see Fig. S8).

2.2.3. Distribution and behavior of particles in the water column

To ensure comparability of the exposure experiments, it was analyzed whether PS-particles (material with lower density) and mussel shell fragments (material with higher density) were suspended in the water column. Therefore, experimental setup and particles were as in the behavior experiments (Table 1, Fig. 1). For this purpose, flow

Table 1

Overview of the used particle types in this study, including mean size ± standard deviation (SD), mean sphericity and the respective density.

Particle type	Mean size ± SD (µm)	Mean sphericity	Density (g/cm^3)	Trade name	Manufacturer
Behavior and molecular experiments					
recycled PET	74 ± 44	0.81	1.41	CleanPET WF	Veolia, Paris, France
PA 66	69 ± 33	0.84	1.15	Ultramid A27 E	BASF, Ludwigshafen am Rhein, Germany
PLA	67 ± 33	0.8	1.24	Ingeo 4043D	NatureWorks, Minnetonka, USA
PS	58 ± 21	0.89	1.05	158 N/L	INEOS Styrolution, Frankfurt am Main, Germany
Mussel shell fragments/ aragonite	20 ± 74	0.91	~2.59 (Hartmann et al., 2016a)	n.a.	in-house produced
Uptake experiment					
Rhodamine B labelled PS	54 ± 23	0.91	~1.05	n.a.	in-house produced
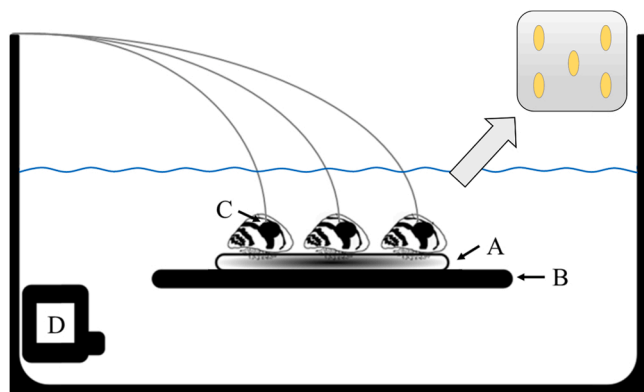
Fig. 1. Schematic experimental setup. Five individuals per aquarium of *D. bugensis* were glued to a ceramic tile (A) and positioned on the inserted glass plate (B). A Hall sensor and a magnet (C) were attached to the valves to record the valve movements. The submersible pump (D) ensures a continuous circular flow. Schematically is also shown the positioning of the mussels on the tile (upper right).

velocities of near-bed regions (corresponding to the position of the mussels) in a small measurement volume (100 μm diameter, 1.3 mm length) were obtained with LDV (TSI Inc.), using two laser beams (532 and 561 nm, 500 mW). The laser was mounted on a two-dimensional traverse system (isel Germany AG, 600 mm travel distance), allowing for the automated measurement of velocity profiles. The LDV was run in coincidence mode to ensure simultaneous sampling. Velocity profiles were taken at six different positions across the ceramic tile (SI Fig. S9).

Friction velocity u_* was calculated from a fit of the temporal mean of horizontal velocity component u to the logarithmic boundary profile $u = \frac{u_*}{\kappa} * \ln\left(\frac{z}{z_0}\right)$, with κ Kármán's constant, z the height over the tile and z_0 roughness length (Huthnance et al., 2002). In addition, we obtained friction velocity as spatial mean of the height-dependent Reynolds stresses $u_* = \frac{1}{n}\sum_{i=1}^{n}\sqrt{-\overline{u'w'}}$, using horizontal ($u'$) and vertical velocity fluctuations (v') (Inoue et al., 2011; Esders et al., 2022). Friction velocities were compared to the critical thresholds for erosion and suspension, which were calculated from particle characteristics, choosing the characteristic diameter at 80 % of sieve passage (Zanke, 2012). The obtained datasets were analyzed with MATLAB and Excel.

2.3. Mussel collection

Quagga mussels (*D. bugensis*) were collected in January 2020 from the river Regnitz near Pettstadt (Germany) (49°49'57.9"N 10°56'55.5"E). They were cut off from rocks with disposable scalpels and transported to the lab in river water. In the lab, the mussels were cleaned (using tap water, brushes, and paper towels) and their size measured. Only those with a 25 ± 5 mm length were used in the experiments. To exclude mixing with the sister species *Dreissena polymorpha*, the species of mussels was determined utilizing the method of Teubner et al. (2016). In this publication, the species determination is based on a morphometric quantification of the angularity (*An*) of the shells (see SI Fig. S1 for examples). From a group of clearly identifiable mussels (5 x *D. bugensis* (*An* ≤ 2.96); 5 x *D. polymorpha* (*An* ≥ 5.05)), the remaining mussels were identified by visual and haptic perception of angularity, as described in Teubner et al. (2016). All remaining mussels were distributed in 12 L aquaria (50 animals per aquarium) initially filled with 3 L river water (originating from the same locations as the mussels). Subsequently, ADaM was slowly applied via silicone tubing up to a volume of 5 L. After another 24 h the river water / ADaM mixture was replaced with 5 L of pure ADaM. Before the experiments, the mussels were acclimated for six weeks in 12 L aquaria filled with 5 L ADaM and maintained at 15 ± 0.5 °C in oxygen saturated conditions by constant air bubbling, and a photoperiod (via fluorescent tubes) of 14 h.

Animals were fed daily *ad libitum* with the green algae *Acutodesmus obliquus*. The constant air bubbling ensured that the algae sank more slowly, making them available to the mussels for a longer time. A complete media exchange was performed every third day.

2.4. Experimental setup

Modified 12 L aquaria (outer dimensions, length x width x height: 30 ×20 x 20 cm; Glass thickness: 0.8 cm) filled with 5 L ADaM were used in the experiments. Glass plates (length x width: 17 ×19 cm; Glass thickness: 0.4 cm) were mounted in the height of 5 cm in these aquaria with aquarium silicone (AquaSil, JBL, Neuhofen, Germany). Four identical glass jars (height: 5 cm) per aquaria were used to stabilize the glass plates at the desired height while the silicone was curing. Before use, the aquaria were soaked in purified water for 24 h, as recommended by the manufacturer, to ensure that no soluble substances from the silicone leach into the medium. During the experiments, the mussels were then placed on the created platforms. With this setup, a free space of ~ 6.1 cm was generated on both sides of the mounted glass plates to enable water circulation. Via submersible pumps (ProFlow t500, JBL, Neuhofen, Germany), in which the outflow was directed underneath the glass plates, a constant circular flow was created, preventing algae or fragments from settling (Fig. 1). The size range of the particles (20–120 μm) was chosen, as mussels of the family Dreissenidae are known to ingest food particles in a range from 20 to 450 μm (Descy et al., 2003; Sprung and Rose, 1988; Grigorovich and Shevtsova, 1995), consequently, fragments in this size range are likely ingested. Due to the circulatory-flow setup in our experiment, neither an upward drift of the lightest material (PS: 1.05 g/cm³) nor a downward drift of the heaviest material could be observed (mussel shell fragments -> mainly aragonite (d: 2.93 g/cm³; crushed shells according to Barbachi et al., d: 2.59 g/cm³ (Barbachi et al., 2017); density of remaining particles: recycled PET: 1.41 g/cm³, PA: 1.15 g/cm³, PLA: 1.24 g/cm³), indicating that mussels were able to ingest the particles.

2.5. Behavior monitoring

2.5.1. Voltage output– Mussel behavior adjustment

Behavior analysis was conducted according to the method described by Hartmann et al., where Hall sensor technology is used to monitor the mussels' valve movements via changes in the voltage output (Hartmann et al., 2016a). In this publication, the threshold between filtrating and closed behavior of the mussels is set as the mean of the voltage output. A preliminary experiment was performed to adjust the voltage outputs to the actual behavior of the mussels we used. This became necessary, as the mussels we used (*D. bugensis*) showed another behavior pattern than the mussels used in the publication of Hartmann et al. (*Anodonta anatina*) (Hartmann et al., 2016a), so that the proposed threshold did not fit for the mussels we used (see Fig. S3 for more details). Therefore, six mussels were glued in groups of two on three small ceramic tiles (1.5 ×5 cm), using a cyanoacrylate adhesive (PlantFix liquid, Dupla, Koblenz, Germany). This specific cyanoacrylate adhesive is recommended for use in tagging projects and behavioral studies of freshwater mussels as it does not disturb the mussels during the experiment and withstands strong removal forces even after long term exposure (Hartmann et al., 2016b). Further, for ethyl 2-cyanoacrylate, tests for aquatic toxicity are not possible and not necessary due to the chemical properties of the registered substance (EC 230–391–5) (ECHA, 2022a), indicating that it has no adverse effect on the mussels in our experiment.

To enable behavior measurements, one 0.2 g N 42 neodymium magnet was glued on the bottom valve and one Hall sensor on the mussels' top valve. These mussels were then optically captured via video cameras (HERO3, GoPro Inc., San Mateo, USA) to determine the most suitable voltage limit, above which a mussel can be considered actively filtrating (Fig. 2). It turned out that no generally valid threshold value (meaning a specific voltage) could be defined since the applied voltage
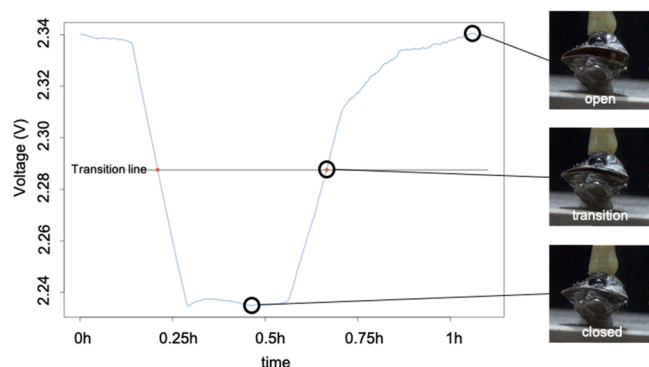
Fig. 2. Exemplary voltage profile gained via Hall sensor technology; the pictures show the mussel's behavior at the respective voltage output.

differed from mussel to mussel. Hence, a threshold suitable for all voltage profiles had to be found. Here, the preliminary experiment revealed that the average voltage of the maximum and minimum voltage output was most appropriate to serve as transition line between filtrating and resting. Transition frequency was then calculated based on the found intersection points with the transition line per day. Filtration activity was considered as the percentage of all data points above the transition line. To ensure that a transition was only counted once, a threshold ($\pm$ 0.25 x SD of the voltage output) around the transition line was applied (see Fig. S3). Furthermore, a moving average over 10 min (120 data points) was calculated to reduce the signal's noise for every data point.

2.5.2. Behavior monitoring during particle exposure

For the actual behavior monitoring experiment, mussels (5 mussels per aquaria, 3 replicate aquaria per treatment (18 aquaria); n = 15 mussels per treatment) were fixed on one ceramic tile (9.5 $\times$ 9.5 cm) using the cyanoacrylate adhesive described above. Additionally, ten mussels per aquarium were added (fixed in groups of two on five ceramic tiles (1.5 $\times$ 5 cm)) for the enzyme and proteomic analyses. To do this, a drop of the cyanoacrylate adhesive was placed on the tile and the mussel was carefully placed on this drop and adjusted to ensure the mussels retains an upright position throughout the experiment. To accelerate the curing of the adhesive, the adhesive joint was rinsed with ADaM several times. Thereby we ensured, that mussels stayed on the designated spot and did not change their position during the measurements which could have led to inaccurate measurements, as for example the position of the sensor could interfere with a normal opening and closing behavior. Further, a single N 42 neodymium magnet (weight: 0.2 g) was glued on the bottom valve and one Hall sensor on the mussels' top valve. At the end of this procedure, every mussel was visually inspected to check whether a normal opening and closing behavior was possible. If necessary, the position of the mussels was adjusted. After 96 h of acclimatization to the experimental setup (Fig. 1), the behavior monitoring started. A schematic representation of the experimental schedule is shown in Fig. 3.

During the 18 days of behavior monitoring, the mussels were fed daily with the green algae *A. obliquus* (0.5 mg C x mussel^{-1} x day^{-1}). The medium was exchanged every third day. During the medium exchange, aquaria were cleaned with brushes and 70 % EtOH to remove remaining

fragments and algae.

Voltage measurements were recorded every 5 s for all 90 mussels (except the time of medium exchange + 1 h). No MP or control particles were added during the first nine days of the experiment to gain a baseline pattern of unstressed behavior. Then 1000 p ml^{-1} of the different polymers and shell fragments were added from the middle water layer of the stock suspensions. We chose this relatively high concentration, as the knowledge on environmental concentrations of MP in this size range is still hampered by methodological constraints, the lack of harmonized methods (Dris et al., 2015b), and a typical sampling mesh size of $\sim$ 330 μm (Li et al., 2018), which makes smaller particles unquantifiable. As the data situation of MP in the environment is scarce in the MP size class we used, we decided to orientate on other publications with MP and *Dreissena*. Here concentrations were used ranging from 500 to 2000 p ml^{-1} (Magni et al., 2019) and 6.4–100000 p ml^{-1} (Weber et al., 2020, 2021). Therefore, we decided to use an intermediate concentration of 1000 p ml^{-1}.

2.6. Biochemical assays

At the end of the experiment (day 18), three randomly picked mussels per aquarium (n = 9/Treatment) were snap frozen in liquid nitrogen and stored at $-$ 80 °C for subsequent biochemical analyses.

The activity of antioxidant enzymes CAT, GPx, SOD, and GST in homogenates of *D. bugensis'* whole soft tissues were analyzed in triplicates of the cytosolic fraction. Whole soft tissue was used following the observation of Binelli et al. (2011), that the small size of the mussels did not allow the use of different tissues due to the small quantity of enzymes contained. The soft tissue of all picked mussels from one aquarium (n = 3) was removed from shells using disposable scalpels. Pooled soft tissue was then homogenized in 4 ml 100 mM phosphate buffer (pH 7.4) containing 100 mM KCl, 1 mM EDTA, 1 mM dithiothreitol (DTT), and protease inhibitors (1/100 v/v) at 4 °C using a high-performance disperser (TP18/10 IKA Werke GmbH & Co. KG, Staufen im Breisgau, Germany). Subsequently, homogenates were centrifuged at 15,000 g for 30 min (4 °C), and the supernatant was used for enzyme assays and protein content determination according to Bradford (ROTIQuant, Carl Roth GmbH, Karlsruhe, Germany) (Bradford, 1976).

As all performed enzyme assays are described elsewhere (CAT (Hadwan, 2018); SOD (McCord, 1999); GPx (Sedaghatfard et al., 2016)), only a summary is given here. In brief, CAT activity in mussel tissues was analyzed based on the protocol of Hadwan (Hadwan, 2018). In this protocol, the CAT activity is measured indirectly at 440 nm through the formation of a stable and colored carbonato-cobaltate (III) complex, which is directly proportional to the rate of dissociation of hydrogen peroxide. SOD activity in mussel tissue was analyzed adopting the protocol of McCord (McCord, 1999). Here the SOD activity was determined at 550 nm via the reduction of cytochrome c (10 μM) by the superoxide anion (O$_2$), which is generated by the enzymatic activity of xanthine oxidase (0.3 U/ml). For GPx activity analysis, the protocol of Sedaghatfard et al. (2016) with slight modifications was used. The NADPH consumption at 340 nm was measured, using H$_2$O$_2$ (0.5 mM) as substrate, glutathione reductase (10 U/ml) to gain a constant level of glutathione (GSH) and sodium azide (NaN$_3$, 1 mM) to inhibit catalase activity. Lastly, GST levels were determined using a commercially available kit (Glutathione-S-Transferase Assay Kit, Sigma Aldrich, St. Louis, USA) at 340 nm with 1-chloro-2,4-dinitrobenzene (CDNB) as
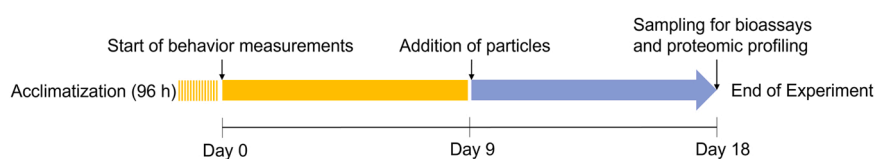
Fig. 3. Schedule of the behavior experiment.

5

co-substrate.

2.7. Uptake of MP into the mussels

To evaluate whether mussels ingest MP particles in the size and shape we used in the main experiment, we conducted an experiment with fluorescently labelled PS fragments (see Table 1). Here, we used the setup as shown in Fig. 1. The mussels were exposed to 1000 p ml^{-1} for 24 h and then snap frozen in liquid nitrogen. Subsequently, the mussels' soft tissues were cryo-sectioned (20 μm, −21 °C) without the use of an embedding medium. These sections were then analyzed using a confocal microscope (Axio Imager.Z2m coupled to an AxioCam MRm (brightfield and fluorescent measurements (ex: 543 nm; em 565 nm)), and to an Axiocam 105 color; all Carl Zeiss AG, Germany) (Fig. 5). Tiles were stitched and channels were merged using a plugin (Preibisch et al., 2009) of Fiji ImageJ 1.53q. Additionally tissue sections were stained with hematoxylin and eosin (H&E) to gain a better overview of the tissues (see SI, Fig. S2).

2.8. Statistical analysis

Processing of the voltage output data was performed as described above. All calculations and statistical analyses for filtration activity, transition frequency, and enzyme activity data were carried out using R Version 4.0.2 (R Core Team, 2021). Data normality was checked using the Shapiro-Wilk test and graphical representation (Q-Q-Plot), while homogeneity of variances was tested using the Levene test function. A standardized linear model (SLiM) was utilized to test for differences in filtration activity and transition frequency between the periods with and without fragments. One-way ANOVAs were computed to test for differences in Δfiltration activity and Δtransition frequency (period with fragments – period without fragments). One-way ANOVAs were also used to test for differences in antioxidant activity. If the one-way ANOVAs identified significant differences, Tukey post hoc tests were computed.

2.9. Proteomic analysis

The proteome analysis was performed on digestive glands tissue. Therefore, per aquaria, another three mussels were randomly picked (n = 9/Treatment) at the end of the experiment (day 18). Digestive glands were dissected with microdissection tools in glass Petri dishes on ice, snap frozen in liquid nitrogen, and subsequently stored at − 80 °C. To 30–40 mg of tissue, sample lysis buffer (7.5 μl per mg frozen tissue) consisting of 6 M urea, 2 M Thiourea, 4 % CHAPS, 30 mM Tris and 1 tablet of protease inhibitor per 5 ml (Complete Ultra tablet mini, Roche) was added. Subsequently, samples were sonicated twice with a cup resonator (BANDELIN electronic GmbH & Co. KG, Berlin, Germany) and then homogenized using QIAshredder (Qiagen, Hilden, Germany) devices (5000x *g*, 1 min). Protein concentrations were determined using the Coomassie Plus (Bradford) Protein Assay (Thermo Fisher Scientific, Waltham, MA, USA).

For in-solution digestion, proteins were reduced in 4.5 mM DTT and alkylated in 8.3 mM iodoacetamide. Samples were diluted to a concentration of 1 M urea, and digestion was performed with trypsin (1/50 enzyme/protein, Promega, Fitchburg, WI, USA) overnight at 37 ∘C. LC-MS/MS analysis was performed using an Ultimate 3000 RSLC (Thermo Fisher Scientific) connected to a Q Exactive HF-X mass spectrometer (Thermo Fisher Scientific). First, 1.6 μg of total protein was injected and loaded onto a trap column (PepMap 100 C18, 100 μm × 2 cm, 5 μM particles, Thermo Scientific) using a flow rate of 5 μl/min and 0.1 % formic acid and 1 % acetonitrile in water as mobile phase (mobile phase A). Next, liquid chromatography was performed with an EASY-Spray column (PepMap RSLC C18, 75 μm × 50 cm, 2 μm particles, Thermo Scientific) and a flow rate of 250 nl/min. Peptide samples were separated with a two-step gradient of mobile phase B (0.1 % formic acid in

acetonitrile) from 3 % B to 25 % B in 160 min, followed by a 10 min ramp to 40 % B. The mass spectrometer was operated in the data-dependent acquisition mode performing a maximum of 15 MS/MS spectra per survey scan.

2.10. Proteomic data processing

For protein and peptide identification, the *de novo* assembly transcriptome of *D. bugensis* from digestive glands (Péden et al., 2019) was *in silico* translated and used to search MS/MS spectra. Protein identification and quantification were done in Proteome Discoverer 2.2 (Thermo Fisher Scientific) with the FDR Confidence set to high (< 1 %) and with MASCOT V2.6.2 (Matrix Science Limited, London, UK) as search engine. To generate a set of proteins differently abundant between treatment and control groups, filtered results were exported and statistically evaluated (e.g. volcano plots) in Perseus V1.5.3.2 (part of the MaxQuant package) (Tyanova et al., 2016). Normalized abundances were log2 transformed, and only proteins present with a minimum number of 3 valid abundance values in at least one group were used for quantification. To handle missing values, the imputation feature of Perseus was used. A Student's T-test was performed (FDR < 0.05), and data were filtered for p-values < 0.01 and log2-fold changes < −0.6 and > 0.6. Differentially abundant proteins were annotated manually, using the best_annotation.gff file from Péden et al. (2019). The mass spectrometry proteomics data have been deposited to the ProteomeXchange Consortium (http://proteomecentral.proteomexchange.org) via the PRIDE partner repository (Perez-Riverol et al., 2019) with the dataset identifier PXD030056.

3. Results

3.1. MP characterization

LD/DIA measurements for all MP revealed that particles had a mean sphericity between 0.80 (PLA) and 0.89 (PS). According to the LD/DIA measurements, MP were in the 20–120 μm size range (Table 1 & SI Fig. S4). The scanning electron micrographs (Fig. 4) confirm that the different particle types were in the same size range and irregularly shaped. Apparently, the PLA and PS particles were of an oval or rounded shape, whereas PA 66 and recycled PET formed more elongated fragments. All MP particles had relatively smooth and rounded edges, and their surface was smooth. In contrast to that, the mussel shell fragments formed somewhat angular, irregularly shaped fragments with clear breaking edges. Furthermore, their surface roughness was increased compared to the MP fragments.

A detailed overview of the chemical analysis of the different polymers is given in the SI (Fig. S5 – 8). All characteristic signals were assigned to each tested polymers (recycled PET, PA 66, PLA, and PS) for the IR measurements. However, IR spectra of recycled PET showed many smaller additional peaks that could not be identified in common IR libraries. Therefore, TGA measurements were performed to measure the degree of inorganic contamination. In all polymer samples, no mass was left at temperatures above 800 °C. Therefore, we assume that no inorganic impurities were present. GC-MS measurements revealed that the recycled PET fragments contained anthranilonitrile, anthranilamide and butylated hydroxytoluene (BHT). Likewise, residual monomers (PS: styrene; PLA: dilactide) and piperazine in PA 66 were identified in the other polymers.

Similar observations were made in the ^{1}H liquid-state NMR spectra of recycled PET, PA 66, PLA, and PS obtained at an external magnetic field of 7.0 T. While all resonances could be assigned for PA 66, PLA and PS, recycled PET exhibits weak additional signals (for more details, see Fig. S6). Their assignment required a higher resolution. The corresponding high-resolution ^{1}H and ^{13}C liquid-state NMR spectra, obtained at an external magnetic field of 16.4 T, revealed, chain defects (5.5 %) that result from side reactions of ethylene glycol (EG) to diethylene
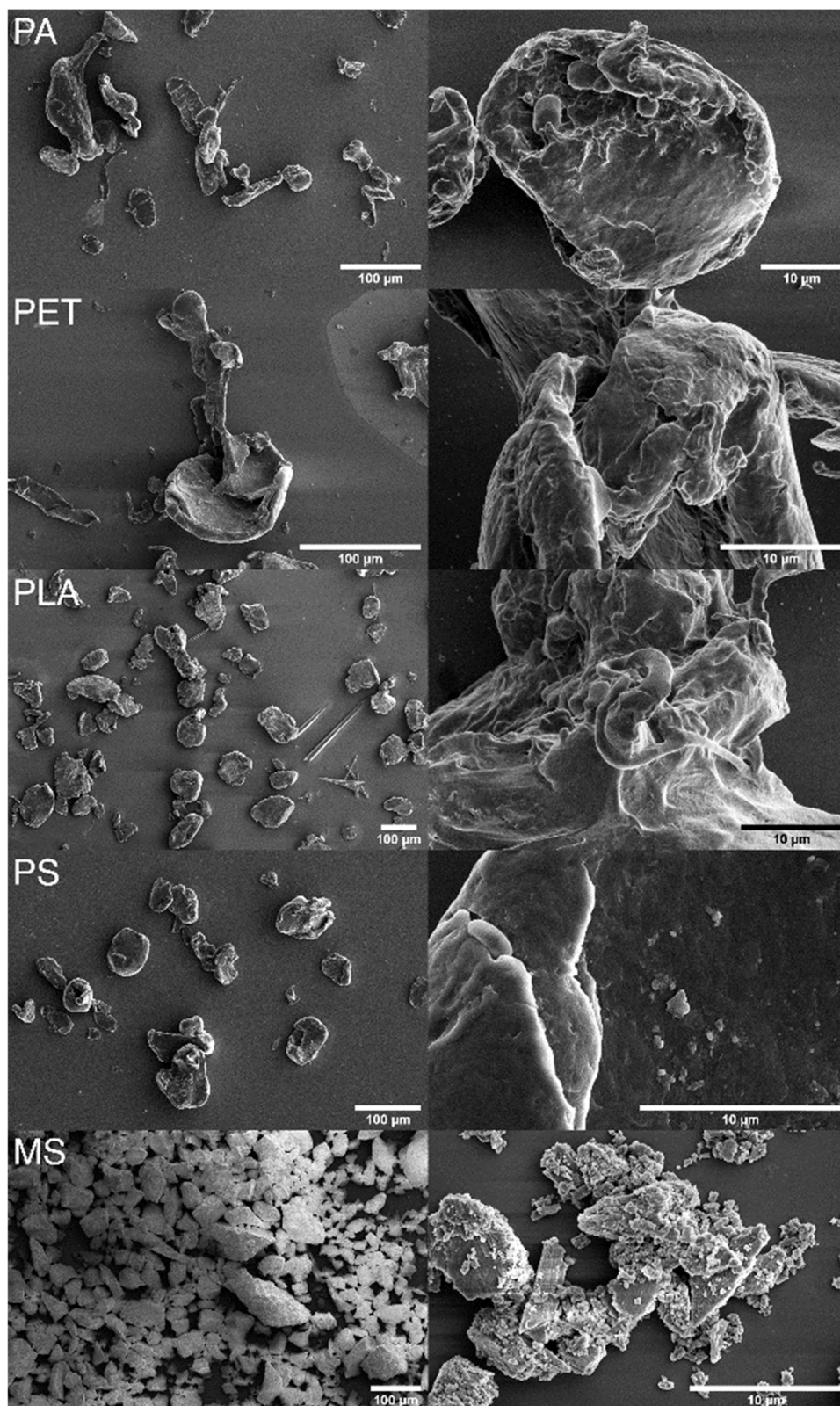
Fig. 4. SEM micrographs of the different used particles in this experiment; on the left: overview pictures; on the right: close ups; PA: polyamide 66; PET: recycled polyethylene terephthalate; PLA: polylactic acid; PS: polystyrene; MS: mussel shell fragments.

glycol (DEG) during the polymerization of PET (Fig. S7 signals c and d). Furthermore, signal groups that match additives like anthranilamide (~ 0.001 %), and modifiers like phenylene-bis-oxazoline (PBO) and iso-phthalic acid (IPA) (~ 1.5 %) were detected (Fig. S7 signals 1, 2 and 3;

for a detailed description, see SI).

3.1.1. LDV measurements – Suspension of particles in the water column
 Friction velocity was calculated from the fit to the logarithmic

7

154

boundary profile and ranged between 11 and 14 $\times 10^{-3}$ m s^{-1}. The eddy correlation method yielded similar values between 9 and 16 $\times 10^{-3}$ m s^{-1}. Friction velocities exceeded the critical threshold of the mussel fragments (9 $\times 10^{-3}$ m s^{-1}) and the PS particles (3 $\times 10^{-3}$ m s^{-1}), leading to erosion of the particles. Since settling velocities were one order of magnitude lower, all particles were transported in suspension in the flow above the ceramic tile at all measurement locations (Zanke, 2012). Additionally, the flow was highly turbulent and characterized by rapid fluctuations of velocity magnitude and direction. For more details regarding the profile of velocity measurements and fluctuations, see SI Fig. S10.

3.2. Ingestion of MP

After 24 h of exposure to Rhodamine B labelled PS, MP was found to be concentrated in the digestive tract of the mussels (Fig. 5 & Fig. S2). Fluorescent signals are clearly visible, showing that the mussels ingested the PS particles.

3.3. Behavioral endpoints

We observed no mortality of bivalves in control and exposure aquaria during the 18 days ongoing measurements (9 days exposure to the MP fragments and shell fragments), which indicates that fragments in this concentration did not induce lethality in the mussels during the exposure period. The output of the Hall sensors was analyzed for the behavioral endpoints filtration activity and transition frequency (n = 3 ×5 animals/ Treatment). ΔFiltration activities (filtration activity in the period with fragments – filtration activity in the period without fragments) did not show any differences between the treatments (One-way ANOVA, $F_{5,84} = 0.81$, p = 0.55). Further, no differences between the two periods (with or without fragments) were detected (SLiM, adjusted $R^2 = 0.005$, p = 0.18) (Fig. 6). Mean filtration activities in the period without fragments ranged from 83.06 ± 10.02 % (PS treatment) to 87.38 ± 3.59 % (recycled PET treatment) and from 83.29 ± 5,71 % (PA 66 treatment) to 86.27 ± 4,03 % (PLA treatment) in the period with fragments.

Like for the filtration activity, also in the Δtransition frequencies (transition frequencies in the period with fragments – transition
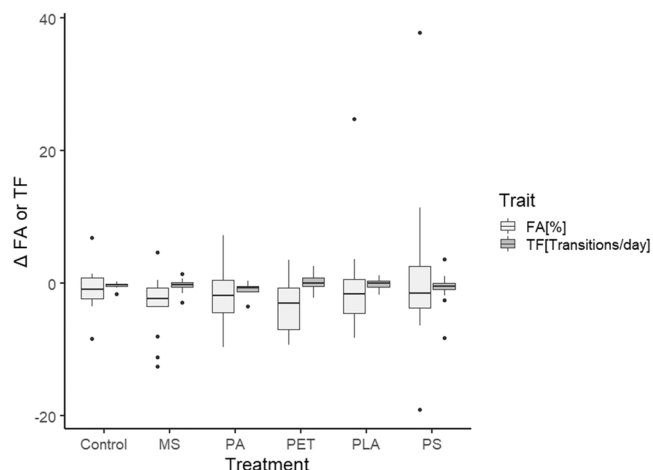
Fig. 6. Boxplot of the behavior of *D. bugensis* expressed as Δfiltration activity (ΔFA) [%] and Δtransition frequency (ΔTF) [transitions/day] (time period with fragments – time period without fragments) after 9 days exposure to 1000 p ml^{-1} of mussel shell fragments (MS), PA 66, PET, PLA, and PS fragments. No significant differences were detected (ΔFA: One-way ANOVA, $F_{5,84} = 0.81$, p = 0.55; FA pretreatment vs. FA treatment: SLiM, adjusted $R^2 = 0.005$, p = 0.18; ΔTF: One-way ANOVA, $F_{5,84} = 1.32$, p = 0.26; TF pretreatment vs. TF treatment: SLiM, adjusted $R^2 = 0.007$, p = 0.13) (n = 3 ×5 animals / Treatment).

frequencies in the period without fragments) no significant differences between the different treatments (One-way ANOVA, $F_{5,84} = 1.32$, p = 0.26) and no difference between the two periods (with or without fragments) were detected (SLiM, adjusted $R^2 = 0.007$, p = 0.13) (Fig. 6). Mean transition frequencies in the period without fragments ranged from 2.66 ± 0.89 transitions/day (control) to 4.65 ± 3.03 transitions/ day (PS treatment) and from 2.35 ± 0.76 transitions/day (control) to 3.91 ± 1.98 transitions/day (PS treatment) in the period with fragments (Fig. 6).
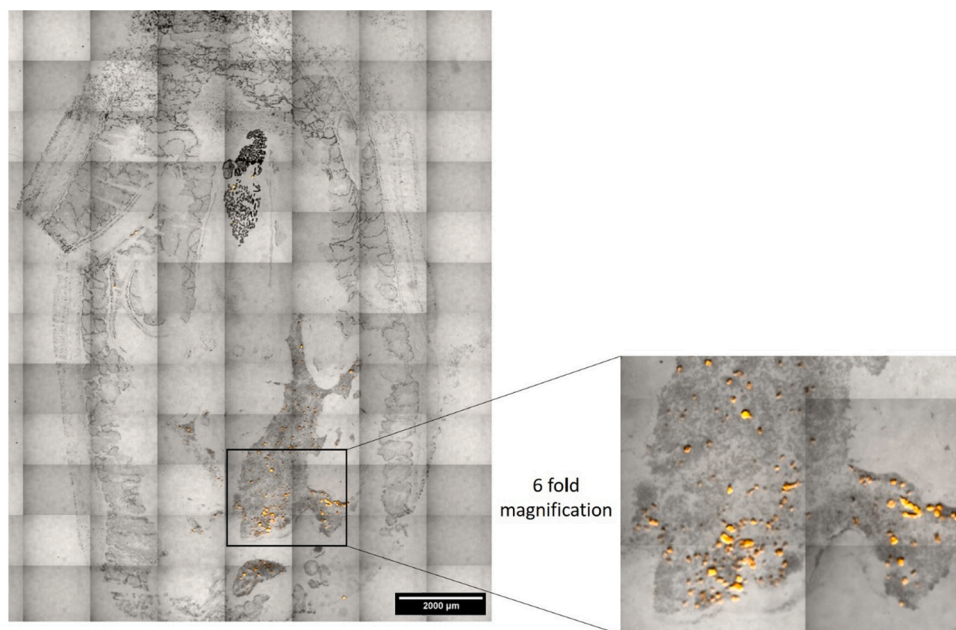
Fig. 5. Stitched tile scan and overlay of brightfield and fluorescent channel; The image shows a cryo-section (20 μm thickness) of *D. bugensis* after ingestion of Rhodamine B labeled PS-MP (orange fluorescence) using a five x objective .

8

7 Publications and manuscripts

3.4. Biochemical alterations

CAT activity showed significant differences between the treatments (One-way ANOVA, $F_{5,48} = 21.64$, $p < 0.001$, Fig. 7A; (n = 3 / Treatment)). The lowest CAT activities were found in the tissues of control mussels and mussels exposed to shell fragments. Between these treatments, no significant differences were observed (Tukey HSD, $p = 0.20$). Mussels exposed to the three petroleum-based MP, recycled PET, PA 66, and PS, showed the highest CAT activity in their tissues, with no differences between them. However, significant differences in CAT activity were observed between the PLA exposed- and the control animals (Tukey HSD, $p < 0.001$) as well as to the animals exposed to mussel shell fragments (Tukey HSD, $p < 0.001$). Mussels exposed to the bio-based PLA showed the broadest range of CAT activity in their tissue, with differences to the control animals (Tukey HSD, $p < 0.001$), PA 66 (Tukey HSD, $p = 0.01$) and PS (Tukey HSD, $p = 0.03$).

GPx activity was the lowest in the tissues of mussels treated with mussel shell fragments, followed by the control animals, and then with a slightly higher activity by the mussels of all MP treatments (Fig. 7B). GPx activity was the highest in tissues of animals exposed to recycled PET. Statistical analysis revealed differences between the treatments (One-way ANOVA, $F_{5,48} = 21.64$, $p < 0.001$), but only for the comparison of PET-treated mussels against mussels exposed to mussel shell fragments, a significant difference was observed (Tukey HSD, $p = 0.048$).

No significant differences were detected for the GST activity (One-way ANOVA, $F_{5,30} = 2.47$, $p = 0.054$, Fig. 7C). The lowest GST activities were again found in tissues of the control animals and mussel tissues exposed to mussel shell fragments. However, all mussel tissues exposed to MP (recycled PET, PA 66, PLA, PS) showed a slightly higher GST activity than tissues exposed to mussel shell fragments and control tissues.

As for GST activity, no significant differences were detectable in SOD activity (One-way ANOVA, $F_{5,12} = 2.08$, $p = 0.138$, Fig. 7D). Here, of the MP treatments, recycled PET and PS caused the highest SOD activity, and the activity of the PA 66-exposed mussels lay in between the upper two and lower three treatments. The PLA exposed mussels showed the lowest activity, followed by the mussel shell fragments exposed and control mussels.

3.5. Proteomic analysis

Using a label-free LC-MS/MS approach, we identified 34,099 peptides that could be assigned to 5502 non-redundant entries of the reference transcriptome database (FDR < 1 %). The entire list of identified proteins can be found in Suppl. Table, sheet S1.

For all comparisons, a Student's t-test led to the detection of proteins which were differently abundant as a trend (p-value < 0.01, log2-fold change < −0.6 and > 0.6). A graphical overview and heatmaps of the corresponding protein intensities are given in Fig. 8. The entire list can be found in Suppl. Table 1, sheets S2 – S10.

However, applying a more stringent Volcano plot analysis including stringent correction for multiple testing and FDR estimation, exclusively the PET treated group displayed significant changes (FDR < 0.05) compared to control and shell fragment treated animals. Furthermore, for recycled PET versus control, we identified 14 differentially abundant proteins (6 in the less abundant group, 8 in the more abundant group, Fig. 9A).

Differentially abundant protein hits were then mapped to the reference transcriptome (Péden et al., 2019), including annotations. The results are summarized in Table 2. Here, protein hits that may be linked to stress responses, like the spermine oxidase (SMOX) -like protein, were found to be increased (Rider et al., 2007).

For recycled PET versus mussel shell fragments, 3 proteins, one of them possibly linked to stress response (glucose-6-phosphate 1-dehydrogenase (G6PD) -like protein) (Venkataraman et al., 2019), were more
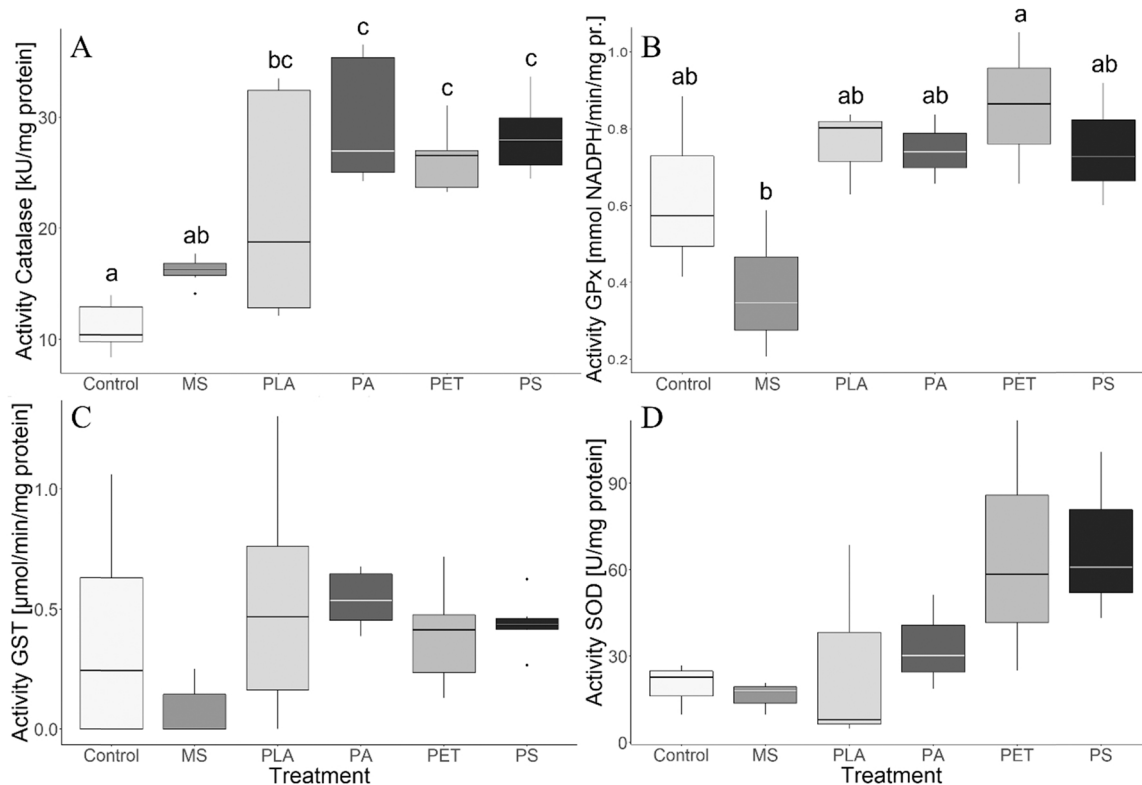
Fig. 7. Activity of the antioxidant enzymes CAT (A), GPx (B), GST (C) and, SOD (D) in whole soft tissue of *D. bugensis* after nine days exposure to mussel shell fragments (MS), recycled PET, PA 66, PLA, and PS fragments. Differing letters (a, b, c) indicate $p \leq 0.05$ (Tukey HSD) (n = 3 / treatment).

9
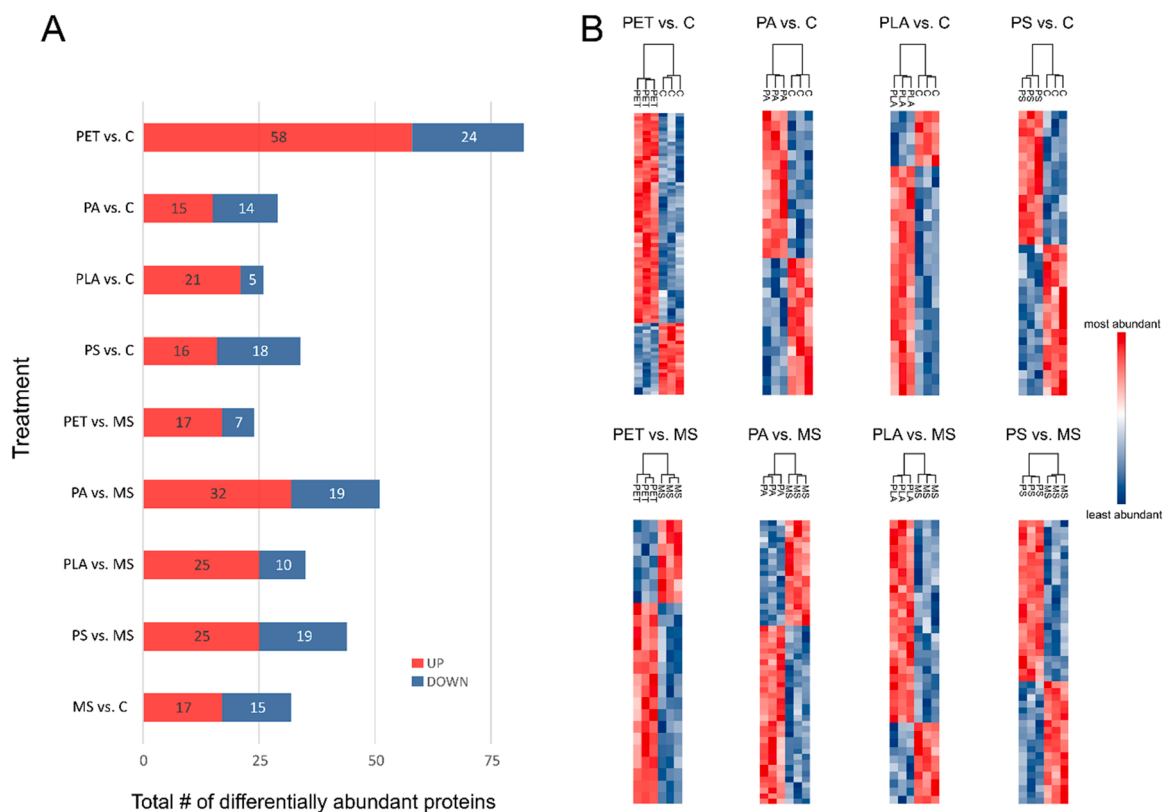
Fig. 8. (A) Overview of differentially abundant proteins for each pairwise comparison (p-value < 0.01; log2-fold change < −0.6 and > 0.6). (B) Hierarchical clustering of normalized intensity values for the corresponding proteins; MS: Mussel shell fragments.
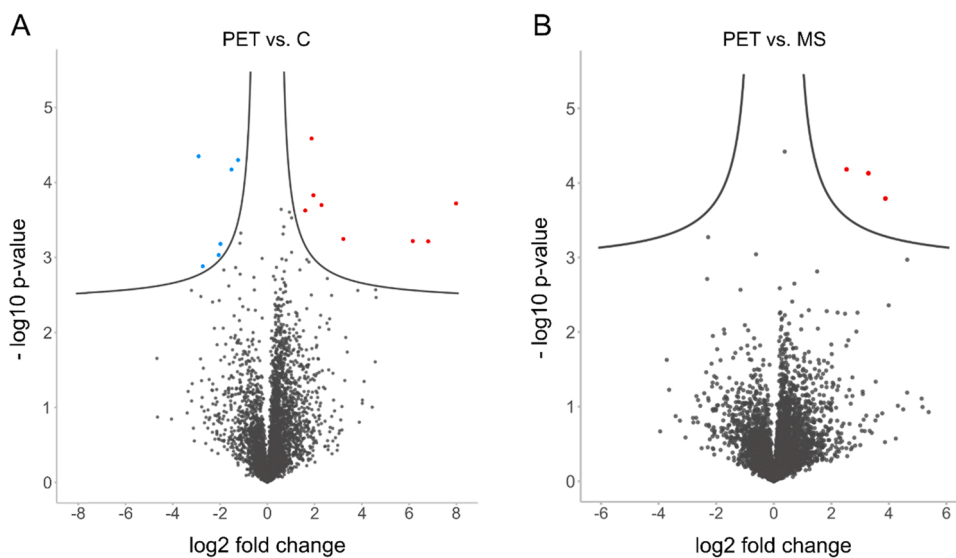
Fig. 9. Volcano plots displaying differentially abundant proteins for the recycled PET treatment (t-test, FDR < 0.05, s0 = 0.1). Proteins less abundant in PET treated animals are marked in blue, more abundant proteins are marked in red. Dark grey proteins are not significantly altered in abundance. (A) PET versus control. (B) PET versus mussel shell fragments (MS).

abundant in the PET treated group (Fig. 9B and Table 3). However, no significant change in the abundance of proteins could be identified for all other pairwise comparisons between treatment and controls.

4. Discussion

4.1. MP properties

The shape and size measurements of the different MP particles via LD/DIA and SEM revealed that they are in a comparable size range (Table 1, Fig. 4 & Fig. S4) and have a similar shape (see mean sphericity Table 1). Furthermore, the recorded surface characteristics of the

Table 2

Differentially abundant proteins in recycled PET vs Control, including their annotation according to Péden et al. (2019). Negative log2-fold changes (LFC) indicate decreased protein abundance in the treated group.

Sequence ID	LFC	p value	Description	Name	Species	
Db_BRAFLDRAFT_56798.2.2	-2.9	0.00004	Uncharacterized protein	XP_002611720	*Branchiostoma floridae*	
Db_LOTGIDRAFT_194221	-2.7	0.00132	Fibrillar collagen NC1 domain-containing protein	XP_009061654	*Lottia gigantea*	
Db_LOC105312657	-2.1	0.00094	PREDICTED: putative GPI-anchored protein PB15E9.01c	XP_011403772	*Amphimedon queenslandica*	
Db_LOC106169915.1.2	-2.0	0.00066	PREDICTED: UPF0587 protein v1g245604-like	XP_013405038	*Lingula anatina*	**decreased**
Db_LOC105318664.6.7	-1.5	0.00007	PREDICTED: fatty acid-binding protein,adipocyte-like	XP_011414186	*Crassostrea gigas*	
Db_LOC105318664.4.7	-1.2	0.00005	PREDICTED: fatty acid-binding protein, adipocyte-like	XP_011414186	*Crassostrea gigas*	
Db_LOC101937497	1.6	0.00024	PREDICTED: protein SCO1 homolog, mitochondrial isoform X1	XP_005305170	*Chrysemys picta bellii*	
Db_LOC105339316.1.2	1.9	0.00003	PREDICTED: spermine oxidase-like	XP_011443107	*Crassostrea gigas*	
Db_LOC101861859	2.0	0.00015	PREDICTED: stromal cell-derived factor 2-like	XP_005111764	*Aplysia californica*	
Db_LOTGIDRAFT_224648.1.2	2.3	0.00020	hypothetical protein LOTGIDRAFT_224648	XP_009046187	*Lottia gigantea*	**increased**
Db_LOC105347340.2.2	3.2	0.00057	PREDICTED: lysosomal alpha-mannosidase isoform X1	XP_011454672	*Crassostrea gigas*	
Db_LOTGIDRAFT_218124.1.9	6.2	0.00061	hypothetical protein LOTGIDRAFT_218124	XP_009059163	*Lottia gigantea*	
Db_LOTGIDRAFT_218124.7.9	6.8	0.00061	hypothetical protein LOTGIDRAFT_218124	XP_009059163	*Lottia gigantea*	
Db_contig_00118	8.0	0.00019	#NV	#NV	#NV	

Table 3

Differentially abundant proteins in PET vs mussel shells, including their annotation according to Péden et al. (2019). Positive log2-fold changes (LFC) indicate increased protein abundance in the treated group.

Sequence ID	LFC	p value	Description	Name	Species	
Db_LOTGIDRAFT_224648.1.2	2.5	0.00007	hypothetical protein LOTGIDRAFT_224648	XP_009046187	*Lottia gigantea*	
Db_LOC101849615.2.4	3.3	0.00007	PREDICTED: glucose-6-phosphate 1-dehydrogenase-like	XP_005097862	*Aplysia californica*	**increased**
Db_LOC105328600.1.4	3.9	0.00016	PREDICTED: enoyl-CoA delta isomerase 2, mitochondrial-like isoform X2	XP_011427847	*Crassostrea gigas*	

different particles are quite similar (Fig. 4), indicating that these aspects only play a minor role for the differing effects we observed in the mussel experiments. This also seems true for the density, as the circulatory-flow setup has kept all particles in the water column (see LDA).

Different analytical methods to analyze the chemical composition of the polymers revealed that MP contain traces of chemicals other than the polymerized plastic. In PA 66 and PLA fragments, the lowest number of additional substances was detected compared to the other polymers. In the PLA samples, thermo-desorption GC-MS measurements revealed a predominant, broad lactide signal, which can be assigned to residual monomers (Inkinen et al., 2011). In the PA 66 particles, piperazine was found, which can be incorporated into polyamides to lower the glass transition temperature and crystallinity (Chen et al., 2002). In the PS fragments, slightly more additional substances were detected than in PA 66 and PLA. Here, for example, styrene was identified, indicating the presence of residual monomers, which can leach into the surrounding medium (Pilevar et al., 2019).

In contrast, the recycled PET fragments contained the most additional chemicals of all characterized polymers. Most prominently, anthranilamide, anthranilonitrile, and BHT were identified. BHT is a synthetic phenolic antioxidant used in food preservation (Wang et al., 2021) and as a thermostabilizer in plastic production (Bach et al., 2012; Sheftel, 2000), while anthranilates are used as scavengers to prevent acetaldehyde leaching from the PET into the beverage (Bach et al., 2012). Observed chain defects caused by DEGs, modifiers like PBO (chain extender) (Scheirs, 2005) and IPA lower the melting temperature and the glass transition temperature (Patkar and Jabarin, 1993; Berg et al., 2019; ILSI Europe Report Series Packaging Materials, 2000). All these properties allow easier thermal and physical degradation, which may accelerate the formation of secondary MP (Galloway et al., 2017) in the environment due to hydrolytic and photolytic degradation (Duvall, 1995). Since the PET we tested came from PET bottles which are used on a massive scale (Plastics Europe, 2021; Kang et al., 2017) and the recyclate is used in a variety of other products like textile fibres or foils (gvm Gesellschaft für Verpackungsmarktforschung, 2020), we assume that millions of tons of PET MP may end up in the environment. Together with the increased bioavailability of residual monomers and additional chemicals due to the increased surface area to volume ratio

evoked by the accelerated fragmentation, MP derived from these materials may be especially hazardous for biota, as some of these compounds are classified as toxic for aquatic organisms (Cope et al., 1997; Netzeva et al., 2005; Cushman et al., 1997).

4.2. Mussels are not able to distinguish between natural and artificial particulate matter

We did not observe any behavioral changes of the mussels after adding additional particulate matter (neither for MP nor for the control particles) (Fig. 6). This is surprising, as mussels have been shown to change their behavior upon exposure to dissolved pollutants like ionic liquids (Costello et al., 2009) and (heavy) metals (Kraak et al., 1994; Vijayavel et al., 2007). Explanations of why mussels did not change their behavior as a reaction to the increased MP-particle load in the media maybe linked to their feeding behavior and natural habitat. As mussels are benthic filter feeders, they are regularly exposed to particulate matter like sand or silt in their natural environment. The mussels used in our experiments originated from the Regnitz River, which hosts Keuper and Jurassic rocks in its catchment area, thus having a consistent sandy and calcareous load (Dotterweich et al., 2003). Therefore, as Weber et al. proposed, there may have been an evolutionary adaption of these mussels to high turbidity and suspended solids (Weber et al., 2020). Hence, our findings indicate that the mussels cannot differentiate between natural particles and artificial particulate contaminants, even in high concentrations, and therefore do not change their behavior when getting in contact with them. Since they do not activate their defensive behavior, they ingest particulate contaminants regardless of their chemical composition, as shown in Fig. 5. This, in turn, may render contamination with particulate pollutants like MP more detrimental for mussels than contamination with dissolved pollutants. Thus, mussel feeding behavior, which is often used as an indicator for pollutants (Hartmann et al., 2016a; Borcherding and Volpers, 1994), may not be suitable for hazard assessment of MP due to its particulate nature.

4.3. Mussels are "blind" to MP, but are affected by it – depending on the polymer type

The analysis of oxidative stress biomarkers indicates adverse effects which differ between the MP exposed mussels, animals exposed to control particles and the mussels without any additional particle load (increased CAT and GPx activities) (Fig. 7A/B). No significant adverse effects were found for SOD activities (Fig. 7D), which supports the hypothesis of Magara et al., that superoxide anion production may not be the main factor of oxidative damage in mussels (Magara et al., 2018). The same accounts for the GST activity (Fig. 7C), which may also play only a minor role in MP toxicity.

CAT activity was significantly altered after exposure to petroleum-based MP (recycled PET, PA 66 and PS), which is in line with other studies (Magara et al., 2018; Magni et al., 2018; Provenza et al., 2020). Interestingly, CAT activities did not differ between control animals and mussels exposed to the natural control fragments (Fig. 7A), indicating a plastic-dependent effect. These findings emphasize the importance of using control particles to be able to differentiate if effects are polymer dependent, and/or particle dependent (Triebskorn et al., 2019). Intriguingly, our results indicate no oxidative stress for PLA, as there is no significant difference in ROS detoxifying enzyme activity compared to the natural control particles, which is somewhat contradictory to other studies with other target organisms. For example, Zimmermann et al. concluded that PLA MP is as toxic as MP derived from conventional plastics to *D. magna* (Zimmermann et al., 2020). Further, Ding et al. stated that PLA does not appear to be more biofriendly than PE when exposed to *Eisenia fetida* (Ding et al., 2021). The contradictory results could be due to different properties of the MP which may even manifest within the same polymer type (Ramsperger et al., 2021). On the other hand, comparisons between studies are made difficult, due to the use of different sizes (Schwarzer et al., 2021), different target organisms and comparisons with other polymer such as PE, PVC and PUR instead of recycled PET, PA66 and PS.

Nevertheless, our finding that PLA is less detrimental for the mussels seems reasonable when comparing the additional substances found in the different polymer samples. Here, the PLA samples only showed one type of lactides (3,6-dimethyl, 1,4-dioxane-2,5-dione; EC_{50} *Daphnia*: 130–250 mg/L (ECHA, 2022b)), which, when leaching out of the MP, appears to be less harmful from an ecotoxicological point of view (Ncube et al., 2020) than substances found in the other polymers, such as styrene found in PS (classified as aquatic chronic 3 according to European Chemicals Agency (ECHA)) or BHT found in the recycled PET (classified as aquatic chronic 1 according to ECHA)).

4.4. Polymer type dependent effects on the digestive glands' proteome

A state-of-the-art LC-high resolution MS/MS approach was applied to test if the induced stress by the various MP types further differs, depending on the chemical compounds contained in the polymer. Here, we found proteins being altered in abundance in all treatment groups. Strikingly, the most prominent and most significant alterations (FDR < 5 %, log2-fold change < −1 and > 1) were observed in the recycled PET treatment. This is in line with our findings from the biochemical assays. The higher number of proteins found in animals exposed to recycled PET vs control (Fig. 9A) may reflect that in the PET group, proteomic alterations are induced by both a general particle ingestion and the polymer type. When comparing recycled PET and ground mussel shells (Fig. 9B), the observed effects are likely to be triggered primarily by the polymer and its additives alone, as the control particles reflect the effects of general particle uptake.

One interesting protein increased in abundance in the recycled PET vs control group is the SMOX-like protein (XP_011443107, LFC = 1.9). SMOX is an enzyme that catalyzes the reaction in which spermine is oxidized to spermidine, which both belong in the group of polyamines. Polyamines are essential elements in nearly all animal and plant cells

and are required for optimal cell growth (Wallace, 2009). Also, a fundamental role of polyamines in the protection against ROS was found (Rider et al., 2007; Matkovics et al., 1993). Furthermore, Hu et al. stated that SMOX is often upregulated in chronic inflammatory conditions in humans and is also linked to increased ROS and DNA damage in various forms of cancers (Hu et al., 2018). This finding thus confirms the increased antioxidant activity described above, indicating adverse effects on mussels. Kournoutou et al. further suggested that certain polyamine compounds may play a significant role in the tolerance of mussels against cadmium (Cd^{2+}) induced stress (Kournoutou et al., 2014). However, because most studies have measured polyamines in unstressed marine bivalves, little is known about the possible effects of polyamine metabolism on stress conditions and the correlation between polyamine levels and biomarkers of oxidative stress and antioxidant defense (Kournoutou et al., 2014). We, therefore, can only assume that the elevated levels of SMOX may be linked to the oxidative stress defense experienced in the biochemical assays after exposure to the recycled PET particles.

When we compared the recycled PET treatment with the particle control, we found 3 proteins increased in abundance. Highly interesting is the G6PD (XP_005097862, LFC = 3.3). This enzyme catalyzes the first step of the oxidative pentose-phosphate pathway, which is a metabolic pathway parallel to glycolysis (Livingstone, 1981), being important in supplying NADPH for the maintenance of the redox equilibrium (GSH/GSSG level; glutathione pathway) (Ho et al., 2013; Georgakouli et al., 2019; Mehta et al., 2000). Further, G6PD is necessary for an optimal response to oxidative stress by nucleated mammalian cells, generally supporting the notion of G6PD as an antioxidant enzyme (Martini and Ursini, 1996). To our knowledge, there are no studies about the pentose-phosphate pathway in *D. bugensis*, but Flores-Nunes et al. found that a 36-h exposure to linear alkylbenzenes led to increased (G6PD) activity in *Crassostrea gigas* (Pacific oyster) digestive glands and gills tissues and stated that their results might represent an adaptive response to linear alkylbenzenes exposure to protect against an increase of for example cellular pro-oxidants (Flores-Nunes et al., 2015). In another study on the pacific oyster, Venkataraman et al. stated that increased abundance of G6PD in *C. gigas* exposed to different environmental stress factors (e.g. higher average temperatures), not only could have maintained transcription and translation processes, but also the levels of cellular and metabolic activity by indirectly dealing with ROS (Venkataraman et al., 2019). The results of the proteomic analysis indicate increased stress caused by recycled PET MP compared to other polymers, supporting the findings of Teng et al. for *C. gigas*, where the results of a weight of evidence (WOE) model analysis suggested that PET MP are more toxic to oysters than PE MP (Teng et al., 2021).

4.5. Adverse effects may be related to chemicals and residual monomers found in MP

Overall, mussels exposed to recycled PET displayed the strongest adverse effects, possibly related to the material properties and chemical compounds found. As parameters like shape, size, and density are similar to the other used particles, the adverse effects could be linked to anthranilamide, anthranilonitrile, BHT, PBO, IPA, and DEG detected via GC-MS and NMR-spectroscopy, which may leach out after being ingested by the mussels. According to toxicity data (EC_{50} *D. polymorpha* 1.3 mg/L) (Cope et al., 1997) for aquatic organisms, BHT may be the most harmful of the identified chemicals, as safety migration limits (SML) (3 mg/kg food) (Bach et al., 2012) are higher than the EC_{50} in *D. polymorpha*. The other two prominent chemicals, anthranilamide (SML: 0.05 mg/kg food) (Welle, 2016) and anthranilonitrile, also show toxicity to aquatic organisms (LC_{50} after 96 h for *Pimephales promelas* 1.59 mmol/L (~215 mg/L) (Netzeva et al., 2005)) and an LC_{50} to fish at 63.42 mg/L respectively (according to ECHA). The modifiers IPA (EC_{50} *D.magna*, >876 mg/L) (Kawamura, 2002), (SML: 5 mg/kg food) (Welle, 2016), DEG (EC_{50} *D.magna*, 10,000–78,500 mg/L) (Manfra et al., 2015)

(SML: 30 mg/kg food) (Welle, 2016) and PBO seem of little concern as they are polymerized into the chains, so the PET would have to degrade completely or be digested before the molecular components are released. Except for BHT, all SMLs are lower than the toxicity threshold. However, as soon as the plastic fragments and the surface area to volume ratio increase, it can be assumed that the additives like BHT or anthranilamide migrate to a greater extent into the surrounding medium, as well as in the digestive tract. Once the mussels ingested the MP, the chemicals we found in the MP could interact with the tissue and then lead to the observed alterations in the proteomic profile and ROS enzyme activity.

Mussels exposed to PA 66 and PS also displayed adverse effects, which may be related to the chemicals and residual monomers found in the MP. For example, styrene (SML under evaluation) (Anon, 2005) was found in PS, which has been shown to cause lysosomal membrane destabilization and DNA strand breaks in mussels (*Mytilus edulis*) (Mamaca et al., 2005) (EC_{50} *D. magna* 4.7 mg/L) (Cushman et al., 1997). Further, piperazine (no SML) found in PA 66 has been shown to cause moderate acute toxicity in *Daphnia* (EC_{50} *D. magna* 105.4 mg/L) (Sigma Aldrich GmbH, 2021).

5. Conclusion

Our results confirm the ingestion of MP by *D. bugensis* after only 24 h of exposure. However, mussels did not change their behavior to avoid or minimize the uptake of MP. On the molecular level, we then found polymer type dependent effects on the mussels (e.g., alterations in ROS detoxifying enzymes), which may be linked to physicochemical properties of the polymers, mainly the chemicals they contain. This could explain the increased toxicity of recycled PET compared to the other polymers, as most harmful chemicals were found in these particles. The chemicals we detected in PET were initially added to PET to improve the physicochemical properties for packaging purposes (Cherif Lahimer et al., 2017). During intended use, these substances are bound, and therefore migration values are well below safety limits (Satish et al., 2012). However, these chemicals may accelerate fragmentation into MP once the PET packaging is carelessly disposed of in the environment. When fragmented to MP, our results show that *D. bugensis* does not sense and react to the presence of MP in the water column. In this way, the particles enter the organism unhindered, which leads to stress responses, indicating sublethal adverse effects of MP exposure. Hence, a useful plastic item, such as a PET plastic bottle, can become a vector for hazardous substances if it enters and fragments in the environment. This could be even more critical when put in an ecological context. With ever increasing MP numbers the animals may be exposed to higher stress levels. Higher stress levels make organisms more susceptible to environmental changes (Greenberg et al., 2002), diseases (Hoffmann and Hercus, 2000) or parasites (Okamura and Feist, 2011). Hence, even sublethal adverse effects as shown here may gradually manifest at the population level and lead to unnoticed irreversible ecosystem changes.

CRediT authorship contribution statement

J.B. and C.L. designed the research study. J.B., L.R., S.R. performed behavior, ROS enzyme experiments, and sampling for proteome analysis. J.B. analyzed the data. J.B and S.R. performed the uptake experiment. L.W. and T.F. performed the proteome analysis. B.P., L.L, M.M., M. S., and S.W. performed physico-chemical particle characterizations and data analysis. JP.B performed the LDV experiment and data analysis. S. F, H.K., T.F., A.G., J.S. and C.L. provided instruments and expert advice. All authors read and commented on the manuscript.

Declaration of Competing Interest

The authors declare that they have no known competing financial interests or personal relationships that could have appeared to influence the work reported in this paper.

Data Availability

The mass spectrometry proteomics data have been deposited to the ProteomeXchange Consortium (http://proteomecentral.proteomexchange. org) via the PRIDE partner repository (R Core Team, 2021) with the dataset identifier PXD030056. Raw data of the real-time valvometry experiment and LDV measurements have been deposited to the opensource repository Zenodo (doi: 10.5281/zenodo.6598998).

Environmental Implication

MP are a major threat to ecosystems worldwide, resulting in a great need to investigate their impacts on ecosystems. To date it is difficult to determine, which physico-chemical properties govern the toxictiy of MP on organisms. In our study we exposed *Dreissena bugensis* to in-depth characterized MP particles (recycled PET, PA 66, PLA and PS) and natural control particles to elucidate polymer-type dependent effects. Thereby, our study contributes to a better understanding of MP hazard assessment. Adverse effects appear to be dependent on specific properties of the particles (for example the chemicals they contain) and on the polymer types themselves.

Appendix A. Supporting information

Supplementary data associated with this article can be found in the online version at doi:10.1016/j.jhazmat.2022.129351.

References

An, D., Na, J., Song, J., Jung, J., 2021. Size-dependent chronic toxicity of fragmented polyethylene microplastics to Daphnia magna. Chemosphere 271, 129591. https:// doi.org/10.1016/J.CHEMOSPHERE.2021.129591.

Anderson, P.J., Warrack, S., Langen, V., Challis, J.K., Hanson, M.L., Rennie, M.D., 2017. Microplastic contamination in lake Winnipeg, Canada. Environ. Pollut. 225, 223–231.

Andrady, A.L., Neal, M.A., 2009. Applications and societal benefits of plastics. Philos. Trans. R. Soc. B Biol. Sci. 364, 1977–1984.

Anon, 2005. Paper and board materials and articles intended to come into contact with foodstuffs. Counc. Eur. Version 2–13.

Bach, C., Dauchy, X., Chagnon, M.-C., Etienne, S., 2012. Chemical compounds and toxicological assessments of drinking water stored in polyethylene terephthalate (PET) bottles: a source of controversy reviewed. Water Res 46, 571–583. https://doi. org/10.1016/j.watres.2011.11.062.

Barbachi, M., Imad, A., Jeffali, F., Boudjellal, K., Bouabaz, M., 2017. Physical characterization of sea shell for a concrete formulation. J. Mater. Environ. Sci. 8, 332–337.

Berg, D., Schaefer, K., Moeller, M., 2019. Impact of the chain extension of poly(ethylene terephthalate) with 1,3-phenylene-bis-oxazoline and N,N′-carbonylbiscaprolactam by reactive extrusion on its properties. Polym. Eng. \ Sci. 59, 284–294 https://doi.org/https://doi.org/10.1002/pen.24903.

Binelli, A., Parolini, M., Pedriali, A., Provini, A., 2011. Antioxidant activity in the zebra mussel (Dreissena polymorpha) in response to triclosan exposure. Water Air. Soil Pollut. 217, 421–430. https://doi.org/10.1007/s11270-010-0597-4.

Borcherding, J., Volpers, W., 1994. The "dreissena-monitor"–first results on the application of this biological early warning system in the continuous monitoring of water quality. Water Sci. Technol. 29, 199–201.

Bradford, M.M., 1976. A rapid and sensitive method for the quantitation of microgram quantities of protein utilizing the principle of protein-dye binding. Anal. Biochem. 72, 248–254.

Chen, X., Zhong, H., Jia, L., Ning, J., Tang, R., Qiao, J., Zhang, Z., 2002. Polyamides derived from piperazine and used for hot-melt adhesives: synthesis and properties. Int. J. Adhes. Adhes. 22, 75–79. https://doi.org/10.1016/S0143-7496(01)00039-2.

Cherif Lahimer, M., Ayed, N., Horriche, J., Belgaied, S., 2017. Characterization of plastic packaging additives: food contact, stability and toxicity. Arab. J. Chem. 10, S1938–S1954. https://doi.org/10.1016/j.arabjc.2013.07.022.

Cope, W.G., Bartsch, M.R., Marking, L.L., 1997. Efficacy of candidate chemicals for preventing attachment of zebra mussels (Dreissena polymorpha). Environ. Toxicol. Chem. Int. J. 16, 1930–1934.

Costello, D.M., Brown, L.M., Lamberti, G.A., 2009. Acute toxic effects of ionic liquids on zebra mussel (Dreissena polymorpha) survival and feeding. Green. Chem. 11, 548–555. https://doi.org/10.1039/b822347e.

Cristaldi, A., Fiore, M., Zuccarello, P., Oliveri Conti, G., Grasso, A., Nicolosi, I., Copat, C., Ferrante, M., 2020. Efficiency of wastewater treatment plants (WWTPs) for microplastic removal: a systematic review. Int. J. Environ. Res. Public Health 17, 8014.

Cushman, J.R., Rausina, G.A., Cruzan, G., Gilbert, J., Williams, E., Harrass, M.C., Sousa, J.V., Putt, A.E., Garvey, N.A., St. Laurent, J.P., Hoberg, J.R., Machado, M.W., 1997. Ecotoxicity hazard assessment of styrene. Ecotoxicol. Environ. Saf. 37, 173–180. https://doi.org/10.1006/eesa.1997.1540.

Descy, J., Everbecq, E., Gosselain, V., Viroux, L., Smitz, J.S., 2003. Modelling the impact of benthic filter-feeders on the composition and biomass of river plankton. Freshw. Biol. 48, 404–417.

Ding, W., Li, Z., Qi, R., Jones, D.L., Liu, Q., Liu, Q., Yan, C., 2021. Effect thresholds for the earthworm Eisenia fetida: toxicity comparison between conventional and biodegradable microplastics. Sci. Total Environ. 781, 146884.

Dotterweich, M., Haberstroh, J., Bork, H., 2003. Frühgeschichtliche Boden- und Reliefentwicklung am Talrand der Regnitz bei Altendorf (Oberfranken) / Prehistoric soil and relief formation at the margin of the Regnitz Valley near Altendorf (Upper Franconia). Die Erde 134, 4.

Dris, R., Imhof, H., Sanchez, W., Gasperi, J., Galgani, F., Tassin, B., Laforsch, C., 2015a. Beyond the ocean: contamination of freshwater ecosystems with (micro-)plastic particles. Environ. Chem. 12 https://doi.org/10.1071/EN14172.

Dris, R., Gasperi, J., Rocher, V., Saad, M., Renault, N., Tassin, B., 2015b. Microplastic contamination in an urban area: a case study in Greater Paris. Environ. Chem. 12, 592–599.

Duvall, D.E., 1995. Environmental degradation of PET and its potential effect on long-term mechanical properties of oriented PET products. Polym. Plast. Technol. Eng. 34, 227–242.

Earth Watch Institute, 2018. Plast. Rivers 1–20.

ECHA. Dilactide. https://echa.europa.eu/de/brief-profile/-/briefprofile/100.002.245, accessed 20 January 2022b.

ECHA Ethyl 2-cyanoacrylate, https://echa.europa.eu/de/registration-dossier/-/registered-dossier/14976/6/2/4, accessed 31 May 2022a.

Esders, E.M., Georgi, C., Babel, W., Thomas, C.K., 2022. Quantitative detection of aerial suspension of particles with a full-frame visual camera for atmospheric wind tunnel studies. Aerosol Sci. Technol. 56, 530–544. https://doi.org/10.1080/02786826.2022.2048789.

Flores-Nunes, F., Mattos, J.J., Zacchi, F.L., Serrano, M.A.S., Piazza, C.E., Sasaki, S.T., Taniguchi, S., Bicego, M.C., Melo, C.M.R., Bainy, A.C.D., 2015. Effect of linear alkylbenzene mixtures and sanitary sewage in biochemical and molecular responses in pacific oyster Crassostrea gigas. Environ. Sci. Pollut. Res. 22, 17386–17396.

Galloway, T.S., Cole, M., Lewis, C., 2017. Interactions of microplastic debris throughout the marine ecosystem. Nat. Ecol. Evol. 1, 1–8. https://doi.org/10.1038/s41559-017-0116.

Georgakouli, K., Fatouros, I.G., Draganidis, D., Papanikolaou, K., Tsimeas, P., Deli, C.K., Jamurtas, A.Z., 2019. Exercise in glucose-6-phosphate dehydrogenase deficiency: Harmful or harmless? a narrative review. Oxid. Med. Cell. Longev. 2019.

Greenberg, N., Carr, J.A., Summers, C.H., 2002. Causes and Consequences of Stress1. Integr. Comp. Biol. 42, 508–516. https://doi.org/10.1093/icb/42.3.508.

Grigorovich, I.A., Shevtsova, L.V., 1995. Effect of Dreissena mussels on the distribution of zooplankton as exemplified by the main Kakhovka Canal. Fifth Int. Zebra Musse Other Aquat. Nuis. Org. Conf. 183–193.

gvm Gesellschaft für Verpackungsmarktforschung, Aufkommen und Verwertung von PET Getränkeflaschen in Deutschland 2019 - Kurzfassung, (2020) 34.

Hadwan, M.H., 2018. Simple spectrophotometric assay for measuring catalase activity in biological tissues. BMC Biochem 19, 1–8. https://doi.org/10.1186/s12858-018-0097-5.

Hartmann, J.T., Beggel, S., Auerswald, K., Stoeckle, B.C., Geist, J., 2016a. Establishing mussel behavior as a biomarker in ecotoxicology. Aquat. Toxicol. 170, 279–288. https://doi.org/10.1016/j.aquatox.2015.06.014.

Hartmann, J.T., Beggel, S., Auerswald, K., Geist, J., 2016b. Determination of the most suitable adhesive for tagging freshwater mussels and its use in an experimental study

of filtration behaviour and biological rhythm. J. Mollusca Stud. 82, 415–421. https://doi.org/10.1093/mollus/eyw003.

Hartmann, N.B., Huffer, T., Thompson, R.C., Hassellöv, M., Verschoor, A., Daugaard, A. E., Rist, S., Karlsson, T., Brennholt, N., Cole, M., 2019. Are we speaking the same language? Recommendations for a definition and categorization framework for plastic debris. Environ. Sci. Technol. 53 (3), 1039–1047.

Ho, H.-Y., Cheng, M.-L., Shiao, M.-S., Chiu, D.T.-Y., 2013. Characterization of global metabolic responses of glucose-6-phosphate dehydrogenase-deficient hepatoma cells to diamide-induced oxidative stress. Free Radic. Biol. Med. 54, 71–84.

Hoffmann, A.A., Hercus, M.J., 2000. Environmental stress as an evolutionary force. Bioscience 50, 217–226. https://doi.org/10.1641/0006-3568(2000)050[0217:ESAAEF]2.3.CO;2.

Hu, T., Sun, D., Zhang, J., Xue, R., Janssen, H.L.A., Tang, W., Dong, L., 2018. Spermine oxidase is upregulated and promotes tumor growth in hepatocellular carcinoma. Hepatol. Res. 48, 967–977.

Huthnance, J.M., Humphery, J.D., Knight, P.J., Chatwin, P.G., Thomsen, L., White, M., 2002. Near-bed turbulence measurements, stress estimates and sediment mobility at the continental shelf edge. Prog. Oceanogr. 52, 171–194. https://doi.org/10.1016/S0079-6611(02)00005-8.

Hwang, J., Choi, D., Han, S., Jung, S.Y., Choi, J., Hong, J., 2020. Potential toxicity of polystyrene microplastic particles. Sci. Rep. 10, 1–12.

ILSI Europe Report Series Packaging Materials, Polyethylene terephthalate (PET) for food packaging applications, Brussels, (2000).

Imhof, H.K., Ivleva, N.P., Schmid, J., Niessner, R., Laforsch, C., 2013. Contamination of beach sediments of a subalpine lake with microplastic particles. Curr. Biol. 23, 867–868.

Inkinen, S., Hakkarainen, M., Albertsson, A.-C., Södergård, A., 2011. From lactic acid to poly (lactic acid)(PLA): characterization and analysis of PLA and its precursors. Biomacromolecules 12, 523–532.

Inoue, T., Glud, R.N., Stahl, H., Hume, A., 2011. Comparison of three different methods for assessing in situ friction velocity: A case study from Loch Etive, Scotland. Limnol. Oceanogr. Methods 9, 275–287. https://doi.org/10.4319/lom.2011.9.275.

Kang, D., Auras, R., Singh, J., 2017. Life cycle assessment of non-alcoholic single-serve polyethylene terephthalate beverage bottles in the state of California. Resour. Conserv. Recycl. 116, 45–52.

M.Y. Kawamura, SIDS Initial Assessment Report for 14th SIAM, 2002).

Klemchuk, P.P., 1990. Hindered amine mechanisms: PartIII- Investigations using isotopic labelling. Polym. Degrad. Stab. 27, 65–74.

Klüttgen, B., Dülmer, U., Engels, M., Ratte, H.T., 1994. ADaM, an artificial freshwater for the culture of zooplankton. Water Res 28, 743–746.

Kournoutou, G.G., Pytharopoulou, S., Leotsinidis, M., Kalpaxis, D.L., 2014. Changes of polyamine pattern in digestive glands of mussel Mytilus galloprovincialis under exposure to cadmium. Comp. Biochem. Physiol. Part C. Toxicol. Pharmacol. 165, 1–8.

Kovats, E., 1958. Gas chromatographic characterization of organic compounds. I. Retention indexes of aliphatic halides, alcohols, aldehydes, and ketones. Helv. Chim. Acta 41, 1915–1932.

Kraak, M.H.S., Toussaint, M., Lavy, D., Davids, C., 1994. Short-term effects of metals on the filtration rate of the zebra mussel Dreissena polymorpha. Environ. Pollut. 84, 139–143.

Li, C., Busquets, R., Campos, L.C., 2020. Assessment of microplastics in freshwater systems: a review. Sci. Total Environ. https://doi.org/10.1016/j.scitotenv.2019.135578.

Li, J., Liu, H., Chen, J.P., 2018. Microplastics in freshwater systems: A review on occurrence, environmental effects, and methods for microplastics detection. Water Res. 137, 362–374.

Livingstone, D.R., 1981. Induction of enzymes as a mechanism for the seasonal control of metabolism in marine invertebrates: glucose-6-phosphate dehydrogenases from the mantle and hepatopancreas of the common mussel Mytilus edulis L. Comp. Biochem. Physiol. Part B Comp. Biochem. 69, 147–156.

Magara, G., Elia, A.C., Syberg, K., Khan, F.R., 2018. Single contaminant and combined exposures of polyethylene microplastics and fluoranthene: accumulation and oxidative stress response in the blue mussel, Mytilus edulis. J. Toxicol. Environ. Heal. Part A. 81, 761–773.

Magni, S., Gagné, F., André, C., Della Torre, C., Auclair, J., Hanana, H., Parenti, C.C., Bonasoro, F., Binelli, A., 2018. Evaluation of uptake and chronic toxicity of virgin polystyrene microbeads in freshwater zebra mussel Dreissena polymorpha (Mollusca: Bivalvia). Sci. Total Environ. 631–632, 778–788. https://doi.org/10.1016/j.scitotenv.2018.03.075.

Magni, S., Della Torre, C., Garrone, G., D'Amato, A., Parenti, C.C., Binelli, A., 2019. First evidence of protein modulation by polystyrene microplastics in a freshwater biological model. Environ. Pollut. 250, 407–415. https://doi.org/10.1016/j.envpol.2019.04.088.

Mamaca, E., Bechmann, R.K., Torgrimsen, S., Aas, E., Bjørnstad, A., Baussant, T., Le, S., 2005. Floch, The neutral red lysosomal retention assay and Comet assay on haemolymph cells from mussels (Mytilus edulis) and fish (Symphodus melops) exposed to styrene. Aquat. Toxicol. 75, 191–201.

Manfra, L., Tornambè, A., Savorelli, F., Rotini, A., Canepa, S., Mannozzi, M., Cicero, A. M., 2015. Ecotoxicity of diethylene glycol and risk assessment for marine environment. J. Hazard. Mater. 284, 130–135.

Martini, G., Ursini, M.V., 1996. A new lease of life for an old enzyme. Bioessays 18, 631–637.

Matkovics, B., Kecskemeti, V., Varga, S.I., Novak, Z., Kertesz, Z., 1993. Antioxidant properties of di-and polyamines. Comp. Biochem. Physiol. B 104, 475–479.

McCord, J.M., 1999. Analysis of superoxide dismutase activity. Curr. Protoc. Toxicol. 00, 7.3.1–7.3.9. https://doi.org/10.1002/0471140856.tx0703s00.

7 Publications and manuscripts

Mehta, A., Mason, P.J., Vulliamy, T.J., 2000. Glucose-6-phosphate dehydrogenase deficiency. Best. Pract. Res. Clin. Haematol. 13, 21–38.

Moore, C.J., 2008. Synthetic polymers in the marine environment: a rapidly increasing, long-term threat. Environ. Res. 108, 131–139.

Ncube, L.K., Ude, A.U., Ogunmuyiwa, E.N., Zulkifli, R., Beas, I.N., 2020. Environmental impact of food packaging materials: a review of contemporary development from conventional plastics to polylactic acid based materials. Materials 13, 4994. https://doi.org/10.3390/ma13214994.

Netzeva, T.I., Worth, A.P., Aldenberg, T., Benigni, R., Cronin, M.T.D., Gramatica, P., Jaworska, J.S., Kahn, S., Klopman, G., Marchant, C.A., 2005. Current status of methods for defining the applicability domain of (quantitative) structure-activity relationships: The report and recommendations of ecvam workshop 52. Altern. Lab. Anim. 33, 155–173.

Ogonowski, M., Schür, C., Jarsén, Å., Gorokhova, E., 2016. The effects of natural and anthropogenic microparticles on individual fitness in Daphnia magna. PLoS One 11, 1–20. https://doi.org/10.1371/journal.pone.0155063.

Ogonowski, M., Gerdes, Z., Gorokhova, E., 2018. What we know and what we think we know about microplastic effects – a critical perspective. Curr. Opin. Environ. Sci. Heal 1, 41–46. https://doi.org/10.1016/j.coesh.2017.09.001.

Okamura, A., Feist, S.W., 2011. Emerging diseases in freshwater systems. Freshw. Biol. 56, 627–637.

Patkar, M., Jabarin, S.A., 1993. Effect of diethylene glycol (DEG) on the crystallization behavior of poly(ethylene terephthalate) (PET). J. Appl. Polym. Sci. 47, 1749–1763. https://doi.org/10.1002/app.1993.070471005.

Péden, R., Poupin, P., Sohm, B., Flayac, J., Giambérini, L., Klopp, C., Louis, F., Pain-Devin, S., Potet, M., Serre, R.-F., 2019. Environmental transcriptomes of invasive dreissena, a model species in ecotoxicology and invasion biology. Sci. Data. 6, 1–8.

Perez-Riverol, Y., Csordas, A., Bai, J., Bernal-Llinares, M., Hewapathirana, S., Kundu, D. J., Inganti, A., Griss, J., Mayer, G., Eisenacher, M., 2019. The PRIDE database and related tools and resources in 2019: improving support for quantification data. Nucleic Acids Res 47, D442–D450.

Pilevar, Z., Bahrami, A., Beikzadeh, S., Hosseini, H., Jafari, S.M., 2019. Migration of styrene monomer from polystyrene packaging materials into foods: characterization and safety evaluation. Trends Food Sci. Technol. 91, 248–261. https://doi.org/10.1016/j.tifs.2019.07.020.

Plastics Europe, Plastics – the Facts 2021, (2021).

Preibisch, S., Saalfeld, S., Tomancak, P., 2009. Globally optimal stitching of tiled 3D microscopic image acquisitions. Bioinformatics 25, 1463–1465.

Provenza, F., Piccardo, M., Terlizzi, A., Renzi, M., 2020. Exposure to pet-made microplastics: particle size and pH effects on biomolecular responses in mussels. Mar. Pollut. Bull. 156, 111228.

R Core Team, 2021. R: A Language and Environment for Statistical Computing. R Foundation for Statistical Computing, Vienna, Austria.

Ramsperger, A., Jasinski, J., Völkl, M., Witzmann, T., Meinhart, M., Jérôme, V., Kretschmer, W.P., Freitag, R., Senker, J., Fery, A., Kress, H., Scheibel, T., Laforsch, C., 2021. Supposedly identical microplastic particles substantially differ in their material properties influencing particle-cell interactions and cellular responses. J. Hazard. Mater., 127961

Renzi, M., Grazioli, E., Blašković, A., 2019. Effects of different microplastic types and surfactant-microplastic mixtures under fasting and feeding conditions: a case study on Daphnia magna. Bull. Environ. Contam. Toxicol. 103, 367–373. https://doi.org/10.1007/s00128-019-02678-y.

Revenga, C., Campbell, I., Abell, R., De Villiers, P., Bryer, M., 2005. Prospects for monitoring freshwater ecosystems towards the 2010 targets. Philos. Trans. R. Soc. B Biol. Sci. 360, 397–413. https://doi.org/10.1098/rstb.2004.1595.

Rider, J.E., Hacker, A., Mackintosh, C.A., Pegg, A.E., Woster, P.M., Casero, R.A., 2007. Spermine and spermidine mediate protection against oxidative damage caused by hydrogen peroxide. Amino Acids 33, 231–240.

Rozman, U., Kalčíková, G., 2022. Seeking for a perfect (non-spherical) microplastic particle – the most comprehensive review on microplastic laboratory research. J. Hazard. Mater. 424, 127529 https://doi.org/10.1016/j.jhazmat.2021.127529.

Ryan, P.G., 2020. Land or sea? What bottles tell us about the origins of beach litter in Kenya. Waste Manag 116, 49–57. https://doi.org/10.1016/j.wasman.2020.07.044.

Ryan, P.G., Dilley, B.J., Ronconi, R.A., Connan, M., 2019. Rapid increase in Asian bottles in the South Atlantic Ocean indicates major debris inputs from ships. Proc. Natl. Acad. Sci. 116, 20892–20897.

Satish, A., Naveena, M.S., Girish, T.K., Leela Bai, S., 2012. Suitability of pet bottles for food contact applications. Indian Food Pack. 97–103.

Scheirs, J., 2005. Additives for the modification of poly(ethylene terephthalate) to produce engineering-grade polymers. In: Long, T.E., Scheirs, J. (Eds.), Mod. Polyesters Chem. Technol. Polyesters Copolyesters. John Wiley & Sons, Hoboken, New Jersey, pp. 495–540.

Schür, C., Zipp, S., Thalau, T., Wagner, M., 2020. Microplastics but not natural particles induce multigenerational effects in Daphnia magna. Environ. Pollut. 260, 113904 https://doi.org/10.1016/j.envpol.2019.113904.

Schür, C., Weil, C., Baum, M., Wallraff, J., Schreier, M., Oehlmann, J., Wagner, M., 2021. Incubation in wastewater reduces the multigenerational effects of microplastics in Daphnia magna. Environ. Sci. Technol. 55, 2491–2499. https://doi.org/10.1021/acs.est.0c07911.

Schwarzer, M., Brehm, J., Vollmer, M., Jasinski, J., Xu, C., Zainuddin, S., Fröhlich, T., Schott, M., Greiner, A., Scheibel, T., Laforsch, C., 2021. Shape, size, and polymer dependent effects of microplastics on Daphnia magna. J. Hazard. Mater., 128136

Sedaghatfard, F., Razavi, S.A., Hedayati, M., Razmi, N., Rahnama, A., 2016. Glutathione peroxidase activity assay with colorimetric method and microplate reading format and comparison with chemiluminescence method. Eur. Online J. Nat. Soc. Sci. 5, 15.

Sheavly, S.B., Register, K.M., 2007. Marine debris & plastics: environmental concerns, sources, impacts and solutions. J. Polym. Environ. 15, 301–305. https://doi.org/10.1007/s10924-007-0074-3.

Sheftel, V.O., 2000. Indirect food additives and polymers: migration and toxicology, first ed. CRC Press,, Boca Raton.

Sigma Aldrich GmbH, SDS on Piperazine - P45907. Accessed 20 January 2022 , 2021).

Sprung, M., Rose, U., 1988. Influence of food size and food quantity on the feeding of the mussel Dreissena polymorpha. Oecologia 77, 526–532.

Teng, J., Zhao, J., Zhu, X., Shan, E., Wang, Q., 2021. Oxidative stress biomarkers, physiological responses and proteomic profiling in oyster (Crassostrea gigas) exposed to microplastics with irregular-shaped PE and PET microplastic. Sci. Total Environ., 147425

Teubner, D., Wesslein, A.K., Rønne, P.B., Veith, M., Frings, C., Paulus, M., 2016. Is a visuo-haptic differentiation of zebra mussel and quagga mussel based on a single external morphometric shell character possible? Aquat. Invasions 11, 145–154. https://doi.org/10.3391/ai.2016.11.2.04.

Triebskorn, R., Braunbeck, T., Grummt, T., Hanslik, L., Huppertsberg, S., Jekel, M., Knepper, T.P., Krais, S., Müller, Y.K., Pittroff, M., Ruhl, A.S., Schmieg, H., Schür, C., Strobel, C., Wagner, M., Zumbülte, N., Köhler, H.R., 2019. Relevance of nano- and microplastics for freshwater ecosystems: a critical review. TrAC - Trends Anal. Chem. 110, 375–392. https://doi.org/10.1016/j.trac.2018.11.023.

Trotter, B., Wilde, M.V., Brehm, J., Dafni, E., Aliu, A., Arnold, G.J., Fröhlich, T., Laforsch, C., 2021. Long-term exposure of Daphnia magna to polystyrene microplastic (PS-MP) leads to alterations of the proteome, morphology and life-history. Sci. Total Environ., 148822

Tyanova, S., Temu, T., Sinitcyn, P., Carlson, A., Hein, M.Y., Geiger, T., Mann, M., Cox, J., 2016. The Perseus computational platform for comprehensive analysis of (prote) omics data. Nat. Methods 13, 731.

Venkataraman, Y.R., Timmins-Schiffman, E., Horwith, M.J., Lowe, A.T., Nunn, B., Vadopalas, B., Spencer, L.H., Roberts, S.B., 2019. Characterization of Pacific oyster Crassostrea gigas proteomic response to natural environmental differences. Mar. Ecol. Prog. Ser. 610, 65–81.

Verschoor, A.J., 2015. Towards a Definition of Microplastics: Considerations for the Specification of Physico-Chemical Properties. National Institute for Public Health and the Environment, Netherlands.

Vijayavel, K., Gopalakrishnan, S., Balasubramanian, M.P., 2007. Sublethal effect of silver and chromium in the green mussel Perna viridis with reference to alterations in oxygen uptake, filtration rate and membrane bound ATPase system as biomarkers. Chemosphere 69, 979–986.

H.M. Wallace, The polyamines: past, present and future, Essays Biochem. 46 , 2009 1–10.

Wang, Y.-W., Li, Y.-N., Lin, Q.-B., Wang, X., Li, Z.-H., Wu, K.-X., 2021. Functional and antioxidant properties of plastic bottle caps incorporated with BHA or BHT. Mater. (Basel) 14, 4545.

Weber, A., Jeckel, N., Wagner, M., 2020. Combined effects of polystyrene microplastics and thermal stress on the freshwater mussel Dreissena polymorpha. Sci. Total Environ. 718, 137253 https://doi.org/10.1016/j.scitotenv.2020.137253.

Weber, A., Jeckel, N., Weil, C., Umbach, S., Brennholt, N., Reifferscheid, G., Wagner, M., 2021. Ingestion and toxicity of polystyrene microplastics in freshwater bivalves. Environ. Toxicol. Chem. 40, 2247–2260.

Welle, F.M., 2016. Verpackungsmaterial aus Polyethylenterephthalat (PET). DLG.

Wieland, S., Balmes, A., Bender, J., Kitzinger, J., Meyer, F., Ramsperger, A.F.R.M., Roeder, F., Tengelmann, C., Wimmer, B.H., Laforsch, C., Kress, H., 2022. From properties to toxicity: comparing microplastics to other airborne microparticles. J. Hazard. Mater., 128151

Zanke, U., 2012. Hydraulik für den Wasserbau. Springer-Verlag.

Zimmermann, L., Göttlich, S., Oehlmann, J., Wagner, M., Völker, C., 2020. What are the drivers of microplastic toxicity? comparing the toxicity of plastic chemicals and particles to Daphnia magna. Environ. Pollut. 267, 115392 https://doi.org/10.1016/j.envpol.2020.115392.

1   # Supplementary Materials for

2

3   **In-depth characterization revealed polymer type and chemical content**
4   **specific effects of microplastics on *Dreissena bugensis*.**

5

6   Julian Brehm, Magdalena V. Wilde, Lukas Reiche, Lisa-Cathrin Leitner, Benedict Petran,

7   Marcel Meinhart, Simon Wieland, Sven Ritschar, Matthias Schott, Jan-Pascal Boos, Sven

8   Frei, Holger Kress, Jürgen Senker, Andreas Greiner, Thomas Fröhlich, Christian Laforsch*

9

10   *Christian Laforsch. Email: Christian.Laforsch@uni-bayreuth.de

11
12

13   **This PDF file includes:**

14   Supplementary Materials and Methods

15   Details for NMR PET measurements

16   Figs. S1 to S10

17   Table S1

18   References

19

20   **Other Supplementary Materials for this manuscript include the following:**

21   Data S1

22

23 **Supplementary Material and Methods**

24 Particle characterization

25 SEM measurements

26 To investigate the morphology of the different particles, 10 µl of each stock suspension were

27 pipetted to pieces of silicon wafers. These were mounted on aluminum stubs (Ø 12 mm, Plano

28 GmbH, Wetzlar, Germany) using carbon conductive tabs (Ø 12 mm, Plano GmbH, Wetzlar,

29 Germany) and dried in a desiccator. The samples were then coated with a 4 nm thick platinum

30 layer (208HR sputter coater, Cressington, Watford, UK). Finally, they were analyzed with a

31 scanning electron microscope (FEI Apreo VolumeScope, Hillsboro, USA) at 3 kV (PA66,

32 recycled PET, PLA) and 5 kV (PS, mussel shell fragments) using an Everhart-Thornley

33 detector.

34 Qa/Qc of used analytical methods

35 Temperature and sensitivity calibration of the DSC measurements were carried out using

36 adamantane, indium, tin, bismuth and caesium chloride as calibration substances. The

37 corresponding melting points were experimentally determined. For the onset value (temperature

38 calibration) respectively the peak area (sensitivity calibration), the quadratic approximation to

39 the theoretical values was calculated, using different weighting of the individual substances.

40 Temperature calibration of the TGA measurements was carried out using indium, bismuth, zinc,

41 aluminum and silver as calibration substances. From the TGA measurements of the substances,

42 the corresponding melting temperatures were calculated by c-DTA. The quadratic

43 approximation of the onset value to the theoretical values was calculated using different

44 weighting of the individual substances.

164

45 The GC-MS device was tuned with perfluorotributylamine (PFTBA) prior to the measurements.

46 For quality assurance every match with the database has been confirmed by comparison with

47 available mass spectra and Kovats indices from the literature. Kovats indices are temperature

48 program and device-independent, column type dependent constants based on the retention time

49 of the analytes, which are a reliable indicator for GC measurements[1]. 1 µL of a qualitative

50 retention time index standard compromising of a mixture of C7 - C33 aliphatic hydrocarbons

51 (100-200 µg/mL per compound in hexane, (No 31080, Restek, Bellefonte, United States) was

52 utilised with the method described above. Peaks of high interest (i.e. anthranilamide, BHT, 2-

53 aminobenzonitrile (anthranilonitrile) were verified by measurements with addition of 1µg of

54 synthetic standards (anthranilamide: Acros organics, 99+%, BHT: Sigma-Aldrich, 99+%,

55 2-Aminobenzonitrile (anthranilonitrile): Fluka, 98%, (0.1µg/µL in $CHCl_3$) (see Fig. S8).

56 Proteomic analysis - Qa

57 The mass spectrometer was operated in the data-dependent acquisition mode performing a

58 maximum of 15 MS/MS spectra per survey scan. For quality assurance and to check the

59 performance of the entire LC-MS/MS setup, 100 ng of a commercial tryptic HeLa digest

60 (Pierce™ HeLa Protein Digest Standard - Thermo Fisher) were measured regularly.

61 Chromatographic peaks of defined peptides were evaluated according to retention times, signal

62 intensities and peak width. MS/MS spectra were analyzed using MASCOT V2.6.2 (Matrix

63 Science Limited, London, UK) and evaluated according to the number of identified peptides

64 and mass accuracy of the spectra. Search parameters were set to: i) Enzyme: Trypsin; ii) Mass

65 tolerance precursor: 10 ppm; iii) Mass tolerance MS/MS: 0.02 Da; iv) Fixed modification:

66 Carbamidomethylation of cysteine; v) Variable modifications: oxidized methionine.

67

68   Additional Details for NMR measurements of PET

69   The ^{1}H NMR spectra obtained at external magnetic fields of 7.0 T (Fig. S6) and 16.4 T (Fig.

70   S7) reveal the characteristic signals of PET at 7.95 ppm and 4.62 ppm (Fig. S7) corresponding

71   to the benzene rings of the terephthalate units and the aliphatic oxyethylene groups of the

72   polymer chains. The signal at 7.92 ppm corresponds to 1.2 % whole cyclic trimer molecules of

73   PET relative to one repeating unit of the main chain. Furthermore, alcohol bearing end groups

74   were observed assigned to signals at 3.99 ppm for the α position and 4.43 ppm for the β position

75   (Fig. S7 signals a and b). With much lower intensity also, the esterification of the OH end

76   groups with TFA-D were found (4.54 ppm and 4.57 ppm). The end group intensity ratio amount

77   to 0.9 mol % matching MWD obtained by the GPC measurements. In addition, the chain defects

78   (5.5%) are visible at 3.95 ppm, and 4.47 ppm resulting from etherification of ethylene glycol

79   (EG) to diethylene glycol (DEG) during the polymerization of PET (Fig. S6 and S7). They are

80   built into the main chain (Fig. S7 signals c and d), which may be desired in some applications

81   to reduce crystallinity and glass transition temperature. The corresponding ^{13}C signals were also

82   observed within the high-resolution ^{13}C NMR spectrum (Fig. S7, signals y, x, t, g, d and c).

83   Furthermore, we observed three characteristic signal groups (Fig. S7 signals 1, 2 and 3) for a

84   difunctionalized (meta-arrangement) benzene ring. They match to additives like

85   Phenylenebisoxazoline (PBO) or isophthalic acid (IPA), which is an impurity in terephthalic

86   acid and amount to 1.5 %. In both cases, it would be polymerized into the PET chain. In

87   addition, the aromatic region exhibits multiple signals in the order of magnitude of 0.1 per mill.

88   Some of which match to the reference measurement of the identified Anthranilamide (GC

89   measurement) and are in the same dimension as the additive would be expected.

90
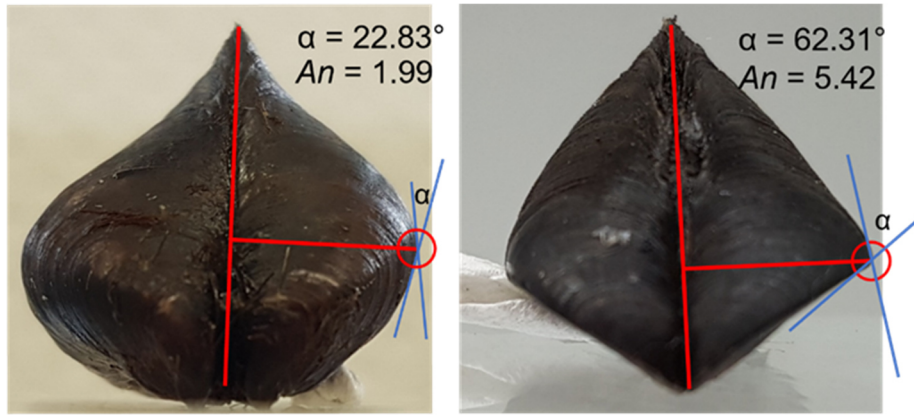
91

92 **Fig. S1. Example for the distinction between *D. bugensis* (left) and *D. polymorpha* (right) according to**

93 **Teubner et al.**[2]**.** Here, valves are divided by a vertical line where the valves meet. Then, the outermost point of

94 the valve is marked. The distance from the central vertical line is then denoted as "width". Then a circle with the

95 radius width/5 is drawn with the outermost point as center. Finally intersections with the contour (blue lines) of

96 the mussels result in the angle "α". The quantitative parameter "angularity" (An) is achieved by α/11.48.

97 Discriminant values for An are An ≤ 3.3 and An ≥ 4.7 for quagga and zebra mussels, respectively.

98

99
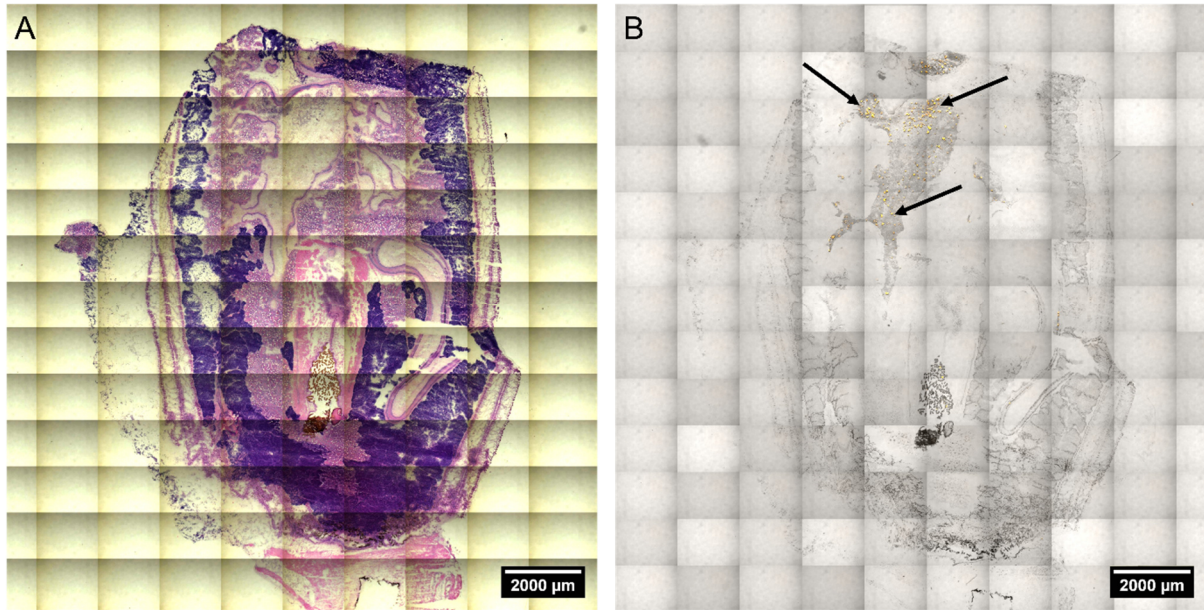
Fig. S2. Stitched tile scans of cryo-sectioned (20µm) mussel soft tissue. (A) H&E stained section; (B) Overlay of brightfield and fluorescent channel (ex: 543 nm; em 565 nm) of the same section. Particles are visible throughout the digestive tract (arrows in B).
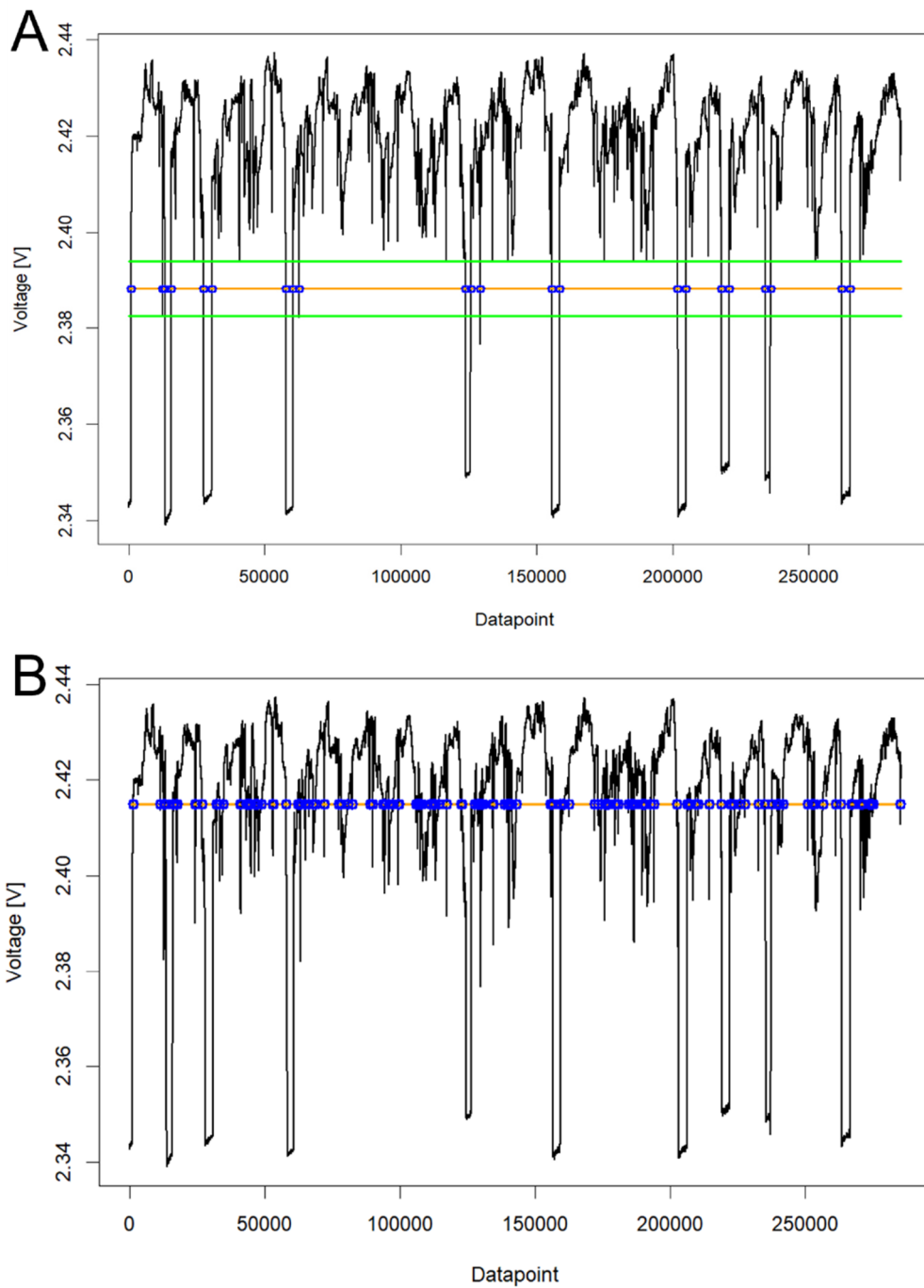
104

105 **Fig. S3. Exemplary voltage curves (black line) after conversion of the raw data.** (A) Voltage curve with new

106 defined threshold (mean of min and max voltage output) to fit the behavior of *D. bugensis*. The orange line

107 represents the transition line. Blue points represent the intersection points of the voltage curve with the transition

108 line. The green lines reflect 0.25 x SD of the voltage output, around the transition line. (B) Voltage curve with the

109 threshold proposed by Hartmann et al., 2016 for *Anodonta anatine* (mean of the voltage output) [3]. The orange

110 line represents the transition line. Blue points represent the intersection points of the voltage curve with the

111 transition line.
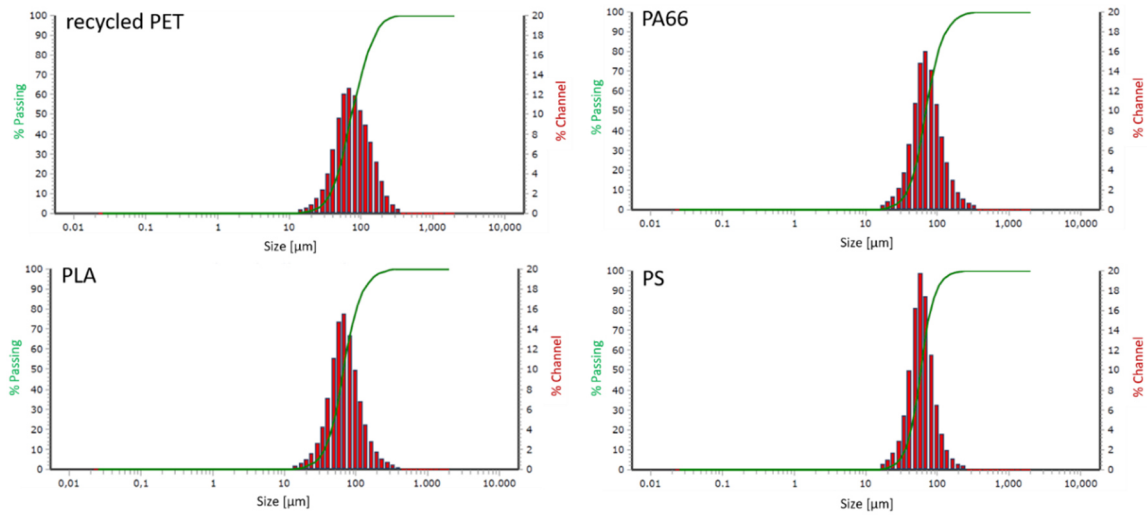
Fig. S4. Details for LD measurements. LD measurements of the different used MPs in this experiment; recycled PET: recycled polyethylene terephthalate PA: polyamide 66; PLA: polylactic acid; PS: polystyrene.
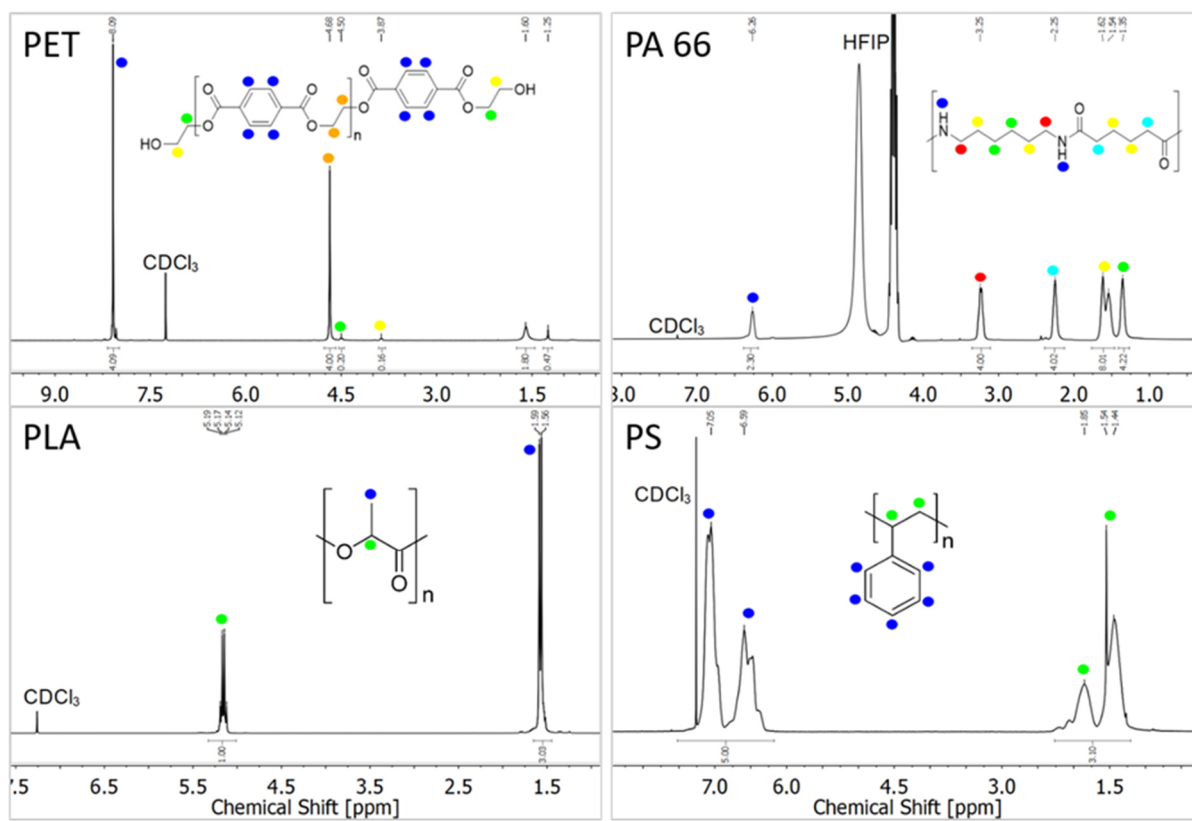
170
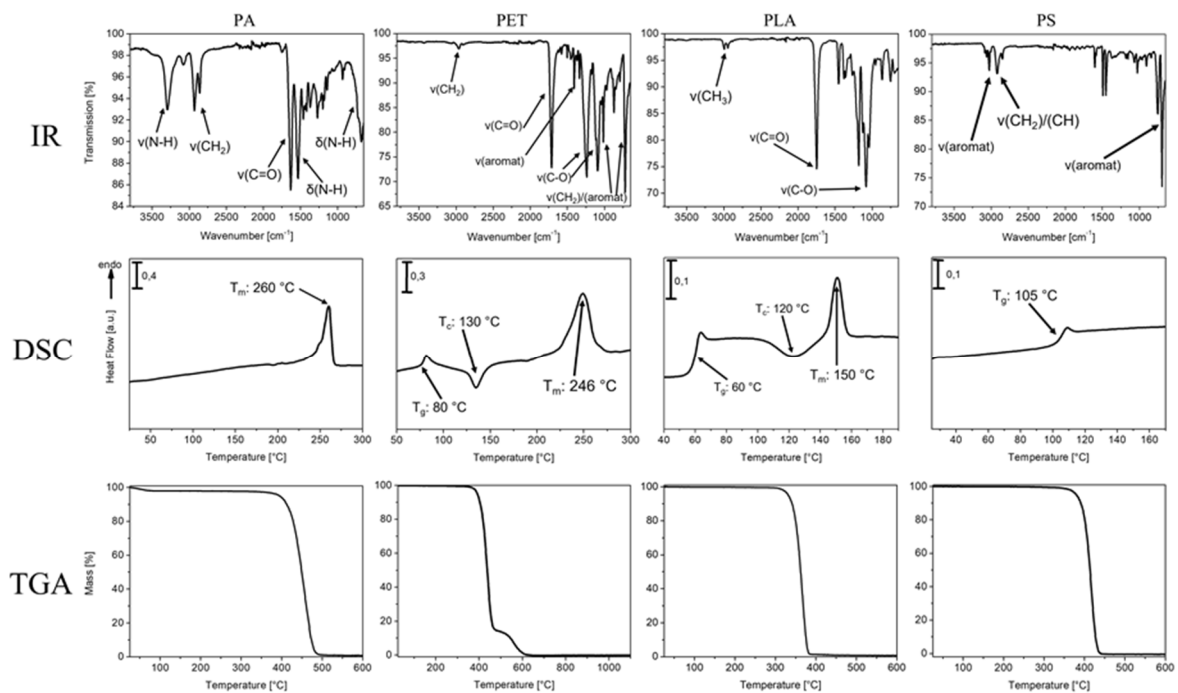
116

117   **Fig. S5. Details for IR, DSC & TGA measurements**. Spectra derived from IR, DSC and TGA measurements
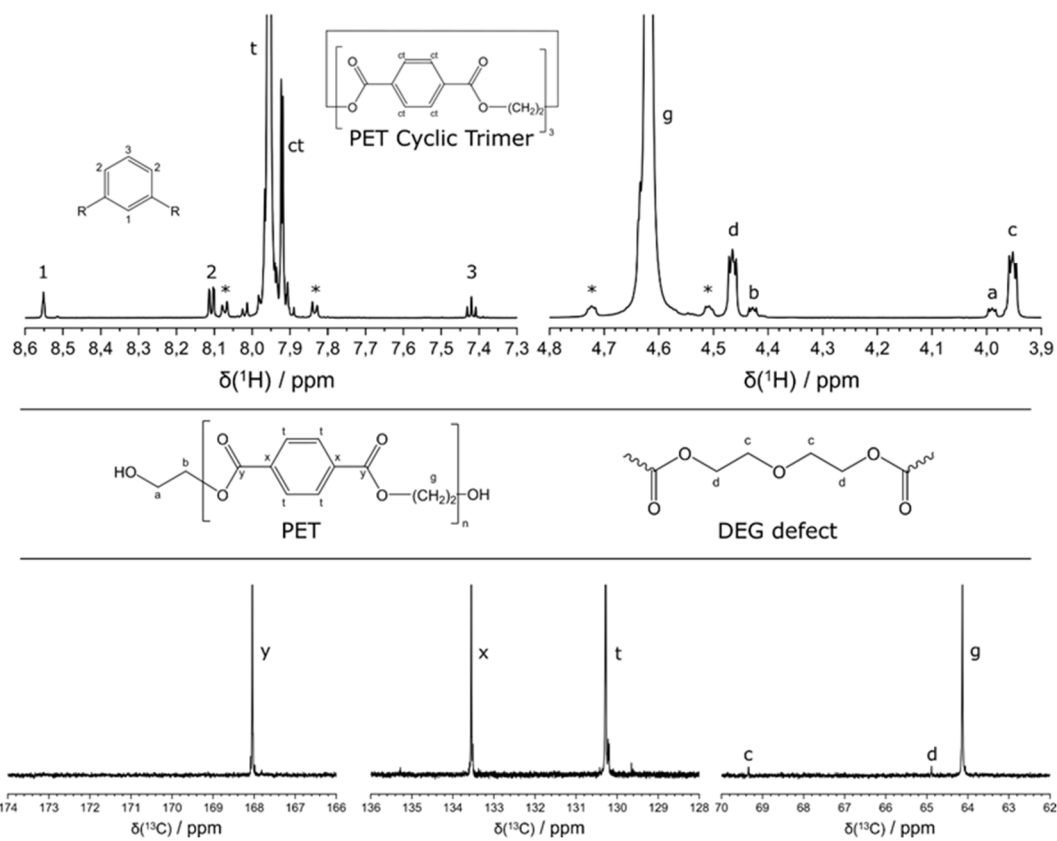
118   for all used polymers

119
120

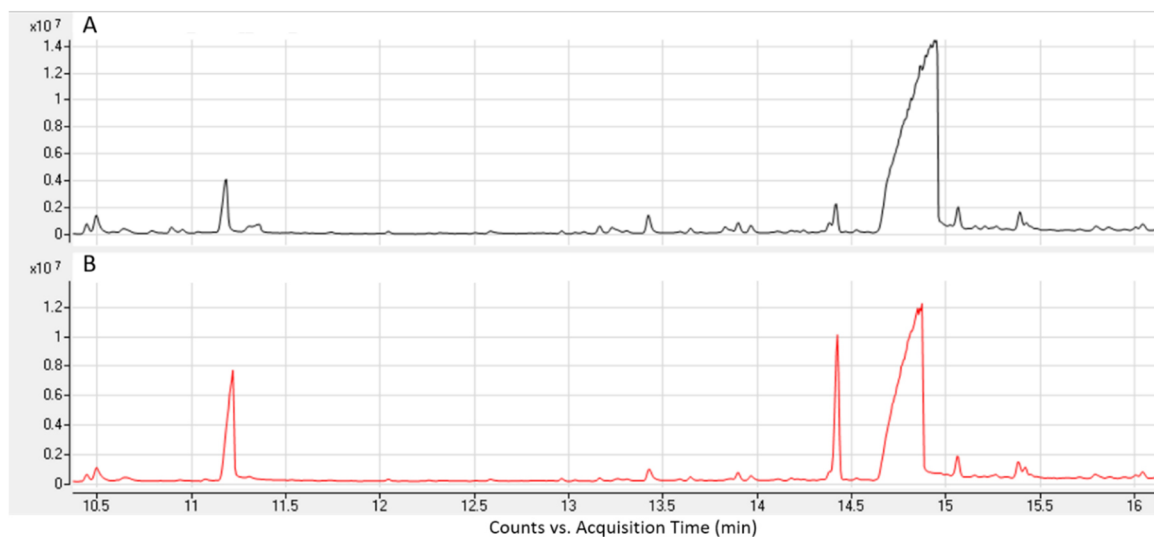Fig. S6. ¹H NMR spectra (B_0 = 7.0 T; v_0 = 300.1 MHz) for all polymer-types used in this study.

121

122

123

124

Fig. S7. ^{1}H and ^{13}C NMR spectra of PET (B_0 = 16.4 T; ν_0(^{1}H) = 700.1 MHz, ν_0 (^{13}C) = 176.0 MHz) in a solvent 3:1 solvent mixture from CDCl$_3$ and TFA-D. ^{13}C satellites are marked with asterisks. Molecule labelling as denoted.

128

129 **Fig. S8. Details for GC-MS measurements of PET.** GC-MS measurements of recycled PET. A: measurement

130 of PET without any additional standards. B: measurement of PET with addition of 1 μg analytical standards

131 (0.1 μg/μL in CHCl$_3$) for anthranilonitrile (11.2 min), BHT (14.4 min) and anthranilamide (14.7 min). Mass

132 spectra and retention times were identical to the peaks of the sample.
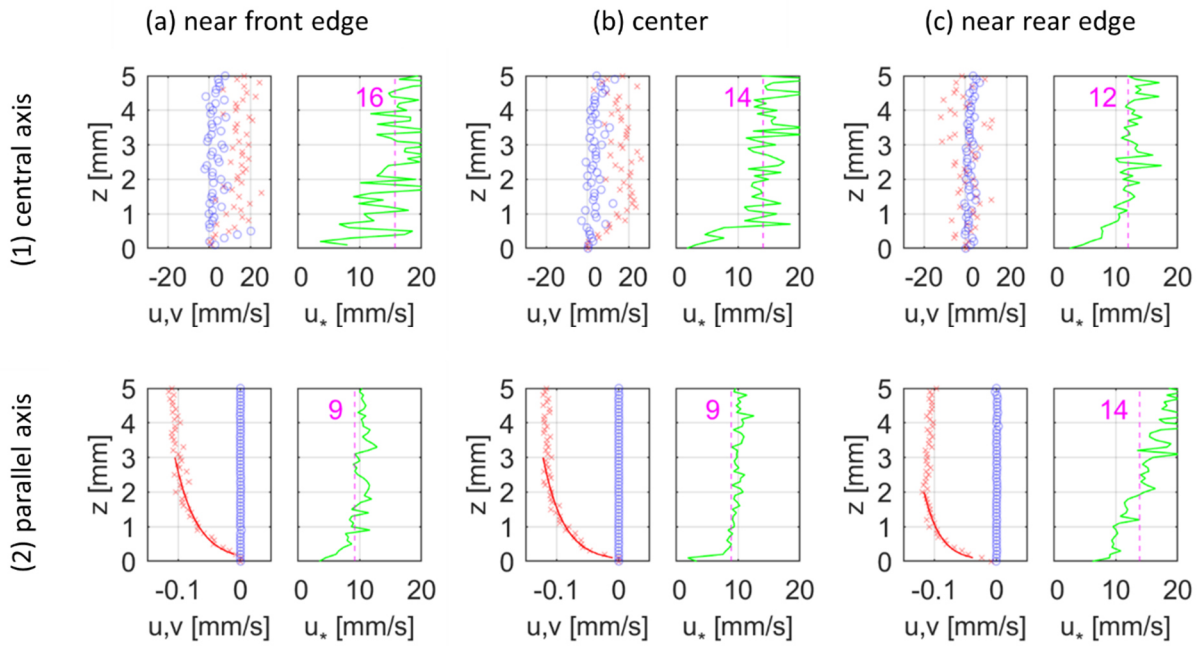
133
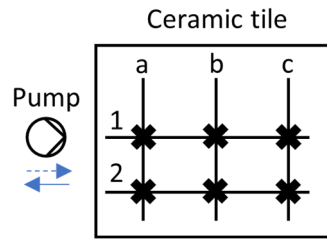
134

135 **Fig. S9. Top view of the velocity measurement locations** along the central axis (1) and a parallel axis (2), at

136 three different longitudinal positions (a) near the front edge, (b) central, (c) near the rear edge. Pump is below the

137 measurement plane, leading to a primary flow to the right below the plane and to the left above the plane.

138

Fig. S10. Profile of velocity measurements and fluctuations (friction velocity from eddy correlation method) evolving above the ceramic tile used for the exposition experiments. Blue circles represent vertical velocities, red crosses horizontal velocities, red lines the fit of horizontal velocities to the logarithmic boundary profile. Green lines show Reynolds stresses and the pink dashed lines friction velocity as its spatial mean. The velocity profile along the central axis (1) showed no pronounced velocity profile, which was caused by rapid fluctuations in the flow. Along the parallel axis (2), a boundary layer was formed and friction velocities from the horizontal velocity profile were 14, 13 and 11 mm/s (from 2a to 2c).

148 **Table S1 Overview of the concentrations of stock suspensions.** Included are mean particle numbers per ml and

149 the standard deviation (SD),

Particle type	PA 66	recycled PET	PLA	PS stock 1	PS stock 2	Mussel shell fragments
Particles/ml	59167	117500	52500	43333	34167	2383333
SD	5204	5000	15612	3819	1443	288675

150

151 **References**

152 [1]   E. Kovats, Gas chromatographic characterization of organic compounds. I. Retention

153   indexes of aliphatic halides, alcohols, aldehydes, and ketones, Helv. Chim. Acta. 41

154   (1958) 1915–1932.

155 [2]   D. Teubner, A.K. Wesslein, P.B. Rønne, M. Veith, C. Frings, M. Paulus, Is a visuo-

156   haptic differentiation of zebra mussel and quagga mussel based on a single external

157   morphometric shell character possible?, Aquat. Invasions. 11 (2016) 145–154.

158   https://doi.org/10.3391/ai.2016.11.2.04.

159 [3]   J.T. Hartmann, S. Beggel, K. Auerswald, B.C. Stoeckle, J. Geist, Establishing mussel

160   behavior as a biomarker in ecotoxicology, Aquat. Toxicol. 170 (2016) 279–288.

161   https://doi.org/10.1016/j.aquatox.2015.06.014.

162

7 Publications and manuscripts

(Eidesstattliche) Versicherungen und Erklärungen

(§ 9 Satz 2 Nr. 3 PromO BayNAT)

Hiermit versichere ich eidesstattlich, dass ich die Arbeit selbstständig verfasst und keine anderen als die von mir angegebenen Quellen und Hilfsmittel benutzt habe (vgl. Art. 97 Abs. 1 Satz 8 BayHIG).

(§ 9 Satz 2 Nr. 3 PromO BayNAT)

Hiermit erkläre ich, dass ich die Dissertation nicht bereits zur Erlangung eines akademischen Grades eingereicht habe und dass ich nicht bereits diese oder eine gleichartige Doktorprüfung endgültig nicht bestanden habe.

(§ 9 Satz 2 Nr. 4 PromO BayNAT)

Hiermit erkläre ich, dass ich Hilfe von gewerblichen Promotionsberatern bzw. -vermittlern oder ähnlichen Dienstleistern weder bisher in Anspruch genommen habe noch künftig in Anspruch nehmen werde.

(§ 9 Satz 2 Nr. 7 PromO BayNAT)

Hiermit erkläre ich mein Einverständnis, dass die elektronische Fassung meiner Dissertation unter Wahrung meiner Urheberrechte und des Datenschutzes einer gesonderten Überprüfung unterzogen werden kann.

(§ 9 Satz 2 Nr. 8 PromO BayNAT)

Hiermit erkläre ich mein Einverständnis, dass bei Verdacht wissenschaftlichen Fehlverhaltens Ermittlungen durch universitätsinterne Organe der wissenschaftlichen Selbstkontrolle stattfinden können.

…………………………………………………………………………………………………

Bayreuth, 20.05.2024   (Jan-Pascal Boos)